

Contents

2.0	SITE CHARACTERISTICS.....	2.1-1
2.1	GEOGRAPHY AND DEMOGRAPHY OF SITE SELECTED	2.1-1
2.1.1	Site Location.....	2.1-1
2.1.2	Site Description	2.1-2
2.1.2.1	Other Activities Within the ISF Site Boundary.....	2.1-3
2.1.2.2	Boundaries for Establishing Effluent Release Limits.....	2.1-3
2.1.3	Population Distribution and Trends.....	2.1-3
2.1.4	Uses of Nearby Land and Waters	2.1-4
2.2	NEARBY INDUSTRIAL, TRANSPORTATION, AND MILITARY FACILITIES..	2.2-1
2.3	METEOROLOGY	2.3-1
2.3.1	Regional Climatology.....	2.3-1
2.3.1.1	Data Sources	2.3-1
2.3.1.2	General Climate.....	2.3-1
2.3.1.2.1	Terrain Influences on Regional Climate.....	2.3-1
2.3.1.2.2	Regional Temperature	2.3-2
2.3.1.2.3	Freeze-Thaw Cycles	2.3-2
2.3.1.2.4	Degree Days	2.3-2
2.3.1.2.5	Subsoil Temperatures	2.3-3
2.3.1.2.6	Regional Precipitation	2.3-3
2.3.1.2.7	Regional Atmospheric Moisture.....	2.3-3
2.3.1.2.8	Regional Winds	2.3-3
2.3.1.2.9	Sky Cover	2.3-4
2.3.1.2.10	Atmospheric Pressure.....	2.3-4
2.3.1.2.11	Air Density	2.3-4
2.3.1.2.12	Other Phenomena	2.3-4
2.3.1.3	Severe Weather.....	2.3-5
2.3.1.3.1	Maximum and Minimum Temperatures.....	2.3-5
2.3.1.3.2	Extreme Winds.....	2.3-5
2.3.1.3.3	Tornadoes	2.3-5
2.3.1.3.4	Dust Devils	2.3-6
2.3.1.3.5	Hurricanes and Tropical Storms.....	2.3-6
2.3.1.3.6	Precipitation Extremes – Recorded Hourly and Daily Precipitation Events	2.3-6
2.3.1.3.7	Precipitation Extremes – Predicted Maximum Storm Events	2.3-6
2.3.1.3.8	Precipitation Extremes – Precipitation Occurrence.....	2.3-7
2.3.1.3.9	Thunderstorms and Lightning	2.3-7
2.3.1.3.10	Snow Storms.....	2.3-7
2.3.1.3.11	Hail and Ice Storms	2.3-8
2.3.2	Local Climatology	2.3-8
2.3.2.1	Data Sources	2.3-8
2.3.2.2	General Climate	2.3-8
2.3.2.3	Topography.....	2.3-8

2.3.3 Onsite Meteorological Monitoring Program	2.3-9
2.3.3.1 Wind Roses.....	2.3-9
2.3.3.2 Observations for Offsite Concentration Assessments	2.3-9
2.3.4 Diffusion Estimates	2.3-9
2.3.4.1 Single Station Modeling – XOQDOQ.....	2.3-10
2.3.4.1.1 Model Operational Theory	2.3-10
2.3.4.1.2 Modeling Assumptions and Input Data.....	2.3-11
2.3.4.1.3 Results	2.3-11
2.3.4.2 Gridded Windfield Modeling - MESODIF.....	2.3-11
2.3.4.2.1 MESODIF Model Description	2.3-11
2.3.4.2.2 MESODIF Modeling Assumptions and Input Data	2.3-12
2.3.4.2.3 MESODIF Results.....	2.3-13
2.4 SURFACE HYDROLOGY	2.4-1
2.4.1 Hydrologic Description	2.4-1
2.4.1.1 Site and Structures	2.4-1
2.4.1.2 Hydrosphere.....	2.4-1
2.4.1.2.1 Mackay Dam	2.4-2
2.4.1.2.2 INEEL Flood Diversion Facility	2.4-2
2.4.2 Floods	2.4-3
2.4.2.1 Flood History	2.4-3
2.4.2.2 Flood Design Considerations.....	2.4-4
2.4.2.3 Effects of Local Intense Precipitation.....	2.4-4
2.4.3 Probable Maximum Flood on Streams and Rivers	2.4-4
2.4.3.1 Probable Maximum Precipitation.....	2.4-5
2.4.3.2 Precipitation Losses	2.4-5
2.4.3.3 Runoff Model.....	2.4-5
2.4.3.4 Probable Maximum Flood Flow	2.4-6
2.4.3.5 Water Level Determinations	2.4-6
2.4.3.6 Coincident Wind-Wave Activity.....	2.4-6
2.4.4 Potential Dam Failures (Seismically Induced)	2.4-7
2.4.4.1 Reservoir Description	2.4-7
2.4.4.2 Dam Failure Permutations	2.4-7
2.4.4.3 Unsteady Flow Analysis of Potential Dam Failures	2.4-7
2.4.4.4 Water Level at ISF Site.....	2.4-8
2.4.5 Probable Maximum Surge and Seiche Flooding	2.4-8
2.4.6 Probable Maximum Tsunami Flooding	2.4-8
2.4.7 Ice Flooding.....	2.4-8
2.4.8 Flooding Protection Requirements	2.4-8
2.4.9 Environmental Acceptance of Effluents	2.4-8
2.5 SUBSURFACE HYDROLOGY	2.5-1
2.5.1 Regional Characteristics	2.5-1
2.5.2 Site Characteristics	2.5-2
2.5.3 Contaminant Transport Analysis	2.5-3
2.6 GEOLOGY AND SEISMOLOGY.....	2.6-1
2.6.1 Basic Geologic and Seismic Information	2.6-1

2.6.1.1	Geomorphology	2.6-1
2.6.1.2	Geologic History	2.6-2
2.6.1.2.1	Paleozoic, Mesozoic, and Early Cenozoic Era History	2.6-2
2.6.1.2.2	Late Cenozoic and Quaternary Era History	2.6-2
2.6.1.2.3	Basin-and-Range Tectonic Activity	2.6-4
2.6.1.3	INEEL/ISF Facility Site Geology	2.6-4
2.6.1.3.1	Topographic and Physiographic Description	2.6-4
2.6.1.3.2	Stratigraphy and Areal Geology	2.6-5
2.6.1.3.3	Structural Geologic Conditions	2.6-8
2.6.1.3.4	Geologic History Related to Regional Geologic History	2.6-9
2.6.1.3.5	Engineering Geological Conditions	2.6-10
2.6.1.3.6	Groundwater Conditions	2.6-10
2.6.2	Vibratory Ground Motion	2.6-10
2.6.2.1	Seismicity	2.6-10
2.6.2.1.1	Regional Setting	2.6-10
2.6.2.1.2	Earthquake History	2.6-10
2.6.2.1.3	Moderate to Large Earthquakes	2.6-12
2.6.2.2	Geologic and Tectonic Characteristics of Site and Region	2.6-13
2.6.2.2.1	Identification and Description of Earthquake Source: Tectonic Provinces	2.6-13
2.6.2.2.2	Identification and Description of Earthquake Source: Faults	2.6-14
2.6.2.2.3	Identification and Description of Earthquake Sources: Volcanic Rift Zones and Axial Volcanic Zone	2.6-19
2.6.2.3	Correlation of Earthquake Activity with Seismic Sources	2.6-19
2.6.2.3.1	Eastern Snake River Plain Province	2.6-19
2.6.2.3.2	Northern Basin and Range Province	2.6-23
2.6.2.3.3	Yellowstone Plateau	2.6-25
2.6.2.3.4	Northern Rocky Mountains	2.6-25
2.6.2.3.5	Maximum Earthquake Potential	2.6-26
2.6.2.3.6	Regional Seismic Wave Transmission Characteristics	2.6-30
2.6.2.4	Probabilistic Seismic Hazard Analysis	2.6-31
2.6.2.4.1	1977 Probabilistic Seismic Hazard Study	2.6-31
2.6.2.4.2	1984 Probabilistic Seismic Hazard Study	2.6-32
2.6.2.4.3	1996 Probabilistic Seismic Hazard Evaluation	2.6-32
2.6.2.4.4	1999 Probabilistic Seismic Hazard Analysis	2.6-34
2.6.2.4.5	Probabilistic Seismic Hazard Applicable to ISF Site	2.6-34
2.6.2.5	Seismic Wave Transmission Characteristics of the ISF Site	2.6-35
2.6.2.5.1	Development of Basecase and Randomized Soil Profiles	2.6-35
2.6.2.5.2	Selection of Mean Ground Motion Hazard Level	2.6-36
2.6.2.6	Design Earthquake Ground Motion	2.6-36
2.6.2.6.1	Development of Horizontal Design Earthquake Ground Motion	2.6-36
2.6.2.6.2	Development of Vertical Design Earthquake Ground Motion	2.6-37
2.6.3	Surface Faulting	2.6-38
2.6.3.1	Geologic Conditions of ISF Site	2.6-38
2.6.3.2	Evidence of Fault Offset	2.6-38
2.6.3.3	Earthquakes Associated with Capable Faults	2.6-39

2.6.3.4	Investigation of Capable Faults	2.6-39
2.6.3.5	Correlation of Epicenters with Capable Faults	2.6-39
2.6.3.6	Description of Capable Faults	2.6-39
2.6.3.7	Zone Requiring Detailed Faulting Studies	2.6-40
2.6.3.8	Results of Faulting Investigations	2.6-40
2.6.4	Stability of Subsurface Materials and Foundations	2.6-40
2.6.4.1	Geologic Features	2.6-40
2.6.4.1.1	Surface or Subsurface Subsidence	2.6-40
2.6.4.1.2	Previous Loading History	2.6-41
2.6.4.1.3	Rock Jointing and Weathering Patterns, Weak Materials	2.6-41
2.6.4.1.4	Unrelieved Residual Stresses	2.6-42
2.6.4.2	Properties of Underlying Materials	2.6-42
2.6.4.3	Plot Plan	2.6-43
2.6.4.4	Soil and Rock Characteristics	2.6-43
2.6.4.5	Excavations and Backfill	2.6-43
2.6.4.6	Groundwater Conditions	2.6-44
2.6.4.7	Response of Soil and Rock to Dynamic Loading	2.6-44
2.6.4.8	Liquefaction Potential	2.6-44
2.6.4.9	Earthquake Design Basis	2.6-44
2.6.4.10	Static Analysis	2.6-44
2.6.4.11	Techniques to Improve Subsurface Conditions	2.6-44
2.6.5	Slope Stability	2.6-44
2.6.5.1	Slope Characteristics	2.6-44
2.6.5.2	Design Criteria and Analyses	2.6-44
2.6.5.3	Logs of Core Borings	2.6-44
2.6.5.4	Compaction Specifications	2.6-45
2.6.6	Volcanism	2.6-45
2.6.6.1	Introduction	2.6-45
2.6.6.2	Potential Volcanic Hazards of the INEEL/ISF Site	2.6-45
2.6.6.2.1	Formation of Eastern Snake River Plain Silicic Calderas and Related Volcanism	2.6-46
2.6.6.2.2	Growth of Rhyolitic Domes, Intrusions, and Related Phenomena	2.6-46
2.6.6.2.3	Basaltic Volcanism and Related Phenomena	2.6-47
2.6.6.2.4	Volcanic Recurrence and Probabilistic Risk for the ISF Site	2.6-49
2.6.6.3	Potential Volcanic Hazards from Distant Sources	2.6-51
2.6.6.3.1	Yellowstone Plateau	2.6-51
2.6.6.3.2	Cascade Volcanoes and Other Western United States Centers	2.6-52
2.6.6.4	Conclusions	2.6-52
2.7	SUMMARY OF SITE CONDITIONS AFFECTING CONSTRUCTION AND OPERATING REQUIREMENTS	2.7-1
2.8	REFERENCES	2.8-1

Tables

Table 2.1-1	Typical Work Force at INEEL Facilities
Table 2.3-1	Historical INEEL Daily Temperature Extremes
Table 2.3-2	Mean and Maximum of Daily Temperature Range for INEEL
Table 2.3-3	Historical Freeze and Thaw Cycles at the INEEL
Table 2.3-4	Historical INEEL Monthly Heating Degree Days and Extremes
Table 2.3-5	Historical INEEL Monthly Cooling Degree Days and Extremes
Table 2.3-6	Historical INEEL Area Precipitation
Table 2.3-7	Historical Precipitation Extremes at INEEL
Table 2.3-8	Historical INEEL Snowfall Amounts
Table 2.3-9	Historical INEEL Dewpoint Temperatures
Table 2.3-10	Historical INEEL Average Wind Speeds
Table 2.3-11	Historical CFA Atmosphere Pressure
Table 2.3-12	DEQ-Estimated Planning-Level Ambient Concentrations INEEL Airshed
Table 2.3-13	Historical INEEL Extremes of Daily Temperatures
Table 2.3-14	Expected INEEL Peak Wind Gusts
Table 2.3-15	Design Basis Tornado
Table 2.3-16	Predicted Maximum Storm Precipitation Amounts
Table 2.3-17	Average Number of Days (percent) with Specified Amounts of Precipitation at the INEEL
Table 2.3-18	Historical INEEL Average Number of Days (percent) with Specified Snowfall Amounts
Table 2.3-19	Historical INEEL Maximum and Average Snow Depths (in inches)
Table 2.3-20	XOQDOQ Input Data and Program Options Used in the INEEL INTEC Dispersion Analysis
Table 2.3-21	MESODIF Input Data and Program Options Used in the INEEL INTEC Dispersion Analysis
Table 2.4-1	Historical Monthly Big Lost River Discharge Near INTEC (Cubic Feet)
Table 2.4-2	Dam and Reservoir Characteristics
Table 2.4-3	Results of Probable Maximum Flood Induced Overtopping Failure of Mackay Dam ⁽¹⁾
Table 2.4-4	Results of Seismic Induced Failure of Mackay Dam During 25-Year Flood ⁽¹⁾
Table 2.4-5	Dam Failure Characteristics
Table 2.5-1	INEEL Production Wells and Annual Volume Pumped
Table 2.6-1	Time Periods of Earthquake Data Completeness
Table 2.6-2	Earthquakes with Magnitudes Greater than 5.5 within 321 Kilometers of INEEL ⁽⁴⁾
Table 2.6-3	Ground Motions Recorded During the Borah Peak Earthquake at CPP-601
Table 2.6-4	Basin and Range Faults Around the Eastern Snake River Plain
Table 2.6-5	Earthquakes within 200 Miles that have Occurred on Tectonic Structures
Table 2.6-6	Historical Earthquakes Possibly Located within the Eastern Snake River Plain
Table 2.6-7	Maximum Magnitudes and Focal Depths of Earthquakes Associated with Dike Injection ^(a)
Table 2.6-8	Maximum Magnitudes Based on Rupture Areas of Normal Faults and Fissures in Eastern Snake River Plain Volcanic Rift Zones

- Table 2.6-9 Probabilistic Seismic Hazard Studies Applicable to the INTEC
Table 2.6-10 Estimated Volcanic-Recurrence Intervals and Corresponding Annual Eruption Probabilities (in parentheses) for Volcanic Zones and Boreholes of the INEEL Area
Table 2.6-11 Strain-Iterated Dynamic Soil Properties
Table 2.6-12 Properties of Soil (Sediments) and Bedrock at INTEC
Table 2.6-13 Hazards Associated with Basaltic Volcanism on the Eastern Snake River Plain

Figures

- Figure 2.1-1 Location Map of the INEEL
Figure 2.1-2 INEEL Vicinity Map (with 50-mile radius line)
Figure 2.1-3 Map of INEEL
Figure 2.1-4 Aerial View of INTEC Showing ISF Site (looking north)
Figure 2.1-5 INTEC Area Plot and Location of ISF Site
Figure 2.1-6 INTEC Area Topographical Map
Figure 2.1-7 Location of the INEEL in Southeastern Idaho
Figure 2.1-8 INEEL Map with Major Drainages
Figure 2.1-9 Distances from the ISF Site to the INEEL Boundary
Figure 2.1-10 Approximate Distribution of Vegetation at the INEEL
Figure 2.1-11 ISF Site Plan
Figure 2.1-12 2000 Census Population Distribution Within 50 Miles of the ISF Facility
Figure 2.1-13 Selected Land Uses at the INEEL and Surrounding Region
Figure 2.2-1 INEEL Primary Facility Areas
Figure 2.3-1 Relief Map of the Eastern Snake River Plain
Figure 2.3-2 Average Monthly Subsoil Temperatures (°F) Sandy Soil Surface
Figure 2.3-3 Average Monthly Subsoil Temperatures (°F) Asphalt Surface
Figure 2.3-4 Topographic Map of the INEEL Area
Figure 2.3-5 Topographical Cross-Sections for TMI-2 ISFSI 50-Mile Radius, North and East Radials
Figure 2.3-6 Topographical Cross-Sections for TMI-2 ISFSI 50-Mile Radius, South and East Radials
Figure 2.3-7 Topographical Cross-Sections for TMI-2 ISFSI 50-Mile Radius, South and West Radials
Figure 2.3-8 Topographical Cross-Sections for TMI-2 ISFSI 50-Mile Radius, North and West Radials
Figure 2.3-9 Topographical Cross-Sections for TMI-2 ISFSI 5-Mile Radius, North and East Radials
Figure 2.3-10 Topographical Cross-Sections for TMI-2 ISFSI 5-Mile Radius, South and East Radials
Figure 2.3-11 Topographical Cross-Sections for TMI-2 ISFSI 5-Mile Radius, South and West Radials
Figure 2.3-12 Topographical Cross-Sections for TMI-2 ISFSI 5-Mile Radius, North and West Radials
Figure 2.3-13 Grid 3 - 10 Meter Level Annual Wind Roses (1980-1982)
Figure 2.3-14 Grid 3 - 10 Meter Level Annual Wind Roses (1980-1982)

- Figure 2.3-15 Grid 3 - 61 Meter Level Annual Wind Roses (1980-1982)
Figure 2.3-16 Grid 3 - 61 Meter Level Annual Wind Roses (1980-1982)
Figure 2.3-17 Wind Observation Locations Within a 50-Mile Radius of ISF Site
Figure 2.3-18 σ_z versus Distance at INEEL
Figure 2.3-19 σ_y versus Distance at INEEL
Figure 2.3-20 Annual Normalized Concentration - 50-Mile Radius (INTEC 1982)
Figure 2.3-21 Annual Normalized Concentration- 5-Mile Radius (INTEC 1982)
Figure 2.3-22 Annual Normalized Total Integrated Concentration (INTEC 1980)
Figure 2.3-23 Annual Normalized Total Integrated Concentration (INTEC 1981)
Figure 2.3-24 Annual Normalized Total Integrated Concentration (INTEC 1982)
Figure 2.3-25 Annual Normalized Total Integrated Concentration (INTEC 1974-1983)
Figure 2.4-1 Big Lost River System on the INEEL
Figure 2.4-2 ISF Facility - Front View
Figure 2.4-3 Hydrograph for PMF-Induced Failure of the Mackay Dam
Figure 2.4-4 Predicted Inundation Area at INEEL for PMF-Induced Overtopping of Mackay Dam
Figure 2.5-1 Relief Map of Idaho with Groundwater Flow Lines
Figure 2.5-2 Groundwater Contours and Directions - INEEL
Figure 2.5-3 Map Showing Production Wells - INEEL
Figure 2.5-4 Depth to Water Table - INEEL
Figure 2.6-1 Physiographic Province Map of the Western United States
Figure 2.6-2 Shade Relief Map of Western United States
Figure 2.6-3 Map of the Overthrust Belt
Figure 2.6-4 Map of Trans-Challis Fault Zone and Challis Volcanic Field
Figure 2.6-5 Calderas in the Track of the Yellowstone Hotspot
Figure 2.6-6 Volcanic Zones on the Eastern Snake River Plain
Figure 2.6-7 Lithographic Logs of the Four INEEL Deep Drill Holes
Figure 2.6-8 Idealized Longitudinal Section of an Eastern Snake River Plain Basalt Lava Flow
Figure 2.6-9 Generalized Geological Map of the INEEL with INTEC Located
Figure 2.6-10 Geologic Cross Section Through the INTEC-TRA Area Showing Anderson's Interpreted Dome
Figure 2.6-11 East-West Geologic Cross Section Through the INTEC-TRA Area
Figure 2.6-12 North-South Geologic Cross Section Through the INTEC-TRA Area
Figure 2.6-13 ISF Site Borehole Locations and Elevation Contours
Figure 2.6-14 Boring B-1 Log
Figure 2.6-15 Boring B-2 Log
Figure 2.6-16 Boring B-3 Log
Figure 2.6-17 Boring B-4 Log
Figure 2.6-18 Boring B-5 Log
Figure 2.6-19 Boring B-6 Log
Figure 2.6-20 Boring B-7 Log
Figure 2.6-21 Boring B-8 Log
Figure 2.6-22 Faults, Volcanic Zones and Historic Earthquakes in the INEEL Region
Figure 2.6-23 Seismic Source Zones in the INEEL Region
Figure 2.6-24 Principle Stress Orientations Affecting the Eastern Snake River Plain
Figure 2.6-25 Strain Rates in the Eastern Snake River Plain and Adjacent Areas

- Figure 2.6-26 Intermountain Seismic Belt and Centennial Tectonic Belt Seismicity Map
- Figure 2.6-27 Earthquake Epicenters in the INEEL Region 1850-1995
- Figure 2.6-28 Map of INEEL Seismic Network Stations and Epicenters of Earthquake
- Figure 2.6-29 Isoseismal Map for the 1959 Hebgen Lake Earthquake
- Figure 2.6-30 Isoseismal Map for the 1983 Borah Peak Earthquake
- Figure 2.6-31 Isoseismal Map for the 1905 Shoshone Earthquake
- Figure 2.6-32 Isoseismal Map for the 1975 Pocatello Valley Earthquake
- Figure 2.6-33 Isoseismal Map for the 1975 Yellowstone Earthquake
- Figure 2.6-34 Isoseismal Map for the 1994 Draney Peak Earthquake
- Figure 2.6-35 Map of the Southern Lemhi Fault
- Figure 2.6-36 Summary of Paleoseismic Results for the Lemhi Fault (Four Trenches)
- Figure 2.6-37 Comparison of Surface Area of the Howe Segment of the Lemhi Fault to the Surface Area of Dike-Induced Normal Faults
- Figure 2.6-38 Deep Borehole Shear Wave Velocity
- Figure 2.6-39 Comparison of the PC 3 (2500 years) Horizontal Rock DBE 5% Damped Response Spectra with the Adjusted Rock UHS for INTEC, TRA, RWMC, and PBF
- Figure 2.6-40 Plots of the Acceleration, Velocity, and Displacement Time Histories for One Horizontal Component of the PC 3 (2500 years) Rock DBE Response Spectrum at INTEC, TRA, RWMC, and PBF
- Figure 2.6-41 Plots of the Acceleration, Velocity, and Displacement Time Histories for the Second Horizontal Component of the PC 3 (2500 years) Rock DBE Response Spectrum at INTEC, TRA, RWMC, and PBF
- Figure 2.6-42 Measured Shear Wave Velocities and Basecase Profile
- Figure 2.6-43 Randomized Shear Wave Velocity Profiles
- Figure 2.6-44 Response of 30 Profiles to 2500-Yr Input Motion (Horizontal 1)
- Figure 2.6-45 Response of 30 Profiles to 2500-Yr Input Motion (Horizontal 2)
- Figure 2.6-46 Strain-Iterated Shear Modulus Versus Depth
- Figure 2.6-47 Strain-Iterated Damping Ratio Versus Depth
- Figure 2.6-48 Soil Property Degradation Models
- Figure 2.6-49 Horizontal Response Spectra of Strain-Iterated Profiles (Horizontal 1)
- Figure 2.6-50 Horizontal Response Spectra of Strain-Iterated Profiles (Horizontal 2)
- Figure 2.6-51 Comparison of Mean Response Spectra (2500-Yr Input Horizontal 1)
- Figure 2.6-52 Comparison of Mean Response Spectra (2500-Yr Input Horizontal 2)
- Figure 2.6-53 Ground Acceleration Time-Histories (mean minus one standard deviation)
- Figure 2.6-54 Ground Acceleration Time-Histories (mean profile)
- Figure 2.6-55 Ground Acceleration Time-Histories (mean plus one standard deviation)
- Figure 2.6-56 Vertical to Horizontal Spectra Ratio
- Figure 2.6-57 Vertical Ground Response Spectrum (mean minus one standard deviation)
- Figure 2.6-58 Vertical Ground Response Spectrum (mean)
- Figure 2.6-59 Vertical Ground Response Spectrum (mean plus one standard deviation)
- Figure 2.6-60 INEEL Volcanic Rift Zones, Axial Volcanic Zones, and Fissures
- Figure 2.6-61 Stress Field and Displacement & Volcanic Rift Zone Structures
- Figure 2.6-62 Map of Volcanic Vents and Volcanic Zones with Estimated Recurrence Intervals

2.0 SITE CHARACTERISTICS

This chapter discusses geography, demography, meteorology, hydrology, seismology, geology, and volcanism as they relate to the Idaho Spent Fuel (ISF) Facility, which is adjacent to the Idaho Nuclear Technology and Engineering Center (INTEC), and is part of the Idaho National Engineering and Environmental Laboratory (INEEL). The geographical location of the ISF Facility, INTEC, and INEEL, the population distribution within and around the INEEL, land and water use, and associated site activities are also discussed.

The discussion of the site characteristics is intended to:

- Identify external natural and man-made phenomena for inclusion in the design basis.
- Characterize local land and water use and population such that individuals likely to be affected are identified.
- Characterize the transport processes that could move released contamination from the site to individuals/populations.

The information presented in this chapter that relates to the Idaho intermountain region, INEEL and INTEC is the same information that was presented for the licensing of the *TMI-2 Independent Spent Fuel Storage Installation (ISFSI) Safety Analysis Report* (hereafter referred to as the TMI-2 ISFSI SAR) (Ref. 2-1).

2.1 GEOGRAPHY AND DEMOGRAPHY OF SITE SELECTED

The following sections contain information concerning the site geography, population, access transportation routes, and land usage.

2.1.1 Site Location

The ISF site is adjacent to the INTEC, on the INEEL. The INEEL is one of nine multi-program laboratories in the U.S. Department of Energy (DOE) complex. The INEEL area measures approximately 60.3 kilometers (37 miles) north to south and about 56 kilometers (34.8 miles) east to west and encompasses 2300 square kilometers (890 square miles). It is in Idaho at the southeast foot of the Lost River, Lemhi, and Beaverhead Mountain ranges of the northwest edge of the Snake River Plain, Idaho. Figure 2.1-1 depicts the location of the INEEL in relation to Idaho and adjacent states, and Figure 2.1-2 shows the location of the INEEL relative to surrounding counties. Most of the INEEL is within Butte County, but portions are also within Bingham, Bonneville, Jefferson, and Clark counties. The ISF site and INTEC are totally within Butte County.

The ISF site is at 43°-34'-05" north latitude, 112°-55'-41" west longitude. The Universal Transverse Mercator coordinates of the ISF site are 344,293 meters east by 4,825,722 meters north. The ISF site is approximately 7.80 acres, as shown on Butte County, Idaho, Section 19 map (T 3 N., R 30 E., B.M.), with the northeast corner located at State Plain Coordinates N 694362.62, E 454717.32. The ISF site property is owned by the DOE and is leased to Foster Wheeler Environmental Corporation (FWENC).

Four major all-weather highways serve the INEEL. The Union Pacific Railroad crosses the southwest corner of the INEEL, and a spur line provides interchange for facilities on the INEEL. Idaho Power Company and Utah Power and Light Company transmission lines supply electrical power to the INEEL. The locations of the highways, railroad tracks, and facilities are shown in Figure 2.1-3. The TMI-2 ISFSI SAR has confirmed that no oil or gas pipelines pass through the INEEL (Ref. 2-1), which would include the ISF Facility site.

The ISF site is adjacent to the INTEC. An aerial photograph of the INTEC and the ISF site is included as Figure 2.1-4, and a site plan showing the location of the INTEC and the ISF site is provided in Figure 2.1-5. A topographical map of the INTEC area is shown in Figure 2.1-6.

2.1.2 Site Description

The INEEL, where the ISF Facility is located, was designated as an exclusion area to build, test, and operate various nuclear reactors and associated facilities. The isolated location was chosen to ensure maximum public safety. The INEEL has no residents. Ingress and egress of site personnel and visiting personnel on official business is strictly controlled. No casual visits are permitted, except for persons driving through the INEEL on the public highways (Figure 2.1-7) and visitors to the Experimental Breeder Reactor I (EBR-I) National Historical Monument, which is open to the public during the summer. The only recreational activities allowed within the INEEL are limited hunting and limited grazing, subject to special requirements (see Section 2.1.4).

The INEEL is in a broad, mostly flat plain averaging 1483 meters (4865 feet) above mean sea level. The Big Lost River runs through the INEEL, close to the northwest corner of the INTEC, approximately 1215 meters (3986 feet) from the ISF site. This section of the river is a runoff channel from the mountains to the northwest. Water flows intermittently during the spring and winter, infiltrating through the basaltic lava rock underlying the INEEL into a huge natural underground reservoir, the Snake River Plain Aquifer, which lies about 137 meters (450 feet) below ground surface. Surface water entering the INEEL sinks below ground surface within the INEEL boundary (Figure 2.1-8).

Figure 2.1-9 indicates the distance from the ISF site to the closest INEEL boundary. The shortest distance from the ISF site to the INEEL boundary is 13.7 kilometers (8.5 miles) to the south. The ISF site is on the INEEL and is remote from major population centers, waterways, and interstate transportation routes. Figure 2.1-5 shows the orientation of the ISF site relative to the adjacent INTEC site.

The typical workforce at INEEL facilities is shown in Table 2.1-1. As of August 2000, there were approximately 4965 employees at the INEEL. These employees live in more than 30 communities adjacent to the INEEL; the largest percentage lives in Idaho Falls. The DOE operates a bus service for INEEL employees from the major communities to the INEEL. The portions of INEEL boundary nearest to adjacent communities are 47 kilometers (29 miles) west of Idaho Falls, 51 kilometers (32 miles) northwest of Blackfoot, 80 kilometers (50 miles) northwest of Pocatello, and 11 kilometers (7 miles) east of Arco.

DOE security forces control access to the INEEL, and may stop traffic and conduct vehicle searches on the INEEL. The Federal Aviation Administration discourages air traffic below approximately 1829 meters (6000 feet). Five commercial airports are within approximately 161 kilometers (100 miles) of the ISF Facility site: 1) 97 kilometers (60 miles) southeast, in Pocatello; 2) 68 kilometers (42 miles) east, in

Idaho Falls; 3) 145 kilometers (90 miles) southwest, in Twin Falls; 4) 97 kilometers (60 miles) west, near Hailey; and 5) 168 kilometers (105 miles) east-northeast, near Jackson, Wyoming. Several smaller gravel-surface landing strips near the INEEL are used primarily for charter flights and crop dusting aircraft. The closest of these is at Atomic City, approximately 18 kilometers (11 miles) southeast of the ISF site.

The principal surface materials at the INEEL are basalt, alluvium, lake bed or lacustrine sediments, slope wash sediments and talus, silicic volcanic rocks, and sedimentary rocks. The natural plant life consists mainly of sagebrush and various grasses (Figure 2.1-10). The vegetation of the INEEL is limited by soil type, meager rainfall, and extended drought periods. A few deciduous trees, principally along the Big Lost River, exist on the INEEL. The most prominent ground cover is a mixture of vegetation consisting of sagebrush (*Artemisia tridentata*) and a variety of grasses (Figure 2.1-10).

The soil at the ISF site is previously disturbed sandy gravel. The flat terrain precludes erosion. The entire INTEC area is kept free from vegetation so there is no fuel for a range fire to the west of the ISF site. Limited undergrowth range fires could approach the site from the east and south. The quantity of fuel for such fires is limited. Such range fires will be addressed by INEEL fire suppression equipment, if necessary.

2.1.2.1 Other Activities Within the ISF Site Boundary

The controlled area boundary for the ISF site, as it was with the TMI-2 ISFSI, is the boundary of the INEEL. The ISF site is surrounded by its own security fence. Many activities occur within the INEEL, but only those activities in the adjacent INTEC could have an impact on the ISF Facility.

Figure 2.1-5 shows the area inside the INTEC boundary. Nuclear fuels are stored and waste from previous fuel processing activities is managed and treated in the INTEC restricted area.

The activities within the ISF site security fence are those related to the administration, operation, or maintenance of the ISF Facility (see Figure 2.1-11).

2.1.2.2 Boundaries for Establishing Effluent Release Limits

The INEEL boundary (property boundary lines), shown in Figure 2.1-3, establishes the controlled area boundary as defined in 10 CFR Part 72 (Ref. 2-2), to protect the public from exposure to airborne radioactivity. Figure 2.1-9 shows the relative position of the ISF site within the controlled area boundary. For more information on radioactivity, see Section 2.2.

Access to the central portion of the INEEL and the ISF Facility is controlled by DOE-contracted security forces, who may, during emergency situations, interrupt traffic on the public highways that cross the INEEL.

2.1.3 Population Distribution and Trends

Population in the region within 80 kilometers (50 miles) was determined to be approximately 128,000 in 2000, based on year 2000 Census data. The average annual growth rate is projected to be 0.8 percent (rate of growth between 1990 and 2000). Therefore, population within the 50-mile radius of the ISF site during the life of the ISF Facility is expected to be approximately 129,000 in 2010, 130,000 in 2020, 131,000 in 2030, and 136,500 in 2035. Figure 2.1-12 shows population density for the 80-kilometer (50-mile) radius

around the ISF Facility. The 80-kilometer (50-mile) radius figure is provided instead of an 8-kilometer (5-mile) radius because there are no residents within 8 kilometers (5 miles). Also shown are the relative locations of the major towns.

For exposure planning purposes, the maximally exposed individual is considered to be at Frenchman's Cabin, at the southern boundary of the INEEL (11 miles from the ISF site). The selection is consistent with other INEEL nuclear facilities.

The nearest populated area to the INEEL is Atomic City, population about 25, approximately 1.6 kilometers (1 mile) from the southern INEEL boundary and about 18 kilometers (11 miles) from the ISF site.

There are no permanent residents, cities, or towns within a 16-kilometer (10-mile) radius of the ISF site. However, several INEEL facilities, such as the Central Facilities Area (CFA), INTEC, Test Reactor Area (TRA), and Radioactive Waste Management Complex (RWMC) and the EBR-I are within 16 kilometers (10 miles) of the ISF site. Because institutional control will restrict access to INEEL lands (Ref. 2-3), population within 16 kilometers (10 miles) of the ISF site is unlikely to change through 2035.

Variations in population are caused by the daily influx of the INEEL workforce. About 2,800 workers are employed within 16 kilometers (10 miles) of the ISF Facility. Highways 20 and 26 pass through the site within 16 kilometers (10 miles) of ISF site. Traffic on these highways, other than the daily site traffic, is related to travel between cities surrounding the INEEL and the many recreational opportunities in the area.

Construction, operation, and decommissioning of the ISF Facility will have a negligible impact on the population of the region.

2.1.4 Uses of Nearby Land and Waters

Categories of land use at the INEEL include facility operations, grazing, general open space, and infrastructure such as roads. Facility operations include industrial and support operations associated with energy research and waste management activities. Land is also used for recreation and environmental research associated with the designation of the INEEL as a National Environmental Research Park. Much of the INEEL is open space not designated for specific uses. Some of this space serves as a buffer zone between INEEL facilities and other land uses. Because about 2 percent (4600 hectares or 11,400 acres) of the total INEEL is used for facilities and operations, it is designated as "rural" for dispersion purposes. Approximately 6 percent of the INEEL, 13,870 hectares (34,260 acres), is devoted to public roads and utility rights-of-way that cross the INEEL. Recreational uses include public tours of general facility areas and EBR-I, and hunting, which is generally restricted to within 0.8 kilometer (0.5 mile) of the INEEL boundary.

Between 121,000 and 142,000 hectares (300,000 and 350,000 acres) are used for cattle and sheep grazing. A 400-hectare (900-acre) portion of this land, at the junction of Idaho State Highways 28 and 33, is used by the U.S. Sheep Experiment Station as a winter feed lot for approximately 6500 sheep. Grazing is not allowed within 3 kilometers (2 miles) of any INEEL nuclear facility, and, to avoid the possibility of milk contamination by long-lived radionuclides, dairy cattle are not permitted. Rights-of-way and grazing permits are granted and administered by the U. S. Department of the Interior Bureau of Land

Management (BLM). Selected land uses at the INEEL and the surrounding region are presented on Figure 2.1-13.

Small communities and towns near the INEEL boundaries include Mud Lake to the east; Arco, Butte City, and Howe to the west; and Atomic City to the south. The larger communities of Idaho Falls/Ammon, Rexburg, Blackfoot, and Pocatello/Chubbuck are east and southeast of the INEEL. The Fort Hall Indian Reservation is southeast of the INEEL.

Recreation and tourist attractions surrounding the INEEL include Craters of the Moon National Monument, Hell's Half Acre Wilderness Study Area; Black Canyon Wilderness Study Area; Camas National Wildlife Refuge; Market Lake State Wildlife Management Area; North Lake State Wildlife Management Area; Yellowstone National Park; Targhee; Caribou-Targhee; Salmon-Challis National Forests; Sawtooth National Recreation Area; Sawtooth Wilderness Area; Sawtooth National Forest; Grand Teton National Park; Jackson Hole recreation complex; and the Snake River (see Figure 2.1-7).

County plans and policies encourage development adjacent to already developed areas to minimize infrastructure extensions and urban sprawl. Because the INEEL is remote from most developed areas, INEEL lands and adjacent areas are not likely to experience residential and commercial development. However, recreational and agricultural uses are expected to increase in the surrounding area in response to greater demand for recreational areas and the conversion of range land to crop land (Ref. 2-4).

The four most prominent tourist/recreation areas in the INEEL area are Yellowstone National Park, approximately 117 kilometers (72 miles) northeast of the INEEL and 160 kilometers (99 miles) from the INTEC; EBR-I, on the INEEL; Craters of the Moon National Monument, approximately 30 kilometers (19 miles) southeast of the INEEL; and the resort areas of Ketchum and Sun Valley, approximately 96 kilometers (59 miles) west of the INEEL and 115 kilometers (72 miles) from the ISF site.

THIS PAGE INTENTIONALLY LEFT BLANK.

2.2 NEARBY INDUSTRIAL, TRANSPORTATION, AND MILITARY FACILITIES

There are no industrial or military facilities within 5 miles of the ISF Facility site. The closest industrial complex to the ISF Facility is in Idaho Falls, approximately 68 kilometers (42 miles) away. The U.S. Navy maintains the only military facility on the INEEL at the Naval Reactor Facilities (NRF) area (Figure 2.2-1), located over 8 kilometers (5 miles) away from the ISF site. NRF's operations support of the U.S. Navy's nuclear-powered fleet through receipt of naval spent fuel for examination and storage preparation and through research and development of materials and equipment.

Nuclear facilities within 8 kilometers (5 miles) of the ISF Facility have been evaluated in accordance with Nuclear Regulatory Commission (NRC) guidelines; CFA, TRA, and Power Burst Facility/Waste Experimental Reduction Facility (PBF/WERF) are within 8 kilometers (5 miles). Activities at these facilities are subject to periodic reviews to ensure worker and public safety. Potential accidents at these facilities are considered in the development of the INEEL emergency management plans.

The ISF Facility is adjacent to the INTEC. The primary missions of the INTEC are to:

- Safely store spent nuclear fuel and prepare it for shipment to an offsite repository.
- Develop technology to safely treat high-level and liquid radioactive waste that resulted from reprocessing spent fuel.
- Remediate past environmental releases.

The primary facilities at INTEC include:

- The Fluorinel Dissolution Process and Fuel Storage Facility (FAST), which is divided into two parts, a spent fuel storage area and the Fluorinel Dissolution Facility.
- The Remote Analytical Laboratory, which is a state-of-the-art facility for remote examination of hazardous and radioactive materials.
- The Fuel Storage Building, which houses three storage pools for spent nuclear fuel.
- The TMI-2 ISFSI, which is a new NRC-licensed dry storage area for spent fuel and debris from the Three-Mile Island accident.
- The High-Level Waste Tank Farm, which includes 11 underground stainless steel storage tanks used to store the radioactive liquid waste generated during the reprocessing of spent fuel and plant decontamination work.
- The New Waste Calcining Facility, which converted liquid high-level radioactive waste from the Tank Farm into a granular solid similar in consistency to sand.
- The INTEC-601/602 Processing Corridors, which were used to chemically separate high enriched uranium (HEU) from dissolved spent fuel during reprocessing and to solidify the recovered HEU for shipment off site.

Because of the distance between the ISF Facility and other INEEL facilities, airborne contamination is the primary potential consequence of an emergency condition at one of the nearby nuclear facilities. The Warning Communications Center at DOE-Idaho Operations Office (DOE-ID) headquarters maintains

continuous site-wide surveillance of all INEEL facilities and transmits warning signals for any unsafe conditions. On receipt of a warning signal, the INEEL Emergency Plan goes into effect, and the appropriate emergency procedures are activated.

Accidents in the nearby nuclear facilities have been evaluated in the facility-specific Safety Analysis Reports. The facilities are built to withstand their design accidents, so the only impact on the ISF Facility from an accident in a nearby facility would likely be airborne contamination. The ISF site would be decontaminated as part of the general recovery from the accident.

Within the nearby INTEC, support operations include maintenance, laboratory operations, security, medical, and others which require the following materials to be handled or stored:

- small amounts of hazardous materials
- temporary waste storage
- satellite fuel storage (propane, gasoline, diesel, etc.)
- small amounts of maintenance materials (solvents, paints, etc.)

As stated in the TMI-2 ISFSI SAR, none of these materials present a hazard to the adjacent buildings within INTEC (Ref. 2-1). Because the ISF Facility is adjacent to INTEC, the same conclusion can be made.

There are no natural gas pipelines, mines or stone quarries, oil or gasoline plants, or other activities in adjacent facilities, from which a fire or explosion could damage the ISF Facility (Ref. 2-1).

The area adjacent to the other INEEL facilities is kept clear of vegetation, therefore, the threat of range or brush fires to these facilities is mitigated.

Aircraft crashes, both commercial flights and helicopter security operations, at the INTEC have been analyzed (Ref. 2-5). These crashes have a frequency of occurrence near the incredible hypothetical range. Crashes into individual INTEC facilities are incredible (less than 9.6×10^{-7} per year). INEEL security has discontinued the routine use of helicopters.

There are no structures tall enough that, if they collapsed, could damage the ISF Facility.

Transportation Routes and Facilities. Public transportation routes nearest the ISF site include U.S. Highways 20/26, which pass approximately 6 kilometers (4 miles) south of the ISF site, and the Mackay Branch of the Union Pacific Railroad, which passes 11 kilometers (7 miles) south of the ISF site (see Figure 2.1-7).

Other roads near the ISF site are the controlled-access roads between INEEL facilities. The nearest road to the ISF site is the East Perimeter Road, which is the western boundary of the ISF site. A railroad spur from the Mackay Branch (which also services only the INEEL) passes within approximately 120 meters (394 feet) west of the ISF Facility. Hazardous materials, including spent nuclear fuels, radioactive waste, and chemicals are transported on these routes. Accidents along these transportation routes are discussed in Chapter 8, *Accident Analysis*.

2.3 METEOROLOGY

2.3.1 Regional Climatology

2.3.1.1 Data Sources

The climatology of the INEEL is well characterized. Research-grade meteorological observations have been continuously taken by the National Oceanic and Atmospheric Administration (NOAA) and its predecessor agencies since 1949. These data have been summarized in *Climatology of the Idaho National Engineering Laboratory, 2nd Edition* (Ref. 2-6).

Idaho Falls 46W, a NOAA meteorological observation station, and a well equipped research tower (Grid 3), are located near the CFA, approximately 3.2 kilometers (2 miles) south of the ISF site.

2.3.1.2 General Climate

2.3.1.2.1 Terrain Influences on Regional Climate

The INEEL is situated on a mile-high area of the Eastern Snake River Plain in southeastern Idaho. Air masses entering the Eastern Snake River Plain, from the west, first cross a mountain barrier, precipitating a large percentage of their moisture. Annual rainfall at the INEEL is light and the region has semi-arid characteristics.

The local northeast-southwest orientation of the Eastern Snake River Plain and bordering mountain ranges channels the prevailing west winds so that a southwest wind predominates over the INEEL. The second most frequent winds come from the northeast. The relatively dry air and infrequent low clouds permit intense solar heating of the surface during the day and rapid radiational cooling at night, so there is a large diurnal range of temperature near the ground.

Because of the moderating influence of the Pacific Ocean, most air masses flowing over this area are warmer during winter and cooler during summer than air masses at similar latitude in the continental climate east of the Continental Divide. The Centennial and Bitterroot mountain ranges keep most of the shallow but intensely cold winter air masses moving south from Canada from entering the Eastern Snake River Plain. Occasionally, the cold air spills over the mountains, and is held in the Eastern Snake River Plain and the INEEL experiences low temperatures for periods lasting a week or longer.

A simplified topographical map of the INEEL area and the Eastern Snake River Plain is presented in Figure 2.3-1 (Ref. 2-6). The height values of the contour lines are given in hundreds of feet above mean sea level. Stipples indicate the area of the plain below 5000 feet. The large dots indicate the location of tower-mounted wind sensors.

Winds at the INEEL are influenced by:

- northwesterly, down-canyon winds that develop in the Little Lost River and Birch Creek Valleys and spill out onto the Eastern Snake River Plain to the southeast
- southwesterly winds that result from redirection of the westerly winds aloft by the mountains bordering the Eastern Snake River Plain

- northerly or northeasterly winds that result from air cooling and descending from the elevated terrain north of INEEL
- reversals in wind directions that occur when shallow surface winds, resulting from surface cooling and density differences, are overcome by winds aloft moving in an opposite direction
- stagnation in areas where light winds converge
- large horizontal eddies that form as a result of convergence, mountain effects, or passing pressure systems associated with larger thermal and moisture fields

These influences combine to result in regional-scale wind trajectories, which rarely maintain their initial direction for long distances or persist for more than a few hours. The impact of this variability on atmospheric transport and dispersion at INEEL is discussed in Section 2.3.4.

2.3.1.2.2 Regional Temperature

The maximum and minimum "normal" temperatures for the ISF Facility were determined using the methodology of NUREG 1536, Section 2.0.V.2.b.1. This methodology uses the highest and lowest ambient temperatures recorded in each year, averaged over the years of record. Input data covered the years 1952 through July 2000, obtained from a nearby NOAA monitoring station.

Table 2.3-1 reflects the averages of the highest and lowest annual average temperatures between 1952 and August 2000 at the NOAA Idaho Falls 46W station. The INEEL maximum and minimum normal temperatures are 98°F and -26°F, respectively.

The smallest daily air temperature range occurs in the winter, while the largest daily air temperature range occurs in the summer. This phenomena is reflected on Table 2.3-2. July and August have mean daily air temperature ranges of 38°F, while December and January have mean daily air temperature ranges of 23°F. Table 2.3-2 also shows that the largest daily air temperature range was 59°F in August and October.

2.3.1.2.3 Freeze-Thaw Cycles

An indication of the amount of weathering to certain materials is the frequency of occurrence of daily freeze-thaw cycles. A freeze/thaw cycle is defined as a day on which the maximum air temperature exceeds 32°F and the minimum air temperature falls to or below 32°F. These data are based on the air temperature at 5 feet in an instrument shelter, which, because of its distance from the ground, may underestimate the actual number of freeze-thaw cycles. Despite this limitation, the data presented in Table 2.3-3 indicate the general frequency and seasonal variation (Ref. 2-6).

The greatest number of cycles occur, as expected, in the spring and fall seasons. On average, 42 percent of the days in the year contain a freeze/thaw cycle.

2.3.1.2.4 Degree Days

A degree-day is another unit of measure based on a specific air temperature. The degree-day concept can be applied to either heating or cooling and is used as a basis for establishing heating and cooling energy requirements and building design considerations. A single heating degree-day is accumulated for each

degree the average daily air temperature is less than 65°F for one day. Conversely, a single cooling degree day is accumulated for each degree the average daily air temperature is greater than 65°F.

The daily trends are evident in Table 2.3-4. January has the highest mean degree-day total of 1517 and July has the lowest total of 29. Monthly heating degree day totals as large as 1726 (December) have been recorded. Table 2.3-4 also shows that the highest single heating degree-day has been 93. On average, locations on the INEEL can be expected to record approximately 8700 degree-days annually.

A historical monthly summary of the cooling degree-days is presented in Table 2.3-5. Cooling is usually not required except during the months of June, July, and August. On average, an annual total of 247 cooling degree-days accumulates at the INEEL (Ref. 2-6).

2.3.1.2.5 Subsoil Temperatures

During a 7-year study sponsored by the DOE, soil temperatures were recorded at the INEEL from thermometer probes placed at 1-foot intervals from depths of 2 through 7 feet beneath a sandy surface, representing the natural terrain with the overlying vegetation removed. Similar measurements were also made under an asphalt road surface. The temperatures at all six levels have been averaged for each month. Isotherms with depth are presented in Figure 2.3-2 and Figure 2.3-3 for both types of surfaces. These figures show a significant difference between the two locations. Under the asphalt, temperatures average approximately 10°F higher in the summer near the surface; in the winter, colder temperatures occur over a longer period and to a greater depth.

2.3.1.2.6 Regional Precipitation

Table 2.3-6 (Ref. 2-6) summarizes the historical average monthly and annual precipitation. The average annual precipitation is 8.72 inches. Maximum observed 24-hour precipitation amounts to less than 2 inches (Table 2.3-7).

About 27 inches of snow falls each year. The maximum yearly total is 59.7 inches, and the smallest total is 6.8 inches. The greatest 24-hour snowfall was 8.6 inches. The ground is usually free of snow from mid-April to mid-November. Table 2.3-8 presents historical snowfall amounts at the CFA (Ref. 2-6).

2.3.1.2.7 Regional Atmospheric Moisture

Table 2.3-9 presents historical monthly averages of wet bulb and dew point temperatures expected at the INEEL site (Ref. 2-6). The moisture content of the air is described by the wet bulb and dew point temperatures. During January (the coldest month) the air temperature averages 16.5°F and the dew point averages 7.4°F. During July the air temperature averages 69°F and the dew point averages 33.5°F. The highest relative humidity is observed in the winter, and the lowest relative humidity is observed in the summer.

2.3.1.2.8 Regional Winds

Historical monthly average wind speeds at the 20 and 250-foot levels are reflected in Table 2.3-10. The months with the highest average wind speed at the 20-foot level are April and May, with a wind speed of 9.3 mph. The month with the lowest average wind speed at the 20-foot level is December, with a wind speed of 5.1 mph.

The wind directions for all the highest hourly speeds listed on Table 2.3-10 are from the west-southwest and the southwest.

Some months show a difference in direction between levels. These differences are attributed to different artifact periods of record.

The maximum instantaneous gust recorded at the CFA 20-foot level was 78 mph from the west-southwest, and 84 mph from the southwest at 250-foot level (see Table 2.3-14).

2.3.1.2.9 Sky Cover

The average daily opaque sky cover for the INEEL is estimated to be as high as seven-tenths in December and as low as three-tenths in July, August, and September. The annual average sky cover is five-tenths (Ref. 2-6).

2.3.1.2.10 Atmospheric Pressure

Measurements of atmospheric pressure are important to many phases of design and operations at the INEEL. Station pressure (actual measured pressure without reduction to sea level), has been recorded continuously at the CFA since February 1950. The station pressure recorded from February 1950 to August 1964 is summarized in Table 2.3-11. The CFA station mercurial barometer standard is at 4937 feet mean sea level. The ISF site is at approximately 4940 feet; therefore, CFA data may be applied to the ISF site (Ref. 2-6).

The average station pressure of 25.06 inches-mercury (in.-Hg) and the highest and lowest recorded pressures of 25.14 in.-Hg and 24.99 in.-Hg, respectively, over the period of record, indicate extremes of station pressure at 24 and 26 in.-Hg. The difference between the highest and lowest pressures recorded in any month over the period of record reflects the development of more intense pressure systems in winter, and weaker systems in summer months. The annual mean daily pressure range is 0.15 in.-Hg, varying from near 0.10 in.-Hg in the summer to 0.20 in.-Hg in the winter. The largest pressure change recorded in one day was 0.680 in.-Hg. Although specific records of the maximum pressure change in 1-hour and a 24-hour period have not been recorded at the INEEL, synoptic and climatological records indicate maximum changes would be bounded by 0.1 in.-Hg per hour and 1 in.-Hg per day.

2.3.1.2.11 Air Density

The average air density at the INEEL is related to pressure. It is computed from the Equation of State using average values of temperature, pressure, and moisture. For sea level, using a standard pressure of 29 in.-Hg and 32°F, a standard density of $1.29 \times 10^{-3} \text{ g/cm}^3$ can be computed.

A normal average temperature of 42.4°F and an average station pressure of 25 in.-Hg gives an average density of $1.06 \times 10^{-3} \text{ g/cm}^3$ for the INEEL (Ref. 2-6).

2.3.1.2.12 Other Phenomena

According to historical INEEL onsite measurement programs, dust concentrations varied from a low of 14.1 micrograms per cubic meter ($\mu\text{g/m}^3$) over a total snow cover to a high of 772 $\mu\text{g/m}^3$ during the summer. In an undisturbed area, even with dust devils present, a concentration of only 151 $\mu\text{g/m}^3$ was

recorded. Annual geometric means of 24-hour particulate samples were approximately $30 \mu\text{g}/\text{m}^3$ (Ref. 2-6).

In relatively undisturbed areas of the INEEL, median dust-particle sizes ranged from 0.330 to 0.425 microns. Less than 1 percent of the ambient particulate is larger than 10 microns, although a few particles reach several hundred microns. Petrographic examinations of dust particles classify the dust as moderately abrasive. Vehicular traffic and activities in construction areas (disturbed areas) contribute more to local high dust concentrations than do strong winds over undisturbed areas.

The Idaho Department of Environmental Quality has analyzed typical dust concentrations in various airsheds within the state and has established estimated background values for pollutants having National Ambient Air Quality Standards (see Table 2.3-12). The U.S. Environmental Protection Agency (EPA) has determined that INEEL air quality is in attainment of applicable National Ambient Air Quality Standards by a wide margin (Ref. 2-7). Existing INEEL air quality poses no potential constraints to ISF site development.

2.3.1.3 Severe Weather

2.3.1.3.1 Maximum and Minimum Temperatures

Historical extremes of daily maximum and minimum daily air temperatures are listed in Table 2.3-13. The maximum difference between the highest and lowest temperatures recorded during a given month was 102°F in December. The largest differences between extremes of monthly daily average temperatures occur in the winter and the smallest differences are between the averages of the summer months (Ref. 2-6).

2.3.1.3.2 Extreme Winds

High wind-speed episodes occur throughout the year, with the highest hourly average winds occurring during winter and spring. At the INEEL, the passage of synoptic frontal systems involves higher and more sustained hourly wind-speed events than those of thunderstorm gust fronts. Downslope winds occasionally cause damage at canyon-mouth locations in the eastern Rocky Mountains. These winds are rare on the Eastern Snake River Plain because the terrain is unfavorable.

The peak wind-speed gusts anticipated at the ISF site at both upper (250 feet) and lower (20 feet) levels are listed by month in Table 2.3-14. Values presented in this table are based on the highest period of record values occurring at CFA. These values will be relevant to maximums occurring over the flat terrain anywhere on the INEEL. Strong gusts may be a result of pressure gradients from large-scale systems, or be a result of a thunderstorm. Because thunderstorms may form at any location and move in any direction, strong gusts can be expected from any direction.

2.3.1.3.3 Tornadoes

A tornado is a violent local vortex in the atmosphere. It is usually accompanied by a funnel-shaped cloud with spiraling winds of high velocity. Tornadoes usually occur in association with thunderstorms, especially those that produce hail. When a vortex cloud reaches the land surface, it is classified as a tornado. If the vortex cloud does not reach the ground surface, it is classified as a funnel cloud.

Most tornadoes in the U.S. occur east of the Rocky Mountains. The total number of tornadoes in Idaho reported to the National Severe Storms Forecast Center (1987) for the years 1950 through 1986 was 58 (Ref. 2-6).

National tornado statistics have been compiled which, when taken with maximum atmospheric moisture content, surrounding geography, and other statistics, allow a realistic assessment of tornado risk. These tornado statistics establish a value for the maximum credible tornado expected at the INEEL. For 1950 to 1994, NOAA records indicate that a total of five funnel clouds have been sighted within the INEEL (Ref. 2-6).

NUREG/CR-4461, *Tornado Climatology of the Contiguous United States*, identifies that the average probability of any tornado occurring in the region that includes the INEEL is $6 \times 10^{-7} \text{ yr}^{-1}$ (return period of 1.66×10^6 years). The probability of a category F-2 (113 mph wind speed) or greater is $1.69 \times 10^{-7} \text{ yr}^{-1}$ (5.91×10^6 year return period). The maximum wind speed with a probability of occurrence of 1×10^{-7} is 171 mph.

The design basis for the ISF site tornado is established by Reg. Guide 1.76, as modified by SECY-93-087 for Tornado Intensity Region III, which is bounding for any tornado expected on the INEEL (Ref. 2-8). The ISF Facility design basis tornado is presented in Table 2.3-15.

2.3.1.3.4 Dust Devils

Although tornadoes are rare at the INEEL, less violent "dust devils" are common in the summer months. Dust devils are small atmospheric vortices that are generated over hot land surfaces. These dust devils pick up dust and pebbles and can overturn, blow down, or carry off unsecured objects. They usually occur on warm sunny days with little or no wind. The dust cloud may be several hundred yards in diameter and extend several hundred feet in the air (Ref. 2-6).

2.3.1.3.5 Hurricanes and Tropical Storms

Because of the moderating influence of the Pacific Ocean and the isolating influence of surrounding mountains, neither hurricanes nor tropical storms occur at the INEEL.

2.3.1.3.6 Precipitation Extremes – Recorded Hourly and Daily Precipitation Events

For precipitation extremes, the highest INEEL value (regardless of location) is cited. The greatest monthly amounts recorded during 1- and 24-hour periods are listed in Table 2.3-7. The high hourly amounts during May and June were the result of heavy thunderstorms. The maximum for 1 hour was 0.54 inches. Precipitation amounts greater than 1 inch per day have occurred during five of the calendar months within the period of record (Ref. 2-6).

2.3.1.3.7 Precipitation Extremes – Predicted Maximum Storm Events

Hershfield (Ref. 2-9) used the long-term precipitation records of more than 1600 stations to develop return periods for 24-hour storms (Table 2.3-16), and short-term records from about 5000 stations to define short return-period storms. From these results he constructed isopluvial maps for the continental United States for storms with return periods of 2 years and 100 years. He then interpolated isopleth maps for other storm durations and return periods. In 1996, Sagendorf analyzed data for all available Upper

SNAKE RIVER STATIONS (INCLUDING INEEL), INDEPENDENTLY VALIDATED THE HERSHFIELD DATA, AND TESTED A FUNCTION TO ADJUST 24-HOUR HERSHFIELD TOTALS TO INEEL STORMS OF SHORTER DURATIONS (REF. 2-10).

2.3.1.3.8 Precipitation Extremes – Precipitation Occurrence

In addition to amounts, frequency of occurrence, and duration of precipitation are frequently used for planning purposes. Table 2.3-17 lists the average number of days (from midnight to midnight) per month (percentage) during which specified amounts of precipitation fell at CFA (Ref. 2-6). These frequencies of occurrence apply to the ISF site.

2.3.1.3.9 Thunderstorms and Lightning

The National Weather Service defines a thunderstorm-day as a day on which thunder is heard at the observing station. Lightning may or may not be seen; rain and/or hail may or may not occur. By this definition, the INEEL may experience, on the average, two or three thunderstorm days each month from June through August. Several individual thunderstorms may occur on each thunderstorm day. Thunderstorms have occurred throughout the year but rarely occur from November to February period.

Surface effects from thunderstorms over the Eastern Snake River Plain are usually much less severe than those in the mountains surrounding the plain or east of the Rocky Mountains. At times, precipitation from the thunderstorm evaporates before reaching the ground so that little or no precipitation may be recorded. Even so, the storm may be accompanied by strong, gusty winds that may produce local dust storms. Cloud-to-ground lightning may occur. Occasionally, rain in excess of the long-period average monthly total may result from a single thunderstorm.

The BLM Interagency Fire Center (Boise) operates a lightning detection system by which the location and number of lightning strikes may be documented, in real time if necessary (Ref. 2-6). Although the INEEL is surveyed by the system, no historical statistics for the area have been compiled. The ISF Facility, including the site security fence and lighting system, will contain grounded lightning protection.

2.3.1.3.10 Snow Storms

Snowfall and snow depth records are available from CFA, the only manned weather station at the INEEL. CFA values are representative of snow conditions at the ISF site. Snowfall is defined as the amount of snow that falls within a given period regardless of the amount that accumulates on the ground. Because snow may melt as it falls, the snowfall amount must occasionally be estimated from the water equivalent of snow. Maximum and minimum totals vary considerably for the period of record (1950 to 1988), particularly in December with a difference of nearly 22 inches. The maximum snowfall in a 24-hour period was 8.6 inches in March (Ref. 2-6).

Table 2.3-18 lists the average number of days (percent) in a given month during which a specified amount of snowfall has been recorded (Ref. 2-6).

Table 2.3-19 lists the averages and the maximum monthly snow depths (Ref. 2-6). The maximum depth ever recorded was 22.3 inches. During periods when several inches of loose snow are present, along with moderate to strong surface winds, considerable blowing and drifting will occur, with drifts accumulating to several feet high.

2.3.1.3.11 Hail and Ice Storms

Although small hail frequently occurs with thunderstorms, damage from hail has not been experienced at the INEEL to date. Crop damage from hail is not unusual in nearby areas. Property damage caused by hail has occurred in Idaho Falls, so damage at the INEEL from hail is possible.

Although brief periods of glazing conditions occasionally accompany a transition from rain to snow and cause slippery sidewalks and roads, they produce insufficient accumulation to damage power or communication lines. Rime icing, which occurs when fog droplets accumulate on objects at temperatures below freezing, is more likely. During the period of record, accumulation on power lines and air intakes has not constrained INEEL operations.

Super-cooled fog or low stratus clouds occasionally occur in winter and may last for several consecutive days, given a snow cover and a persistent high-pressure system.

2.3.2 Local Climatology

2.3.2.1 Data Sources

A site-specific climatology report prepared in 1989 by NOAA contains the most applicable site-specific data for ISF site climatologic conditions (Ref. 2-6).

2.3.2.2 General Climate

The local climatology data for the ISF Facility site is represented in Section 2.3.1, *Regional Climatology*. The regional climatological data is representative of the local climatological data as it was obtained from meteorological observation stations within a 5-mile radius of the ISF Facility site.

2.3.2.3 Topography

Regional topography in the INEEL area is presented in Figure 2.3-4. A detailed topographical survey at 2-foot contour intervals for the 8-kilometer (5-mile) radius of the INTEC site, adjacent to the ISF site, was compiled from DOE drawings B50-001-ASC, plates 16, 17, 21, and 22. Topographic cross-sections were produced for each of 16 radii corresponding to the 16-point compass directions from the TMI-2 ISFSI site to the 8-kilometer (5-mile) and 80 kilometer (50-mile) limits. These cross sections, presented in Figure 2.3-5, Figure 2.3-6, Figure 2.3-7, Figure 2.3-8, Figure 2.3-9, Figure 2.3-10, Figure 2.3-11, and Figure 2.3-12 are representative of the ISF site regional topography because the ISF site is adjacent to the INTEC.

The 80 kilometer (50 mile) cross section is presented in lieu of the required 16-kilometer (10-mile) cross section, to provide a cross sectional representation that reflects the regional terrain. The 16-kilometer (10-mile) cross section would be similar to the 8-kilometer (5-mile) cross section.

The terrain features cause a subtle channeling of the diurnal low wind-speed flows, even over the valley floor where relative topographic relief is small. This influence can be seen under both daytime surface-heating and nocturnal surface-cooling conditions. Terrain surrounding the INEEL also is known to channel and redirect the upper level (global scale) winds and determine the character of their interaction

with the valley surface. Down-valley winds formed in the surrounding valleys and interaction of the mountains with nearby frontal systems are also significant causes of valley winds.

2.3.3 Onsite Meteorological Monitoring Program

2.3.3.1 Wind Roses

Grid 3, research-grade meteorological tower, is the wind station closest to the ISF site. Grid 3 is integrated with the INEEL emergency dose prediction system maintained by NOAA. With two levels of wind instrumentation (10 and 61 meters) and three levels of temperature instrumentation, it provides wind and temperature data for use in ISF site climatology. Grid 3 wind instrumentation spans the full height of the tower with continuous wind data reduced for climatological use.

Stability wind roses for Grid 3 at 10 meters and 61 meters are presented in Figure 2.3-13, Figure 2.3-14, Figure 2.3-15, and Figure 2.3-16 (Ref. 2-1). These sensor heights mirror atmospheric heights in which transport and dispersion from surface and elevated (stack) releases, respectively, may occur. Because they are above much of the friction layer, the winds at 61 meters (200 feet) are representative of release heights above that level.

2.3.3.2 Observations for Offsite Concentration Assessments

Wind data have been collected continuously since the 1950s at a large number of stations in the vicinity of the INEEL. During ISF Facility operations, weather data will continue to be obtained from Grid 3. Data may also be used from the 26 additional telemetry towers maintained by NOAA for use in near real-time offsite concentration assessments.

Figure 2.3-17 shows wind observation station locations within a 50-mile radius to the ISF site (Ref. 2-6). At each location, wind sensors are sited at the National Weather Service standard height of 10 meters (32 feet). Equipment specifications, maintenance standards, and data analysis procedures are established by DOE-ID and, as stated in the TMI-2 ISFSI SAR, conform to the requirements of NRC Regulatory Guide 1.23, National Weather Service protocols, and quality assurance requirements of EPA QAMS 005/80 (Refs. 2-7 and 2-11).

2.3.4 Diffusion Estimates

Dispersion modeling performed by NOAA, ARLFRD for INEEL sources was used in the TMI-2 ISFSI analysis as the basis for diffusion estimates. Because the ISF site is adjacent to the INTEC, where the TMI-2 ISFSI is located, the TMI-2 ISFSI dispersion model is applicable.

Total integrated concentrations for two different spatial scales were calculated by DOE for TMI-2 ISFSI using normalized emission rates and four different sets of meteorological data to simulate the release and dispersion of pollutants from the TMI-2 ISFSI site. Regional-scale modeling using a variable-trajectory Gaussian puff model (MESIDIF) was performed to determine the spatial and temporal variations in the normalized concentration patterns. A single sector-averaged Gaussian plume model (XOQDOQ) was used to compare regional and local impacts (Ref. 2-12).

2.3.4.1 Single Station Modeling – XOQDOQ

The NRC uses the computer program XOQDOQ in its independent meteorological evaluations of continuous and anticipated intermittent releases from commercial nuclear power reactors. The program implements the assumptions outlined in Section C (excluding Cla and Cib) of NRC Regulatory Guide 1.111 (Ref. 2-13). Annual relative effluent concentrations (X/Q) and annual average relative deposition, (D/Q) are calculated at user-specified locations, and at various standard radial distances and segments for downwind sectors. Possible intermittent (e.g., containment or purge) releases that occur during routine operation may also be evaluated using the program. Evaluation of intermittent releases provides both X/Q and D/Q values at various standard locations, as well as user-specified points of interest.

2.3.4.1.1 Model Operational Theory

The computer program XOQDOQ is based on the theory that radioactive material released to the atmosphere will have a normal (Gaussian) distribution about the plume centerline. In predicting effluent concentrations for longer time periods, the Gaussian distribution is assumed to be evenly distributed within the directional sector. A straight-line trajectory is assumed between the point of release and the receptors.

The plume rise equation used in XOQDOQ is taken from Briggs (Refs. 2-14 and 2-15). Plume rise is calculated as a function of stability. Effective plume height is then given as the sum of plume rise and the physical stack height.

For a specific receptor and source configuration, a long-term estimate of X is obtained by solving the dispersion equation for each meteorological condition assigned by the user, then summing the concentrations after weighting each by its frequency of occurrence.

The sum of the frequencies for each long-term analysis (e.g., seasonal or annual) should be near unity. A 1-hour occurrence of a particular meteorological condition will be included in an annual joint frequency distribution as $(1 \text{ hour/year}) / (8760 \text{ hours/year}) = 0.00011$, and in a seasonal (quarter annual) array as 0.00045.

The representative speeds usually assigned to the six climatological wind speed categories are 0.67, 2.45, 4.47, 6.93, 9.61, and 12.52 meters per second (0-3, 4-6, 7-10, 11-16, 17-21 and 21 knots per second). These ranges are user-specified.

The horizontal and vertical dispersion parameters (sigma y and sigma z) used in XOQDOQ are in the form of continuous functions of downwind distance and stability.

XOQDOQ allows specifications of sigma y and sigma z from measured curves obtained from actual field studies at INEEL. The main advantages of using this approach are: 1) the stability classification scheme may be used on easily obtained parameters, and 2) the relationships of sigma y and sigma z under low wind speed, inversion conditions are allowed to depart from a power law function, and thus make the results more realistic. This option was exercised in the computer analyses presented in this section. The curves are presented in Figure 2.3-18 and Figure 2.3-19. Model operational theory is described in Sagendorf, et al. (Ref. 2-12).

The six stability categories (S = 1 through 6 in order of increasing atmospheric stability, 4 being neutral) of the joint frequency distribution are defined on the basis of the criteria. The classification is based on ground-level meteorological observations only (surface wind speed, cloud cover, ceiling) supplemented by solar elevation data (latitude, time of day, and the time of year). Thus the stability estimates can be obtained for any site at which suitable observations have been made.

2.3.4.1.2 Modeling Assumptions and Input Data

For the TMI-2 ISFSI, at the INTEC site, four XOQDOQ runs were made to examine the relationship between local and regional effluent concentration patterns. Two spatial scales were used: 0 to 8 kilometers (0 to 5 miles) from the source and 0 to 80 kilometers (0 to 50 miles) from the source. The INTEC was examined for each scale. Meteorological conditions at INTEC were represented by the joint frequency distribution of 1982 wind and stability data from the telemetry station at the PBF as a "worst likely" situation. Because INTEC is adjacent to the ISF site, the conclusions for INTEC are applicable to the ISF site.

Several XOQDOQ options may be exercised when executing the program. Table 2.3-20 summarizes the options used in previous modeling for the INEEL (Ref. 2-16).

2.3.4.1.3 Results

Figure 2.3-20 and Figure 2.3-21 present annual normalized concentrations of effluents calculated by XOQDOQ (Ref. 2-16). Overall concentration patterns consist of bimodal distributions extending along the annual prevailing wind directions (approximately southwest and northeast).

Figure 2.3-20 presents the concentration isopleths out to an 80-kilometer (50-mile) radius due to normalized emissions from INTEC. The concentration pattern exhibits a strong southwest to northeast distribution with little buildup in the northwest-southeast direction, except for a small tertiary lobe toward the south-southeast.

Figure 2.3-21 presents the concentration isopleths out to a radius of 8 kilometers (5 miles) from the normalized emission source at INTEC. Again, there is a bimodal distribution with major axis from southwest to northeast. The case exhibits a slightly wider concentration distribution at the northern lobe. The tertiary lobe extending southeast is much less developed on this spatial scale. Note the maximum concentration area centered about 0.8 kilometer (0.5 mile) northeast of the source. This feature was not evident on the regional scale (80 kilometer [50 mile]) radius.

2.3.4.2 Gridded Windfield Modeling - MESODIF

2.3.4.2.1 MESODIF Model Description

MESODIF is a regional-scale variable-trajectory Gaussian puff model developed at NOAA's Air Resources Laboratory at the INEEL (Ref. 2-17). It takes into account the spatial and temporal variations in the advection, diffusion, transformation, and removal mechanisms governing plume dispersion. It differs from the conventional Gaussian plume approach in that MESODIF simulates the deformation of a continuous plume by a time-varying, vertically uniform horizontal wind field. MESODIF simulates a continuous point source by superpositioning discrete puffs of a circular, horizontal cross-section. Each puff is advected as an element with its time history, independent of preceding or succeeding puffs. The

dimensions of an individual puff are proportional to its travel distance (or travel time). A continuous plume is represented by the serial releasing of sufficient numbers of discrete puffs (finite plume segments). With suitable input parameters, MESODIF can reproduce the results of a conventional Gaussian plume model in the near field from a source. Since its initial formulation, MESODIF has been modified by others and offered by EPA as one of the Users Network of Applied Models for Air Pollution Version IV Series under the name MESOPUFF.

A continuous point source is often used to examine the effects of spatial and temporal variations of the low-altitude wind flows upon time-integrated concentration estimates. Because the transporting regional wind surrounding the INTEC exhibits curving, recirculating, and at times stagnating flows, a Gaussian simple continuous point source type of equation could not be used in MESODIF (because the resulting plume geometry would be inapplicable). Because the continuous point source equation is an integration of the more general Gaussian instantaneous point-source, this instantaneous point-source equation is the beginning point for MESODIF.

The sigma values used in MESODIF are the Pasquill A through F stratifications of values measured from continuous plume releases of 0.5-hour to 1-hour duration. The application of these rates to puff diffusion tends to slightly overestimate the dilution (underestimate the concentration) of puffs within the first few kilometers. The specifications of sigma values versus stability categories and trajectory distances primarily apply to distances of a few kilometers. These curves have been extrapolated to regional-scale distances in several INEEL field studies.

In application, the MESODIF model disperses plume effluent through the advective transport of puff centers and through the diffusion of effluent puffs about their individual centers. The transport of puffs is determined from a horizontal field of spatially and temporally varying winds.

For vertical dispersion, a capping stable layer or restricting lid to upward diffusion is considered. The height of the base of the capping lid or stable layer is denoted as "L." In MESODIF, L is specified each hour to account for known diurnal variability of the depth of mixing. An hourly value of L is applied uniformly throughout the computation area.

The source emission strength Q may be specified each hour if desired. For the INTEC site analysis, it has been held constant at one unit per hour; each puff then contains one unit divided among the number of puffs released per hour. Removal mechanisms such as dry deposition, precipitation scavenging, and chemical and photochemical changes are not incorporated. The two essential parts of the computation are: 1) the determination of the locations of the puffs as they are carried by the wind, and 2) the calculation of the growth and subsequent dilution of each puff. A third portion of the computation involves the determination of the contribution of the puffs to the time-integrated dosage on any array of grid points. The concentration is computed and accumulated for each grid point within the radius of influence of each puff.

2.3.4.2.2 MESODIF Modeling Assumptions and Input Data

For TMI-2 ISFSI, the DOE completed a series of MESODIF runs to examine the spatial and temporal variations that would occur in the normalized concentration patterns for various source locations and for different periods of meteorological data. INTEC was modeled using MESODIF, normalized emission rates, surface releases, and a meteorological data set for 1980, 1981, and 1982 (Ref. 2-16). Also, a long-

term average of 10 years of meteorological data has been used to produce annual long-term mean concentrations for 1974 through 1983). For the INTEC source location the 1974 through 1983, 1980, 1981, and 1982 data sets were used. Key input parameters for the MESODIF modeling are summarized in Table 2.3-21 (Ref. 2-16).

2.3.4.2.3 MESODIF Results

Figure 2.3-22, Figure 2.3-23, Figure 2.3-24, and Figure 2.3-25 present isopleths of annual normalized total integrated concentration calculated by MESODIF. Concentration patterns overall are quite similar for the meteorological years and emission source locations (Ref. 2-16). The figures show a bimodal distribution with lobes extending along the annual prevailing wind directions for this area (southwest and northeast) and a rapid decrease in concentration with distance.

Figure 2.3-22 presents concentration isopleths for normalized emissions from the TMI-2 ISFSI site with 1980 meteorological data. The concentration pattern exhibits all of the general characteristics identified above. In addition, there is evidence of a minor tertiary concentration lobe extending southeast.

Figure 2.3-23 presents concentration isopleths for normalized emissions from the TMI-2 ISFSI site with 1981 meteorological data. Again, concentration patterns are similar to 1980 with slightly less development in the tertiary lobe. Concentration isopleths due to normalized emissions from the TMI-2 ISFSI site, calculated using 1982 meteorological data, are presented in Figure 2.3-24. Concentration patterns are similar to the other 2 years but the magnitude of the concentrations appears somewhat lower in 1982. For 1982, the area enclosed by a line of given magnitude is generally smaller in 1982 than in 1980 or 1981, indicating low concentrations closer to the source in 1982 than in either 1980 or 1981.

Figure 2.3-25 presents the 10-year mean concentration isopleths for normalized TMI-2 ISFSI emissions calculated using the 1974 through 1983 meteorological data sets. These long-term mean isopleths exhibit all of the general characteristics shown by the isopleths for each individual year. The long-term mean isopleths are most like the isopleths calculated using 1982 meteorology in spatial distribution – the southwest-northeast extensions dominate, there is little tertiary lobe development, and the maximum concentration areas near the source are more confined and localized than in the other study years. Thus, it appears that the 1982 meteorological data set used in the TMI-2 ISFSI site modeling is most representative of long-term meteorological patterns.

THIS PAGE INTENTIONALLY LEFT BLANK.

2.4 SURFACE HYDROLOGY

The following sections discuss the hydrology of the region, the INEEL, and the ISF Facility site as it pertains to the design basis, performance requirements, and operation of the ISF Facility.

2.4.1 Hydrologic Description

The INEEL is in the Pioneer Basin, a closed topographic depression on the Eastern Snake River Plain that receives intermittent runoff from the Big Lost River, Little Lost River, and Birch Creek drainage basins (Figure 2.1-8). The Pioneer Basin is not crossed by any perennial streams because the permeability of alluvium and underlying rock causes the water to infiltrate into the ground. The largest stream, the Big Lost River, enters the INEEL near the southern end from the west and, during exceptionally wet years, flows in a large arc northeast to the foot of the Lemhi Mountain Range, where it ends in a series of playas (sinks). The only other naturally occurring stream on the INEEL is Birch Creek, which enters from the north. This stream is usually dry except during heavy spring runoff, when water may flow onto the INEEL. The Little Lost River approaches the INEEL from the northwest through Howe and ends in a playa just off the INEEL.

The Big Lost River is the most important element affecting the surface water hydrology of the INEEL and INTEC. (Figure 2.4-1) The Big Lost River discharges an average of 2.6×10^8 cubic meters per year (211,000 acre-feet per year) below Mackay Dam, 48 kilometers (30 miles) northwest of Arco (Ref. 2-18). The largest recorded annual flow of the Big Lost River for the entire period of record occurred in 1984 and amounted to 5.8×10^8 cubic meters per year (476,000 acre-feet per year), measured below Mackay Dam. The second largest annual flow occurred in 1965 and amounted to roughly three-quarters of the 1984 record (Ref. 2-19).

Other than these intermittent streams, playas, and manmade percolation, infiltration, and evaporation ponds, there is little surface water at the INEEL. Surface water that reaches the INEEL is not used for consumption (e.g., irrigation, manufacturing, or drinking) and no future uses of surface water that reaches the INEEL are identified.

2.4.1.1 Site and Structures

Vertical control for the ISF Facility design is based on the 1988 Geodetic Survey, North American Vertical Datum (NAVD 88). Elevation references, from others, are based on an INEEL site-specific datum (1986 Flood Study Datum) developed from the 1929 Geodetic Survey Datum (NGVD 1929).

The ISF site is adjacent to the southeastern portion of INTEC, about 1200 meters (4000 feet) from the Big Lost River channel. The ISF site grade access elevation will be 1499 meters (4917 feet) at the existing ground surface, as shown in Figure 2.4-2. Grading will provide for positive drainage of runoff away from the ISF Facility structures. Runoff will be directed to the existing storm drainage areas. The final grade is not expected to result in changes to the natural drainage patterns in the ISF site area.

2.4.1.2 Hydrosphere

Stream flows from the Little Lost River and Birch Creek seldom reach the INEEL (Figure 2.1-8) and would not affect the ISF site, as they are to the north. The Little Lost River drains the slopes of the Lemhi

and Lost River ranges. Water in the Little Lost River is diverted seasonally for irrigation north of Howe, Idaho, and does not flow onto the INEEL. Birch Creek originates from springs below Gilmore Summit in the Beaverhead Mountains and flows southeast onto the Snake River Plain. The water in the creek is diverted north of the INEEL for irrigation and hydropower purposes. In the winter, when the water is not being used for irrigation, flows are returned via a manmade channel to the main Birch Creek channel within the INEEL boundary. The channel leads to a gravel pit near Playa 4, approximately 6.4 kilometers (4 miles) north of TAN. Here it infiltrates the channel and gravel pit bottom, thereby recharging the Snake River Plain Aquifer.

The Big Lost River is the principal natural surface-water feature on the INEEL and the only stream potentially affecting the ISF Facility. It flows southeast from Mackay Dam, through the Big Lost River Basin past Arco, Idaho, and onto the Snake River Plain. Stream flows are often depleted by irrigation diversions and infiltration losses before reaching the INEEL. When flow in the Big Lost River reaches the INEEL, it is either diverted to the Flood Diversion Facility or flows north across the INEEL in a shallow, gravel-filled channel to its terminus in the Big Lost River playas, where its flow is lost to evaporation and infiltration recharging the Snake River Plain Aquifer. For monthly discharge of the Big Lost River at Lincoln Boulevard near the INTEC, see Table 2.4-1.

Major control on the Big Lost River upstream of the ISF site includes the Mackay Dam and the INEEL Flood Diversion Facility. See Table 2.4-2 for Mackay Dam and INEEL Flood Diversion Facility reservoir characteristics.

2.4.1.2.1 Mackay Dam

Mackay Dam, about 72 kilometers (45 miles) upstream from the INEEL, impounds water from the Big Lost River for irrigation purposes downstream. Mackay Dam is a 433-meter (1430-foot) long, 24-meter (79-foot) high earth-filled dam built for the Big Lost River Irrigation District. The dam was completed in 1917 and has a storage capacity of $5.0 \times 10^7 \text{ m}^3$ (44,500 acre-feet) and surface area of 502 hectares (1241 acres) at a water surface elevation of 1849 meters (6066.5 feet) (Table 2.4-2). There is an ungated overflow spillway with a weir length of 23 meters (75 feet) at elevation 1849 meters (6066.5 feet) near the west abutment of the dam. The spillway is designed for a discharge of 92 cubic meters per second (m^3/s) (3250 cubic feet per second [cfs]) with 1.2 meters (4 feet) of freeboard on the dam. The outlet works are also located near the west abutment and extend through the embankment and under the spillway to form an outlet channel. The outlet works consist of five motor-operated slide gates measuring 1.2 by 1.4 meters (4 by 8 feet) mounted in an upstream control tower. The arched-roof outlet tunnel measures 3 by 3 meter (10 by 10 foot), and reaches 152 meter (500 feet) downstream into a 3 meter (10-foot) diameter steel pipe, which extends to the outlet. At the outlet, the pipe branches into six 1.2 meter (4-foot) diameter pipes emptying into a stilling basin at the toe of the dam. The total discharge capacity of Mackay Dam is less than $283 \text{ m}^3/\text{s}$ (10,000 cfs). Water from the Big Lost River is impounded for the irrigation of about 57,500 acres of land downstream from the reservoir and for recreational opportunities. Another 10,200 acres of land upstream from the reservoir are also irrigated with Big Lost River water.

2.4.1.2.2 INEEL Flood Diversion Facility

The INEEL Flood Diversion Facility includes a diversion dam, dikes, and spreading areas about 16 kilometers (10 miles) upstream from INTEC. The Flood Diversion Facility was constructed in 1958 and enlarged in 1984 to reduce the threat of flood at the INEEL from the Big Lost River. The Flood Diversion

Facility controls or divides the flow in the Big Lost River between the spreading areas to the south and the playas to the north. The water can be temporarily stored until it infiltrates into the ground, thus precluding flows of flood size past the INTEC and other INEEL facilities. The spreading areas (A, B, C, and D) and the playas (1, 2, 3, and 4) are shown in Figure 2.4-1. The Flood Diversion Facility has an elevation between 1533.1 and 1543.7 meters (5030 and 5064.7 feet); the INTEC lies at about 1498 meters (4917 feet). The playas, about 29 kilometers (18 miles) downstream from INTEC, lie between an elevation of 1456.9 and 1460 meters (4780 and 4790 feet).

The Flood Diversion Facility diversion dam consists of a small earthen diversion dam and headgate that diverts water from the main channel, through a connecting channel, and into a series of four natural depressions called spreading areas. Flow in the diversion channel is uncontrolled at discharges that exceed the capacity of the culverts. The diversion channel can carry $204 \text{ m}^3/\text{s}$ (7200 cfs) from the Big Lost River channel into the spreading areas. Two low swales southwest of the main channel will carry an additional $59 \text{ m}^3/\text{s}$ (2100 cfs), for a combined diversion capacity of $263 \text{ m}^3/\text{s}$ (9300 cfs) (Ref. 2-20). The capacity of the spreading areas is about $7.2 \times 10^7 \text{ m}^3/\text{s}$ (58,000 acre-feet) at an elevation of 1530 meters (5050 feet) (Ref. 2-21). An overflow weir in Spreading Area D allows water to drain southwest, off the INEEL. To date, runoff from the Big Lost River has never exceeded the capacity of the spreading areas (Ref. 2-22). Gates placed on two corrugated-steel culverts control flow downstream onto the INEEL. At full capacity, the culverts can handle up to $25.5 \text{ m}^3/\text{s}$ (900 cfs) of flow through the diversion dam downstream onto the INEEL.

There are no users of the surface water that reaches the INEEL.

2.4.2 Floods

Because this is not a flood-dry site, as defined in American National Standards Institute/American Nuclear Society-2.8-1981, the following analysis is presented.

2.4.2.1 Flood History

A study of recorded discharge data from several U.S. Geological Survey (USGS) stream flow stations along the Big Lost River upstream of the INEEL suggests a history of low-magnitude floods (Ref. 2-23). Flooding in the Big Lost River basin is associated with peak flows during the snowmelt season and occasional flooding caused by ice jams in the stream channel. Big Lost River flows seem to be attenuated by the gravels, deep alluvium, and permeable basalt found in the channel bed. These stream flow losses, combined with controlled stream flow, diversion canals, and irrigation use, significantly affect the natural flood peaks. Downstream of the INEEL, the local semi-arid climate, relief, and geology combine to regulate local runoff. Local flooding in the past has been associated with unseasonably warm temperatures and rain on frozen ground, as the following local flood history describes.

1965 Flood. A record snow pack occurred in the Big Lost River basin in the winter of 1964-65. The maximum runoff occurred in late June. The Mackay Reservoir was full and most of the runoff passed down to the basin and through the Flood Diversion Facility on the INEEL. During the flood peak (June 29, 1965), approximately $51 \text{ m}^3/\text{s}$ (1,800 cfs) were diverted to the spreading areas from a peak flow of $62 \text{ m}^3/\text{s}$ (2215 cfs). The Big Lost River overflowed its banks above Arco through most of June. On the INEEL, the flood was controlled by the Flood Diversion Facility and by storage and infiltration in the river channels, playas, and sinks. The water did not reach the end of the Big Lost River channel at the

Birch Creek playa. This flood exhibited the largest crest and largest water volume to be discharged onto the INEEL in 65 years of record. Significant as it was, this flood caused no damage to INEEL facilities.

1984 Flood. High stream flows in the Big Lost River and a severe cold spell during the winter of 1983-84 caused ice jams that threatened localized flooding. Ice buildup in Spreading Area A (Figure 2.4-1) resulted in waters backing up in the diversion channel and ultimately threatening to overtop Dike 1. The high stream flows in the Big Lost River in 1983 and 1984 were largely the result of the Borah Peak earthquake of October 28, 1983. The earthquake created new springs upstream of Mackay Reservoir, which significantly increased the inflows to the reservoir. Outflows from the reservoir were also increased to reduce the storage behind the dam. Downstream INEEL facilities were not threatened or damaged by this accumulation of ice in the diversion channel.

In response to this flood threat, the Diversion Area was upgraded to provide additional flood control, increasing the diversion channel flow capacity of 71 m³/s (2500 cfs) to over 255 m³/s (9000 cfs).

During the winter months there is generally no flow in the Big Lost River downstream on the INEEL. If there is, however, the flow is diverted to the Flood Diversion Facility to avoid the accumulation of ice in the main channel, reducing the possibility of flooding downstream. The review of the historical information since the TMI-2 ISFSI was licensed, determined that no flooding or inundation from storms or runoff has caused recent flooding of the INTEC and ISF site area.

2.4.2.2 Flood Design Considerations

As noted above, no flooding or inundation from storms or runoff has caused flooding of the ISF site to date. The ISF site is slightly below the probable maximum flood elevation (4917 feet versus probable maximum flood nominal elevation of 4921 feet) based on NAVD 88 datum. Chapter 8, *Accident Analysis*, addresses the consequences of flooding at the ISF site. Such flooding would not cause structural damage or create significant offsite radiological consequences.

2.4.2.3 Effects of Local Intense Precipitation

Normal rainfall is generally higher in the mountains to the west than it is in the Pioneer Basin. For average, highest, and lowest total monthly and annual precipitation at CFA from January 1950 to December 1988, see Table 2.3-6. Thunderstorms are infrequent on the INEEL, and the total amount of rain generated during a thunderstorm is usually relatively small because of the arid climate of the Snake River Plain.

2.4.3 Probable Maximum Flood on Streams and Rivers

The probable maximum flood represents the hypothetical flood considered to be the most severe flood event reasonably possible, based on hydro-meteorological application of maximum precipitation and other hydrologic factors. The probable maximum flood may be caused by either an unusually severe storm or some catastrophic event, such as a dam failure. The probable maximum flood resulting from an overtopping failure of the Mackay Dam caused by an extreme precipitation event is the bounding scenario for INEEL facilities. Figure 2.4-3 represents the probable maximum flood hydrograph and Figure 2.4-4 is the inundation map for the probable maximum flood-induced failure of Mackay Dam. Table 2.4-3

provides information on the peak water-surface elevation, peak flow, water velocity, and time of wave arrival at several downstream locations for this dam failure scenario.

Information presented in this section reflects the data provided in the TMI-2 ISFSI SAR (Ref. 2-1). The TMI-2 ISFSI SAR was based on the *Flood Routing Analysis for a Failure of Mackay Dam* prepared for the DOE to provide the basis for assessing and developing flood protection systems for the INEEL (Ref. 2-24).

2.4.3.1 Probable Maximum Precipitation

The probable maximum precipitation for the drainage basin above Mackay Dam is based on a 48-hour general storm in June, preceded 3 days in time by an antecedent storm with a magnitude of 40 percent of the 48-hour storm (Ref. 2-24). This scenario provides for no flow losses to the ground. It represents situations in which the ground may be frozen or fully saturated. The peak flow for the probable maximum flood is 82,100 cfs, occurring 154 hours after the beginning of the storm. The probable maximum flood estimate falls within the 50,000 to 200,000 cfs Myers envelope curve used by the U.S. Army Corps of Engineers. The probable maximum flood peak flow is almost 20 times higher than the highest flow of 4420 cfs recorded at Howell Ranch, a USGS station approximately 27 kilometers (17 miles) northwest of the dam. The probable maximum flood is based on the maximum potential for critical hydro-meteorological conditions to occur, not on probabilities or historical flood frequencies.

2.4.3.2 Precipitation Losses

The Big Lost River leaves the mountains at Arco. Below this point, the topography and drainage characteristics change along the river. The area is a low, flat plain with basalt bedrock. The drainage from most of the Pioneer Basin is integrated with the Big Lost River. Locally, some depressions in the basalt receive intermittent runoff. There is seldom enough precipitation in this area to exceed the infiltration capacity of the soil to create intermittent streams to the Big Lost River.

2.4.3.3 Runoff Model

The combined Big Lost River Basin and Pioneer Basin range in elevation from 1454 meters (4784 feet) to over 3830 meters (12,600 feet). Thus, this area has over 375 meters (8800 feet) of relief, resulting in large differences in temperature and climate at any given time. The low land in the Pioneer Basin is subject to periods of warm wind, rain, and snowmelt during the winter. These conditions cause runoff and minor flooding in the lower basins during regional storms and substantially increase the snow pack in the uplands. The largest documented runoffs in the lower parts of the basins have occurred in January, February, or March; the maximum runoff from the highlands is usually in May or June. Generally, frost leaves the ground in the Pioneer Basin and the valley floors of the mountain basins in March or April; the permeable soils and gravels can then accept surface water by infiltration before most of the snow pack starts to melt. Most surface water reaching the Pioneer Basin from the tributary drainage basins eventually infiltrates beneath the soil and rock to the groundwater reservoir. The remainder is lost through evaporation.

2.4.3.4 Probable Maximum Flood Flow

Because the spillway of Mackay Dam is not adequate to pass the effects of the probable maximum precipitation safely, overtopping and subsequent breaching of the dam due to this probable maximum precipitation storm were analyzed. During this projected overtopping failure, the inflow is sufficient to raise the water surface above an elevation of 1852 meters (6077 feet), 0.3 meter (1 foot) above the crest of the dam. A trapezoidal breach was assumed to develop over a 1-hour period and extend to the base of the dam. The computer code DAMBRK, developed by the National Weather Service, was used in the flood-routing analysis (Ref. 2-24).

The peak flow resulting from the probable maximum precipitation-induced overtopping failure is 306,700 cfs in the reach immediately downstream of the Mackay Dam (Table 2.4-3). This peak flow attenuates to 71,850 cfs at the INEEL Diversion Dam and to 66,830 cfs at INTEC. The flood wave reaches the INEEL Diversion Dam in 10 hours and the INTEC in 13.5 hours. Water velocities are approximately 1 to 3 feet/second downstream on the INEEL.

2.4.3.5 Water Level Determinations

The computer program DAMBRK identified the water levels at specified locations for the probable maximum flood-induced overtopping failure (Ref. 2-24). Peak water surface elevations, flow, velocity, and time of the wave arrival are identified in Table 2.4-3.

The data in these tables is based on an INEEL site-specific vertical datum (1986 Flood Study Elevation datum) adjusted from the NGVD 1929 datum.

The elevations reflected in the *Flood Routing Analysis for a Failure of Mackay Dam* (Ref. 2-24) differ from the NAVD 88 datum by 3.71 feet. Therefore, to convert 1986 Flood Study elevations to NAVD 88 datum elevations, 3.71 feet must be added to the 1986 Flood Study elevation.

The worst flooding condition at the INTEC results from the failure of Mackay Dam due to the probable maximum precipitation storm. The floodwaters within the ISF Facility area would reach up to 1499.83 meters (nominally 4921 feet) based on the NAVD 88 datum. The final graded ground surface elevation at the ISF site will be 1498.7 meters (4917 feet). The first floor elevation of the ISF facilities is at elevation 1498.8 meters (4917.5 feet). The Transfer Area floor is at 4917.5 feet, the Storage Area floor is at 4918 feet, and the Cask Receipt Area is at 4913.2 feet. The effects of the flood waters on important to safety (ITS) equipment and the actions to mitigate the effects of flooding are reflected in Chapter 8, *Accident Analysis*.

2.4.3.6 Coincident Wind-Wave Activity

Wind activity at the INEEL coincident with the largest projected flood crest could not produce waves that would exceed 0.2 meter (0.5 foot), primarily because of the shallow depth of water surrounding most INTEC buildings (Ref. 2-25). Thus, the static and dynamic effects of wave activity would be negligible.

2.4.4 Potential Dam Failures (Seismically Induced)

Mackay Dam was classified as a high-hazard dam by the State of Idaho in a 1978 inspection that utilized the U.S. Army Corps of Engineers guideline for safety inspection of dams (Ref. 2-25). This classification is based on the concentration of people and property downstream, the size of the dam, and its storage capacity, not on any aspect of the dam's current condition or operation.

Mackay Dam is in a region of historical seismicity, as evidenced by the 1983 Borah Peak earthquake. The performance of the dam during this earthquake demonstrated the stability of the embankment during moderate ground motion; however, Mackay Dam was built without any seismic design criteria. Therefore, a seismically induced dam failure has been analyzed to determine potential impacts at the INEEL (Ref. 2-24). This analysis assumed a postulated seismic failure of Mackay Dam during an inflow to the reservoir equal to the 25-year recurrence interval flood (peak flow 4030 cfs). Because a seismic event could potentially disrupt a significant part of the dam's structure, the breach was assumed to be trapezoidal, extending to the bottom of the structure at an elevation of 5997 feet, and developing over a 1-hour period. The peak flow from the seismic dam failure in the reach immediately downstream of the dam is 107,480 cfs (Table 2.4-4). This peak flow attenuates to 45,410 cfs at the INEEL Flood Diversion Facility Dam and to 39,080 cfs at the INTEC. The leading edge of the wave reaches the INEEL diversion dam in about 12 hours and the INTEC in about 16 hours. Average water velocities on the INEEL are 1 to 3 feet per second.

2.4.4.1 Reservoir Description

See Section 2.4.1.2 for information related to Mackay Dam and INEEL Flood Diversion Facility Dam.

2.4.4.2 Dam Failure Permutations

Sections 2.4.3 and 2.4.4 discuss, respectively, the projected overtopping dam failure due to the probable maximum precipitation, and a seismically induced dam failure. Other dam failure permutations examined include two hydraulic (piping) failures concurrent with 100-year and 500-year inflow floods to the reservoir under this scenario. The INEEL Flood Diversion Facility Dam would be overtopped by the floodwaters released by the failure of Mackay Dam. This overtopping of the INEEL Flood Diversion Facility Dam will contribute to the flooding downstream on the INEEL. The DAMBRK analysis assumes that the INEEL diversion dam begins to fail when floodwaters reach 5065 feet, an overtopping depth of 0.3 foot. Because of the small size of this dam, the breach is assumed to be fully developed after 0.1 hour, an essentially instantaneous failure. Characteristics of the four hypothetical dam failures analyzed are provided in Table 2.4-5.

2.4.4.3 Unsteady Flow Analysis of Potential Dam Failures

The flood from dam failure would initially travel down a valley between basalt flows. The initial velocity would be high near the failure, but the average velocity would decrease to approximately 1 foot per second (fps) near the INEEL Flood Diversion Facility Dam. Water entering the INEEL Flood Diversion Facility Dam from this flood is much less than the actual capacity of the spreading areas. Water that bypasses the Flood Diversion Facility would continue to spread out across the floodplain and have a peak water velocity of 2.7 fps at INTEC.

2.4.4.4 Water Level at ISF Site

The ISF Facility design basis is a probable maximum flood on the Big Lost River as described in Section 2.4.3.

2.4.5 Probable Maximum Surge and Seiche Flooding

The INEEL, on the Eastern Snake River Plain, is remote from major bodies of water; therefore, surge and seiche flooding are not potential natural phenomena.

2.4.6 Probable Maximum Tsunami Flooding

The Eastern Snake River Plain, on which the INEEL is located, is remote from major bodies of water; therefore, tsunami flooding at the INEEL is not a potential natural phenomenon.

2.4.7 Ice Flooding

Ice flooding is not a threat at the INEEL because, during the winter months, flow of the Big Lost River is diverted to the Flood Diversion Facility to avoid ice accumulation in the main channel downstream of the diversion dam. Possible ice jams upstream of the diversion dam are of no concern because overflowing of the banks at that location can cause no damage to the INTEC.

2.4.8 Flooding Protection Requirements

Chapter 8, *Accident Analysis*, addresses the flood protection requirements at the ISF site.

2.4.9 Environmental Acceptance of Effluents

The ISF Facility design permits portions of the buildings to be flooded in the event of the design basis flood. Contamination to the outside of the facility was analyzed and is discussed in Chapter 8, *Accident Analysis*.

There are no liquid discharges to the environment, therefore, the surface hydrology is not affected by any effluents. The ISF Facility liquid systems have limited interfaces with the environment, therefore, there are limited scenarios that could yield an inadvertent release of effluents to the environment. The ISF Facility site is sloped to the southeast to allow stormwater to be routed to a storm drain ditch. It is anticipated that any inadvertent release of liquid effluent would also follow this path and be collected in the storm drain ditch.

Any liquid that did infiltrate the ground surface would not greatly affect the regional groundwater quality. This conclusion is based on previous groundwater computer modeling done of the vadose zone. The vadose (unsaturated) zone extends from the ground surface down to the water table (aquifer). Within the vadose zone, water and air occupy openings in the geologic materials. Subsurface water in the vadose zone is referred to as vadose water. At the INEEL this complex zone consists of surface sediments (primarily clay and silt, with some sand and gravel) and many relatively thin basaltic lava flows, with some sedimentary interbeds. The vadose zone protects the groundwater by filtering many contaminants through adsorption, buffering dissolved chemical wastes, and the slowing transport of contaminated liquids to the aquifer. The vadose zone also protects the aquifer by storing large volumes of liquid or

dissolved contaminants released to the environment through spills or migration from disposal pits or ponds, allowing natural decay processes to occur (Ref. 2-26).

THIS PAGE INTENTIONALLY LEFT BLANK.

2.5 SUBSURFACE HYDROLOGY

The INEEL is in the Eastern Snake River Plain and is underlain by the Snake River Plain Aquifer. A description and discussion of this aquifer provides the essence of the INEEL subsurface hydrology. Because the ISF site geohydrology is encompassed within the INEEL geohydrology, they are interrelated; therefore, the INEEL geohydrology is presented in this section. Much of the information presented in this section is from the USGS. Since 1949, the USGS has maintained a monitoring network of the INEEL to determine hydrologic trends of the Snake River Plain Aquifer.

2.5.1 Regional Characteristics

The Snake River Plain Aquifer is characterized as a thick sequence of basalts and sedimentary interbeds filling a large and structural basin about 322 kilometers (200 miles) long and 80 to 129 kilometers (50 to 70 miles) wide in southeastern Idaho (Figure 2.5-1). The INEEL is underlain with basalt flows 3 to 23 meters (10 to 75 feet) thick with interbedded layers of fluvial, lacustrine, windblown, and pyroclastic sediments. The basalt and sediment underlying the INEEL are saturated at depth, and together form the Snake River Plain Aquifer. Most of the permeability occurs along the upper and lower contacts of successive basaltic flows, which have large and irregular fractures, fissures, and other voids. These discontinuities lead to a large degree of heterogeneity and anisotropy in the hydraulic properties of the aquifer.

The Big Lost River, entering the topographic depression of the Eastern Snake River Plain, is the only significant natural recharge to the aquifer. The Big Lost River drains more than 2254 square kilometers (1400 square miles) of mountainous area that includes parts of the Lost River Range and the Pioneer Range west of the INEEL. Flow in the Big Lost River infiltrates the Snake River Plain Aquifer along its channel and at sinks and playas at the river's end. Other surface drainages to the Snake River Plain Aquifer include Birch Creek, Little Lost River, and Camas Creek.

Groundwater generally flows northeast to southwest at an average hydraulic gradient of approximately 1 meter (4 feet) per mile (Figure 2.5-2). Nearly 8×10^9 cubic meters (2.8×10^{11} cubic feet) of water is discharged by the aquifer annually. Most of the discharge occurs as spring flow between Hagerman and Twin Falls. About 2.6×10^9 cubic meters (9.1×10^{10} cubic feet) of irrigation water are pumped from the Snake River Plain Aquifer in a typical year. About half of this water reenters the ground as return flow to the aquifer.

The altitude of the regional groundwater surface underlying the INEEL ranges from an elevation of about 1402 meters (4600 feet) in the north to about 1341 meters (4400 feet) near the southwest boundary of the INEEL. Due to the large volume of water and the hydraulic gradient, reversing the aquifer flow is highly unlikely.

The Snake River Plain Aquifer, one of the largest and most productive groundwater resources in the United States. The aquifer is listed as a Class I aquifer and was designated by the EPA as a sole-source aquifer in 1991. Groundwater from this aquifer supplies essentially all drinking water consumed in the Eastern Snake River Plain.

The Snake River Plain Aquifer is the only source of water used at the INEEL. Figure 2.5-3 shows the wells where water is being withdrawn within 8 kilometers (5 miles) of the ISF site. Table 2.5-1 lists the

INEEL production wells, the depth of each well, the depth to water at each well, and the annual volume of water withdrawn from each well. The wells withdraw water from the main body of the Snake River Plain Aquifer. The water withdrawn from each well is used for potable water, ground maintenance, and necessary INEEL operations. The ISF Facility will use groundwater provided from the INTEC and will not require any additional wells.

The underflow (i.e., that amount of water passing directly under the INEEL boundaries) of the INEEL is approximately 1.8×10^9 cubic meters per year (4.7×10^{11} gallons per year); consumption is less than 1 percent of the INEEL underflow and less than 0.1 percent of the total annual aquifer discharge.

Irrigated agriculture provides a significant portion of the economic base for southern Idaho, and the Snake River Plain Aquifer plays a major role in meeting irrigation requirements. The aquifer provides groundwater for irrigation of over one-third of the 3 million irrigated acres of the Snake River Plain. It is estimated that over 127,000 people depend on the aquifer for domestic and municipal water needs. Total domestic water consumption is approximately 46,000 acre-feet per year and groundwater discharge from well pumpage equals approximately 1.92 million acre-feet (Ref. 2-27).

2.5.2 Site Characteristics

The Snake River Plain Aquifer at the INEEL ranges from 61 meters (200 feet) below ground surface in the northern sectors to about 274 meters (900 feet) below ground surface in the southern sectors. Figure 2.5-4 shows the contours of depth to the water table at the INEEL.

The transmissivity of the aquifer generally ranges from 1.3×10^4 to 1.2×10^8 cubic meters per day per meter (1.0×10^6 to 1.0×10^8 gallons per day per foot). The average value for transmissivity is 6.2×10^4 cubic meters per day per meter (5.0×10^6 gallons per day per foot). Measured coefficients of the aquifer are highly variable both spatially and temporally, ranging from 0.001 to 0.2 and averaging 0.15. The effective porosity ranges from 5 to 10 percent.

Because of abundant rain and snowfall in the surrounding mountains, groundwater from the Snake River Plain Aquifer is low in dissolved solids and is satisfactory for most purposes without treatment. The groundwater contains calcium and magnesium carbonate as the major dissolved solids. The groundwater has a pH range of 7.7 to 9.6 with a median of 8.01 (Ref. 2-28).

Low levels of radioactive contamination are present in the groundwater near the ISF site, due to past disposal of wastewater using an injection well at INTEC. Since the use of the well was discontinued and the well was sealed, the contaminant levels have been dropping steadily. The major radionuclides in the contamination are ^3H , ^{90}Sr , and ^{137}Cs .

The ISF site does not have any monitoring wells. There are no groundwater recharge areas within the influence of the installation. Small amounts of groundwater are used in operation of the ISF Facility. This water comes from existing INTEC wells.

2.5.3 Contaminant Transport Analysis

The ISF Facility does not have any liquid discharges to the environment, therefore, there is no means during normal operation for contamination to be transported to the subsurface hydrology. The ISF Facility does not effect any users of the Snake River Plain Aquifer.

The ISF Facility design permits portions of the buildings to be flooded in the event of the design basis flood. Refer to Chapter 8, *Accident Analysis*.

THIS PAGE INTENTIONALLY LEFT BLANK.

2.6 GEOLOGY AND SEISMOLOGY

2.6.1 Basic Geologic and Seismic Information

2.6.1.1 Geomorphology

The INEEL is on the eastern portion of the Snake River Plain Province (Figure 2.6-1), a broad low-relief basin floored with basaltic lava flows and terrigenous sediments (sediment derived directly from the destruction of rocks on the earth's surface). The Snake River Plain is about 80 to 100 kilometers (50 to 62 miles) wide and over 560 kilometers (348 miles) long. It extends in a broad arc from the Idaho-Oregon border on the west to the Yellowstone plateau on the east. The Snake River Plain transects and sharply contrasts with the mountainous country of the northern Basin-and-Range Province and the Idaho Batholith (Figure 2.6-2). Surface elevations on the Snake River Plain decrease continually and gradually from about 2000 meters (6562 feet) near Yellowstone to about 650 meters (2132 feet) near the Idaho-Oregon border (Ref. 2-29). Summits of mountains surrounding the Plain range up to 3700 meters (12,140 feet) in elevation, producing a maximum elevation contrast of about 2300 meters (7545 feet).

The northern Basin-and-Range Province, which bounds the Snake River Plain on the south, is composed of north-to-northwest trending mountain ranges (with peaks up to 3700 meters high) separated by intervening basins (1400 to 1600 meters in elevation) filled with terrestrial sediments and volcanic rocks. Individual mountain ranges in the vicinity of the Snake River Plain are up to 200 kilometers (124 miles) long and 30 kilometers (19 miles) wide. They are sharply separated from the intervening basins by late Tertiary to Quaternary normal faults (Ref. 2-30). The basins are 5 to 20 kilometers (3 to 12 miles) wide and grade onto the Eastern Snake River Plain.

The Yellowstone Plateau, at the northeastern end of the Eastern Snake River Plain, is a high volcanic plateau underlain by Pleistocene rhyolitic volcanic rocks (Figure 2.6-1 and Figure 2.6-2). With elevations of about 2100 to 2600 meters (6890 to 8530 feet), it is significantly higher than the Snake River Plain but not as high as the mountain summits of the northern Basin-and-Range Province. The Plateau is characterized by extremely high heat flow from the surface, high temperatures at shallow depths, abundant hot spring, fumarolic and geyser activity, and landforms controlled by thick rhyolitic lava flows (Refs. 2-31, 2-32 and 2-33). These characteristics reflect recent volcanic activity in the area (2 million years ago to several tens of thousands of years ago) (Ref. 2-33).

The Idaho Batholith, which adjoins the northern margin of the central Snake River Plain, is characterized by a large area of irregular mountainous terrain with peaks ranging in elevation from 2400 to 3700 meters (7870 to 12,140 feet) (Ref. 2-34). Streams dissecting the area usually have dendritic drainage patterns reflecting the homogeneous nature of the underlying granitic rocks that comprise the batholith.

The four physiographic provinces described here (the Eastern Snake River Plain, the northern Basin-and-Range Province, the Yellowstone Plateau, and the Idaho Batholith) also correspond to tectonic or seismotectonic provinces. Each province has a different seismogenic potential, determined by the nature of its intrinsic tectonic processes. The nature and seismogenic potential of these tectonic processes is discussed in Section 2.6.2, Vibratory Ground Motion.

2.6.1.2 Geologic History

2.6.1.2.1 Paleozoic, Mesozoic, and Early Cenozoic Era History

The mountains northwest of the Eastern Snake River Plain, near the INEEL, are composed of thick sequences of late Precambrian through Pennsylvanian sedimentary strata. The Precambrian through lower Ordovician rocks are mostly clastic (shale, quartzite), whereas the upper Ordovician through Pennsylvanian rocks are mostly carbonates (dolomites, limestone). They occur within westward dipping thrust sheets that formed during east-directed Mesozoic compressional tectonism (Refs. 2-35 and 2-36).

During the Paleozoic and Mesozoic eras, continental shelf carbonates (limestone and dolomites) were deposited in a north-trending belt, which included southeastern Idaho, along the western margin of the North American continent (Ref. 2-37). Thrust faulting accompanied the deposition of these sediments in the Paleozoic era (Antler orogeny), in the Paleozoic/Mesozoic era (Sonoma orogeny), and again in Mesozoic/Cenozoic era (Sevier/Laramide orogenies). This thrust faulting produced the Idaho/Wyoming thrust belt (overthrust belt) that extends through eastern Idaho (Figure 2.6-3). In the early Cenozoic era, eastward-directed thrust faults and belts of deformation may have continued uninterrupted through southeast Idaho.

Large volumes of granitic rock were emplaced by igneous intrusion into the upper crust during Mesozoic and early Cenozoic eras, thrusting to produce the Idaho Batholith in central Idaho (Figure 2.6-3). Subduction of the Pacific plate beneath the North American plate caused large-scale melting of the lithosphere throughout the western cordillera. In addition to the Idaho Batholith, the Sierra Nevada Batholith and other large granitic intrusive bodies were formed during this time.

In the early Cenozoic era, northwest to southeast-directed extension produced the northeast-trending Trans-Challis fault zone and the associated Custer and Panther Creek grabens (Figure 2.6-4). Accompanying volcanism caused caldera subsidence along the trend of the grabens. Volcanic rocks of the Challis volcanic field, which covers much of south-central Idaho adjacent to the northwestern margin of the Eastern Snake River Plain, were erupted from sources along the Trans-Challis zone and elsewhere in south-central Idaho.

2.6.1.2.2 Late Cenozoic and Quaternary Era History

The Yellowstone Hotspot

The processes that caused development of the Eastern Snake River Plain began about 17 million years ago. A rising plume of anomalously hot rocks in the earth's mantle (the Yellowstone Hotspot) first impinged on the base of the lithosphere at that time. Because the mantle plume is rooted deep in the earth, it has remained relatively stationary while the lithosphere and crust (North American plate) have shifted across it due to plate tectonic processes. Approximately 17 million years ago, the North American plate was positioned so that the area now located in north-central Nevada was directly above the hotspot. As plate tectonic activity has moved the plate southwestward at about 3.5 centimeters per year (1.4 inches/year), the hotspot has left distinctive effects, evidenced by a broad crescent-shaped plain extending from Yellowstone National Park to north-central Nevada.

The effects of the Yellowstone Hotspot on the lithosphere and crust have been profound. Two types of large-scale melting have occurred. First, melting of the hot mantle material in the rising plume itself and generated basaltic melts (magmas) that migrated into the crust about 20 kilometers (12 miles). This melting was due to the decrease in pressure on high-temperature mantle material as it moved from great depth. Second, melting of crustal rocks produced granitic melts that migrated upward to near-surface reservoirs and caused widespread explosive and effusive rhyolitic volcanism typical of that at Yellowstone National Park. This melting was due to heating of crustal rocks by the much hotter basaltic magmas that rose from the mantle plume.

The observable surface effects of the Hotspot today include widespread, large-volume sheets of rhyolitic volcanic rocks emplaced by explosive processes, large-volume rhyolitic lava flows, calderas from which the rhyolitic volcanic rocks erupted, elevated topography in the area directly over the hotspot due to buoyant effects of the hotspot, and the basin of the Eastern Snake River Plain, which was caused by subsidence as plate motion moved volcanic highlands southwestward from the hotspot.

Calderas from which the rhyolitic volcanic rocks erupted are typically 30 to 70 kilometers (19 to 43 miles) across. They resulted from foundering of the roof of shallow magma chambers as voluminous explosive eruptions occurred. As the roofs foundered into the evacuated magma chamber, the resulting depressions were filled with thick sequences of rhyolitic volcanic rocks. As the North American plate migrated to the southwest across the Yellowstone Hotspot, a string of calderas and volcanic fields formed in the wake of the hotspot (Figure 2.6-5). When the surface cooled along this string of volcanic fields, the Eastern Snake River Plain was formed.

Modifications to Crustal Structure Resulting from Hotspot Processes

In addition to large-scale melting and volcanism, the melting processes associated with the hotspot significantly modified the crust beneath the Eastern Snake River Plain. The crystallization of large volumes of basaltic magma in the mid-crust produced a layer of anomalously dense rock roughly 10 kilometers (6 miles) thick. The added weight of this material to the crust, along with the contraction due to cooling after passing over the hotspot, has caused the Eastern Snake River Plain to subside in elevation by about 2 kilometers (1 mile) during the past 4 million years.

Basalt Volcanism and Sedimentation in the Subsiding Eastern Snake River Plain Basin

The subsidence of the Eastern Snake River Plain has produced an elongated northeast-trending basin in which two types of materials have accumulated to a depth of up to 2 kilometers (1 mile). These two types of materials are: 1) basalt lava flows that were generated by residual heat in the upper mantle beneath the plain and rose to the surface, onto the subsiding basin; and 2) sedimentary material deposits that have formed interbeds between lava flows. The sediments are composed of clays, gravels, sands, and silts that were deposited by wind action, streams such as the Big Lost River, and lakes such as Mud Lake and its much larger ancient predecessor, Lake Terretton.

The accumulation of these two types of rocks in the Eastern Snake River Plain has resulted in the observed sequence of interlayered basalt lava flows and sedimentary interbeds. Volcanism is a sporadic process. During the long periods of quiescence between volcanic periods, sediments accumulated to thicknesses of less than 1 meter (3.3 feet) to greater than 60 meters (197 feet). During short periods of

volcanic activity, several lava flows commonly accumulated to thicknesses reaching several tens of meters.

2.6.1.2.3 Basin-and-Range Tectonic Activity

The Basin-and-Range Province of the western United States (Figure 2.6-1) is a region of extending crust, high elevations, high heat flow, and extensive Cenozoic era volcanism (Ref. 2-38). The north to north-northwest trends of normal faults and mountain ranges in the Province, as well as various types of in situ stress determinations, (Ref. 2-39) show that the area is subjected to east-west to northeast-southwest directed tension. In the northern Basin-and-Range Province, which is transected by the Eastern Snake River Plain, the extension produces north-trending normal faults and mountain ranges on the southern side of the Eastern Snake River Plain and northwest-trending ones on the northern side. The mountain ranges are caused by block faulting: as extension stretches the area, the brittle upper crust (upper 10 to 16 kilometers) can respond only by breaking into blocks that rotate slightly along the faults between to produce long, narrow mountain ranges with intervening basins (valleys).

The rugged topography and high elevations characteristic of these mountain ranges die out at the margins of the Eastern Snake River Plain (Figure 2.6-2) and give way to the relatively flat and low-lying topography characteristic of the Plain. The activity on the normal faults that bound the ranges must also die out at the plain margins, else the mountain ranges would continue across.

2.6.1.3 INEEL/ISF Facility Site Geology

2.6.1.3.1 Topographic and Physiographic Description

INEEL Area

The topographic relief of the Eastern Snake River Plain is subdued with respect to the surrounding Basin-and-Range Province. Total relief of the floor of the plain in the INEEL area is about 200 meters (656 feet), ranging from 1460 meters (4790 feet) at Big Lost River Sinks to about 1650 meters (5413 feet) on the northeast-trending axial ridge of the plain (Figure 2.3-4). Four prominent buttes along the axial ridge of the plain stand noticeably higher than the Plain. Big Southern Butte (2308 meters), Cedar Butte (1776 meters), Middle Butte (1948 meters), and East Butte (2003 meters) offer additional relief of 120 to 650 meters above the axial ridge.

The axial ridge, known as the axial volcanic zone, constrains the Snake River to the southeastern edge of the Plain and causes rivers from the mountains north of the plain to drain into closed basins (Ref. 2-40). The most prominent example is the Big Lost River, which flows onto the plain near Arco, turns northeastward in the southwestern part of the INEEL, and flows north to the Big Lost River Sinks in the northern part of the INEEL. The Little Lost River and Birch Creek also empty into playas in the northern part of the INEEL.

Much of the Snake River Plain is rough, uneven topography due to the character of the numerous basalt lava flows that make up the surface. The topography is characterized by lobate forms, numerous steep-walled closed depressions and mounds, and anastomosed fissures. Erosional processes have not established classic drainage patterns. Streams tend to be intermittent, wandering, and blind as they follow lava flow contacts and lava channels, commonly ending in closed depressions.

In many areas the lava flow topography is softened by deposition of windblown silt into fissures and depressions. In some areas, silt deposition has been so great that the topography is dominated by dune forms and rolling terrain with little or no basalt at the surface. Development of intermittent lakes and ponds in many closed depressions in the lava flow surface has resulted in deposition of fine silts and clays, producing small flat-floored playas (Ref. 2-41).

ISF Facility Site

The ISF Facility site is in a flat area near the Big Lost River in the south central part of the INEEL adjacent to the INTEC (Figure 2.3-4). The area is underlain by about 8 to 10 meters (25 to 30 feet) of Big Lost River alluvial silts, sands, and gravels, which lie on an alternating sequence of basalt lava flows and interbedded sediments extending to a depth of about 600 to 700 meters (1968 to 2297 feet). Landforms in the vicinity of the ISF site consist of the braided channels of the Big Lost River to the west and north of the site, and irregular flow lobes of basalt lavas to the east of the ISF site.

2.6.1.3.2 Stratigraphy and Areal Geology

INEEL Area

Stratigraphy. During the past 4 million years, the Eastern Snake River Plain, including the INEEL area, has experienced volcanic activity, mostly in the form of mild outpourings of basaltic lava flows. Vents for the basaltic volcanism are concentrated in northwest trending volcanic rift zones and along the axial volcanic zone (Refs. 2-40 and 2-42) (Figure 2.6-6). Sediments deposited by wind action, streams, and lakes have also accumulated in the Eastern Snake River Plain, concurrent with the basaltic lava flows. Lithologic logs of four INEEL deep holes (more than 2000 feet deep) (Figure 2.6-7), and hundreds of shallower drilled holes show that an inter layered sequence of basalt lava flows and poorly consolidated sedimentary interbeds, known as the Snake River Group, occur to depths of 1 to 2 kilometers beneath the INEEL (Refs. 2-40, 2-41, 2-29). This sequence is underlain by a large, but unknown, thickness of late Tertiary era rhyolitic volcanic rocks.

Sedimentary interbeds within the Snake River Group are of diverse origins. These include silts deposited by wind action; silts, sands, and gravels deposited by streams such as the Big Lost River; and clays, silts, and sands deposited in playas and lakes such as Mud Lake and its much larger Pleistocene era predecessor, Lake Terreton. These sedimentary processes continue to operate today, producing surficial deposits of alluvial, aeolian, and lacustrine/playa origin.

The interlayering of unconsolidated and poorly consolidated sediments within the basalts has several implications for facilities at the INEEL.

- The interbedded sediments are composed mostly of fine-grained materials (silts and clays) with low permeability and high absorption capabilities. Therefore, they retard the downward migration of water and contaminants to the water table (Ref. 2-41).
- The low permeability of the sedimentary interbeds commonly causes localized perched water zones beneath some INEEL infiltration ponds (Refs. 2-43 and 2-44) and beneath natural infiltration/recharge zones such as the Big Lost River channel and sinks at flood stage.
- They can represent confining or semi-confining layers in the aquifer, thereby affecting the manner in which water (and contaminants) move vertically and horizontally.

- The alternating high and low seismic velocities associated with basalts and poorly consolidated sedimentary interbeds, respectively, cause greater-than-normal attenuation of earthquake strong ground motions (Refs. 2-45, 2-46, 2-47).
- The unconsolidated sands and clays intercalated within the hard, brittle basalts make drilling and downhole geophysical logging difficult, increasing the expense and time necessary for development of exploratory borings and monitoring wells at the INEEL.

Areal Geology. Surface rocks on and near the INEEL are mostly Quaternary period basalt lava flows, the upper part of the Snake River Group, ranging in age from less than 15,000 years to more than 730,000 years (Figure 2.6-9) (Ref. 2-48). A wide band of Quaternary mainstream alluvium extends along the course of the Big Lost River from the southwestern corner of the INEEL to the Lost River sinks area in north-central INEEL. Lacustrine deposits of clays and sands from ancient Lake Terreton occur in the northern part of the INEEL. Beach sands deposited by Lake Terreton were reworked by winds in late Pleistocene and Holocene periods to form large dune fields in the northeastern part of the INEEL (Refs. 2-41 and 2-49). Several Quaternary period rhyolite domes occur along the axial volcanic zone near the south and southeast borders (Ref. 2-40). Paleozoic era limestone, late-Tertiary period rhyolitic volcanic rocks, and large alluvial fans occur in limited areas along the northwest margin of the INEEL (Ref. 2-48).

Vertical and Horizontal Facies of Basalt Lavas. Figure 2.6-8 shows an idealized section showing distribution of vertical and horizontal facies variation in Eastern Snake River Plain basalt lava flows. From bottom to top, basalt lava flows typically are composed of a basal rubble zone, a lower vesicular zone, a massive columnar jointed zone, an upper vesicular and fissured zone, and a cap of platy jointed crust.

The near-vent facies of lava flows is typified by thin, vesicular, platy flows (shelly pahoehoe). Pyroclastic ash and breccia layers are commonly interleaved within the thin flow layers. With distance from the vent, the shelly pahoehoe grades rapidly into the layered facies structure, described above, which typifies the medial and distal portions of the lava flow (Figure 2.6-8). Deflation pits, in which solidified crust has subsided over areas where lava has drained away, are common throughout the flow but more numerous near the terminus.

Sediment Facies. Sediments of diverse origins occur covering and interbedded with basalts of the Eastern Snake River Plain. Surface lava flows throughout INEEL and surrounding regions are covered by varying thicknesses of windblown silt (loess). Alluvial sands and gravels are common along the Big Lost River channel through the site, and lacustrine clays deposited in Pleistocene Lake Terreton are common in the northern and northeastern part of the site (Figure 2.6-9). Since the sedimentary depositional processes operating in the geologic past are similar to those operating today, these same types of sediments make up the interbeds in the subsurface.

INTEC and ISF Facility Area

Stratigraphy. Through FWENC geotechnical work, the subsurface soils under the ISF site were found to generally consist of about 2 to 5 feet (0.6 to 1.5 meters) of dense sandy gravel, overlying about 25 feet (7.6 meters) of dense sand and gravel. Basalt bedrock was encountered at depths between 25 and 30 feet (7.6 and 9.1 meters) below ground surface.

Sedimentary interbeds within the Snake River Group beneath the INTEC are composed mostly of silts, clayey silts and sandy silts. Cross sections showing the positions and thicknesses of interbeds are shown in Figure 2.6-10, Figure 2.6-11, and Figure 2.6-12. These sections show that an interbed occurs at a depth of about 45 to 60 meters below the surface. Several more interbeds are shown to occur between 60 to 180 meters (197 to 590 feet), and they presumably occur throughout the entire thickness of the basalt section because they are present in deep exploration well INEEL-1 (Figure 2.6-7), which is located approximately 5 kilometers north of the ISF Facility site, and WO-2, which is located about 5 kilometers east of the ISF Facility site.

Based on analysis of geophysical logs of wells, examination of drill core from core-holes, chemical analyses of core samples, and radiometric age determinations, 23 basalt lava-flow groups have been identified in the first 213 meters (700 feet) beneath the INTEC, adjacent to the ISF site (Ref. 2-50). In general, the age of the youngest basalt lava flow under the INTEC is between 100,000 and 200,000 years. The oldest lava is about 640,000 years.

Correlations based on regional mapping and analysis of well and drill hole data throughout the INEEL provide knowledge of the source areas for some of the flow groups. Many others have unknown source areas and unknown areal distributions because their source vents have been buried by later flows or sediments, and the current distribution of drill-holes does not provide sufficient subsurface information to identify all vent locations.

Basalt lava flow groups make up about 85 percent of the upper 213 meters (700 feet) beneath INTEC. The remaining 15 percent consist of sediment layers. The surficial sediment ranges in thickness from less than 2 meters to about 24 meters (a few feet to 80 feet), with the thickest areas lying west of INTEC and south of TRA. Surficial sediment is mostly composed of sandy and silty gravels deposited by the Big Lost River during late Pleistocene period. Sediment layers from deeper in the section are composed of both aeolian silts and sands and alluvial sediments.

Surficial sediment at the INTEC is thicker than most layers in the vadose zone beneath the INTEC. The sediment layers in the vadose zone range in thickness from 1 meter (3 feet) to 4.7 meters (15 feet). Sediment layers are thicker at greater depths in the sequence. At depths of about 500 meters (1640 feet) and greater, several interbeds 10 to 30 meters (30 to 100 feet) thick occur, and the average sediment layer thickness from 500 meters (1640 feet) deep to the base of the basalt-sediment sequence is about 8.4 meters (28 feet). On an INEEL-wide basis, sediment layer thickness distributions are similar to the INTEC. For INEEL wells and borings, the sediment layers tend to be thinner at depths of less than 305 meters (1000 feet). The sediment layers tend to be thicker in the northern part of the INEEL at an average of 5 meters (16 feet) than in the southern and southeastern parts at an average of 2 meters (7 feet).

Areal Geology. The INTEC lies just southeast of the channel of the Big Lost River in the south-central part of the INEEL (Figure 2.3-4 and Figure 2.1-6). In this area, the Big Lost River has a broad low-relief floodplain about 6 kilometers (3.7 miles) wide, bounded on the southeast and northwest by outcrops of basalt lava flows (Figure 2.6-9). The INTEC, adjacent to the ISF Facility site, is constructed on late Pleistocene alluvial gravels above the Holocene floodplain, which lies northwest of the river channel between the INTEC and TRA. Numerous abandoned channels and perhaps braided channels of the Big Lost River characterize the Holocene floodplain. The presently active channel, which is dry most of the time, is incised into the Holocene floodplain deposits by about 1.5 to 2 meters (5 to 7 feet), and is floored

by sands and fine gravels. The Pleistocene floodplain deposit, on which the INTEC is located, shows no evidence in aerial photographs of recent channels or braids of the river. Subdued meander-scroll topography is present over large areas of the Pleistocene surface, especially south and southwest of the INTEC. The surface is covered by sagebrush and the meander-scrolls are recognizable mainly from tonal anomalies on aerial photographs. Based on degree of soil development, the deposits that make up this surface were laid down during periods of high runoff during retreat of the most recent (Pinedale) glaciers, probably about 15,000 to 20,000 years ago (Ref. 2-51).

The landforms outside the floodplain are dominated by lava flow surface morphology that has been subdued somewhat by deposition of loess and fine aeolian sand in low areas and in the lee of ridges and hills. The lava flow surfaces are characterized by rugged but low relief topography. Due to deflation of parts of the surface during waning stages of volcanic activity, there are numerous closed basins separated by undeformed ridges. The largest of the basins commonly contain thin playa deposits that cover the basin floors. The ridges are riddled with anatomizing fissures roughly parallel to the margins of the collapsed basins. Many of the outcrops show columnar jointing that produces a hexagonal or polygonal pattern of fractures on the outcrop surface.

The basalts at the surface just east of the INTEC (Figure 2.6-9) and perhaps beneath the surficial sediment layer are about 230,000 years old, and flowed from vents about 14 kilometers (9 miles) southeast of the site (Ref. 2-48). Basalt flows beneath those at the surface are older and range in age to as much as 4.3 million years at the base of the basalt sequence (Ref. 2-40). These basalts have accumulated in the Eastern Snake River Plain that has continuously subsided at a rate of about 0.5 millimeter per year since passage of the Yellowstone Hotspot about 4.3 million years ago.

In contrast to vent locations for surface basalts, the source vents for basalts in the subsurface are poorly known. It is clear that some of the subsurface basalts erupted from the volcanic vent at AEC Butte about 3 kilometers (2 miles) northwest of the ISF site. Others came from vents in the Lava Ridge-Hells Half Acre volcanic rift zone, the axial volcanic zone, and possibly the Arco volcanic rift zone (see Section 2.6.6, *Volcanism*).

Basalts in the ISF site area, and throughout the Eastern Snake River Plain, are olivine tholeiites. They are mostly phryitic and contain up to 20 percent by volume phenocrysts of olivine and plagioclase. The groundmass is composed of olivine, plagioclase, clinopyroxene, magnetite, ilmenite, and minor amounts of apatite, glass, rutile, and oxidation products.

2.6.1.3.3 Structural Geologic Conditions

The cross sections through the INTEC site area constructed by Anderson (Ref. 2-50) suggest the possibility of folding and faulting of basalt lava flows in the subsurface. In the cross-section shown in Figure 2.6-10, a domal structure is interpreted in rocks older than the DE4 flow and in an area approximately 0.6 kilometers west of the INTEC. Since the structure does not show up in other sections through the area (Figure 2.6-11 and Figure 2.6-12), its true configuration and significance is uncertain.

In fact, the correlations based on gamma logs and geochemical analyses of core samples suggest that the stratigraphy is nearly horizontal beneath the INTEC-TRA area. Potassium-argon (K-Ar) dating and paleomagnetic inclinations suggest that discontinuities exist at depths of greater than 91 meters (300 feet) in rocks older than about 300,000 years, and that faults or a fold exists there.

Individual basalt lava flows have well-developed fissure sets that formed during emplacement of the lava. These fissures result from bending of the solidified lava crust as still-molten lava flows away, leaving deflated areas (Figure 2.6-8). In addition, post-solidification cooling joints develop in the lava flows, usually producing columnar joints with polygonal patterns. These emplacement- and cooling-related fissures and joints are ubiquitous in Eastern Snake River Plain lava flows; they are not through-going tectonic structures, and they should not be viewed as indications of folding or faulting. They are separate and distinct from fissuring related to dike injection in volcanic rift zones, which is a seismogenic process and has significance for seismic hazards.

The typical shape of the upper surface of a lava flow is irregular and rugged. High plateaus correspond to inflated areas, where the lava beneath the solidified crusts remained in place and solidified. Low areas correspond to basins and pits, where lava has escaped from beneath the solidified crust and allowed the crust to collapse to elevations as much as 9 to 12 meters (30 to 40 feet) below the inflated areas. Concentric fissures that developed in the collapsing crust because of removal of support from below commonly mark the margins of the pits and craters.

Field explorations of the ISF site have been performed. Subsurface explorations included drilling soil borings, excavating test pits, performing field geotechnical tests, collecting soil samples, and geophysical surveys/testing (Ref. 2-51).

Eight (8) geotechnical borings were drilled to obtain subsurface information to support the design and construction of the facility (see Figure 2.6-13). Borings were 8 inches in diameter and drilled to approximately 30 to 45 feet (9 to 13 meters) below ground surface. The logs of the exploratory borings are presented in Figure 2.6-14 through Figure 2.6-21.

Based on the observations of the soils in the borings and test pits, the subsurface soils encountered at this site generally consisted of about 2 to 5 feet (0.6 to 1.5 meters) of dense sandy gravel, overlying about 25 feet (7.6 meters) of dense sand and gravel. Basalt bedrock was encountered at depths between 25 and 30 feet (7.6 and 9.1 meters) below the ground surface. No concentric fissures were encountered.

2.6.1.3.4 Geologic History Related to Regional Geologic History

The geologic history at the ISF site and its relationship to regional geologic history can be summarized as follows:

- Eruption of voluminous, explosive silicic volcanic rocks during passage of the Yellowstone Hotspot beneath the area, 6.5 to 4.3 million years ago.
- Subsidence of the area as the hotspot passed with coeval eruption of basaltic lavas and accumulation of clastic sediments in the Eastern Snake River Plain basin.
- Accumulation of about 700 to 1000 meters (2300 to 3280 feet) of interbedded basalts and sediments, the Snake River Group, from 4.3 million years ago to present.
- Establishment of the Big Lost River's course through the central part of INEEL, probably within the last 0.5 to 1.0 million years. Upstream of the town of Arco the river's course is controlled by the positions of Basin-and-Range block-fault mountain ranges; downstream it is controlled by the positions of volcanic zones and the local slope of the surface of the Eastern Snake River Plain.

- The last volcanism at the ISF site occurred approximately 230,000 years ago. Since that time Big Lost River alluvium has accumulated to a depth of about 9 to 18 meters (29 to 59 feet).

2.6.1.3.5 Engineering Geological Conditions

See Section 2.6.4, *Stability of Subsurface Materials and Foundations*.

2.6.1.3.6 Groundwater Conditions

See Section 2.5, *Subsurface Hydrology*, for information related to groundwater under the ISF site.

2.6.2 Vibratory Ground Motion

2.6.2.1 Seismicity

2.6.2.1.1 Regional Setting

The Eastern Snake River Plain is defined as the eastern portion of the Snake River Plain extending from the Yellowstone Plateau to the Great Rift (Figure 2.6-22). The relatively aseismic Eastern Snake River Plain is surrounded by the seismically active Intermountain Seismic Belt and Centennial Tectonic Belt (Figure 2.6-22). The Intermountain Seismic Belt is a zone of concentrated seismicity that extends from northwestern Montana through the Yellowstone Plateau, southeastern Idaho, central Utah, and into southern Nevada. It is divided into three parts: the northern (Montana), central (Idaho), and southern (Nevada and Utah) Intermountain Seismic Belt. North of the Eastern Snake River Plain a branch of the Intermountain Seismic Belt extending from Hebgen Lake, Montana, westward into central Idaho (Figure 2.6-22) has been characterized as an independent zone of earthquake activity referred to as the Centennial Tectonic Belt. Smith and Arabasz (Ref. 2-52) consider the Centennial Tectonic Belt (formerly the Idaho Seismic Zone) a part of the central Intermountain Seismic Belt that “wraps around” the Eastern Snake River Plain. In the following discussions, this zone of seismicity will be referred to as the Centennial Tectonic Belt to distinguish it from the north-trending zone of seismicity within the central and northern Intermountain Seismic Belt (Figure 2.6-22).

Figure 2.6-24 shows a compilation of the minimum principle stress directions for the Eastern Snake River Plain region, derived from focal mechanisms, geologic indicators, and borehole breakouts. The minimum principal stress directions indicate northeast-trending extension northwest of the Eastern Snake River Plain and more east-trending directions south of the Eastern Snake River Plain. Although a rotation in the stress field may occur somewhere within the Eastern Snake River Plain, the plain appears to be subjected to the same extensional stress field as the surrounding region. Strain rates have been compiled by Eddington et al. (Ref. 2-53) for the Eastern Snake River Plain region. Strain rates for the region around the Eastern Snake River Plain range from 1.1×10^{-15} per second for Yellowstone Plateau to 3.8×10^{-17} per second for the Intermountain Seismic Belt. Preliminary estimates for the Eastern Snake River Plain are 1×10^{-16} per second based on the amount of extension measured in the Eastern Snake River Plain volcanic rift zones for the Holocene, similar to strain rates outside the Eastern Snake River Plain (Ref. 2-54).

2.6.2.1.2 Earthquake History

Earthquakes of magnitudes greater than 2.0 for the years 1850 to 1995 (shown in Figure 2.6-26 and Figure 2.6-27) were compiled from the following sources:

Agency	Dates
INEEL	1986-1995
USGS	1986-1995
Montana Bureau of Mines and Geology	1986-1995
United States Bureau of Reclamation	1986-1995
University of Utah Seismograph Stations	1986-1995
Engdahl and Rinehart (Ref. 2-55)	1880-1985
State Seismicity Maps for Idaho, Wyoming, Montana, Utah, and Nevada, USGS Denver, Colorado	1850-1985

The earthquake data were initially compiled by Woodward-Clyde Consultants (Ref. 2-46) for the years 1884-1989, then updated by Woodward-Clyde Federal Services (Ref. 2-47) to include earthquakes in 1991 and 1992, and again (Ref. 2-56) to include earthquakes occurring during 1993-1995.

For the central Intermountain Seismic Belt, the earthquake record extends back to November 10, 1884, the date of the first documented earthquake (M_L 6.3), which occurred near Paris, Idaho. Before the 1960s, seismographic coverage of the Eastern Snake River Plain and surrounding Basin-and-Range Province was relatively poor, with only earthquakes larger than magnitude 5.0 recorded by seismographs worldwide. The detection of earthquakes before this time was based on felt reports and damage reports by local residents. Such epicentral locations may be in error by 100 kilometers (62 miles) or more (Ref. 2-46). Over 90 percent of the earthquakes shown in Figure 2.6-27 have occurred during 1970 to 1995. The epicenters have been determined from localized seismic networks within the intermountain region. Epicentral errors for this time period could range from up to 20 kilometers (12 miles) depending on the number and spatial distribution of the seismic stations recording the event.

In the early 1960s, seismographs were installed in the intermountain area by the University of Utah Seismographic Stations (Figure 2.6-28). The USGS installed and operated a seismic network at Yellowstone National Park, Wyoming from 1970 to 1981; from 1983 to present, it has been operated by the University of Utah Seismographic Stations. Seismic stations were installed near Teton Dam, Idaho (currently operated by Brigham Young University-Idaho) beginning in 1980, in southwestern Montana (operated by Montana Bureau of Mines and Geology) starting in 1981, and in western Wyoming near Jackson Lake (operated by U.S. Bureau of Reclamation) during 1986. With additional seismic stations, smaller magnitude earthquakes will be detected.

Local seismic monitoring within the Eastern Snake River Plain began in December 1971, when a seismic station was installed at INEEL (Ref. 2-57). By 1979, this network included five stations within and near the boundaries of the Eastern Snake River Plain. Additional seismic stations were added to the network beginning in 1986. Currently, the INEEL seismic network consists of 26 seismic stations (Figure 2.6-28).

Earthquake data have been compiled by the INEEL seismic network for a 27-year period, from 1972 through 1999, primarily covering the Eastern Snake River Plain. During this period, approximately 19 microearthquakes have been located within or near the boundary of the Eastern Snake River Plain, indicating that infrequent, small-magnitude earthquakes (magnitude less than 1.5) may be characteristic of Eastern Snake River Plain seismicity (Refs. 2-58 and 2-59). Although 13 of these microearthquakes have occurred near or within the INEEL boundary, Jackson and others (Ref. 2-58) indicate that the INEEL area of the Eastern Snake River Plain is not more microseismically active than other areas, but rather that the INEEL seismic network has an adequate detection threshold (magnitude = 0) to record these small events.

Figure 2.6-27 shows that 1850 through 1995 earthquakes ($M_l > 2.5$) were located in the Intermountain Seismic Belt and Centennial Tectonic Belt, but not within the Eastern Snake River Plain. Also, earthquakes are located closest to the margins of the Eastern Snake River Plain near the Yellowstone Plateau, and farthest (up to 70 kilometers [40 miles]) away from the Eastern Snake River Plain margins near the Great Rift and Pocatello. From similar compilations of earthquake data, several investigators have concluded that the Eastern Snake River Plain is aseismic (Refs. 2-60, 2-61, 2-62 and 2-52). Contemporary seismic monitoring of the Eastern Snake River Plain (1972 – 1995) suggests that only infrequent small-magnitude earthquakes (20 events over 27 years of $M_l \leq 1.5$) occur within the Eastern Snake River Plain, as compared to the thousands of events of similar and larger size within the surrounding region. Although it is recognized that historic earthquakes may have occurred within the Eastern Snake River Plain, their large location uncertainties do not support origins within the Eastern Snake River Plain, particularly when other geologic and geophysical data are considered.

Based on the number of seismic stations operating over specific time intervals, periods of completeness can be established for various magnitudes. The periods of completeness are the time periods over which independent earthquakes (excluding aftershocks) can be considered to be completely detected (Ref. 2-46). Table 2.6-1 shows the periods of completeness for various magnitudes of the earthquake data shown in Figure 2.6-22. The completeness periods indicate that, for historic times, the database for larger magnitude earthquakes is more complete than for smaller magnitude events.

2.6.2.1.3 Moderate to Large Earthquakes

Moderate to large earthquakes of magnitudes greater than 5.5 have occurred within a 200-mile (321-kilometer) radius of the ISF site and are shown on Figure 2.6-22. For these events, Table 2.6-2 lists the earthquakes with Modified Mercalli greater than 5.5 with the largest magnitude computed, moment magnitude if computed, and Modified Mercalli intensities at the epicenter and documented in the vicinity of the ISF site. Of the events listed in this table, six have documented effects in the ISF site area.

1959 Hebgen Lake Earthquake. The largest earthquake in the region had a surface-wave magnitude of M_s 7.5. The earthquake occurred within the Intermountain Seismic Belt on August 17, 1959, at Hebgen Lake, Montana (Figure 2.6-29) (Ref. 2-63), 190 kilometers (118 miles) northeast of the INTEC site. The ISF site is located in what was a Modified Mercalli intensity zone VI. Although the earthquake was felt at the INEEL, it caused no damage to INEEL facilities (Ref. 2-64).

Borah Peak, Idaho Earthquake. This earthquake had a surface-wave magnitude of M_s 7.3. The earthquake occurred on October 28, 1983, in the Centennial Tectonic Belt 89 kilometers (55 miles) from the INTEC. The earthquake resulted from normal faulting along the Lost River fault (Ref. 2-65). The epicenter was in the Thousand Springs valley near the western flank of Borah Peak (Ref. 2-66). Substantial damage occurred to masonry structures in the communities of Mackay and Challis, Idaho, near the epicentral area (Ref. 2-64).

The ISF site is located in what was a Modified Mercalli Intensity zone VI (Figure 2.6-30) (Ref. 2-67). Inspections of existing INTEC facilities following the earthquake revealed no apparent structural or component damage that would compromise structural integrity at INTEC.

At the time of the Borah Peak earthquake, the INEEL had 15 strong-motion accelerographs in operation. Peak horizontal accelerations recorded at INEEL ranged from 0.022g to 0.078g for basement and free-field sites (Ref. 2-68).

Table 2.6-3 shows the corrected peak accelerations, velocities, and displacements measured by the three strong-motion accelerographs at INTEC facilities, 89 kilometers (55 miles) from the Borah Peak epicenter (Ref. 2-69).

Shoshone, Idaho, Earthquake. This 1905 earthquake, M_l 5.5, was reported to have occurred in the south-central portion of the Snake River Plain. It was felt in Idaho, Utah, Nevada, and Oregon. Although the INEEL did not start operations until 1949, the isoseismal map determined by Oaks for the Shoshone earthquake suggests that the ISF site would have been within a Modified Mercalli intensity zone IV (Figure 2.6-31) (Ref. 2-70).

Pocatello Valley, Utah, Earthquake. This 1975 earthquake, M_b 6.1, occurred near the Idaho-Utah border. An isoseismal map developed by Cook and Nye shows that the ISF site is located in what was a Modified Mercalli intensity zone III (Figure 2.6-32) (Ref. 2-71). It was reported that the earthquake was felt out to a distance of 305 kilometers (190 miles). No damage was reported at the INEEL.

Yellowstone Park, Wyoming, Earthquake. This 1975 earthquake, M_l 6.1, was located in the central portion of Yellowstone National Park. The earthquake was reportedly not felt at the INEEL (Figure 2.6-33) (Ref. 2-72).

Draney Peak, Idaho, Earthquake. This 1994 earthquake, M_w 5.7, occurred in Idaho, 18 kilometers (11 miles) west of Afton, Wyoming. The earthquake was reported to be felt in parts of southeastern Idaho but was not reportedly felt at the INEEL (Figure 2.6-34) (Ref. 2-73).

2.6.2.2 Geologic and Tectonic Characteristics of Site and Region

2.6.2.2.1 Identification and Description of Earthquake Source: Tectonic Provinces

The tectonic provinces of most concern for seismic and volcanic hazards at INEEL are the Eastern Snake River Plain and the northern Basin-and-Range Province (Figure 2.6-1). Other provinces close enough to INEEL to require consideration, especially for probabilistic seismic hazard assessments, are the Yellowstone Plateau and the Idaho Batholith.

The Eastern Snake River Plain is distinguished from the surrounding provinces by subdued topography, lower elevations, absence of Basin-and-Range faults and mountain ranges (Figure 2.6-2), and historic aseismicity (Figure 2.6-28) (Ref. 2-74). In addition, it is associated with a regional gravity high (Ref. 2-75), positive aeromagnetic anomaly (Ref. 2-76), and high seismic velocity (Ref. 2-77) reflecting zones of dense, magnetic mafic rocks near the surface and in the mid-crust beneath the Plain. The zone of mafic material in the mid-crust is believed to represent the zone of accumulation and solidification of mafic magmas generated by the Yellowstone Hotspot as it passed beneath the Eastern Snake River Plain.

The northern Basin-and-Range Province is distinguished by north-northwest trending block-fault mountain ranges that formed in response to east-northeast directed extension. North-northwest-trending normal faults bounding these ranges have accumulated up to 2 kilometers (1.2 miles) of vertical

displacement during the Late Tertiary and Quaternary (Ref. 2-30). Seismicity and Holocene paleoseismicity in the northern Basin-and-Range Province are concentrated on those parts of the faults that lie in a parabolic zone that passes through the Yellowstone Plateau and flanks both sides of the Eastern Snake River Plain (Figure 2.6-22 and Figure 2.6-27) (Refs. 2-74 and 2-30). The limbs of the parabolic zone are closest to the Eastern Snake River Plain near the Yellowstone Plateau and diverge outward from the Eastern Snake River Plain margin with distance to the southwest. In the vicinity of INEEL, the limbs lie about 40 to 50 kilometers (31 miles) from the margins of the Eastern Snake River Plain. Historic moderate to large earthquakes that have occurred in the parabolic zone include the 1983 Borah Peak, 1959 Hebgen Lake, 1975 Pocatello Valley, 1975 Yellowstone, 1934 Hansel Valley, and 1994 Draney Peak earthquakes.

The Yellowstone Plateau is distinguished by exceptionally high heat flow (Refs. 2-30 and 2-31), low seismic velocities at shallow crustal levels (Refs. 2-78 and 2-32), abundant hot spring and geyser activity (Refs. 2-79 and 2-80), persistent swarms of seismic activity, and rapid rise and fall (centimeter-scale inflation and deflation within months to years) of land surface elevations (Ref. 2-78). The area has experienced rapid and continuing uplift during the late Quaternary over the Yellowstone hotspot, near areas (northeastern Eastern Snake River Plain) that are rapidly subsiding. This results in development of large faults with high slip rates (Ref. 2-30) and with trends inconsistent with the direction of regional extension (for example, the Centennial, Teton, and Hebgen/Red Canyon faults, Figure 2.6-22) (Refs. 2-53, 2-63, and 2-81). In addition, the Yellowstone Plateau has much greater seismicity than either the Eastern Snake River Plain or the northeastern Basin-and-Range Province (Ref. 2-52), possibly resulting from interaction of regional extension with rapid local vertical crustal movements, from hydrothermal activity, and from magma movements in shallow chambers. Voluminous Quaternary explosive silicic volcanism (Ref. 2-66), significant delays in teleseismic P-waves beneath the caldera area (Refs. 2-82 and 2-83), and the 5-kilometers (3-miles) depth limit of seismicity within the caldera all suggest extremely high temperatures and presence of magma in the crust and upper mantle (Ref. 2-78).

The Idaho Batholith is distinguished by high, rugged topography, sparsity of Basin-and-Range Province faults, and absence of late Tertiary and Quaternary volcanism (Figure 2.6-1 and Figure 2.6-2). Seismicity is much less intense than that observed in the Basin-and-Range Province (Ref. 2-76), with maximum magnitudes of about 5. The Batholith appears to have been relatively unaffected by regional extension, perhaps because the granitic rocks are stronger or more coherent than rocks in the Basin-and-Range Province to the east and southwest.

2.6.2.2.2 Identification and Description of Earthquake Source: Faults

Faults of several ages and origins occur in the INEEL region. Some old and inactive, presenting no earthquake threat; others are capable of generating earthquakes that could affect INEEL facilities. A detailed correlation of faults with earthquakes is presented in Section 2.6.2.3, Correlation of Earthquake Activity with Seismic Sources.

Mesozoic thrust faults occur in the mountain ranges bordering the Eastern Snake River Plain (Figure 2.6-3) (Refs. 2-35 and 2-36). They formed during a period of east-directed thrusting related to the Sevier orogeny. They are gently westward dipping structures that separate major Paleozoic thrust sheets. These faults are mostly inactive at the present, because the compressional forces that created them at about 60 million years ago no longer exist.

However, it is possible that steeply dipping parts (ramps) of some of the thrust faults have been reactivated by Basin-and-Range normal faults in Late Tertiary to recent times (Ref. 2-84).

Eocene to Oligocene normal faults trend northward across the Lost River, Lemhi, and Beaverhead ranges north of the Eastern Snake River Plain (Refs. 2-84 and 2-85). Although these faults have several kilometers of accumulated displacement, their orientation with respect to the present stress field is such that they have little tendency for movement. Therefore they are not active today and pose no threat for earthquake hazards.

Basin-and-Range normal faults (Figure 2.6-22) of Miocene to Holocene age bound the northwest-trending mountain ranges north and south of the Eastern Snake River Plain (Ref. 2-86). These faults have accumulated up to 3 kilometers (1.8 miles) of displacement in the past 4 to 7 million years ago and are still active, as evidenced by fault scarps cutting latest Quaternary and Holocene alluvial fan deposits and by the occurrence of the 1983 Borah Peak earthquake. Table 2.6-4 summarizes the important characteristics of most Basin-and-Range normal faults around the Eastern Snake River Plain.

The closest of these faults to INEEL facilities, the Lost River, Lemhi, and Beaverhead faults (Figure 2.6-22), each bound the southwest side of a mountain range, producing typical Basin-and-Range half graben. These are large normal faults that extend from the northern margin of the Eastern Snake River Plain northwards to the Salmon River. Based on seismic and paleoseismic investigations, they are capable of generating earthquakes of magnitude 7 or larger (Refs. 2-87 and 2-88). Because of their size, activity, and proximity to many INEEL facilities, they control much of the INEEL seismic hazard.

Lemhi fault. Detailed paleoseismic and structural investigations have been performed on the southern Lemhi fault (Refs. 2-88 and 2-89). Results are:

- Segmentation of the southern Lemhi fault is redefined based on timing of paleoseismic events and on detailed mapping of the structure of the fault in bedrock and surficial deposits (Figure 2.6-27).
- The most recent earthquake events on the various segments range from 15 to 24 thousand years ago.
- There is evidence for temporal clustering of earthquake events (i.e., clusters of several events) over a few thousand years separated by long intervals (tens of thousands of years) of quiescence.
- Maximum magnitude of earthquakes in the southern part of the fault is estimated to be moment magnitude 7.15 (Refs. 2-55 and 2-47).
- Bedrock structural features of the southern part of the fault suggest that Quaternary displacement dies out at the south end of the Lemhi Range, and that significant seismogenic fault movements do not extend onto the Eastern Snake River Plain (Figure 2.6-35). Seismic reflection lines along the extended trace of the fault onto the Eastern Snake River Plain also show that recognizable offset of rock layers does not extend for more than 1 kilometer (0.6 mile) from the end of the range (Ref. 2-47).
- The horizontal distance from the inferred southern terminus of the fault to the ISF site is approximately 26.5 kilometers (16 miles).

- The best estimate of slip rate for the southern segment of the fault is 0.15 millimeters per year. In the 1996 probabilistic seismic hazard investigation the slip rate is allowed to range up to 1 millimeter per year to account for uncertainties in temporal clustering characteristics (Ref. 2-47).

Lost River Fault. The Lost River fault is slightly farther from the ISF site than the Lemhi fault, but poses similar seismic hazard because potential maximum magnitudes are slightly larger. Detailed paleoseismic and structural investigations of the segments closest to the INEEL, the Arco and Pass Creek segments (Refs. 2-89, 2-90, and 2-88), produced the following results:

- Activity on both segments is more recent than previously believed. The two most recent events on the Arco segment are between 21 ± 4 and 20 ± 4 thousand ($\pm 2\sigma$) years old; the three most recent events on the Pass Creek segment are between 18 ± 3 and 17 ± 4 thousand years old. Because of the overlap in age estimates (within 2σ), the two most recent events on both segments may have been contemporaneous.
- Ages of individual earthquake events indicate temporal clustering. Recurrence intervals vary from around 1000 years or less to 40,000 years or more on both segments.
- Paleomagnitude estimates based on vertical displacements yield a range of moment magnitudes from 6.6 to 7.3 for the Arco segment and 6.7 to 7.5 for the Pass Creek segment. The range of values results from assumptions as to whether measured displacements represent average or maximum values of displacement. Maximum magnitude estimates based on segment length for the Arco segment are moment magnitude 6.6-6.8, and for the Pass Creek segment moment magnitude 6.7.
- The Arco segment may extend south of the terminus of the Lost River range for several kilometers onto the Eastern Snake River Plain and into the northwestern end of the Arco volcanic rift zone.
- The horizontal distance from the southern exposed trace of the fault to the ISF site is 29 kilometers (18 miles).
- The best estimate of slip rate for the southern segment of the fault is 0.12 millimeter per year. In the 1996 probabilistic seismic hazard assessment slip rate was allowed to range from 0.05 millimeter per year to 1.0 millimeter per year to account for uncertainties in temporal clustering characteristics.

Beaverhead Fault. Although considerably farther from the ISF site (approximately 52 kilometers [32 miles] horizontal distance) than the Lemhi and Lost River faults, earthquakes on this fault will contribute to the probabilistic hazard assessment. No trenching investigations have been done for the fault, but surface mapping and studies of scarp characteristics furnish general information about its paleoseismology (Refs. 2-91 and 2-92). The southernmost two segments of the Beaverhead fault (the Blue Dome and Nicholia segments), those closest to the INEEL, seem to have quite different faulting histories. The Blue Dome segment (the southernmost segment) has no scarps in alluvium, even though the range front is steep and straight, suggesting geologically recent faulting. Both the range front morphology and the lack of scarps in alluvium suggest that the most recent surface faulting occurred more than 100,000 years ago. In addition, the exposure of bedrock on both sides of the fault scarp at the southern end of the range suggests that total vertical displacement is much smaller here than in segments farther north. Slip rate estimates for the Blue Dome segment range from 0.02 millimeter per year to 0.3 millimeter per year.

In contrast, the Nicholia segment (the next closest segment to the ISF site) is characterized by scarps that cut all alluvium except Holocene alluvium. In fact, scarps in Pinedale-age alluvium suggest that the most recent earthquake event was about 15,000 years ago, and slip rate estimates range up to 1 millimeter per year.

Grand Valley-Star Valley Fault. The active portions of the Grand Valley-Star Valley fault system are more than 160 kilometers (100 miles) from the ISF site and contribute significantly less to the seismic hazard than the Lost River, Lemhi, and Beaverhead faults northwest of the Eastern Snake River Plain. The northern terminus of the Grand Valley-Star Valley fault may extend as far as the town of Rexburg, about 90 kilometers (56 miles) from the ISF site (Ref. 2-93). Field investigations by Anders and others (Ref. 2-74), Piety and others (Ref. 2-94), and McCalpin and others (Ref. 2-95) have shown that the northern part of this fault system was active from about 4 million to 2 million years ago, but since then has been inactive. The southern end of the fault, in the Alpine and Star Valley area, however, experienced late Pleistocene and Holocene earthquake activity. Piety and others estimated a maximum credible earthquake of M_i 7.5 for the Grand Valley-Star Valley fault based on comparison of scarp heights and fault, displacements with those of historic earthquakes in the Intermountain Seismic Belt (Ref. 2-94).

The northwest boundary of the Eastern Snake River Plain has been investigated as a possible source of earthquakes that could contribute to the seismic hazards of INEEL facilities (Ref. 2-96). There is no evidence to support active faulting of postulated northeast-trending normal or strike-slip faults (Refs. 2-97 and 2-77) along the northwest boundary of the Eastern Snake River Plain. The abrupt termination of the northwest-trending mountain ranges at the margins of the Eastern Snake River Plain (Figure 2.6-2), the discontinuity observed in some geophysical surveys (refraction seismic, gravity, and magnetotelluric) at the northwest boundary of the Eastern Snake River Plain (Refs. 2-97, 2-77, 2-98, and 2-99), and the aseismic nature of the Eastern Snake River Plain relative to the surrounding seismically active region have been interpreted by some investigators (Refs. 2-100, 2-101, 2-98, and 2-102) to suggest the presence of active boundary faults along the margins of the Eastern Snake River Plain.

Formation of the Eastern Snake River Plain related to migration of the crust over the Yellowstone Hotspot (Refs. 2-103 and 2-30), the lack of geologic evidence (i.e., northeast-trending fault scarps) for large normal faults along the margins of the Eastern Snake River Plain (Refs. 2-71, 2-104, and 2-105), and seismologic and volcanic evidence indicating that the Eastern Snake River Plain and surrounding Basin-and-Range regions are subjected to northeast-directed extension (Refs. 2-40, 2-39, 2-58, and 2-106) do not support the possibility of active subsurface faults. The strain-rate (or extension-rate) estimates for the Eastern Snake River Plain (Ref. 2-54) are consistent with those estimated for areas outside the Eastern Snake River Plain. The Eastern Snake River Plain is a broad volcanic basin and does not resemble continental rift systems such as the Rio Grande rift or the East African Rift, which are large graben structures bounded by active normal faults.

In further efforts to look for possible recent fault activity along the margins of the Eastern Snake River Plain, a small northeast-trending topographic scarp (Ref. 2-49) on an alluvial fan on the southeast side of the Arco Hills was trenched in 1989. The results of the logging by the Idaho Geological Survey, under subcontract to EG&G Idaho, showed no evidence for faulting. The scarp was formed from some surficial processes, perhaps aeolian modifications to a fire scar (Ref. 2-105).

Other investigations have been conducted on northeast-trending faults at the southern terminations of the Lemhi Range and Beaverhead Mountains near the margins of the Eastern Snake River Plain (Refs. 2-71, 2-104, and 2-89). Results indicate that these faults were active more than 2 million years ago because they do not displace sediments and volcanic rocks younger than 2 million years and they have small lengths, generally less than 10 kilometers (6 miles), and small total displacements.

Nontectonic lineaments on and near INEEL can be observed from the air, on aerial photographs, and on satellite images. One of the most pronounced of these, the Principal Lineament, has been studied extensively and shown to be caused by aeolian modifications to a large fire scar (Ref. 2-107). This process produces many lineaments and perhaps even small topographic scarps on the Eastern Snake River Plain. Other lineaments are caused by unmodified fire scars, linear stream drainages, alignments of vegetative or soil contrast with unknown causes, fluvial (stream, river) deposits, paleoflood deposits, and aeolian deposits (dunes) (Refs. 2-108 and 2-105).

Late Tertiary caldera boundary faults are postulated to exist in the silicic volcanic rocks beneath the Snake River Group. There are several bases for this postulation:

- Calderas like those on the Yellowstone Plateau today must have been associated with the late-Tertiary silicic volcanic fields occurring along the margins of the Eastern Snake River Plain.
- In some areas (southern ends of the Lemhi and Beaverhead Ranges near INEEL, and northern ends of the Caribou and Snake River Ranges near Rexburg), structures interpreted to be caldera boundary structures have been recognized (Ref. 2-109).
- The great thicknesses of silicic volcanic rocks observed in INEEL deep exploration holes, INEEL-1 and WO-2 (Figure 2.6-7), suggest that they were emplaced into an intra-caldera setting.

The exact sizes, shapes, and locations of the buried calderas is uncertain, but interpretations have been made (Figure 2.6-5) on the basis of geophysical anomalies, positions of volcanic fields, flow-direction indicators in ash flow sheets, and paleomagnetic data (Refs. 2-110 and 2-42). Several general observations are possible. Caldera size is such that some of them are likely to span the entire width of the Eastern Snake River Plain. Caldera shape, and thus the configuration of associated caldera boundary faults, are generally circular to oval. Given the tendency for calderas to overlap each other (Figure 2.6-5), it is likely that most of the Eastern Snake River Plain boundary is characterized by caldera boundary faults buried beneath the edges of the Snake River Group. Caldera boundary faults can explain, in a manner consistent with data and concepts, Pankratz and Ackermann's interpreted buried fault along the northwest margin of the Eastern Snake River Plain (Ref. 2-97).

Several lines of evidence show that the calderas are no longer active because the causative heat source has moved to a new position beneath Yellowstone. The possibility of reactivation of the faults due to contemporary tectonism should be considered, but does not seem to be a cause for concern for two reasons:

- Because the faults have a circular to oval configuration, they are not likely have long sections oriented properly for movement in contemporary stress fields.
- No late-Pleistocene or Holocene faulting that could be related to reactivation of these faults is observed on the Eastern Snake River Plain (Ref. 2-108).

2.6.2.2.3 Identification and Description of Earthquake Sources: Volcanic Rift Zones and Axial Volcanic Zone

Volcanic vents on the Eastern Snake River Plain are concentrated in northwest-trending and northeast-trending linear belts (Figure 2.3-4). The northwest-trending belts have associated ground deformation features and are referred to as volcanic rift zones. The ground deformation features are fissures, faults, grabens, and monoclines that form due to dilational stresses above the tops of basalt dikes as magma moves from depth to the surface. Three well defined volcanic rift zones occur in the INEEL region of the Eastern Snake River Plain, the Great Rift volcanic rift zone (which extends southeastward from Craters of the Moon National Monument), the Arco volcanic rift zone (which extends southeast from Arco across the southwestern corner of the INEEL), and the Lava Ridge-Hells Half Acre volcanic rift zone (which extends from the south end of the Lemhi Range to the Hells Half Acre lava field) (Figure 2.3-4). A fourth volcanic rift zone, the Howe-East Butte volcanic rift zone, has been postulated, but it is an ill-defined zone consisting only of a few vents that are several hundred thousand years old (Ref. 2-42).

By analogy with active volcanic rift zones in other parts of the world (e.g., Iceland and Hawaii), it can be inferred that volcanic rift zones are sources of earthquakes during periods of volcanic activity. The magnitudes of volcanic rift zone earthquakes are small (less than 5.5), but because of their proximity to INEEL facilities their contributions to both deterministic and probabilistic seismic hazards have been assessed (Refs. 2-55 and 2-88).

Some volcanic vents on the Eastern Snake River Plain are concentrated in a northeast-trending zone along the axis of the Eastern Snake River Plain (Figure 2.3-4). This is called the axial volcanic zone to distinguish it from volcanic rift zones. It is important to make this distinction because the axial volcanic zone does not contain northeast-trending ground deformation features that would qualify it to be a volcanic rift zone. The few ground deformation features in the axial volcanic zone are northwest-trending fissures. This indicates that the volcanic vents in the axial volcanic zone are fed by northwest-trending dikes and that, even though it is not a volcanic rift zone, seismicity can be associated with volcanism there. Thus it also has been evaluated in deterministic and probabilistic seismic hazards assessment (Refs. 2-55 and 2-47).

2.6.2.3 Correlation of Earthquake Activity with Seismic Sources

Table 2.6-5 lists earthquakes with magnitudes greater than 5.5 that have occurred within a 200-mile (321-kilometer) radius around the ISF site, and that can be correlated with tectonic structures. Table 2.6-5 includes the seismic moments, focal mechanisms, focal depths, rupture lengths, and horizontal and vertical displacements computed by various seismological methods for these earthquakes. The following discussion of earthquakes and their relationships to geologic structures or provinces is separated into areas based on tectonic provinces.

2.6.2.3.1 Eastern Snake River Plain Province

Stover and others (Ref. 2-111) noted 14 historic earthquakes possibly located within the Snake River Plain. Figure 2.6-22 shows their locations; Table 2.6-6 lists their dates of occurrence, intensities, magnitudes (if reported), and location uncertainties. Earthquakes listed in Table 2.6-6 occurring between 1905 and 1937 have locations based on felt reports, with large location errors. The earthquakes listed for

1954, 1964, and 1969 have instrumentally determined locations, but due to the lack of local seismic networks before 1970, they also have large location errors.

In compiling earthquake data (pre-1970) into the Decade of North American Geology catalog for the western U. S., Engdahl and Rinehart (Refs. 2-112 and 2-55) selected only large magnitude earthquakes to represent earthquake source zones. Source zones were defined by using instrumentally located epicenters (post-1970) to determine seismically active areas. Within these areas, only large magnitude earthquakes (pre-1970) would be retained in the catalog. Thus, Figure 2.6-22 excludes the epicenters for eight of the possible Snake River Plain events due to their low intensities (hence, low magnitudes) and large location errors, and only includes the epicenters for the 1905 (Richter magnitude 5.5) Shoshone, 1928 (Richter magnitude 5.2), and 1937 (Richter magnitude 5.4) events. Although the epicenters for the 1928 and 1937 events are near the Idaho-Nevada border outside of the Snake River Plain boundaries, Woodward-Clyde Consultants (Ref. 2-46) included them within the Snake River Plain since Smith and Arabasz (Ref. 2-52) extended the Snake River Plain boundary to the Idaho-Nevada border. More commonly, the Snake River Plain boundaries are defined by topographic features that separate the flat, low-lying Snake River Plain region from the surrounding mountainous Basin-and-Range Province.

Figure 2.6-27 shows that from 1850 through 1995, the 1905 earthquake near Shoshone, Idaho, is the only event located within the Snake River Plain. The November 11, 1905, Shoshone earthquake occurred before there was instrumental monitoring in Idaho and, since its location was based on felt reports, it may have an error of 100 kilometers (62 miles) or more. This earthquake is significant to assessing seismic hazards at INEEL, because it may have originated within the Snake River Plain.

1905 Shoshone Earthquake

Recently, Oaks (Ref. 2-70) conducted a comprehensive investigation of historical records throughout an eight-state region to determine the magnitude and epicenter of the Shoshone earthquake. For the investigation, historical documents were sought from Nevada, Oregon, Idaho, Utah, Wyoming, Montana, California, Colorado, and Washington, D.C. Primary sources included original field notes of the Department of Agriculture weather observers reports, daily and monthly journal notations by U.S. Army Surgeons and other scientific and military personnel at U.S. Army command posts, personal diaries, and church records. Secondary sources, those transcribed from primary sources for use in another document, included newspapers, journal articles, books, maps, reports, and earthquake catalogs.

From a compilation of damage reports, Oaks (Ref. 2-70) determined the Modified Mercalli intensity for towns in Idaho, Utah, Nevada, and Oregon. Figure 2.6-31 shows the contours for intensities IV and V, and the possible location of the epicenter near the Idaho-Utah border. Both Shoshone, Idaho, and Elko, Nevada, reported damage that corresponds to intensity VI. It is noted that for other earthquakes these towns report higher intensities than surrounding towns (Ref. 2-66). A Richter magnitude of 5.5 ± 0.5 was estimated for the Shoshone earthquake, based on notes of seismic-wave amplitudes observed on a seismogram recorded by a station in Canada and measurements of the area within of the intensity V contour. Comparison of the intensity contours for the 1905 earthquake with earthquakes occurring near the Idaho-Utah border in 1934 (M_i 6.6), 1962 (M_i 5.7), and 1975 (M_i 6.0) also provides further support for an origin outside the Snake River Plain. Even though this study suggests the earthquake epicenter may have been outside the Snake River Plain, recent seismic hazards assessments at INEEL have estimated the level of ground motions from an earthquake similar in size to the 1905 Shoshone earthquake occurring within the Eastern Snake River Plain near the INEEL.

Hypotheses for Aseismic Nature of Eastern Snake River Plain

Earthquakes up to surface-wave magnitude 7.5 associated with Basin-and-Range faults have occurred in the Intermountain Seismic Belt, but only small magnitude earthquakes (Richter magnitude less than 1.5) have been detected instrumentally in the Eastern Snake River Plain. In addition, the rate of seismicity (number of earthquakes per unit of time) is much lower in the Eastern Snake River Plain than in the Intermountain Seismic Belt and Centennial Tectonic Belt (Ref. 2-58). Several investigators have attempted to explain the comparative aseismicity of the Eastern Snake River Plain. Their analyses have considered the distribution of instrumental seismicity and active faults, topography (surficial geologic features), the geologic history of formation of the Eastern Snake River Plain and the Basin-and-Range Province, tectonic stress patterns, crustal heat flow, and crustal- and upper-mantle compositions and properties. Earthquakes in the Centennial Tectonic Belt and Intermountain Seismic Belt indicate that the region around the Eastern Snake River Plain is subjected to a tectonic extensional stress field that actively extends the crust by normal faulting, which over millions of years produces mountains and valleys. The Eastern Snake River Plain is also subjected to this same stress field and possibly similar strain rates (Figures 2.6-24 and 2.6-25), but Basin-and-Range-style normal faults are not present within the Eastern Snake River Plain, leading investigators to propose alternative mechanisms for extensional deformation:

- **Aseismic Creep.** Smith and Sbar (Ref. 2-60) and Brott and others (Ref. 2-113) suggest that deformation occurs by creep in response to high crustal temperatures beneath the Eastern Snake River Plain. Comparisons of heat-flow data in and outside the Eastern Snake River Plain suggests that temperatures are higher beneath the Eastern Snake River Plain (Refs. 2-113, 2-114, and 2-115). Unlike the Basin-and-Range Province, where brittle deformation (rock fracture) and associated earthquakes raise the mountains and lower the valleys, the Eastern Snake River Plain experiences only ductile deformation (aseismic creep) because high temperatures in the crust preclude brittle deformation.
- **Crustal Strength.** Anders and others (Ref. 2-74) suggest that the Eastern Snake River Plain and the region adjacent to its boundary (the "collapse shadow") have increased integrated-lithospheric strength. They propose that the presence of a mid-crustal mafic intrusion strengthens the crust so that it is too strong to fracture. Smith and Arabasz (Ref. 2-52) also suggested that the mid-crustal mafic body beneath the Eastern Snake River Plain may increase crustal strength and thereby reduce the seismic capability of the Eastern Snake River Plain.
- **Dike Injection.** Parsons and Thompson (Ref. 2-116) proposed that magma overpressure through dike injection suppresses normal faulting and associated seismicity by altering the local stress field. In addition, the intrusion of numerous northwest-trending dikes during the long-term history of intermittent basaltic volcanism allows extension on the Eastern Snake River Plain to keep pace with tectonic extension occurring in the surrounding Basin-and-Range Province or Intermountain Seismic Belt (Refs. 2-40 and 2-106). Dike intrusion extends the crust because pressurized magma dilates the walls of the dike by a meter or more with each intrusion event.
- **Crustal Strain Rates.** Anders and Sleep (Ref. 2-117) suggest that the introduction of mantle-derived mafic magmas into the mid-crust increases the strain rate in the region directly over the hotspot (e.g., the contemporary high seismicity rate within the Yellowstone Plateau). Cooling and crystallization of the mid-crustal mafic magmas as the crust moves away from the hotspot causes

the strain rate to decrease to low levels (the current situation within the Eastern Snake River Plain). Several million years are required; after that before-strain rates climb to pre-hotspot levels.

Causes of Eastern Snake River Plain Microearthquakes

Investigators have also suggested possible mechanisms for microearthquakes that occur within the Eastern Snake River Plain. Because the Eastern Snake River Plain is a volcanic province, magmatic processes are a possible mechanism for the low-level microearthquakes. Brott and others (Ref. 2-113) suggested that microearthquakes may be a result of subsidence due to cooling and contraction of the Eastern Snake River Plain following the passage of the hotspot. Pelton and others (Ref. 2-59) suggested association with dike-injection or mass loading of the crust by the rhyolite domes near the axis of the Eastern Snake River Plain. Jackson and others (Ref. 2-58) observed that the microearthquakes that have occurred in the Eastern Snake River Plain from 1972 through 1995 do not have the distinct spatial or temporal patterns observed for contemporary dike-injection events at Kilauea, Hawaii, or Krafla, Iceland (Refs. 2-118, 2-119, 2-120) and therefore are not likely due to magmatic processes. Although no detailed analyses of mass loading and its role in producing microearthquakes within the Eastern Snake River Plain has been performed, Jackson and others (Ref. 2-58) attribute the occurrence of microearthquakes (Richter magnitude less than 1.5) to small-scale faulting in the shallow crust, in response to the regional extensional tectonic stress field. This interpretation is supported by two composite focal mechanisms for microearthquakes within the Eastern Snake River Plain that suggest predominantly normal faulting with northeast to southwest oriented T-axis.

Volcanic Seismicity

Several volcanic rift zones occur on the Eastern Snake River Plain in the vicinity of the INEEL (see Section 2.6.6 for a complete description). In addition to volcanic vents, the volcanic rift zones contain fissures, monoclinical flexures, normal faults, and graben, all of which are induced by shallow dike intrusion during periods of volcanic activity. Seismic studies at active volcanic rift zones, such as in Hawaii and Iceland, and theoretical and physical models of the resulting surficial deformation features indicate that dike-injection can produce small normal faults that extend to or slightly below the top of the dike (up to 4 kilometers [2.4 miles]) (Refs. 2-121, 2-122, 2-123, 2-124, and 2-125).

Because a dike-injection event has not been observed within an Eastern Snake River Plain rift zone, two methods are used to estimate maximum magnitudes of earthquakes that could be associated with future dike-injection events. The first method uses analogy to active volcanic rift zones of the world to estimate the maximum magnitude of earthquakes that would accompany future Eastern Snake River Plain volcanism (Table 2.6-7). In the active volcanic rift zones of Iceland, Hawaii, and east Africa, small earthquakes, commonly less than 4.5 in magnitude, accompany basalt dike injection, although magnitude 5.5 earthquakes have been observed (Refs. 2-126, 2-127, 2-128, and 2-55). Rubin suggests that some small normal faults form aseismically during multiple dike-injection events (Ref. 2-129). Bjornsson and others observed offsets of up to 2 meters (6.5 feet) along normal faults during intrusion into the Krafla volcanic rift zone, Iceland, while the largest associated earthquake was magnitude 3.8 (Ref. 2-130).

The second method for estimation of the upper bound maximum magnitude of seismicity associated with potential future dike-injection events on the Eastern Snake River Plain uses the empirically based relationship of fault-area versus moment magnitude developed by Wells and Coppersmith (Ref. 2-131). Table 2.6-6 shows the range of magnitudes, $3.3 \leq M_w \leq 5.3$, derived from the fault area vs. moment

magnitude relationship for normal fault lengths within the Arco and Lava Ridge-Hells Half Acre volcanic rift zones (Ref. 2-90). These values are somewhat similar to the observational values shown in Table 2.6-7. Using this relationship to estimate the maximum magnitude results in an upper bound for several reasons (Ref. 2-127): 1) deformation can occur aseismically and seismic moment release may be small compared to total moment released through inelastic deformation (Refs. 2-132, 2-133, and 2-129); 2) faults rupture in small increments in tandem with dike propagation; 3) dike-induced normal faults have shallow downdip widths resulting in small areas for rupture (Ref. 2-134); 4) using magnitude-fault area relationships assumes rupture along the entire length, but observations indicate that the faults move in small increments or even aseismically; and 5) the relationship of moment magnitude to fault area assumes a crustal value for rigidity (3×10^{11} dyne/cm²) which may be lower for near-surface volcanic rocks, to appropriately describe volume changes (approximately $0.5\text{--}1.8 \times 10^{11}$ dyne/cm²) (Refs. 2-132, 2-133, and 2-135).

Recurrence intervals of the dike-induced seismicity within the Eastern Snake River Plain volcanic rift zones are based on the volcanic rock record (Ref. 2-40). For the current INEEL probabilistic assessment, the maximum magnitude (M_w 5.5) earthquake is assumed to occur during each dike-injection episode even though observational seismicity during dike-injection events in Iceland and Hawaii show that most episodes of dike injection are accompanied by earthquakes of magnitude 3.5 or less.

2.6.2.3.2 Northern Basin and Range Province

Centennial Tectonic Belt

The 1983 surface-wave magnitude 7.3 Borah Peak, Idaho, earthquake is the largest event to occur in the Centennial Tectonic Belt (Figure 2.6-22 and Figure 2.6-27). Figure 2.6-30 shows a map of the Borah Peak earthquake intensity distribution (Ref. 2-67). The focus of the earthquake was at a depth of 16 ± 4 kilometers (9.9 ± 2.4 miles), near the base of the seismogenic crust, at the south end of the Thousand Springs segment of the Lost River fault (Ref. 2-86). It ruptured to the northwest producing 36 kilometers (22 miles) of surface faulting along the Thousand Springs segment and a portion of the Warm Springs segment. It also produced a surface scarp with a maximum of 2.7 meters (8.8 feet) of vertical displacement (Ref. 2-65). The Borah Peak mainshock and aftershocks define a normal fault dipping 40 to 50 degrees to the southwest, which is consistent with dips determined from first motions, body-wave analysis, and geodetic observations (Table 2.6-5) (Ref. 2-66). The stress drop determined from seismic moment is 17 bars, and from geologic data is 12 bars. Even considering the possible sources of error in the calculations, the stress drop probably did not exceed 75 bars, suggesting that the Borah Peak earthquake was a low stress-drop event, compared to other normal faulting earthquakes in the same magnitude range (Ref. 2-86).

Red Rock Valley. This August 20, 1999, M_b 5.3 earthquake was felt throughout the region, to distances of 325 kilometers (202 miles). Items were knocked from shelves in the epicentral area, but no significant damage was reported. The mainshock had a focal depth of 10 ± 1 kilometers (6 ± 0.6 miles). P-wave first motion data from the mainshock and largest aftershock indicate predominantly dip-slip on a northwest-trending, moderately dipping normal fault. The earthquake and aftershocks are interpreted to be associated with a crossover structural zone between the east-dipping Red Rock normal fault and the west-dipping Monument Hill fault, range-bounding faults with later Quaternary displacements (Ref. 2-136).

Intermountain Seismic Belt

Several moderate- to large-magnitude earthquakes can be correlated to tectonic structures within the central part of the Intermountain Seismic Belt near the Eastern Snake River Plain (Figure 2.6-22).

Hansel Valley. The March 12, 1934, M_L 6.6, Hansel Valley, Utah, earthquake was felt over an area of 440,000 square kilometers (169,885 square miles) and reached Modified Mercalli intensity VIII (Ref. 2-79).

Shenon (Ref. 2-137) mapped north-trending subparallel fractures displacing salt flats and unconsolidated late Quaternary sediments in the southwestern part of Hansel Valley over an area 6 kilometers (3.7 miles) wide and 12 kilometers (7.4 miles) long. Up to 50 centimeters of vertical displacement and 25 centimeters horizontal offset were reported by dePolo and others (Ref. 2-138). The focal mechanism from seismic wave-form modeling by Doser (Ref. 2-139) indicates that the main shock occurred along a strike-slip fault with left-lateral slip on a northeast-trending structure. The event originated at a focal depth of 8 to 10 kilometers (3.7 to 7.4 miles) and had a subsurface rupture length of 11 kilometers (6.8 miles) (Ref. 2-139).

Cache Valley. Reanalysis of seismograms for the August 30, 1962, M_s 5.7, Cache Valley earthquake indicates that it may be associated with the Temple Ridge fault, a less prominent feature with only 500 meters (1640 feet) of Neogene throw, located east of the East Cache fault (Ref. 2-140). Focal depth is estimated to be 10 ± 2 kilometers (7.4 ± 1.2 miles) and focal mechanisms from first motions and body wave analysis suggest predominantly dip-slip normal faulting with dips of 49 and 58 degrees, respectively, to the west, and small components of right-lateral strike-slip motion (Refs. 2-141 and 2-140). Woodward-Clyde Consultants (Ref. 2-46) estimated Brune and RMS stress drops of 25.2 ± 5.2 bars and 45 ± 4 bars, respectively.

Pocatello Valley. The March 28, 1975, M_b 6.1, Pocatello Valley earthquake occurred along a northeast-trending structure with a large left-lateral component of slip (Ref. 2-142).

Figure 2.6-32 shows the Modified Mercalli intensity distribution (Ref. 2-71). Studies of the aftershock sequence were consistent with a fault dip of 39 degrees to the northwest (Ref. 2-143). The event originated at a focal depth of about 9 kilometers (5.6 miles) (Table 2.6-5) and has an inferred stress drop of about 50 bars for initial faulting (Ref. 2-142).

Draney Peak. The February 3, 1994, M_w 5.7 Draney Peak earthquake occurred along buried subsidiary structures in the hanging wall of the Star Valley normal fault. The mainshock focal mechanism indicates normal slip along a northerly-striking fault. Hypocenters in the 25- to 30-kilometer (15- to 18-miles) long north-south trending aftershock zone form two diffuse, non-copolar zones dipping east-northeast. Aftershock focal mechanisms show predominantly normal faulting with a mixture of dip-slip, strike-slip, and some reverse mechanisms (Ref. 2-144).

2.6.2.3.3 Yellowstone Plateau

Hebgen Lake Earthquake

The August 18, 1959, surface-wave magnitude 7.5, Hebgen Lake earthquake is the largest event to occur in the Intermountain Seismic Belt region. Figure 2.6-29 shows the Modified Mercalli intensity distribution (Ref. 2-145). Seismic wave-form analysis by Doser (Ref. 2-63) indicates that the main shock was a double event consisting of subevent one, an M_b 6.3 followed 5 seconds later by subevent two, an M_b 7.0. Doser's analysis also suggests that the rupture occurred along one or more fault planes with east-west strike orientations (Table 2.6-5) slightly discordant with the trace of surface faulting along the Hebgen and Red Canyon faults. Maximum vertical displacements of 6.7 meters (22 feet) over a surface scarp length of 23 kilometers (14 miles) and 6.1 meters (20 feet) over 14.5 kilometers (9 miles) were observed along the Red Canyon and Hebgen faults (Refs. 2-100 and 2-146). A 1-meter (3-foot) scarp was observed along a 3-kilometer (1.8-mile) segment of a fault adjacent to Madison Canyon, but it is difficult to determine whether it was related to coseismic movement associated with the Hebgen Lake earthquake (Ref. 2-100).

Focal mechanisms derived from first motions and body-wave analysis for the subevents indicates normal faulting with dips ranging between 40 to 60° to the southwest. Subevent 1 initiated at a focal depth of 10 kilometers (6.2 miles) and subevent 2 at 15 kilometers (9.3 miles). The estimated stress drop for the main shock is 115 bars (Ref. 2-63).

Yellowstone Caldera

The June 30, 1975, M 6.1, Yellowstone Park earthquake occurred near the northern rim of the Yellowstone Caldera. Figure 2.6-33 shows the Modified Mercalli intensity distribution. The focal depth of this event was shallow, 6 kilometers (3.7 miles). Aftershock studies and first motions suggest normal faulting along a northwest-trending structure dipping about 70 degrees to the northeast (Ref 2-147).

2.6.2.3.4 Northern Rocky Mountains

Clarkston Valley

The July 10, 1925, magnitude 6.8, Clarkston, Montana, earthquake was felt over an 800,000-square-kilometer area and reached a Modified Mercalli intensity of VIII in the epicentral area (Ref. 2-52). Although this earthquake was large, it produced no surface scarp, but some ground cracks were observed (Ref. 2-148). Seismic wave analysis indicates a focal depth of 9 kilometers (5.6 miles), a rupture length of 25 kilometers (15.5 miles), and oblique normal slip on a northwesterly-dipping plane (Table 2.6-5) (Ref. 2-149).

Virginia City

The November 23, 1947, magnitude 6.3 Virginia City earthquake may be associated with rupture along a portion of the northwest-trending Madison Canyon fault, based on first motions (Ref. 2-150). Reanalysis using seismic waveforms suggests a combination of strike-slip and dip-slip faulting (right-lateral oblique slip) along a normal fault striking east-west. Doser suggests that fault motion at depth in this part of the Hebgen Lake/Madison region occurs along structures striking nearly east-west and that the northwest strike of surface faulting may reflect the trend of preexisting weaknesses that the earthquake ruptures

exploited as they propagated to the surface. The event originated at a focal depth of about 8 kilometers (5 miles) (Ref. 2-149).

2.6.2.3.5 Maximum Earthquake Potential

Patterns of seismicity and locations of mapped faults have been used to assess potential sources of future earthquakes for estimating ground shaking at INEEL. As shown in Figure 2.6-23, the sources and maximum magnitudes of earthquakes that could produce the maximum levels of ground motions at the ISF site include: (1) a magnitude 7.15 earthquake at the southern end of the Lemhi fault; (2) a magnitude 7.25 earthquake at the southern end of the Lost River fault; (3) a magnitude 5.5 earthquake associated with dike injection in either the Arco or the Lava Ridge-Hell's Half Acre volcanic rift zone and the axial volcanic zone; (4) a background magnitude 5.5 earthquake in the Eastern Snake River Plain; and (5) a background earthquake with magnitude up to 6.75 in the northern Basin-and-Range Province (Ref. 2-47). Ground motion contributions from other sources such as the postulated Eastern Snake River Plain boundary fault, northern Basin-and-Range Province, Yellowstone Plateau, and Idaho Batholith are significantly smaller due to their distant locations or lower maximum magnitudes.

Lemhi Fault-Howe Segment

The Howe segment, at the southern end of the Lemhi fault, is the closest part of the Lemhi fault to the INEEL (Figure 2.6-35). The ISF site is about 26 kilometers (16.1 miles) from the mapped southern termination of the Howe segment (Ref. 2-47). The most recent event (MRE) occurred between 15,000 and 24,000 years ago (Ref. 2-88). The lengths of the Howe and Fallert Springs (the segment just north of the Howe segment (Figure 2.6-36) segments are approximately 15 to 20 kilometers (9.3 to 12.4 miles) and 25 to 30 kilometers (15.5 to 18.6 miles), respectively (Refs. 2-155, 2-152, and 2-91). Recent paleoseismic investigations (four trenches excavated across the segments) by Woodward-Clyde Consultants (Refs. 2-46 and 2-88) indicate that the MRE could have ruptured portions of both the Howe and Fallert Springs segments, resulting in a total length of 35 kilometers (21.7 miles). For the MRE, maximum and average displacements are 2.5 and 1.5 meters, respectively (Ref. 2-88). The maximum magnitude estimated for the southern Lemhi fault is 7.15, based on empirical data from Wells and Coppersmith (Ref. 2-131) using: (1) surface rupture length; (2) subsurface rupture length; (3) rupture area (length x down-dip extent; 31 x 21 kilometers (19 x 13 miles) (Figure 2.6-37); (4) maximum displacement; and (5) average displacement (Refs. 2-46 and 2-47). The slip rate of 0.1 millimeter/year for both the Howe and Fallert Springs segments is lower than the estimated 0.3 millimeter/year for the Thousand Springs segment of the Lost River fault, indicating that the Howe segment is less active (Ref. 2-65).

Lost River Fault-Arco Segment

The Arco segment is at the southern end of the Lost River fault and is the part of the fault closest to the INEEL (Figure 2.6-23). The north and south ends of the Arco segment have been mapped at different locations by various investigators. The northern terminus was originally mapped at King Mountain (Refs. 2-49 and 2-153), but has more recently been established at Ramshorn Canyon (Refs. 2-65, 2-154, 2-85, and 2-155). Woodward Clyde Federal Services (Ref. 2-47) use the Ramshorn Canyon terminus in their detailed analysis of fault behavior. The location of the southern terminus is less certain. Three scenarios are possible. Scenario 1: The fault ends about 1 kilometer (0.6 mile) south of Arco, where scarps that are mapped along the main range front disappear under alluvium in the Arco Basin (21 kilometer [13 miles] total length, 9 kilometer [5 miles] west of the INEEL boundary). Scenario 2: The

fault ends about 2 kilometers (1.2 miles) south of the range-front scarps in an area west of Butte City where scarps in basalt lava flows occur. Most evidence (Refs. 2-47 and 2-90) supports this interpretation (25 kilometer [15.5 miles] total length, 7 kilometers [4.3 miles] west of the INEEL boundary). Scenario 3: suggests that the terminus may lie 7 kilometers (4.3 miles) southeast of Butte City at a set of monoclinial flexures in the northwest end of the Arco volcanic rift zone (30 kilometer [18.6 miles] total length, 1 kilometers [0.6 mile] west of the INEEL boundary). Each of these scenarios is used in the 1996 probabilistic seismic hazards assessment for INEEL (Ref. 2-56).

The most recent and penultimate events on the Arco segment occurred between 21 ± 4 and 20 ± 4 thousand years ago, possibly with contemporaneous rupture on the Pass Creek segment to the north. Maximum magnitude estimates for the Arco segment range from 6.6 to 7.3 (Ref. 2-156). The uncertainty in magnitude is due to uncertainty in rupture length, uncertainty in assumptions that the measured displacements represent average or maximum values, and the apparent discrepancy between length-based and displacement-based magnitudes. The net vertical displacement at the Arco Peak site (on the Arco segment) averages 1.2 to 1.5 meters (3.9 to 4.9 feet) per event. The best estimate of slip rate between 58,000 and 20,000 years ago is 0.12 millimeters per year (Refs. 2-65 and 2-156).

Beaverhead Fault–Blue Dome Segment

The Blue Dome segment is at the southern-most end of the Beaverhead fault (Figure 2.6-23). The ISF site is 52 kilometers (32 miles) horizontal distance from the Blue Dome segment. Stickney and Bartholomew (Ref. 2-157) estimate the MRE at more than 30,000 years ago. More recent mapping in the area suggests that it has not been active for several hundred thousand years because no scarps are present on Quaternary alluvial fans (Ref. 2-92). The length of the segment is estimated to be about 25 kilometers (15.5 miles). Woodward-Clyde Consultants (Ref. 2-46) estimates a maximum magnitude of 7.0 for an earthquake on along the Blue Dome fault, based on analogy to the Lemhi and Lost River faults further to the west. Several investigators suggest that this segment has a slip rate of 0.02 mm/year to 0.3 mm/year (Ref. 2-65).

Eastern Snake River Plain Volcanic Zones

Volcanic vents are not randomly distributed on the Eastern Snake River Plain, but occur in discrete zones. Most vents occur in northwest-trending volcanic rift zones and a concentration of vents also occurs along the axis of the Eastern Snake River Plain. Volcanic rift zones on the Eastern Snake River Plain contain a variety of structures, other than volcanic vents, that suggest an association with shallow northwest-trending dikes in the subsurface. These structures include fissures, fissure swarms, fault scarps, and monoclines, all of which have been observed in active volcanic rift zones of Iceland and Hawaii and demonstrated to be associated with shallow dike intrusion (Refs. 2-123 and 2-124). The great age range of exposed volcanic rift zones on the Eastern Snake River Plain (from over 1 million years to 2000 years (Refs. 2-40 and 2-42) suggest that basaltic volcanism throughout the history of the Eastern Snake River Plain has been fed by volcanic rift zone processes. The northwest trend of volcanic rift zones and the dikes that produce them is controlled by the regional northeast-directed extensional stress field (Ref. 2-39). The same stress field produces northwest-trending normal faults, northwest-trending fault-block mountain ranges, in the Basin-and-Range province to the north and south of the Eastern Snake River Plain.

The long-term (about 4 million years ago to present) intrusion of northwest-trending basalt dikes into the Eastern Snake River Plain has accommodated northeast-directed extension that was elsewhere

accommodated by normal faulting (Ref. 2-106). The supplanting of normal faulting and its associated earthquakes in the Eastern Snake River Plain by dike intrusion is the mechanism that best explains the relatively aseismic nature of the Eastern Snake River Plain with respect to the surrounding Basin-and-Range Province and Yellowstone Plateau (Refs. 2-116 and 2-126).

Arco Volcanic Rift Zone

The Arco volcanic rift zone extends from the southern end of the Lost River Range across the southwestern corner of the INEEL (Figure 2.6-23). The ISF site is about 14 kilometers (8.7 miles) away from the closest point on the boundary of the rift zone. The rift zone is about 8 kilometers (5 miles) wide and 20 kilometers (12.4 miles) long (Refs. 2-157 and 2-48). Small normal faults within the rift zone are 5 to 6 kilometers (3 to 3.7 miles) in length, have maximum cumulative vertical offsets of about 12 meters (39 feet) (multiple offsets) and are postulated to extend to a depth of 2 kilometers (1.2 miles) below the surface (Refs. 2-121, 2-47, 2-46). A set of fissures in the Box Canyon graben area is collinear with the small normal faults (Table 2.6-8) bounding the graben, which results in a total length of 8 kilometers (5 miles). Based on the compilation of earthquake data for active rift zones, a maximum magnitude of 5.5 is assumed possible for future dike-injection events within the rift zone. This is consistent with a magnitude of 5.2, based on the assumption that an earthquake associated with dike injection ruptures a fault area of 16 square kilometers (length x depth; 8 x 2 kilometers [5 x 1.2 miles]; Figure 2.6-37) (Refs. 2-46 and 2-47). The most recent volcanic activity in the central part of the volcanic rift zone appears to have been about 95,000 years ago (Refs. 2-159, 2-48, 2-158, and 2-160). The 10,000 to 13,000 year old Cerro Grande and North and South Robbers lava flows occur at the southern end of the volcanic rift zone at its intersection with the axial volcanic zone (Ref. 2-48).

Lava Ridge-Hell's Half Acre Volcanic Rift Zone

The Lava Ridge-Hell's Half-Acre volcanic rift zone extends from the southern end of the Lemhi range across the INEEL to the southeastern corner (Figure 2.6-23). The ISF site is about 28 kilometers (17.4 miles) away from the closest point on the boundary of the rift zone. The rift zone is 3 to 6 kilometers (1.8 to 3.7 miles) wide and 50 kilometers (31 miles) long. At the southern end of the rift zone, two sets of fissures, which may or may not be associated with small normal faults (Table 2.6-8), are about 4 kilometers (2.5 miles) in length (Ref. 2-108). Because portions of the fissures are covered by younger lava flows, the fissure sets could extend 11 kilometers (6.8 miles) farther south. A maximum magnitude of 5.5 was assumed possible for earthquakes associated with future dike-injection events within the Lava Ridge-Hell's Half-Acre rift zone, based on the compilation of earthquake data shown in Table 2.6-7. This is consistent with a magnitude of 5.5, which was estimated using fault area (15 x 3 kilometers = 30 square kilometers [18.6 square miles]) and assuming rupture along the entire fissure lengths (Refs 2-46 and 2-47). The most recent volcanic activity within the Lava Ridge-Hell's Half-Acre rift zone occurred with the eruption of the Hell's Half Acre volcanic field at its intersection with the axial volcanic zone about 5200 years ago (Refs. 2-158 and 2-48).

Howe-East Butte Volcanic Rift Zone

The postulated Howe-East Butte volcanic rift zone extends across the central portion of the INEEL from the range front south of Howe to East Butte (Figure 2.6-23). It is poorly expressed surficially and is mostly covered by fluvial and lacustrine sediment (Ref. 2-161). The ISF site is within the postulated Howe-East Butte volcanic rift zone. Woodward-Clyde Consultants (Refs. 2-46 and 2-47) consider the

maximum magnitude for the Howe-East Butte to be 5.5, similar to the Arco and Lava Ridge-Hell's Half-Acre volcanic rift zones. Volcanic vents in the Howe-East Butte volcanic rift zone are dated at 580,000 to 641,000 years old (Ref. 2-48), and a conservative minimum age for the Howe-East Butte volcanic rift zone is 230,000 years, based on the age of lava flows from the axial volcanic zone that cover volcanic rift zone structures and vents (Ref. 2-48).

Axial Volcanic Zone

The axial volcanic zone is located along the Eastern Snake River Plain axis and crosses portions of the INEEL's southern and eastern boundary. The ISF site is about 13 kilometers (8 miles) from the closest point of the axial volcanic zone boundary. Dike-induced structures are near the intersections of the Arco and Lava Ridge-Hell's Half Acre volcanic rift zones with the axial volcanic zone. Thus, a maximum magnitude of 5.5 is assumed possible, based on the interpretation that dike injection mechanisms in the axial volcanic zone are similar to those in other Eastern Snake River Plain volcanic rift zones. The most recent volcanic activity took place about 5000 years ago at the Hells Half Acre lava field (Refs. 2-159 and 2-48).

Great Rift Volcanic Rift Zone

The Great Rift volcanic rift zone crosses the Eastern Snake River Plain in the northwest to southeast direction. It is about 70 kilometers (45 miles) in total length, but is divided into three segments with slightly different trends. The three segments range in length from 15 to 30 kilometers. The ISF site is 45 kilometers northwest from the closest approach of the Great Rift.

The dimensions of fissure sets along the Great Rift are similar to those in the Lava Ridge-Hell's Half Acre volcanic rift zone; thus, a magnitude 5.5 is possible for earthquakes associated with future dike intrusion events. The most recent volcanic activity in the Great Rift occurred about 2000 years ago (Ref. 2-159). Because of the great distance of the Great Rift from the ISF site, ground motions resulting from volcanic seismicity will be less than ground motions from Eastern Snake River Plain background seismicity and seismicity associated with closer volcanic rift zones.

Eastern Snake River Plain Background Province

Although instrumental seismicity indicates that the Eastern Snake River Plain is relatively aseismic, an earthquake similar in size to the 1905 Shoshone event is considered possible within the Eastern Snake River Plain. For estimating ground motions at INEEL, an earthquake of maximum magnitude 5.5 is postulated to occur anywhere within a 25-kilometer radius of each facility. This is referred to as a "background earthquake" and is commonly used for design of commercial nuclear reactors to assess effects from earthquakes that may occur on unknown faults (those without surface exposures).

Northern Basin and Range Background Province

The northern Basin and Range background source region surrounds the Eastern Snake River Plain. Excluding known normal faults that are capable of generating magnitude 7.0 events, a background earthquake with a maximum magnitude of 6.75 is possible within this source region on unknown or "blind" faults (Refs. 2-46 and 2-47). Doser suggests that earthquakes of magnitude 6.0 to 6.75 could occur in the intermountain seismic belt without producing surface rupture, and thus would leave no

geologic record of their occurrence (Ref. 2-162). An example of this phenomena is the 1975 ML 6.0 Pocatello Valley earthquake near the Idaho-Utah border. This event occurred on a "blind" (not evident in surface geology) cross-fault that trended transverse to the trend of nearby Basin and Range normal faults (Ref. 2-143).

Idaho Batholith Background Province

The Idaho Batholith is a seismically quiet region and its boundaries are defined by the extent of granitic rocks associated with the batholith. No extensive or well-defined Quaternary faults are mapped within the Idaho Batholith (Refs. 2-46 and 2-47). Although seismographic coverage is poor (a detection threshold of $M \geq 3$), it appears to have a low seismic potential (Ref. 2-48). Woodward-Clyde Consultants estimated the maximum magnitude to be Mw 5.5 (Refs. 2-46 and 2-47).

Yellowstone Plateau Background Province

The Yellowstone Plateau is the topographically high region of the Yellowstone volcanic field and surrounding areas. The elevation of the plateau averages approximately 2500 meters (8202 feet) and, in addition to the Yellowstone Caldera, it includes the Beartooth uplift to the east, the Hebgen Lake fault zone to the west, and the Teton Range to the south. It is an area of extremely high heat flow, profuse seismicity, abundant geothermal activity, low seismic velocity, low gravity, and rapid vertical crustal movements, all of which suggest high temperatures and perhaps magma bodies at relatively shallow depths in the crust (Ref. 2-92). Since detailed recording began in 1973, the maximum magnitude of seismicity within the Yellowstone Caldera has been about 4.5 and the focal depths have been less than 10 kilometers (6.2 miles). Outside the caldera and along the Caldera rim, Yellowstone Plateau seismicity attains a greater focal depth (approximately 20 kilometers [12.4 miles]) and greater magnitude. It includes the 1959 Hebgen Lake (M_S 7.5) event, largest earthquake in the Intermountain Seismic Belt and the 1975 Yellowstone Park (M_L 6.1) earthquake. Thus, the maximum magnitude of Yellowstone Plateau seismicity is assumed to be M_S 7.5 for the INEEL probabilistic seismic hazards assessment (Refs. 2-47 and 2-56).

2.6.2.3.6 Regional Seismic Wave Transmission Characteristics

For the ground motion modeling studies, regional attenuation was characterized by a frequency-dependent quality factor, $Q(f)$. Singh and Herrman (Ref. 2-163) determined a regional crustal coda Q_0 of 450 and h of 0.2 for $Q(f)$ in the Basin and Range northwest of the Eastern Snake River Plain. Braille and others (Ref. 164) observed high attenuation in the 1978 Eastern Snake River Plain seismic refraction experiment within the Eastern Snake River Plain for the P-wave quality factor Q_p . They attributed it to low Q values in the volcanic rocks (Q_p 20 to 200) and throughout the crust (Q_p 160 to 300). Woodward-Clyde Consultants (Refs. 2-45, 2-56) used the model parameters of Q_0 and h from Singh and Herrman (Ref. 2-196) in their deterministic analyses. They also suggest that the relatively short source-to-site distance of 20 km does not significantly attenuate earthquake ground motions.

Near-Surface Geological Attenuation

Woodward-Clyde Consultants (Ref. 2-45) indicate that near-surface geology (0 to 5 km depth) has a significant influence on earthquake ground motions at a site. The INEEL resides upon the Eastern Snake River Plain which is covered with basalt lava flows and sediments. Boreholes throughout the INEEL site

indicate the basalt is interbedded with sedimentary layers; in some areas, the percentage of interbeds reached 50 percent.

This unique stratigraphy has the affect of deamplifying or decreasing the level of earthquake ground motions because seismic waves travel through a sequence of alternating high (basalt) and low (sediments) velocity zones that tend to scatter the seismic energy. Also, seismic energy is intrinsically dampened by the sedimentary interbeds. The net effect of the interbedded basalt is to reduce the level of earthquake ground motions when compared to a homogeneous basalt (no interbeds) (Refs. 2-45, 2-56, 2-47). The amount of deamplification is dependent on the difference between the velocities for the basalt and sedimentary layers, but probably is in the range of 20 to 25 percent.

Figure 2.6-38 shows the shear-wave velocity (V_s) profile determined to estimate earthquake ground motions at the INTEC (Refs. 2-56, 2-47). The velocity model was derived from using well and borehole logs located at and near INTEC. Since the velocity model has large contrasts (basalt vs. sediment), the velocity profiles were smoothed to taper the large effects of scattering which resulted in low-amplitude spectra. Regional earthquakes were digitally recorded near two boreholes at TRA (about 3 km northwest of the TMI-2 ISFSI site). These data were used to estimate the near-surface attenuation, k , and to determine the amount of smoothing in the velocity profiles.

2.6.2.4 Probabilistic Seismic Hazard Analysis

Both deterministic and probabilistic seismic hazard studies to evaluate potential earthquake ground motions have been conducted at the INEEL since the early 1970s for establishing seismic design criteria. Since that time, ground motion seismology and federal regulations (NRC and DOE) have continued to evolve, and geoscience investigations have continued at INEEL. To keep pace with these changes, site-specific deterministic and probabilistic ground motion studies were completed for the INEEL facility areas during the 1990s. These studies formed the basis for development of site-specific probabilistic and deterministic ground motions at the TMI-2 ISFSI site. Recent changes in NRC requirements for power reactors allow for the use of probabilistic seismic design parameters (Ref. 2-165). DOE-ID has also updated the *DOE/ID Architectural Engineering Standards* to include probabilistic seismic design parameters for the INTEC (Ref. 2-166). The ISF design earthquake parameters are based on the recent probabilistic analysis results for INEEL and are discussed in Section 2.6.2.4.5.

The probabilistic approach to the seismic design was approved by the NRC for the TMI-2 ISFSI. An exemption request was submitted to the NRC with the ISF Facility License Application.

2.6.2.4.1 1977 Probabilistic Seismic Hazard Study

In 1977, a probabilistic seismic hazard study was conducted by Agbabian Associates (Ref. 2-167) for the New Waste Calcining Facility site at the INTEC to calculate the probability of experiencing the design earthquake during the service life of the facility (Table 2.6-9). The procedure used the mathematical model of Der Kiureghian and Ang (Ref. 2-168). The investigators used three source areas having magnitude ranges from 6.75 to 7.5 with corresponding intensities of IX-X and recurrence intervals based on a limited historical earthquake catalog. They developed intensity attenuation relationships using five regional earthquakes (1935 MMI VII Helena, Montana; 1959 MMI X Hebgen Lake, Montana; 1962 MMI VII Richmond, Utah; 1967 MMI VII Tushar-Sevier Central, Utah; and 1975 MMI VII Pocatello Valley,

Idaho). Their results suggested that for a peak horizontal acceleration of 0.40 g on rock, there is 0.01 percent chance of exceedance in 100 years (Table 2.6-9).

2.6.2.4.2 1984 Probabilistic Seismic Hazard Study

In a 1984 probabilistic seismic hazard study, Tera Corporation calculated probabilities of peak horizontal accelerations for the Argonne National Laboratory West site on the INEEL. They developed seismic hazard maps for all of the INEEL including the INTEC.

Their methodology used the Tera (Ref. 2-169) model developed from the work of Mortgat et al (Ref. 2-170). They specified nine source regions, three of which included the major range-bounding faults (Lost River, Lemhi, and Beaverhead). The magnitudes for the source regions ranged from 6.5 to 7.75. The recurrence intervals for the sources regions were derived from a 17-year earthquake record of the local region.

The attenuation relationship was based on Campbell (Ref. 2-171) and Tera (Ref. 2-172) incorporating values of crustal attenuation determined from regional earthquake recordings (Ref. 2-163) and the results of the Eastern Snake River Plain refraction survey (Ref. 2-77). For the INTEC, the resulting seismic hazard maps show 0.18 g at a return period of 1,000 years and 0.30 g at a return period of 10,000 years (Table 2.6-9).

2.6.2.4.3 1996 Probabilistic Seismic Hazard Evaluation

The 1996 probabilistic seismic hazards evaluation by Woodward-Clyde Federal Services (Ref. 2-47) was conducted for the INEEL facility areas including the INTEC. This study has undergone extensive peer review and provides the basis for developing seismic design parameters to be used at the INEEL.

The probabilistic methodology used in the study is based on Cornell (Ref. 2-173) and Youngs and Coppersmith (Ref. 2-174). It provides for explicit inclusion of the range of scientifically defensible seismologic and tectonic interpretations, including seismic source characterization and ground motion attenuation models (consistent with approaches in NRC Regulatory Guide 1.165, "Identification and Characterization of Seismic Sources and Determination of Safe Shutdown Earthquake Ground Motions," Sections C 1 through 3). Uncertainties in conceptual models and parameters were incorporated into the hazard through use of logic trees. Sensitivity analyses were performed to examine the important contributors to the total hazard and to the uncertainties in the hazard. This evaluation incorporated results of all geologic, seismologic, and geophysical investigations conducted for the INEEL since the 1960s.

Earthquake magnitudes and recurrence rates were assessed for the earthquake sources that contribute to potential ground motions at the INTEC site. The four closest sources (Figure 2.6-23) that contribute to the hazard at INTEC include:

- Basin-and-Range normal faults, characterized by magnitudes ranging from M_w 6.5 to 7.75 based on fault dimensions (surface length, displacements, and area) and recurrence methods based on slip rates or recurrence intervals.
- Northern Basin-and-Range background seismicity which is characterized by magnitudes ranging from M_w 6.25 to 6.75 and recurrence models are based on the historical earthquake record (1884 to 1992).

- Eastern Snake River Plain background seismicity, characterized by magnitudes ranging from M_w 5.0 to 6.0 based on the possible occurrence of the 1905 Shoshone earthquake within the Snake River Plain. Because the Eastern Snake River Plain is aseismic, the recurrence is estimated by assuming that one-third of the time earthquakes of this magnitude range occur in the Eastern Snake River Plain and two thirds of the time earthquakes of this magnitude range occur outside the Eastern Snake River Plain.
- Volcanic rift zones of the Eastern Snake River Plain, characterized by magnitudes ranging from 4.5 to 5.5 based on analogy with other active volcanic rift zones and measurements of fault dimensions for small normal faults produced by dike injection within the volcanic rift zones. The recurrence intervals are based on the recurrence of volcanism (Table 2.6-10).

A site-specific attenuation relationship was developed for the INTEC site using the stochastic numerical ground motion modeling approach (Refs. 2-47 and 2-45) and results of shear-wave velocity measured in boreholes at the INTEC. In addition, four empirical ground motion attenuation relationships (unmodified for style of faulting factors), that represent the uncertainty in empirical modeling of earthquake ground motions, were used in the study. The site-specific stochastic attenuation relationship was weighted at 0.6 because it is representative of the Eastern Snake River Plain geological conditions, which are vastly different from typical California sites. The empirical attenuation relationships (Refs. 2-45 and 2-175) were weighted individually based on their relative applicability, but total to a combined weight of 0.4.

Results of the INEEL seismic hazard evaluation significant to the ISF Facility include (Ref. 2-47):

- The ISF Facility is located within the Eastern Snake River Plain, which is characterized by a low rate of seismicity and small magnitude earthquakes. Thus, the background earthquakes within the Eastern Snake River Plain contribute little to the hazard at the ISF Facility.
- There is little contribution from the volcanic rift zones because the volcanic episodes have long recurrence intervals (more than 15,000 years) and any associated seismicity is characterized by small magnitude (less than 5.5) earthquakes.
- In general, the stochastic relationship results in lower motions at short periods than the empirical relationships because of the interbedded volcanic stratigraphy, which has a lower velocity gradient in the upper 1 kilometer (0.6 mile) than homogeneous rock, and the alternating high and low velocities, which tend to dampen out high-frequency ground motions.
- At shorter return periods (less than 2000 years) the hazard is dominated by the northern Basin-and-Range background seismicity due in part to the extremely low level of seismicity in the Eastern Snake River Plain and the long recurrence intervals of the Basin-and-Range faults.
- The Basin-and-Range faults contribute more to the hazard at 10,000 years because this return period approaches the average recurrence interval of the faults.

The results of the 1996 probabilistic seismic hazard evaluation are for rock in the form of mean peak horizontal accelerations and uniform equal hazard spectra for return periods of 500, 1000, 2000, and 10,000 years. For the INTEC, the peak horizontal acceleration is 0.13 g at a return period of 2000 years (Table 2.6-9).

2.6.2.4.4 1999 Probabilistic Seismic Hazard Analysis

In 1999, URS Greiner Woodward-Clyde Federal Services recomputed the probabilistic seismic hazards for all INEEL facility areas evaluated in 1996, including the INTEC, to incorporate stochastic modeling and empirical attenuation relationships more applicable for extensional tectonic regimes (Refs. 2-176 and 2-177).

Specifically, the stress drop median in the stochastic modeling was reduced from 75 to 50 bars based on recent evaluations of stress drops and extensional attenuation relationships (Refs. 2-47, 2-178, 2-179, 2-180 and 2-181). The distribution for the site-specific stochastic modeling has a median of 50 bars (0.6 weight) with a range of 25 bars (0.2 weight), 75 bars (0.15 weight), and 150 bars (0.05 weight) to include a range of uncertainty about the preferred value.

The empirical attenuation relationships used in this analysis were based on adjustments for extensional tectonic regimes used for the Yucca Mountain Site Characterization Project (Yucca Mountain Project). The Yucca Mountain Project ground-motion experts recognized that use of empirical attenuation relationships based primarily on California strong ground motions (strike-slip and thrust faulting earthquakes) for seismic hazard assessments in the Basin-and-Range Province would overestimate ground motions of normal faulting earthquakes. To address this issue, the Yucca Mountain Project ground-motion experts developed scaling relationships that account for differences in earthquake sources of California strike-slip versus normal faulting to modify the empirical attenuation relationships (Ref. 2-182). For recomputation of the INEEL seismic hazards, only scaling relationships and similar weighting distribution were adopted to modify the empirical attenuation relationships selected by the Yucca Mountain Project ground-motion experts for applicability to extensional tectonic regimes (Refs. 2-176 and 2-177).

Regulatory Guide 1.165 (Appendix C) recommends supplementing the probabilistic seismic hazard by response spectra shapes of the dominant earthquakes at low (1 to 2.5 Hertz [Hz]) and intermediate (5 to 10 Hz) frequencies to arrive at the design earthquake response spectrum. In this analysis, the recomputed rock uniform hazard spectra were deaggregated to determine the contributions from dominant earthquakes at low and intermediate frequencies. The uniform hazard spectra were then supplemented by these results of the deaggregation to derive the smoothed, 5 percent damped horizontal rock response spectra at 1000, 2000, and 10,000 years return periods, in accordance with the steps outlined in Regulatory Guide 1.165. The vertical rock response spectra were obtained by multiplying the vertical to horizontal spectral ratios developed for the INEEL to the horizontal response spectra.

The peak horizontal accelerations for rock at 1000, 2000, and 10,000 years return periods were calculated to be 0.09g, 0.11g, and 0.18g respectively. The peak vertical accelerations for rock were 0.07g, 0.09g, and 0.14g at 1000, 2000, and 10,000 years return periods respectively.

2.6.2.4.5 Probabilistic Seismic Hazard Applicable to ISF Site

Payne et al. (Ref. 2-183) adjusted the rock uniform hazard spectra at 2000 and 10,000 years return periods developed for the INTEC by URSG-WCFS in 1999 (Refs. 2-176 and 2-177) to be applicable to larger facility areas at INEEL. The larger facility areas included the INTEC, TRA, RWMC, and PBF. The 2000-year return period uniform hazard spectra was also increased by 8 percent to account for a 2500-year return period in anticipation of revisions to the *DOE-ID Architectural Engineering Standards*

(Ref. 2-166). The adjusted 2,500-year return-period rock uniform hazard spectra are also applicable to the ISF site in developing the design earthquake parameters.

The horizontal rock design earthquake response spectra were developed by incorporating smoothed, broadened regions of the peak accelerations, velocities, and displacements defined by the adjusted 2500-year return-period rock uniform hazard spectra. Portions of the rock design earthquake response spectra were adjusted to ensure conservatism for the structural design process. Figure 2.6-39 reflects the 2500-year return period horizontal rock design earthquake response spectra for 5 percent damping compared to the adjusted 2500-year return-period rock uniform hazard spectra. The peak ground acceleration (PGA) at the rock outcrop is 0.123g. Two statistically independent horizontal time histories (Figure 2.6-40 and Figure 2.6-41) were developed from the 2500-year return period horizontal rock response spectrum in accordance with the requirements of Seismic Analysis of Safety-Related Nuclear Structures (ASCE-98). The enveloping criteria used for matching the time histories with the design earthquake response spectra also satisfy the requirements of Standard Review Plan 3.7.1 (Ref. 2-184). These horizontal rock time histories constitute the control motions for the ISF site for performing the site soil response analysis.

The 2500-year return-period vertical rock design earthquake response spectra were calculated using the vertical to horizontal (V/H) spectral ratios developed for the INEEL.

2.6.2.5 Seismic Wave Transmission Characteristics of the ISF Site

2.6.2.5.1 Development of Basecase and Randomized Soil Profiles

Geotechnical investigations of the INEEL ISF site included eight boreholes and eight test pits to characterize the soil. Downhole measurements were conducted in two of the boreholes to establish shear-wave and compression-wave velocity data for the soil layers. Four seismic refraction lines were also run (Figure 2.6-13). The INEEL ISF site is underlain by dense to very dense sandy gravel over basalt rock. The dense sandy gravel extends from the ground surface to an average depth of about 2.5 feet. Most of this layer will be removed as construction progresses. The very dense sandy gravel ranges to about 25 to 30 feet below the ground surface where it is underlain by basalt rock. The soil layers at the ISF site are uniform over the proposed locations for the buildings and the depth to bedrock is shallower than at other areas of INTEC (including the TMI-2 site). The static and dynamic properties of subsurface materials determined from the site geotechnical and geophysical investigations were used in the development of base case soil profiles.

The base case soil profile was defined by the depth to each soil and rock layer. S-wave velocities and unit weight for each layer was developed from soil measurement at the ISF site (Figure 2.6-42) (Ref. 2-185). From the base case shear wave velocity and soil profile, the computer program RANPAR (Ref. 2-186) was used to generate 30 site-dependent, randomized soil profiles. Both shear wave velocity and total depth of profile were randomized. The statistical variation for development of the randomized soil profiles was based on site-specific soil data from borings and shear-wave measurements taken at various locations on the INTEC site (all within about one-half mile [0.8 kilometer] of the ISF facility). The resulting 30 randomized shear wave velocity profiles are presented in Figure 2.6-43, showing the mean minus one standard deviation, the mean, and the mean plus one standard deviation profiles with the 30 randomized profiles.

2.6.2.5.2 Selection of Mean Ground Motion Hazard Level

The mean horizontal ground motion hazard was developed by calculating the response of the 30 profiles to each of the two horizontal components of the 2500-year return-period rock motions. The computer program ProShake (Ref. 2-187) was used to calculate the response. Figure 2.6-44 and Figure 2.6-45 show the results of the individual response calculations, along with the mean results, in the form of 5 percent damped response spectra in each of the two horizontal directions. The mean values presented in these figures are representative of the mean ground motion hazard that may be expected at the site. The response spectral values are computed at the frequencies recommended in Standard Review Plan 3.7.1. The peak ground accelerations of the calculated responses are plotted at a period of 0.01 seconds.

A specific “design earthquake” response spectra at the ground surface is not defined for the ISF site because the actual time histories from the soil response analysis, along with their associated strain-iterated soil properties are preserved for direct input into the soil structure interaction analysis. However, the mean ground motion hazard curves thus developed, if smoothed and broadened, could be considered the free-field horizontal design response spectra for the site.

2.6.2.6 Design Earthquake Ground Motion

To account for uncertainties in the soil-structure interaction analysis, the approach used was to vary the soil shear modulus between an upper and lower bound about the best estimate value. The goal of the site response analysis was to develop three sets of three-component surface acceleration time histories (corresponding to three sets of strain-iterated soil properties) whose mean response spectral values were consistent with the mean level of ground motion hazard presented above. These three sets of ground motion time histories, two horizontal and one vertical, were developed from site-specific analyses as described in the following sections.

2.6.2.6.1 Development of Horizontal Design Earthquake Ground Motion

From each of the 30 soil response analyses, strain-iterated shear modulus and damping ratio versus depth profiles were obtained, as shown in Figure 2.6-46 and Figure 2.6-47 respectively. The soil degradation models used in the iteration calculations are shown in Figure 2.6-48 (Ref. 2-185). The mean minus one standard deviation, the mean, and the mean plus one standard deviation strain-iterated profiles were then calculated from the data in these figures for each of the two horizontal directions. The strain-iterated dynamic soil properties for the three soil profiles are presented in Table 2.6-11.

The soil response analyses, using the program ProShake, were then performed on the mean minus one standard deviation, the mean, and the mean plus one standard deviation strain-iterated profiles in each horizontal direction using the same input rock motions, holding the soil properties constant. The results of these analyses are presented in the form of 5-percent damped acceleration response spectra at the ground surface in Figure 2.6-49 and Figure 2.6-50 for each of the two horizontal directions respectively.

The mean spectral values of the three response spectra presented in Figure 2.6-49 and Figure 2.6-50 are plotted against the mean of the 30 randomized cases (representing the mean ground motion hazard level) in Figure 2.6-51 and Figure 2.6-52. The two mean response spectra are reasonably similar. Thus, the three horizontal acceleration time histories corresponding to the three response spectra in each of the two horizontal directions are consistent with the mean levels of ground motion hazard.

The three free-field horizontal design earthquake time histories for each of the two components of horizontal ground motions, corresponding to the mean minus one standard deviation, the mean, and the mean plus one standard deviation strain-iterated soil profiles, are presented in Figure 2.6-53, Figure 2.6-54, and Figure 2.6-55 respectively.

2.6.2.6.2 Development of Vertical Design Earthquake Ground Motion

As previously discussed, the vertical design earthquake time histories developed at the bedrock outcrop by Payne et al. (Ref. 2-183) are not appropriate for use in soil response or soil-structure interaction analyses.

1. The current state of knowledge for seismology is in debate about whether the vertical component of earthquake motions can be modeled solely from vertically propagating compressional (P) wave.
2. The vertical response spectra at rock were developed from the V/H ratio which includes higher motions at frequencies between 10 and 30 Hz based on empirical data. The empirical data account for the content of the seismic waves generating the vertical motions. Thus, propagating the vertical component of the earthquake time histories through a soil column may result in unnecessary conservatism.

The vertical design earthquake ground motion for the INEEL ISF site was developed by performing the following steps:

1. The response spectra for the horizontal design earthquake ground motion time-histories discussed in Section 2.6.2.6.1 were multiplied by the empirical ratio of vertical to horizontal ground motions applicable to INEEL as shown in Figure 2.6-56. This resulted in target vertical ground surface acceleration response spectra at 2-percent and 5-percent damping.
2. For each pair of horizontal ground surface motions, the vertical-to-horizontal ratio was applied to the component of horizontal motion with the slightly higher spectral response to develop a target vertical response spectrum. A total of three vertical target response spectra (corresponding to the three soil profiles) were developed from the three pairs of horizontal ground surface motions.
3. A previously recorded vertical acceleration time-history that has the characteristics desired in the final vertical ground surface motion was selected. The criteria considered in selecting previously recorded vertical ground motion for spectral matching included: 1) seismic sources in an extensional tectonic regime, preferably in the Basin-and-Range Province of the western United States; 2) seismic moment magnitude and the source-to site distance ranges; and 3) the site subsurface conditions. The Anderson Dam Left Abutment motion was chosen for use in the spectral matching analyses.
4. The computer program RASCAL (Ref. 2-188) was used to develop a vertical ground surface acceleration time-history using the vertical ground surface response spectrum for 2-percent damping (from step 1) and the phase spectrum of the selected recorded motion (step 2) as input.

5. Baseline correction of the resulting time-history was performed using the computer program BASECOR (Ref. 2-189).
6. The individual values of the spectral match by RASCAL for the 2-percent damping target spectra were checked to ensure that they were at or above the target between 0.25 Hz and 50 Hz. Portions of the 2-percent spectrum and the entire 5-percent spectrum were checked that no more than 5 points fell below the target spectrum, and that all the points that fell below the target spectrum were within 10 percent of the target in accordance with NUREG-0800 and NUREG/CR-5437 (Refs. 2-184 and 2-190).
7. There were a few points that did not meet the requirements for enveloping. Therefore, additional spectral matching of the time histories was performed using the program RSPMATCH to better fit the target spectra. After processing by RSPMATCH, the resulting vertical time histories were again baseline corrected with the program BASECOR to minimize the displacement drive.
8. The durations of the final artificial vertical time histories were checked to be similar to that of the horizontal time-histories.

Figure 2.6-57, Figure 2.6-58, and Figure 2.6-59, show the vertical target spectra and the final vertical ground-surface acceleration response spectra for 5-percent damping for the mean minus one standard deviation, the mean, and the mean plus one standard deviation strain-iterated soil profiles, respectively. The three vertical acceleration time histories corresponding to these three vertical ground-surface response spectra are plotted in Figure 2.6-53, Figure 2.6-54, and Figure 2.6-55.

2.6.3 Surface Faulting

Surface faulting, defined as the rupture of the earth's surface due to tectonic or magmatic activity, is of concern in some areas of the INEEL, but not at the ISF site itself. The only place on the INEEL that could be affected by surface faulting related to tectonic activity is near the southern tip of the Lemhi fault, which is approximately 40 kilometers (25 miles) from the ISF site (Figure 2.6-22 and Figure 2.6-35). Surface faulting associated with an earthquake on the Howe and Fallert Springs segments could extend into the INEEL for a distance of several kilometers in the area just east of the Big Lost River sinks.

Surface faulting is of concern in volcanic rift zones. Areas in and near the Arco and the Lava Ridge-Hells Half Acre volcanic rift zones (Figure 2.6-22) have the greatest potential for such dike-induced surface faulting. Also, the fissures north of the Naval Reactor Facilities (Figure 2.6-60) appear to be dike-induced fissures. The potential recurrence of such fissuring is tied closely to periods of volcanic activity in volcanic rift zones.

2.6.3.1 Geologic Conditions of ISF Site

See Section 2.6.1.3.2, *Stratigraphy and Areal Geology - ISF Site*.

2.6.3.2 Evidence of Fault Offset

No evidence for fault offset at or near the surface exists in the immediate vicinity of the ISF site or INTEC. Several lineaments are visible on aerial photographs and Landsat images. These lineaments are

mostly northeast-trending alignments of contrasting density and distribution of vegetation whose origin is most likely due to aeolian modifications of old range-fire scars.

A dense array of borings in the INTEC area adjacent to the ISF site, and several excavations to bedrock, have revealed no evidence of surface ruptures or displacements in the near-surface basalt lava flows. Geologic cross sections based on lithologic and geophysical logs of many of these holes show no evidence of near-surface faulting.

Lithologic relationships in numerous borings and wells in the INTEC area show no evidence for folding or faulting in the subsurface. Although some basalt lava flows are present in parts of the area and absent in others, it has been demonstrated that they have not been structurally disrupted. Their discontinuous distribution is due to pinching out of lava that flowed into the Big Lost River valley from vents to the southeast and southwest.

2.6.3.3 Earthquakes Associated with Capable Faults

No capable faults have been identified in the INTEC area, and no significant earthquakes have been recorded or reported in the area. Several microearthquakes have been recorded in the INEEL area since 1972, but they were not felt and they do not define or correlate with faults.

2.6.3.4 Investigation of Capable Faults

See Section 2.6.2.2.2, *Identification and Description of Earthquake Sources: Faults*.

2.6.3.5 Correlation of Epicenters with Capable Faults

The only earthquake epicenters in the INTEC area are microearthquakes. They are not correlated with, nor do they define, capable faults. There are no capable faults in the INTEC area.

2.6.3.6 Description of Capable Faults

There are no capable faults within 8 kilometers (5 miles) of the ISF site. However, at a distance of 9 kilometers (6 miles), just northwest of the Naval Reactor Facility, is an east-trending, 2-kilometer (1.2-miles) long fissure that has a section about 335 meters (1100 feet) long with vertical displacement of about 2 meters (7 feet) (Ref. 2-108). A little over 2 kilometers (1 mile) northwest of this fissure is a shorter northwest-trending fissure (Figure 2.6-60). Although these fissures are outside the 8-kilometer (5-mile) radius stipulated by regulation, the small amount of existing information relating to their origin and age is presented here.

These appear to be dike-induced fissures like those in the Eastern Snake River Plain volcanic rift zones, but they occur outside of well-defined volcanic rift zones. The east trend of the southernmost fissure is not consistent with the trend of fissures that would form under the present northeast directed extensional stress field. They occur within the postulated Howe-East Butte volcanic rift zone, the most poorly defined volcanic rift zone on the Eastern Snake River Plain. It has the lowest vent density, and, if the fissures northwest of Naval Reactor Facility are part of it, only two fissures. The lava fields within the postulated volcanic rift zone are 300,000 to 600,000 years old (Ref. 2-42).

The age of the fissures can be constrained only within broad limits. They cut rocks that are 400,000 to 730,000 years old (Ref. 2-48), so they must be younger than that. They are covered in places by recent (younger than 5000 years) alluvial sediments (Ref. 2-49), so they must be older than that. Although some untried methods could be applied to try to further constrain their age, the chances of success are small.

Information available from geologic mapping of the fissures northwest of Naval Reactor Facility and from mapping of volcanic rift zones elsewhere on the Eastern Snake River Plain suggests that the Naval Reactor Facility fissures do not pose a surface-faulting threat to the ISF site. The evidence is:

- The fissures possess many of the characteristics of volcanic rift zone fissures (dike-induced fissures), i.e., mostly dilational displacement, local zones of minor vertical displacement, west to northwest trend, magnitude of dilation and minor vertical offset consistent with injection of a single dike. They do not appear to be tectonic faults.
- Because the age of basalt lavas and four volcanic vents in the area (Ref. 2-48) are between 400,000 and 700,000 years old, it is likely, but not proven, that the fissures are close to that age also. This is because the fissures require dike intrusion for their formation and the most likely time for dike intrusion to have happened was during or soon after the development of the volcanic vents in the area.
- No recognized tectonic faults occur near the fissures.
- The section of the southernmost fissure with vertical displacement is so short (approximately 1100 feet [355 kilometers]) that any prehistoric seismicity associated with its formation would have been low magnitude.

2.6.3.7 Zone Requiring Detailed Faulting Studies

No recorded earthquakes or structures are present within 5 miles (8 kilometers) of the ISF site. Also, the fissures north of Naval Reactor Facility are more than 5 miles (8 kilometers) from the ISF site. Therefore, there is no zone requiring detailed faulting studies.

2.6.3.8 Results of Faulting Investigations

No detailed faulting investigations are necessary within the 8-kilometer (5-mile) radius and none have been done for the fissures northwest of Naval Reactor Facility.

2.6.4 Stability of Subsurface Materials and Foundations

2.6.4.1 Geologic Features

2.6.4.1.1 Surface or Subsurface Subsidence

Due to the nature of geologic materials and the processes of their formation, several conditions can contribute to subsidence. As summarized below, none of these conditions exist at the ISF site.

Lava Tubes

Lava tubes are linear open cavities that allow lava to flow from its source vent. Their observed dimensions in basalts of the Eastern Snake River Plain range up to several tens of kilometers in length

and 10 meters (32 feet) in diameter. No lava tubes are recognized in the lava flows at or near the ISF site, and the dense pattern of borings in the INTEC area has revealed none in the subsurface. The potential for subsidence due to lava tubes at the ISF site is extremely low.

Interflow Rubble Zones

In some areas of the Eastern Snake River Plain and the INEEL, interflow rubble zones with large void volumes have been observed in outcrops and in borings. However, none have been revealed in the drilling in the INTEC area.

Fine-Grained Sediments

Surficial sediments at the ISF site are alluvial deposits of the Big Lost River and consist mostly of sandy gravels and gravelly sands. Their thickness ranges from 8 to 10 meters (25 to 30 feet), and they are underlain by basalt bedrock. Under the adjacent INTEC, some boreholes identified a 1- to 2-meter (3-foot to 7-foot) thick clay layer just above the basalt bedrock however, this clay layer is not present on the ISF site. Several sediment interbeds ranging from 1 to 6 meters (3 to 20 feet) thick occur within the basalt bedrock between some of the lava flows. These interbeds occur at depths of about 30 meters (100 feet), 46 meters (150 feet), 61 meters (200 feet), 84 meters (275 feet), 122 meters (400 feet), 177 meters (580 feet), and 216 meters (710 feet) (Ref. 2-191). The interbeds are composed mostly of fine-grained silty sands with some clay lenses. Due to infiltration of water from settling ponds, sewage lagoons, and pipe leaks from the INTEC, some of the interbeds are saturated with perched water bodies. The surficial sediments are not saturated except in the area directly beneath the settling ponds at the south end of the INTEC, over 305 meters (1000 feet) from the ISF site. The surficial sediments are not saturated, except in the area directly beneath the settling ponds at the south end of the INTEC, over 305 meters (1000 feet) from the ISF site.

2.6.4.1.2 Previous Loading History

Rocks at the surface of the Eastern Snake River Plain have no previous loading history. The slow subsidence of the Eastern Snake River Plain basin during the past 4 million years has resulted in the continuous accumulation of the basalts and sediments of the Snake River Group. Rocks and sediments at the surface have never been subjected to lithostatic or tectonic loading.

2.6.4.1.3 Rock Jointing and Weathering Patterns, Weak Materials

Previous geotechnical studies provided information on two types of discontinuity that exist in the rocks beneath the INTEC area, adjacent to the ISF site. The first is discontinuity between lava flows, a result of the emplacement process of the lava flows. The zones between lava flows typically are characterized by a layer of rubble or breccia (Figure 2.6-8), composed of blocks of basalt that broke from the advancing front of the overlying lava flow and formed a layer of broken blocks over which the flow advanced. These interflow rubble zones range up to a meter thick and commonly possess a great amount of void space between blocks. After burial, that void space can remain open and contribute to groundwater flow in the aquifer, or it can become filled with silty sediments and become a barrier to water flow. In addition to basal rubble zones, development of fissures in the upper part of lava flows is common during emplacement. This development is caused by bending and tilting of solidified crust (sometimes several meters thick) during flow of still-molten lava beneath. Fissures developed by this process can be up to

2 meters (7 feet) wide and 3 to 5 meters (10 to 16 feet) deep. They form complex, irregular patterns on the lava flow surface and often are crudely parallel to the edge of the flow. They are occasionally filled by surficial sediments before burial by younger lava flows.

The second type of structural discontinuity in lava flows is related to cooling and contraction of the lava flow after solidification. This process produces columnar jointing in the lava flow, with columns polygonal in cross section and perpendicular to the lava flow surfaces (Figure 2.6-8). The cooling process also causes development of platy joints parallel to and near the upper and lower surfaces of the lava flow. These two sets of joints cause the basalt to break into columnar blocks and irregular plates when it is weathered and eroded or when it is broken by excavation or mining.

Fine-grained sedimentary interbeds between lava flows can cause structural weakness in some areas, but at the INTEC, adjacent to the ISF site, the first interbed occurs at a depth over 30 meters (98 feet) and would not affect foundation integrity. Surficial sediments, being composed of gravels and coarse sands, are not prone to structural weakness.

2.6.4.1.4 Unrelieved Residual Stresses

Geologic units at and near the surface at the ISF site, and throughout the Eastern Snake River Plain, have never been buried to greater depths than they are at present, and thus they have not acquired residual stresses from great lithostatic or tectonic loads. The stresses generated during cooling and contraction of the basalt lavas were relieved by development of the columnar jointing and platy fracture patterns.

2.6.4.2 Properties of Underlying Materials

The following properties of underlying materials are contained in the *Idaho Spent Fuel Project Geotechnical Engineering Report* (Ref. 2.51), where applicable.

Grain-size classification is a reflection of the material makeup of the subsurface materials. Observations of the solids in the borings and test pits at the central ISF site reflect conditions of about 2 to 5 feet (0.6 to 1.5 meters) of dense sandy gravel, overlaying about 25 feet (7.6 meters) of very dense sand and gravel. Basalt bedrock was encountered between 25 and 30 feet (7.6 and 9.1 meters) below ground surface (see Figure 2.6-14 through Figure 2.6-21).

Atterberg limits relate to the plasticity characteristics of the clays and other cohesive sediments of the soil. Atterberg limits cannot be effectively determined on sediments with low cohesive properties, like those at the ISF site.

Moisture content is the weight of water per unit weight of solids. Because the moisture content of gravels and sands from the ISF site area is so low, generally less than 10 percent, reflecting the unsaturated condition of the soils, there is little potential for either liquefaction or for consolidation.

Unit weight is the weight of solids per cubic foot of soil. The design value for the ISF site soil was taken as 135 pounds per cubic foot, based on laboratory results.

Shear modulus (G) is the ratio of shear stress to shear strain. Shear modulus values for the ISF site are reflected in Table 2.6-11.

Poisson's Ratio is the ratio of transverse to axial strain. Value was calculated to be 0.33 for the soils on the ISF site, based on the average value of shear and compression waves. Most sands worldwide have values from 0.3 to 0.35, so the alluvial soils on the ISF site are fairly typical.

Damping is a measure of the vibration energy-absorbing characteristic of the soil. The damping values for the ISF site are reflected on Table 2.6-11.

Consolidation characteristics consist of the coefficient of consolidation (C_v), and the compression index (C_c). For non-cohesive, granular soils (as those at the ISF site) the transfer of load to the soil framework is immediate and there is little time dependent behavior.

Seismic wave velocities are the velocities at which seismic waves travel through material. The seismic compression wave (V_p) is the velocity at which a seismic compression wave travels through the material, often referred to as primary-wave velocity. Shear velocity (V_s) is the velocity at which a seismic shear wave travels through the material, often referred to as secondary-wave velocity. The seismic wave velocities for the ISF site are reflected on Table 2.6-11.

Density is a measure of the site soil density with respect to the possible range of densities for that particular soil type. The relative densities reported for soils in the INTEC area are mostly in the range of 40 to 100 percent, corresponding to dense to very dense sands, and thus have a low potential for further compaction or liquefaction.

Porosity is the fraction or percentage of bulk volume not occupied by solids (i.e., the fraction or percentage of bulk volume occupied by voids or pores). Porosity reported for INTEC area soils are in a range of 30 to 40 percent and are slightly lower than porosity for most graded gravels and sands composed of rounded grains (36 to 46 percent).

Strength characteristics (shear strength) are parameters that describe the resistance to shear. They are cohesion or interparticle attraction (C), and the angle of internal friction or the resistance to interparticle slip (ϕ). The C values for the sandy gravel soil are considered to be zero, indicating a cohesionless soil. The angle of internal friction for ISF site sandy gravels ranges from 35 to 46 degrees. This indicates a relatively high resistance to interparticle slip.

2.6.4.3 Plot Plan

Figure 2.6-13 details the location of borings and graphic profiles with the locations of ISF Facility structures.

2.6.4.4 Soil and Rock Characteristics

Table 2.6-11 and Table 2.6-12 detail the static and dynamic engineering properties of materials underlying INTEC and the ISF site.

2.6.4.5 Excavations and Backfill

The excavations at the ISF site will be for the installation of site utilities and foundation excavations. Native soils are suitable for use as backfill material when properly compacted.

2.6.4.6 Groundwater Conditions

The construction and operation of the ISF Facility will not affect groundwater, and the groundwater will not affect the ISF Facility, as detailed in Section 2.5.

2.6.4.7 Response of Soil and Rock to Dynamic Loading

Table 2.6-11 provides analysis of the ISF site soil and rock in response to dynamic loading.

2.6.4.8 Liquefaction Potential

Liquefaction is a process in which seismic shear waves cause an increase in the pore water pressure in noncohesive soil strata. This increase of pore pressure in noncohesive soil strata reduces effective stress confining the soil. The reduction in effective confining stress reduces the shear modulus of the soil, which results in increased soil deformation.

The alluvial deposits above the basalt at the ISF site are mostly sand and gravel with an average gravel content of about 44 percent. Because this material is coarse and far above the water table, liquefaction is not a concern at the ISF site (Ref. 2-51).

2.6.4.9 Earthquake Design Basis

See Section 2.6.2, *Vibratory Ground Motions*.

2.6.4.10 Static Analysis

Static analysis of foundations is performed as part of the facility structural design, to ensure stability of the foundations against overturning, sliding, and excess bearing pressures.

2.6.4.11 Techniques to Improve Subsurface Conditions

No improvements in subsurface conditions are necessary.

2.6.5 Slope Stability

Slopes in the ISF site area are small (Figure 2.6-13), a few feet per mile at most, and pose no threat for instability or landsliding.

2.6.5.1 Slope Characteristics

There are no slopes, natural or engineered, on the ISF site.

2.6.5.2 Design Criteria and Analyses

Design criteria and analyses for slope stability are not applicable to the ISF site.

2.6.5.3 Logs of Core Borings

No borrow areas are anticipated.

2.6.5.4 Compaction Specifications

Site construction specification will require that the facility footprint and pavement areas be cleared of any vegetation and debris. Fill required to bring the site to grade or to backfill excavations, will be placed in loose lifts not to exceed 12 inches (34 centimeters). Each lift will be moisture conditioned to near optimum moisture content prior to compaction. Fill will be compacted as determined by ASTM D 1557.

2.6.6 Volcanism

2.6.6.1 Introduction

Basaltic and rhyolitic volcanism has affected the Eastern Snake River Plain since 10 million years ago, and has continued into recent geological time. No historical eruptions have occurred on the Eastern Snake River Plain, but as recently as 2100 years ago, lava flows issued from the Great Rift, about 25 kilometers (15 miles) southwest of the INEEL. Other Holocene epoch basaltic lava fields near the southern INEEL boundary range from about 5000 and 13,000 years in age (Ref. 2-159). Many basaltic vents and three rhyolitic vents within the present INEEL boundary erupted between about 200,000 and 1.2 million years ago (Ref. 2-48). For these reasons, an assessment of volcanic hazards at the ISF site is warranted, and such an evaluation is based on the record of past volcanism in the region.

This section summarizes information on the timing, distribution, and eruptive character of volcanism that could affect the ISF site. Potential volcanic hazards are grouped into two categories: 1) those related to volcanic sources within the INEEL area, and 2) those related to distant sources outside the Eastern Snake River Plain. For near-field volcanism, the volcanic history of the Eastern Snake River Plain and the INEEL area (Figure 2.6-5, Figure 2.6-6 and Figure 2.6-9) dictates that three varieties of volcanism be evaluated:

- the formation of future silicic calderas and associate eruptions of voluminous ash and pumice, as occurred in the INEEL area between about 6.5 and 4.3 million years ago, during passage of the Yellowstone mantle plume (Ref. 2-30) (Figure 2.6-5)
- the growth of new silicic lava domes near INEEL, as occurred at Big Southern Butte (0.3 million years ago), East Butte (0.6 million years ago) and elsewhere along the axial volcanic zone near the southern portion of the INEEL (Figure 2.6-9) (Ref. 2-48)
- phenomena related to Quaternary Eastern Snake River Plain basaltic volcanism, largely involving the effusion of lava flows and magma-induced ground fissuring across the INEEL area (Figure 2.6-6)

Potential impacts from distant volcanic sources include: 1) pyroclastic flows or tephra fall from explosive-silicic eruptions of the Yellowstone plateau, 100 to 200 kilometers (62 to 124 miles) northeast of the INEEL; and 2) tephra fall from the Cascade volcanoes and other explosive volcanic centers in the western United States.

2.6.6.2 Potential Volcanic Hazards of the INEEL/ISF Site

The nature and timing of volcanism is reconstructed from interpretation of Eastern Snake River Plain volcanic deposits, and from the results of potassium-argon dating of volcanic rocks. Observations of historical volcanic phenomena are also useful toward understanding prehistoric INEEL volcanism,

particularly the volcanic rift zone eruptions of Iceland and Hawaii, and the growth of silicic lava domes at volcanic centers along the Pacific Rim.

2.6.6.2.1 Formation of Eastern Snake River Plain Silicic Calderas and Related Volcanism

Explosive, voluminous eruptions of silicic pumice and ash and associated caldera collapse occurred on the Eastern Snake River Plain during passage of the Yellowstone Hotspot between about 6.5 and 4.3 million years ago (Refs. 2-30 and 2-29) (Figure 2.6-5). Tephra-fall and pyroclastic-flow deposits from these eruptions, known as the Heise volcanism, were dispersed over tens of thousands of square kilometers in southern Idaho and adjoining states.

The risk of explosive silicic volcanism and caldera formation in the INEEL area and at the ISF site is negligible for the following reasons.

- The mantle plume (Yellowstone Hotspot) - the apparent energy source of voluminous, caldera-forming, silicic volcanism on the Eastern Snake River Plain - has now moved under the Yellowstone Plateau, 100 to 200 kilometers (62 to 124 miles) northeast of the INEEL, and accounts for the Quaternary period silicic volcanism and ongoing hydrothermal activity of that area (Refs. 2-29 and 2-30).
- Thermal modeling and geophysical studies of the Eastern Snake River Plain crustal structure (Ref. 2-77) show that the silicic magma chambers inferred to have existed in the shallow crust of the Eastern Snake River Plain during the late Tertiary period are now entirely solidified and are therefore incapable of erupting.
- The recurrence intervals (quiescent periods) between major caldera eruptions on the Eastern Snake River Plain and the Yellowstone Plateau lasted 0.5 to 1.7 million years. Therefore, 2.5 to 8 recurrence intervals (it has been 4.3 million years since the last such Eastern Snake River Plain eruption) have elapsed in the INEEL area. This suggests that caldera-related silicic volcanism has ceased.
- The time-transgressive pattern of the Eastern Snake River Plain-Yellowstone silicic volcanism suggests that explosive silicic volcanism expires after basaltic lava flows have filled the calderas. On the Eastern Snake River Plain, the late-Tertiary silicic calderas are buried by up to several kilometers of late-Tertiary to Quaternary basalt and sediment.
- Geothermal, geophysical, and geodetic anomalies indicate the presence of large shallow silicic magma chambers at such places as Yellowstone National Park and Long Valley, California. The anomalies include extremely high heat flow, low seismic velocities at shallow crustal levels, abundant hot spring and geyser activity, persistent swarms of seismic activity, and rapid rise and fall of land surface elevations (Refs. 2-31, 2-32, 2-78, 2-79, and 2-80). None of these phenomena occur beneath the Eastern Snake River Plain.

2.6.6.2.2 Growth of Rhyolitic Domes, Intrusions, and Related Phenomena

Volcanic domes are steep-sided mounds of lava, commonly of silicic (rhyolitic) composition. The magma is too viscous to flow more than a few kilometers from the vent. The growth of domes is predominantly an effusive process, and blocks of the surrounding terrain can be uplifted and tilted as the viscous magma

approaches the surface (Ref. 2-192). Growing domes are steep sided, unstable, and therefore prone to slope failure. In addition, dome lavas commonly contain sufficient dissolved gas to generate small explosions. As a result, small-volume tephra-fall deposits and blocky pyroclastic flows are frequently associated with dome growth.

During the past 1.2 million years several small rhyolite domes were emplaced in the INEEL area along the axial volcanic zone (Figure 2.6-9): Big Southern Butte (0.3 million years ago), Cedar Butte (0.4 million years ago), East Butte (0.6 million years ago), Middle Butte (inferred as uplifted by a shallow silicic intrusion; uplifted basalt dated at 1.1 million years), and an unnamed butte (1.2 million years) (Refs. 2-192 and 2-193). The estimated recurrence interval for the Eastern Snake River Plain silicic-dome effusion in the INEEL area is 200,000 years (5×10^{-6} per year), based on these 5 domes, emplaced within a one-million-year period (1.2 million years ago to 0.3 million years ago).

The Quaternary rhyolitic domes postdate the earlier caldera-related silicic volcanism by about 3 million years, and they are compositionally dissimilar to the caldera rhyolites, suggesting a distinct phenomenon. Although tephra falls and small-volume pyroclastic flows are commonly associated with silicic-dome growth, no such deposits have been identified in the INEEL area, probably because they have been covered by younger basaltic lava and sediment. Several centimeters of tephra could accumulate 10 kilometers (6 miles) or more downwind of growing volcanic domes. Given the flat terrain of the Eastern Snake River Plain, the major effects of dome effusion, intrusion and uplift, pyroclastic volcanism and corrosive gases would likely be restricted to within about 5 kilometers (3 miles) of a growing volcanic dome. Any fumes and tephra associated with dome growth along the axial volcanic zone would probably be carried northeastward along the southern INEEL boundary, and eventually off site, by prevailing southwesterly winds.

Based on the apparent 200,000 year recurrence interval (5×10^{-6} per year) and the likely restriction of hazardous phenomena to near-vent areas, the probability of a silicic dome affecting the central and northern portion of the INEEL (including the ISF site) is judged to be small (less than 10^{-6} per year). The most likely area of future silicic-dome emplacement is along the axial volcanic zone; hence, the probabilistic risk of impact on southern-INEEL facilities would be somewhat higher, but still less than 10^{-6} per year.

2.6.6.2.3 Basaltic Volcanism and Related Phenomena

With the exception of localized and infrequent silicic dome volcanism (Figure 2.6-9), Quaternary volcanism of the INEEL area has been predominantly basaltic. Potassium-argon dating of lava flows demonstrates that basaltic vents on the INEEL range in age from more than 1 million years on the northern portion of the INEEL, to about 0.2 million years on the southern portion of the INEEL near the axial volcanic zone (Ref. 2-48). Although their vents are not situated on the INEEL, four Holocene epoch basalt lava fields erupted along the axial volcanic zone between about 13,000 and 5000 years ago. In one case, the 13,400 years old Cerro Grande lava field crossed what is now the southern INEEL boundary. Quaternary period basaltic volcanism on the Eastern Snake River Plain has involved mostly mild, effusive outpourings of fluid lava flows from eruptive fissures and small, low-lying shield volcanoes (Ref. 2-192).

Volcanic Rift Zones

Basaltic vents are not randomly disseminated across the INEEL area, but tend to concentrate in northwest-trending, linear belts known as volcanic rift zones (Figure 2.6-60) (Ref. 2-42). These belts are marked by basaltic vents as well as open fissures, monoclines and small normal faults—structures produced during propagation of vertical dikes that fed the surface eruptions (Figure 2.6-61). Eastern Snake River Plain volcanic rift zones are inferred to be underlain by basaltic-dike swarms, based on their surface-deformation features and their equivocal correspondence with positive aeromagnetic and gravity anomalies (Ref. 2-194). Eastern Snake River Plain volcanic rift zones are polygenetic features, i.e., were apparently active through numerous cycles of volcanism. The Great Rift (Figure 2.6-6) has well-developed volcanic landforms and surface-deformation features that formed during eight cycles of Holocene volcanism (Ref. 2-195).

The Arco volcanic rift zone is more diffuse and diachronous, with fissures and vents dispersed across an 8-kilometer (5-mile) wide belt (Figure 2.6-6 and Figure 2.6-62), formed by multiple cycles of volcanism between 600,000 to 10,000 years ago. The Lava Ridge-Hells Half Acre volcanic rift zone is strongly diachronous; its northern portion is occupied by lavas greater than 1 million years old, and its southern terminus is marked by the 5200-year-old Hells Half Acre lava field and dike-induced fissures (Figure 2.6-6 and Figure 2.6-62). Its central region is poorly developed, and is marked by a single monocline that was likely induced by dike intrusion (Figure 2.6-62). The Howe-East Butte volcanic rift zone is poorly expressed surficially, and is largely covered by fluvial and lacustrine sediment on the central portion of the INEEL; five vents and several isolated fissures are associated with a positive, northwest-trending aeromagnetic anomaly (Ref. 2-161).

Axial Volcanic Zone

The most voluminous and recent volcanism in the INEEL area occurred during the past 1.2 million years along the axial volcanic zone, a broad, northeast-trending constructional-volcanic highland consisting of coalesced basaltic-shield volcanoes, tephra cones, and isolated silicic domes. The axial volcanic zone forms a topographic divide along the Eastern Snake River Plain axis. It differs from volcanic rift zones because northwest-trending fissure swarms that typify volcanic rift zones are rare, and its overall topographic orientation is perpendicular to the regional stress field. Basaltic dike intrusion processes along the axial volcanic zone are probably similar to those of volcanic rift zones, but increased magma supply along the Eastern Snake River Plain axis and the predominance of large shield volcanoes has apparently covered most of the dike-induced surface deformation along the axial volcanic zone.

Volcanic Hazards at the ISF Site

Table 2.6-13 lists hazards associated with the Eastern Snake River Plain basaltic volcanism, based on interpretation of the Eastern Snake River Plain eruption products and analogy with historical observations of rift-zone volcanism in Hawaii and Iceland. The most significant hazard is lava flows inundating or burning facilities. Such flows vary greatly in volume and may cover a few square kilometers to 400 square kilometers (154 square miles) or more (Ref. 2-42). On gentle terrain such as the Eastern Snake River Plain, lava flows would generally move downslope at a few meters per minute. Large lava flows on the Eastern Snake River Plain seldom exceed 30 kilometers (19 miles) in length, and most are less than 12 kilometers (7 miles) long.

Borehole investigations and outcrop studies indicate that most Eastern Snake River Plain basaltic lava flows are less than 10 meters (33 feet) thick, and taper to several meters in thickness at flow edges. They are therefore unlikely to surmount major topographic or manmade obstacles. The general topography and vent locations of the INEEL area (Figure 2.3-4 and Figure 2.6-62) suggest that future lavas will most likely erupt from vents along the axial volcanic zone or at the intersections of that zone with the volcanic rift zones, from which they could flow toward the central portion of the INEEL and the ISF site.

2.6.6.2.4 Volcanic Recurrence and Probabilistic Risk for the ISF Site

Table 2.6-10 gives estimated volcanic recurrence intervals for INEEL volcanic zones and boring sites, estimated by summing individual vents and fissures in the respective volcanic zones, and dividing that sum by the total time period of volcanism within each zone. This approach gives minimum-recurrence estimates and is conservative, because it is assumed that every vent or fissure (or set of fissures, when they could be confidently grouped as cogenetic) represents a single eruptive episode. It is more likely that each eruptive episode involved eruptions from several vents and the opening of multiple fissures, based on the record of Holocene epoch volcanism and on analysis of the generation, rise, and storage of Eastern Snake River Plain magma (Ref. 2-193).

In general, Table 2.6-10, Figure 2.6-62 suggest that the shortest recurrence intervals (16,000 to 17,000 years), the most recent volcanism (Holocene lava fields), and hence the most probable areas of future basaltic volcanism and ground deformation, are the axial volcanic zone and the Arco volcanic rift zone. In this context, the INEEL Volcanism Working Group estimated the conditional probability of basaltic volcanism to affect a south-central portion of the INEEL as less than 10^{-5} per year.

For the ISF site, the probability of inundation can be more closely estimated by employing the parameters contributing to the probability. The parameters that are important to the estimation of probability include:

- volcanic recurrence interval of the source zone or zones
- topographic setting of the site and the potential sources
- lengths and areas of lava flows
- distance from the site to potential sources of lava
- potential for mitigation of the lava flow hazard

The three cases below illustrate the estimation of inundation probability.

Volcanic Source Zone	Case 1 – Probability of eruption at a random site within the source zone	Case 2 – Probability of inundation at a random site within the source zone	Case 3 – Probability of Inundation at ISF site
Combined axial volcanic zone and Arco volcanic rift zone	$6 \times 10^{-5}/\text{yr}$	$2.6 \times 10^{-6}/\text{yr}$	$5.2 \times 10^{-6}/\text{yr}$ without mitigation 10^{-6} to $10^{-7}/\text{yr}$ with mitigation

Case 1 illustrates the probability of an eruption anywhere within the volcanic source zone. It is based on the number of vents and fissure sets within the Arco volcanic rift zone and the axial volcanic zone and the age range of volcanism for those zones. It is simply the “source term,” or “recurrence term” for a zone or region, and contains no information about the magnitude of the event. It is derived by dividing the number of vent/fissure sets into the age range of volcanism, as illustrated in Table 2.6-10. It is the highest

probability of the three cases because it allows for the volcanism to occur anywhere within the combined area of the two zones and makes no prediction for any particular spot. Therefore, it is not applicable to any specific site.

Case 2 illustrates the probability of inundation of a random site within the volcanic source zone. This case goes beyond Case 1 by incorporating a “magnitude” term, and making some assessment of the likelihood that some site will be affected. The assessment of likelihood is achieved by taking into account the area of coverage of the average lava flow in relation to the total area of the source zone. Because it selects no specific spot, it ignores the effects of topography, the distance from potential sources and the potential for mitigation. It is estimated by simply multiplying the result of Case 1 (6×10^{-5} per year) by the ratio of average area covered by a typical the Eastern Snake River Plain lava flow to the total area of the volcanic source zone. The result (2.6×10^{-6} per year) is analogous to the estimation made by the INEEL Volcanism Working Group, and is in fact less than 10^{-5} per year, as the group predicted.

Case 3 is the probability of inundation at the ISF site. This assessment goes beyond Case 2 because it deals with a specific site. Therefore, the topographic setting, the statistics of lava flow length, and the potential for mitigation can be brought to bear on the problem. The ISF site lies outside the volcanic source zone, and its topographic setting in the Big Lost River valley defines the specific part of the volcanic source zone that can send lava flows on a path towards the site. This volcanic source zone is called the “critical volcanic source area.” It is defined on the south, southeast, and southwest by the topographic divide that separates the Big Lost River drainage basin from that of the Snake River. Lavas that erupt south of that divide will flow south, away from the ISF site, and are of no concern for lava inundation at the site. It is defined on the north by the northern edge of the volcanic source zone. Lavas originating from the axial volcanic zone northeast of East Butte will not flow toward the ISF site.

The critical volcanic source area encompasses 660 square kilometers (254 square miles) of the total 2270 square kilometers (876 square miles) of the combined Arco volcanic rift zone and the axial volcanic zone. In addition, the ISF site is over 10 kilometers (6 miles) (50th percentile lava flow length) from the closest approach of the critical volcanic source area (Figure 2.6-62) and most of the source area is farther than 16 kilometers (9 miles) from the site. Using the 70th percentile distance of 16 kilometers (9 miles), only 30 percent of flows from that distance will reach the site; therefore, the annual probability of inundation is 5.2×10^{-6} . This is obtained by multiplying the Case 1 probability (6×10^{-5} per year) by the percentage of the total area of the source zone encompassed by the critical volcanic source area (29 percent) and by the percentage of lava flows from the critical volcanic source area that will reach the site (30 percent). This estimated annual probability of inundation at the site (5.2×10^{-6}) is conservative for several reasons, as described below.

- The critical volcanic source area is farther from the site than the 70th percentile distance (some of it is twice that distance); therefore, much smaller percentages of lava flows will reach the site from those distances.
- The probability of eruption within the volcanic source zone is conservative because the vents are double-counted in the overlap zones of the volcanic rift zones with the axial volcanic zone. Removing this conservatism alone will reduce the annual probability of inundation at the site to 3.8×10^{-6} .
- No allowance is made for mitigation. Although the effectiveness of mitigation is difficult to assess, it is likely that actions can be taken to mitigate the hazard. The INEEL seismic network

can detect seismicity associated with rising magma from the mantle, and has appropriate station spacing to accurately locate the most likely areas of eruption. Seismicity-detected ascent rates of basaltic magmas from source regions 40 to 60 kilometers (25 to 37 miles) deep beneath Kilauea and Mauna Loa volcanoes, Hawaii, show that several weeks to several months are required for magma to rise to upper crustal chambers beneath the volcano summits. Because the magma source beneath the Eastern Snake River Plain is 50 to 200 kilometers (31 to 124 miles) deep, the seismic network may provide similar warning time even though the tectonic setting of the Eastern Snake River Plain is different from Hawaii's (Ref. 2-195).

- Basaltic lava flows on the Eastern Snake River Plain have relatively low flow velocities because of low topographic gradients. Analogy to flow velocities in other similar terrains shows that velocities of about 2 kilometers (1 mile) per day are most likely, and thus it would take several days for lava from most of the critical volcanic source area to reach the ISF site. The warning time for ISF site personnel would likely be in the range of weeks to months. Given a month or more of warning, various mitigation actions could be taken and likely be successful.

Potential mitigation actions include removal of the spent nuclear fuel canisters from the area, building of earthen berms around the facility, building of earthen berms in the flow path to slow or divert the advance, cooling of the lava flow front with water sprays to slow or divert the advance, and use of explosives at or near the vent area to divert lava flow. Some of these strategies have been used successfully in Iceland and in Italy, and are likely to be successful here. Even if mitigation were successful only half the time, the inundation probability would be further reduced to less than 2×10^{-6} per year; higher potential of success is more likely and would reduce the probabilities into the 10^{-6} to 10^{-7} range.

2.6.6.3 Potential Volcanic Hazards from Distant Sources

The Volcanism Working Group studied locations and general characteristics of potentially hazardous volcanoes in the western United States. The selective analysis below supports the general conclusion that significant impacts to the INEEL from distant volcanic eruptions are highly improbable.

2.6.6.3.1 Yellowstone Plateau

Geologic and geophysical investigations indicate that the mantle plume that left its 15-million-year track across southern Idaho and formed the Snake River Plain now resides beneath the Yellowstone Plateau. This explains the crustal structure, high heat flow, geothermal features, and explosive silicic volcanism of that area. The Yellowstone Plateau volcanic field has produced more than 6×10^{12} cubic meters (7.8×10^{12} cubic yards) of silicic tephra, largely in the form of tephra-fall and pyroclastic-flow deposits, in 3 cycles of explosive, caldera-related volcanism during the past 2.1 million years ago (Ref. 2-32). Ash layers from Yellowstone have been identified in the Quaternary stratigraphic record across much of western North America. Eruptions of this magnitude are rare in the worldwide geologic record. The three climactic Yellowstone eruptions occurred 2.1 million years ago, 1.3 million years ago, and 0.6 million years ago, for an average recurrence interval of 700,000 years (Ref. 2-79).

Hazards at the ISF site from potential Yellowstone eruptions include blanketing by pyroclastic flows or volcanic ash. The facility lies about 160 kilometers (99 miles) from the Yellowstone caldera rim and more than 200 kilometers (124 miles) from the Hot Springs Basin area of northeastern Yellowstone, a likely

site of future eruptions. Large-volume pyroclastic flows from Yellowstone, the Eastern Snake River Plain and elsewhere, traveling on relatively flat terrain, generally have a maximum runout distance of 100 to 150 kilometers (62 to 93 miles). Hence, the likelihood of pyroclastic flows from even the largest Yellowstone eruptions reaching the INEEL is essentially nonexistent, because of the great distance and intervening topographic barriers.

Although there is no direct relationship between ashfall thickness and damage parameters, the historical eruptions of Mt. St. Helens in Washington State demonstrate that the infrastructure of a technologically advanced nation can accommodate about 8 centimeters (3 inches) of ash without serious long-term consequences. Ash fall thickness from Yellowstone could exceed 8 centimeters (3 inches) if there were an eruption greater than 4.0×10^{10} cubic meters (5.2×10^{10} cubic yards), and if wind conditions dispersed the ash cloud directly over the INEEL. Such conditions are conceivable in light of past Yellowstone volcanism, but are highly improbable because prevailing winds would not likely direct ash toward the INEEL and because the recurrence intervals of such events are extremely long (0.5 to 1 million years). Less than 5 centimeters (2 inches) of Yellowstone ash have been found on the Eastern Snake River Plain at INEEL-equivalent distances.

2.6.6.3.2 Cascade Volcanoes and Other Western United States Centers

The Cascade volcanoes of northern California, Oregon, and Washington have produced many Quaternary period tephra layers, some of them widely dispersed across the western United States. These centers lie 700 to 800 kilometers (435 to 497 miles) west of the INEEL, at distances and prevailing-wind directions that prevent all but the largest ashfall eruptions from impacting the INEEL area. The Mazama ash is a voluminous and widespread ash layer that erupted from what is now Crater Lake, Oregon, and is a product of the largest known Cascade eruption. In the INEEL area, the Mazama ash is 0.5 to 2 centimeters (0.2 to 0.8 inches) thick (Ref. 2-19). Theoretical considerations and field measurements indicate that less than 6 centimeters of Mazama ash would have fallen on the INEEL, if the dispersal axis of the cloud were directly overhead. This effectively eliminates the Cascade volcanoes as sources of significant ashfall at the INEEL.

A similar conclusion is reached for other western United States volcanoes, such as the Long Valley caldera, which erupted about 600,000 years ago and produced the 6.0×10^{11} cubic meters (7.8×10^{11} cubic yards) Bishop Tuff. Long Valley is more than 800 kilometers (496 miles) southwest of the INEEL. Significant ash fall could be expected only for improbable conditions and at extremely long recurrence intervals.

2.6.6.4 Conclusions

Hazards associated with INEEL-area volcanism as well as distant volcanic sources are evaluated. The most significant hazards and risks to the ISF site are associated with basaltic volcanism and related phenomena from Eastern Snake River Plain vents.

For volcanic areas such as the Eastern Snake River Plain, with no historical volcanism and an incomplete chronologic record of prehistoric volcanism, assessments of potential volcanic hazards and volcanic risk are based on interpretation of the long-term geologic records and on the documented effects of historical eruptions in analog regions such as Iceland and Hawaii. Volcanic hazards to the ISF site are related to future basaltic and rhyolitic eruptions along volcanic rift zones and the axial volcanic zone. The most

significant volcanic hazard to the INEEL is the inundation or burning of facilities by basaltic lava flows from volcanic rift zones. A significant related hazard is disruption of facilities due to ground deformation accompanying magma intrusion along volcanic rift zones: opening of fissures, normal faulting, broad-region tilting and uplift within several kilometers of vents. Other, less significant basaltic hazards include volcanic-gas emission and disruption of groundwater.

Available geologic map data and geochronometry of the INEEL basalt lava flows suggest minimum (most conservative) volcanic recurrence intervals of 10^{-4} to 10^{-5} per year, for the axial volcanic zone and the Arco and Lava Ridge-Hells Half Acre volcanic rift zones. The probabilistic risk of basalt-lava inundation or intrusion-related ground disturbance is therefore estimated to be less than 10^{-5} per year for the ISF site and other sites on the southern portions of the INEEL. Risk from these phenomena at northern portions of the INEEL is still lower because volcanism there has been less frequent and less recent. The probability of significant impact from all other volcanic phenomena (e.g., growth of new rhyolite domes on the Eastern Snake River Plain or tephra falls thicker than 8 centimeters from non-Eastern Snake River Plain vents) is estimated to be less than 10^{-5} per year, because of great distance, infrequency, low volume, and topographic or atmospheric barriers to the dispersal of tephra on the INEEL.

THIS PAGE INTENTIONALLY LEFT BLANK.

2.7 SUMMARY OF SITE CONDITIONS AFFECTING CONSTRUCTION AND OPERATING REQUIREMENTS

The ISF Facility will be located within the boundaries of the INEEL and will not add appreciably to the impact of the INEEL on the local environment, infrastructure, labor, or population.

The finished grade of the ISF Facility is at an elevation of 4917 feet. The site will slope gradually to the southeast corner, where a stormwater retention basin will be located during construction (4910 feet).

Dust at the construction site will be controlled with the occasional application of water.

Accumulated snow will be removed and deposited where melting will not flood the construction site or adjacent operating areas.

The following design bases for important to safety structures, systems and components are related to the site characteristics for the ISF Facility (see Chapter 3).

- The ISF Facility is designed for the normal maximum and minimum temperatures of the INEEL, 98°F to -26°F.
- The ISF Facility is designed for a snow load of 30 psf.
- The ISF Facility is designed to accommodate a probable maximum flood.
- The ISF Facility is designed to withstand a tornado event with wind speeds up to 200 mph.
- The ISF Facility is designed to withstand a 2,500-year return period seismic event with a horizontal peak acceleration at rock of 0.123g.

THIS PAGE INTENTIONALLY LEFT BLANK.

2.8 REFERENCES

- 2-1. DOE (1997), *Idaho National Engineering and Environmental Laboratories (INEEL) Three Mile Island Unit 2 (TMI-2) Independent Spent Fuel Storage Installation (ISFSI) Safety Analysis Report*, U.S. Department of Energy, Idaho Operations Office, Idaho Falls, Idaho.
- 2-2. Title 10, Code of Federal Regulations, Part 72, *Licensing Requirements for the Independent Storage of Spent Nuclear Fuel and High-Level Radioactive Waste*, Washington, D.C.
- 2-3. DOE (1996), *Comprehensive Facility and Land Use Plan*, DOE/ID-10514, U.S. Department of Energy, Idaho Operations Office, Idaho Falls, ID, March.
- 2-4. DOE-ID (1993), *Idaho National Engineering Laboratory Long-Term Land Use Future Scenarios*, DOE/ID-10440, U.S. Department of Energy, Idaho Operations Office, Idaho Falls, ID.
- 2-5. Lee, L. G., J. M. Mines, and B. B. Webb (1994), *Assessment of Aircraft Impact Probabilities at the Idaho Chemical Processing Plant*, Westinghouse Idaho Nuclear Company, WINCO-1137.
- 2-6. Clawson, K.L., G.E. Start, and N.R. Ricks, (1989), *Climatology of the Idaho National Engineering Laboratory, 2nd Edition*, DOE/ID-12118, U.S. Department of Commerce, National Oceanic and Atmospheric Administration, Environmental Research Laboratories, Air Resources Laboratory, Field Research Division, Idaho Falls, ID, p. 155.
- 2-7. Idaho Department of Environmental Quality (1996), *Statewide Background Values - Ambient Concentration for Pollutants for which National Ambient Air Quality Standards Have Been Established*, April.
- 2-8. U.S. Nuclear Regulatory Commission (1993), SECY-93-087 USNRC Policy Issue: *Policy, Technical, and Licensing Issues Pertaining to Evolutionary and Advanced Light Water Reactor (ALWR) Designs*, SECY-93-087, April 2.
- 2-9. Hershfield, D.M. (1961), *Rainfall Frequency Atlas of the United States*, U.S. Weather Bureau Technical Paper No. 40, U.S. Department of Commerce, Washington, D.C.
- 2-10. Sagendorf, J.F. (1996), *Precipitation Frequency and Intensity at the Idaho National Engineering Laboratory*, NOAA Technical Memorandum, National Oceanic and Atmospheric Administration, Environmental Research Laboratories, Idaho Falls, Idaho, June 21.
- 2-11. EPA QAMS 005/80, *Interim Guidelines for Preparing Quality Assurance Project Plans*.
- 2-12. Sagendorf, et al. (1982), *XOQDOQ: Computer Program for the Meteorological Evaluation of Routine Effluent Releases at Nuclear Power Stations*, NUREG/CR-2919, J.F. Sagendorf, J.T. Goll, and W.F. Sandusky, U.S. Nuclear Regulatory Commission, Washington, D.C.
- 2-13. U.S. Nuclear Regulatory Commission (1977), Regulatory Guide 1.111, *Methods for Estimating Atmospheric Transport and Dispersion of Gaseous Effluents in Routine Releases from Light-Water-Cooled Reactors*, Rev. 1, July.

- 2-14. Briggs, J.B. (1971), *Some Recent Analyses of Plume Rise Observations, Proceedings of the Second International Clean Air Act Congress*, edited by H.M. England and W.T. Barry, Academic Press, N.Y.
- 2-15. Briggs, J.B. (1972), "Discussion on Chimney Plumes in Neutral and Stable Surroundings," *Atmospheric Environment*, pp. 507-510.
- 2-16. NOAA (1984), *Climatology of the Idaho National Engineering Laboratory, Site Specific Summary NPR Primary and Alternate Site (Draft)*, IDO-12048B, G.E. Start, ed., November.
- 2-17. Start, G.E. and L.L. Wendell (1974), *Regional Effluent Dispersion Calculations Considering Spatial and Temporal Meteorological Variations*, NOAA Technical Memorandum ERL-ARL-44, National Oceanic and Atmospheric Administration, Washington, D.C.
- 2-18. Barraclough, J.T. and R.G. Jensen (1975), *Hydrologic Data for the Idaho National Engineering Laboratory Site, 1971 to 1973*, U.S. Geological Survey Open File Report 75-318 (IDO-22052), January.
- 2-19. Fischer, D.R., R.G. Jensen, and J.R. Pitman (1989), *Hydrologic Conditions at the Idaho National Engineering Laboratory, 1982-1985*, U.S. Geological Survey Open File Report 89-4008, DOE/ID-22078, December.
- 2-20. Bennett, C.M. (1986), *Capacity of the Diversion Channel Below the Flood-Control Dam on the Big Lost River at the Idaho National Engineering Laboratory*, U.S. Geological Survey, Water-Resources Investigations Report 86-4204.
- 2-21. McKinney, J.D. (1985), *Big Lost River 1983-1984 Flood Threat*, EG&G Report PPD-FPB-002.
- 2-22. Carrigan, P.H., Jr. (1972), *Probability of Exceeding Capacity of Flood Control System at the National Reactor Testing Station, Idaho*, U.S. Geological Survey Open file Report IDO-22052, January.
- 2-23. Koslow, K.N. and J.A. Tullis (1983), *Characterization of Big Lost River Floods with Recurrence Intervals Greater than 25 Years*, RE-PB-83-044, EG&G Idaho, Inc., Idaho Falls, Idaho, November.
- 2-24. Koslow, K.N. and D.H. Van Haaften (1986), *Flood Routing Analysis for a Failure of Mackay Dam*, EGG-EP-7184, EG&G Idaho Inc., Idaho Falls, ID.
- 2-25. U.S. Department of the Army Corps of Engineers (1977), *National Program of Inspection of Dams Report, Vol. 1, Appendix D, Recommended Guidelines for Safety Inspection of Dams*, Office of the Chief of Engineers.
- 2-26. DOE (1995), *Department of Energy Programmatic Spent Nuclear Fuel Management and Idaho National Engineering Laboratory Environmental Restoration and Waste Management Programs Final Environmental Impact Statement*, DOE/EIS-0203-F, April.

- 2-27. EPA 910/9-90-020, *EPA Support Document for the EPA Designation of the Eastern Snake River Plain Aquifer as a Sole Source Aquifer*, August 1990.
- 2-28. Cecil, D. and Orr, B.R. (1991), *Hydrologic Conditions and Distribution of Selected Chemical Constituents in Water, Snake River Plain Aquifer, Idaho National Engineering Laboratory, Idaho 1986 to 1988*, U.S. Geological Survey Open File Report 91-4047, DOE/ID-22096, August.
- 2-29. Malde, H.E. (1991), "Quaternary Geology and Structural History of the Snake River Plain, Idaho and Oregon," *Quaternary Non-glacial Geology, Conterminous United States*; Boulder, Colorado, Geological Society of America, The Geology of North America, v. K-2, pp. 251-281.
- 2-30. Pierce, K.L. and Morgan, L.A. (1992), "The Track of the Yellowstone Hotspot: Volcanism, Faulting, and Uplift," *Regional Geology of eastern Idaho and Western Wyoming*; Geological Society of American Memoir 179, pp. 1-54.
- 2-31. Morgan, P., Blackwell, D.D., Spafford, R.E., and Smith, R.B. (1977), "Heat Flow Measurements in Yellowstone Lake and the Thermal Structure of the Yellowstone Caldera," *Journal of Geophysical Research*, v. 82, pp. 3719-3732.
- 2-32. Smith, R.B. and R.L. Christiansen (1980), "Yellowstone Park as a Window on the Earth's Interior," *Scientific American*, v. 242, no. 2, pp. 104-117.
- 2-33. Christiansen, R.L. (1984), "Yellowstone Magmatic Evolution: Its Bearing on Understanding Large-volume Explosive Volcanism;" *Explosive Volcanism: Inception, Evolution, and Hazards*; National Academy Press, Washington, D.C., pp. 84-95.
- 2-34. Thelin, G.P. and R.J. Pike. (1991), *Landforms of the Conterminous United States - A Digital Shaded Relief Portrayal*; U.S. Geological Survey Miscellaneous Investigations Map 2206, scale 1:3,500,000.
- 2-35. Link, P.K., B. Skipp, M.H. Hait, S.U. Janecke, and B.R. Burton. (1988), *Structural and Stratigraphic Transect of South-central Idaho: A Field Guide to the Lost River, White Knob, Pioneer, Boulder, and Smoky Mountains*; Idaho Geological Survey Bulletin 27, pp. 5-42.
- 2-36. Skipp, B. and M.H. Hait (1977), *Allochthons Along the Northeast Margin of the Snake River Plain, Idaho*; Wyoming Geological Association 29th Annual Field Conference Guidebook, pp. 499-515.
- 2-37. Oldow, J.S., A.W. Bally, H.G. Ave'Lallement, and W.P. Leeman (1989), "Phanerozoic Evolution of the North American Cordillera: United States and Canada," *The Geology of North America: An overview*. Geological Society of America, Decade of North America Geology, v. A, pp. 139-232.
- 2-38. Eaton, G.P. (1982) *The Basin and Range Province: Origin and Tectonic Significance*, Annual Reviews of Earth and Planetary Science, v.10, pp 409-440.

- 2-39. Zoback, M.L. and M.D. Zoback (1989), "Tectonic Stress Field of the Continental United States," *Geophysical Framework of the Continental United States*, L.C. Pakiser and W.D. Mooney, editors, Geological Society of America Memoir 172, pp. 523-539.
- 2-40. Hackett, W.R. and R.P. Smith (1992), "Quaternary Volcanism, Tectonics, and Sedimentation in the Idaho National Engineering Laboratory Area," *Field Guide to Geologic Excursions in Utah and Adjacent Areas of Nevada, Idaho, and Wyoming*, Utah Geological Survey, Miscellaneous Publication 92-3, pp. 1-17.
- 2-41. Nace, R.L., P.T. Voegely, J.R. Jones and S. Deutsch (1975), *Generalized Geologic Framework of the National Reactor Testing Station, Idaho*; U.S. Geological Survey Professional Paper 725-B, 49 pp.
- 2-42. Kuntz, M.A., H.R. Covington, and L.J. Schorr (1992), "An Overview of Basaltic Volcanism of the Eastern Snake River Plain, Idaho," *Regional Geology of Eastern Idaho and Western Wyoming*, M.A. Kuntz and L.B. Platt, eds., Geological Society of America Memoir 179, pp. 227-267.
- 2-43. Hull, L.C. (1989), *Conceptual Model and Description of the Affected Environment for the TRA Warm Waste Pond (Waste Management Unit TRA-03)*; EG&G Informal Report, EGG-ER-8644.
- 2-44. Bennett, C.M. (1990). *Streamflow Losses and Groundwater Level Changes Along the Big Lost River at the Idaho National Engineering Laboratory, Idaho*, U.S. Geological Survey Water-Resources Investigative Report 90-4067.
- 2-45. Woodward-Clyde Consultants (1990), *Earthquake Strong Ground Motion Estimates for the Idaho National Engineering Laboratory: Final Report, Volume I: Summary, Volume II: Methodology and Analyses, and Volume III: Appendices*, EG&G Idaho, Inc. Informal Report EGG-BG-9350.
- 2-46. Woodward-Clyde Consultants (1992), *Earthquake Strong Ground Motion Evaluations for the Proposed New Production Reactor at the Idaho National Engineering Laboratory, Volume I: Deterministic Evaluation and Volume II: Probabilistic Evaluation*, EG&G Idaho, Inc. Informal Report EGG-GEO-10304.
- 2-47. Woodward-Clyde Federal Services (1996), *Site Specific Probabilistic Seismic Hazard Analysis for the INEL*, Final Report, Lockheed Idaho Technologies Company, Technical Report INEL-95/0536.
- 2-48. Kuntz, M. A., B. Skipp, M.A. Lanphere, W.E. Scott, K.L. Pierce, G.B. Dalrymple, D.E. Champion, G.F. Embree, W.R. Page, L.A. Morgan, R.P. Smith, W.R. Hackett, and D.W. Rodgers (1994), *Geologic Map of the Idaho National Engineering Laboratory and Adjoining Areas, Eastern Idaho*; U.S. Geological Survey Miscellaneous Investigations Map 1-2330, 1:100,000 scale.
- 2-49. Scott, W.E. (1982), *Surficial Geologic Map of the Eastern Snake River Plain and Adjacent Areas, Idaho and Wyoming*; U.S. Geological Survey Miscellaneous Investigation Map I-1372, scale 1:250,000.

- 2-50. Anderson, S.R. (1991), *Stratigraphy of the Unsaturated Zone and Uppermost Part of the Snake River Plain Aquifer at the Idaho Chemical Processing Plant and Test Reactors Area, Idaho National Engineering Laboratory, Idaho*, U.S. Geological Survey Water Resources Investigative Report 91-4010, 71 pp.
- 2-51. Foster Wheeler Environmental Corporation (2001), *Idaho Spent Fuel Project Geotechnical Engineering Report*, ISF-FW-RPT-0012.
- 2-52. Smith, R.B. and W.J. Arabasz (1991), *Seismicity of the Intermountain Seismic Belt*, in *Neotectonics of North America*, D.B. Slemmons, E.R. Engdahl, M.D. Zoback, and D.D. Blackwell, eds., Geological Society of America, Decade Map Vol. 1, Boulder Colorado, pp. 185-228.
- 2-53. Eddington, P.J.K., R.B. Smith, and C.R. Renggli (1987), "Kinematics of Basin and Range Intraplate Extension," *Continental Extensional Tectonics*, Geological Society Special Publication No. 28, pp. 371-392.
- 2-54. Hackett, W.R., R.P. Smith, and N.E. Josten (1991), *Interaction of Quaternary Volcanic and Tectonic Processes, Eastern Snake River Plain*, Geological Society of America, Abstracts with Programs v. 23, p. 32.
- 2-55. Engdahl, E.R. and W.A. Rinehart (1991), "Seismicity Map of North America Project," *Neotectonics of North America*, D.B. Slemmons, E.R. Engdahl, M.D. Zoback and D.D. Blackwell, eds., Geological Society of America Decade Map Volume 1, pp. 21-27.
- 2-56. Woodward-Clyde Federal Services (1997), letter transmittal of *Update Earthquake Catalog 1884-1995*, Ivan Wong letter, December 30, Oakland, California.
- 2-57. King, J.J., T.E. Doyle, and S.M. Jackson (1987), "Seismicity of the Eastern Snake River Plain Region, Idaho, Prior to the Borah Peak, Idaho Earthquake: October 1972 - October 1983," *Bulletin of the Seismological Society of America*, v. 77, no. 3, pp. 809-818.
- 2-58. Jackson, S.M., I.G. Wong, G.S. Carpenter, D.M. Anderson, and S.M. Martin (1993), "Contemporary Seismicity in the Eastern Snake River Plain, Idaho Based on Microearthquake Monitoring," *Bulletin of the Seismological Society of America*, v. 83, pp. 680-695.
- 2-59. Pelton, J.R., R.J. Vincent, and N.J. Anderson (1990), "Microearthquakes in the Middle Butte/East Butte Area, Eastern Snake River Plain, Idaho," *Bulletin of the Seismological Society of America*, v. 80, no. 1, pp. 209-212.
- 2-60. Smith, R.B., and M.L. Sbar (1974), "Contemporary Tectonics and Seismicity of the Western United States with Emphasis on the Intermountain Seismic Belt," *Bulletin of the Geological Society of America*, 85, pp. 1205-1218.
- 2-61. Smith, R.B. (1978), "Seismicity, Crustal Structure, and Intraplate Tectonics of the Interior of the Western Cordillera," in Smith, R.B. and Eaton, G.P., editors, *Cenozoic Tectonics and Regional Geophysics of the Western Cordillera*, Geological Society of America Memoir 152, pp. 111-144.

- 2-62. Smith, R. B., W.D. Richins, and D.I. Doser (1985), "The 1983 Borah Peak, Idaho Earthquake: Regional Seismicity, Kinematics of Faulting, and Tectonic Mechanism," in *Proceedings of Conference XXVIII on the Borah Peak, Idaho Earthquake*, U. S. Geological Survey Open-File Report 85-290, pp. 236-263.
- 2-63. Doser, D.I. (1985), "Source Parameters and Faulting Processes of the 1959 Hebgen Lake, Montana, Earthquake Sequence," *Journal of Geophysical Research*, v. 90, no. B6, pp. 4537-4555.
- 2-64. Gorman, V.W. and R.C. Guenzler (1983), *The 1983 Borah Peak Earthquake and INEL Structural Performance*, EG&G Informal Report EGG-EA-6501, 76 pp.
- 2-65. Crone, A.J., M.N. Machette, M.G. Bonilla, J.J. Lienkaemper, K.L. Pierce, W.E. Scott, and R.C. Bucknam (1987), "Surface faulting accompanying the Borah Peak earthquake and segmentation of the Lost River fault, central Idaho," *Bulletin of the Seismological Society of America*, v. 77, no. 3, pp. 739-770.
- 2-66. Richins, W.D., J.C. Pechmann, R.B. Smith, C.J. Langer, S.K. Goter, J.E. Zollweg, and J.J. King (1987), "The 1983 Borah Peak, Idaho Earthquake and its Aftershocks," *Bulletin of the Seismological Society of America*, v. 77, no. 3, pp. 694-723.
- 2-67. Stover, C.W. (1985). "The Borah Peak, Idaho earthquake of October 28, 1983 - Isoseismal map and intensity distribution," *Earthquake Spectra*, 2, No. 1, pp. 11-21.
- 2-68. Jackson, S. M. (1985). *Acceleration Data from the 1983 Borah Peak, ID earthquake Recorded at the Idaho National Engineering Laboratory*, in *Workshop XXVIII on the Borah Peak, ID Earthquake*, U. S. Geological Survey Open File Report 85-290, pp. 385-400.
- 2-69. Jackson, S. M., J.J. King, D.M. Anderson, G.S. Carpenter, and H.A. Adams (1991) *Strong Ground Motion Data Recorded at the Idaho National Engineering Laboratory during the 1983 Borah Peak, Idaho, earthquake*; EG&G Idaho, Inc., Idaho Falls, Idaho. Informal Report EGG-BG-9249, 136 pp.
- 2-70. Oaks, S.D. (1992), *Historical Seismicity Investigation for the November 11, 1905 earthquake*; EG&G Informal Report EGG-GEO-10203, 106 pp.
- 2-71. Cook, K.L. and R.K. Nye (1979). *Effects of the Pocatello Valley (Idaho-Utah border) earthquake of March 28, 1975 (UTC)*, *Earthquake Studies in Utah 1850 to 1978*, W.J. Arabasz, R.B. Smith, and W.D. Richins, editors, pp. 445-457.
- 2-72. Stover, C.W., R.B. Simson, and W. Person (1977), "Earthquake in the United States, April-June 1975", *U.S. Geological Survey Circular 749-B*, 29 pp.
- 2-73. Dewey, J. (1994), Letter transmittal of the 1994 Draney Peak, Idaho Earthquake Isoseismals, U.S. Geological Survey, March 4, Denver, Colorado.
- 2-74. Anders, M.H., J.W. Geissman, L.A. Piety, and J.T. Sullivan (1989), "Parabolic Distribution Of Circumeastern Snake River Plain Seismicity and Latest Quaternary Faulting: Migratory Pattern

- and Association with the Yellowstone Hotspot;" *Journal of Geophysical Research*, v. 94, no. B2, pp.1589-1621.
- 2-75. Bankey, V., M. Webring, D.R. Mabey, M.D. Kleinkopf, and E.H. Bennett (1985), *Complete Bouguer Gravity Anomaly Map of Idaho*, U.S. Geological Survey Map MF-1773.
- 2-76. Zeitz, I., F.P. Gilbert, and J.R. Kirby (1978). *Aeromagnetic Map of Idaho*, U.S. Geological Survey Map GP-920.
- 2-77. Sparlin, M.A., L.W. Braile, and R.B. Smith (1982), "Crustal Structure of the Eastern Snake River Plain Determined from Ray Trace Modeling of Seismic Refraction Data," *Journal of Geophysical Research*, v. 87, no. B4, pp. 2619-2633.
- 2-78. Smith, R.B. and L.W. Braile. (1993), Topographic Signature, Space-Time Evolution, and Physical Properties of the Yellowstone-Snake River Plain Volcanic System: the Yellowstone Hotspot, in A.W. Snoke, J.R. Steidtmann, and S.M. Roberts, editors, *Geology of Wyoming*, Geological Survey of Wyoming Memoir No. 5, pp. 694-754.
- 2-79. Christiansen, R.L. (1989), "The Yellowstone Plateau-Island Park Region," in K.L. Ruebelmann, editor, *Snake River Plain-Yellowstone Volcanic Province, Field Trip Guidebook T305*, 28th International Geological Congress, American Geophysical Union, Washington, D.C., pp. 14-37.
- 2-80. White, D.E., R.O. Fournier, L.J.P. Muffler, and A.H. Truesdale. (1975), *Physical results of research drilling in thermal areas of Yellowstone National Park, Wyoming*, U.S. Geological Survey Professional Paper 892, 70 pp.
- 2-81. Peyton, S.L., R.B. Smith, and J.C. Pechmann (1991), *Seismotectonics of the Yellowstone-Hebgen Lake Region from Earthquake Focal Mechanisms and Stress Field Inversion*, EOS 72, pp. 335-336.
- 2-82. Iyer, H.M., J.R. Evans, G. Zandt, R.M. Stewart, J. Coakley and J. Rolloff (1981), "A Deep Magma Body Under the Yellowstone Caldera: Delineation Using Teleseismic P-wave Residuals and Tectonic Interpretation," *Geological Society of America Bulletin*, v. 92, pp. 1471-1646.
- 2-83. Evans, J.R. (1982), "Compressional Wave Velocity Structure of the Upper 350 km Under the Eastern Snake River Plain Near Rexburg, Idaho," *Journal of Geophysical Research*, v. 87, pp. 2654-2670.
- 2-84. Smith, R.B. and R.L. Bruhn (1984), "Intraplate Extensional Tectonics of the Eastern Basin-Range: Inferences on Structural Style from Seismic Reflection Data, Regional Tectonics, and Thermal-Mechanical Models of Brittle-Ductile Deformation," *Journal of Geophysical Research*, v. 89, pp. 5733-5762.
- 2-85. Janecke, S.U. (1992), "Kinematics and Timing of Three Superimposed Extensional Systems, East Central Idaho: Evidence for an Eocene Tectonic Transition," *Tectonics*, v. 11, no. 6, pp. 1121-1138.

- 2-86. Scott, W. E., K. L. Pierce, and M. H. Hait, Jr. (1985), "Quaternary Tectonic Setting of the 1983 Borah Peak Earthquake, Central Idaho;" *Bulletin of the Seismological Society of America*, v. 75, no. 4, pp. 053-1066.
- 2-87. Doser, D.I. and R.B. Smith (1985), "Source Parameters of the 28 October 1983 Borah Peak, Idaho, Earthquake from Body Wave Analysis," *Bulletin of the Seismological Society of America* 75, pp. 1041-1051.
- 2-88. Woodward-Clyde Consultants (1992), *Paleoseismic Investigations of the Southern Lemhi Fault, Idaho*, EG&G Idaho, Inc., Informal Report EGG-GEO- 10178, 32 pp.
- 2-89. Bruhn, R.L, D. Wu, and J-J. Lee (1992), *Final Report on the Structure of the Southern Lemhi and Arco Fault Zone, Idaho*; EG&G Idaho, Inc., Informal Report EGG-NPR-10680, 6 plates, 26 pp.
- 2-90. Jackson, S.M., G.S. Carpenter, R.P. Smith, and J.L. Casper (1995), *Seismic Reflection Project Near the Southern Terminations of the Lost River and Lemhi Faults, Eastern Snake River Plain, Idaho*; Idaho National Engineering Laboratory Technical Report, INEL-95/0489.
- 2-91. Haller, K.M. (1988), *Segmentation of the Lemhi and Beaverhead faults, East- central Idaho, and Red Rock fault, Southwest Montana, During the Late Quaternary*, M.S. Thesis, University of Colorado, 141 pp.
- 2-92. Embree, G.F. (1989), *Neogene Fault Activity in Southern Beaverhead Range Adjacent to the Eastern Snake River Plain and Birch Creek Valley, Idaho*, unpublished report and map, submitted to EG&G Idaho Inc., Idaho Falls, Idaho.
- 2-93. Williams, E.J. and G.F. Embree (1980), "Pleistocene Movement on Rexburg Fault, Eastern Idaho (Abstract)," *Geological Society of America Abstract with Program*, Rocky Mountain Section, v. 12, no. 6, p. 308.
- 2-94. Piety, L.A., C.K. Wood, J.D. Gilbert, J.T. Sullivan, and M.H. Anders (1986), *Seismotectonic Study for Palisades Dam and Reservoir, Palisades Project*, U.S. Bureau of Reclamation, Engineering Research Center, Seismotectonic Div., Denver, CO, and Pacific Northwest Region Geology Branch, Boise, ID, Seismotectonic Report 86-3, 198 pp.
- 2-95. McCalpin, J.P., L.A. Piety, and M.H. Anders (1990), *Part 1. Latest Quaternary Faulting and Structural Evolution of Star Valley, Wyoming*, in *Geologic Field Tours of Western Wyoming and Parts of Adjacent Idaho, Montana, and Utah*, S. Roberts, ed., Geological Survey of Wyoming Public Information Circular No. 29, pp. 5-14.
- 2-96. EG&G Idaho, Inc. (1985), *INEL Environmental Characterization Report*, EG&G Idaho, Inc. Informal Report EGG-NP-6688, three volumes.
- 2-97. Pankratz, L.W. and H.D. Ackerman (1982), "Structure Along the Northwest Edge of the Snake River Plain Interpreted from Seismic Refraction," *Journal of Geophysical Research*, v. 84, no. B4, pp. 2676-2682.

- 2-98. Mabey, D.R. (1978), "Regional Gravity and Magnetic Anomalies in the Eastern Snake River Plain, Idaho, U.S. Geological Survey," *Journal of Research*, v. 6, pp. 553-562.
- 2-99. Stanley, W.D. (1982), "Magnetotelluric Soundings on the Idaho National Engineering Laboratory Facility, Idaho," *Journal of Geophysical Research*, 87, pp. 2683-2691.
- 2-100. Myers, W.B. and W. Hamilton (1964), "Deformation Accompanying the Hebgen Lake Earthquake of August 17, 1959," *U.S. Geological Survey Bulletin*, 435-I, pp. 55-98.
- 2-101. Corbett, M.K. (1975), *Structural Development of the Eastern Snake River Plain, Idaho as an Intracontinental Rift*, Geological Society of America Abstracts with Programs 7, pp. 599-600.
- 2-102. Hamilton, W. (1987), *Plate-Tectonic Evolution of the Western U.S.A.*, Episodes 10, pp. 271-301.
- 2-103. Morgan, W.J. (1972), *Plate Motions and Deep Mantle Convection*; Geological Society of America Memoir 132, pp. 7-22.
- 2-104. Zentner, N.C. (1989), *Neogene Normal Faults Related to the Structural Origin of the Eastern Snake River Plain, Idaho*, unpublished M.S. Thesis, Idaho State University, 48 pp.
- 2-105. Breckenridge, R.M. and K.L. Othberg (1991), *Geologic Interpretation of a Trench Excavation Near Arco Hills on the Northwest Margin of the INEL, Snake River Plain, Idaho*; Idaho Geological Survey Technical Report 91-2, 20 pp.
- 2-106. Rodgers, D.W., W.R. Hackett, and H.T. Ore (1990), "Extension of the Yellowstone Plateau, Eastern Snake River Plain, and Owyhee Plateau," *Geology*, v. 18, pp. 1138-1141.
- 2-107. Morin-Jansen, A. (1987), *Study of the Principle Lineament and Associated Lineaments*; Masters Thesis, Idaho State University, Pocatello.
- 2-108. Golder Associates (1992), *New Production Reactor Site Characterization, Volume I: Volcanic Zones Mapping Report, Volume II: Regional Geomorphic Study, and Volume III: NPR Site Geologic Report*; EG&G Informal Report EGG-NPR-10625.
- 2-109. Morgan, L.A. (1988), *Explosive Rhyolitic Volcanism of the Eastern Snake River Plain* (unpublished, Ph.D. Thesis), Manoa, University of Hawaii, 191 pp.
- 2-110. Smith, R.B. and L.W. Braile (1994), "The Yellowstone Hotspot," *Journal of Volcanology and Geothermal Research*, v. 61, pp.121-187.
- 2-111. Stover, C.W., G.E. Reagor, and S.T. Algermissen (1986), *Seismicity Map of the State of Idaho*, U.S. Geological Survey Map MF1857.
- 2-112. Engdahl, E.R. and W.A. Rinehart (1988), "Seismicity Map of North America, Continent-scale Map-004," *Decade of North American Geology*, Geological Society of America, Scale 1:5,000,000, 4 sheets.

- 2-113. Brott, C.A., D.D. Blackwell, and J.P. Ziagos (1981), "Thermal and Tectonic Implications of Heat Flow in the Eastern Snake River Plain, Idaho," *Journal of Geophysical Research*, v. 86, pp. 11709-11734.
- 2-114. Blackwell, D.D. (1989), "Regional Implications of Heat Flow of the Snake River Plain, Northwestern United States," *Tectonophysics*, v. 164, pp. 323-343.
- 2-115. Blackwell, D. D. (1992), *Heat Flow Modeling of the Snake River Plain*, EG&G Informal Report EGG-C91-103450, 109 pp.
- 2-116. Parsons, T. and G. Thompson (1991), "The Role of Magma Overpressure in Suppressing Earthquakes and Topography: Worldwide Examples," *Science*, v. 253, p. 1399-1402.
- 2-117. Anders, M.H. and N.H. Sleep (1992), "Magmatism and Extension: The Thermal and Mechanical Effects of the Yellowstone Hotspot," *Journal of Geophysical Research*, v. 97, pp. 15379- 15393.
- 2-118. Brandsdottir, B. and P. Einarsson (1979), "Seismic Activity Associated with the September 1977 Deflagration of the Krafla Central Volcano in Northeastern Iceland," *Journal of Volcanology and Geothermal Research*, v. 6, pp. 197-212.
- 2-119. Einarsson, P. and B. Brandsdottir (1980), "Seismological Evidence for Lateral Magma Intrusion During the July 1978 Deflation of the Krafla Volcano in Northeastern- Iceland," *Journal of Geophysics*, v. 47, pp. 160-165.
- 2-120. Klein, F.W., R.Y. Koyanagi, J.S. Nakata, and W.R. Tanigawa (1987), "The Seismicity of Kilauea's Magma System," in *Volcanism in Hawaii*, R.W. Decker, T.L. Wright, and P.H. Stauffer eds., U. S. Geological Survey Professional Paper 1350, pp. 1019-1185.
- 2-121. Mastin, L.G. and D.D. Pollard (1988), "Surface Deformation and Shallow Dike Intrusion Processes at Inyo Craters, Long Valley, California," *Journal of Geophysical Research*, v. 93, pp. 13,221-13,235.
- 2-122. Ryan, M.P. (1987), "Neutral Buoyancy and the Mechanical Evolution of Magmatic Systems," in *Magmatic Processes: Physiochemical Principles*, The Geochemical Society Special Publication No. 1, B.O. Mysen, ed., pp. 259-287.
- 2-123. Rubin, A.M., and D.D. Pollard (1987), "Origins of Blade-like Dikes in Volcanic Rift Zones," in *Volcanism in Hawaii*, R.W. Decker, T.L. Wright, and P.H. Stauffer eds., U.S. Geological Survey Professional Paper 1350, pp. 1449-1470.
- 2-124. Rubin, A.M., and D.D. Pollard (1988), "Dike-induced Faulting in Rift Zones of Iceland and Afar," *Geology*, v. 16, pp. 413-417.
- 2-125. Rubin, A. M. (1990), "A Comparison of Rift-Zone Tectonics in Iceland and Hawaii," *Bulletin of Volcanology*, v. 52, pp. 302-319.

- 2-126. Smith, R.P., S.M. Jackson, and W.R. Hackett (1996), "Paleoseismology and Seismic Hazards Evaluations in Extensional Volcanic Terrains," *Journal of Geophysical Research*, v.101, p.6277-6292.
- 2-127. Hackett, W.R., S.M. Jackson, and R.P. Smith (1996), "Paleoseismology in Volcanic Environments," in J.P. McCalpin, ed., *Paleoseismology*, Academic Press, New York.
- 2-128. Jackson, S. M. (1994), *Magnitudes of Earthquakes Associated with Basalt Dike Intrusion for use in INEL Seismic Hazards Evaluations*, Informal Report, INEL 94/0132, 44 pp., Lockheed Idaho Technologies Company, Idaho Falls, ID.
- 2-129. Rubin, A.M. (1992), "Dike-induced Faulting and Graben Subsidence in Volcanic Rift Zones," *Journal of Geophysical Research*, v. 97, pp. 1839-1858.
- 2-130. Bjornsson, A., K. Saemundsson, P. Einarsson, E. Tyggvason, and K. Gronvald (1977), "Current Rifting Episode in North Iceland," *Nature*, v. 266, pp. 318-323.
- 2-131. Wells, D.L. and Coppersmith, K.J. (1994), "New Empirical Relationships Among Magnitude, Rupture Length, Rupture Area, and Surface Displacement," *Bulletin of the Seismological Society of America*, v. 84, pp. 974-1002.
- 2-132. Filson, J., T. Simkin, and L-K. Leu (1973), "Seismicity of a Caldera Collapse: Galapagos Islands 1968," *Journal of Geophysical Research*, v. 78, pp. 8591-8622.
- 2-133. Stein, R.S., P. Briole, J.C. Ruegg, P. Tapponnier, and F. Gasse (1991), "Contemporary, Holocene, and Quaternary Deformation of the Asal Rift, Djibouti: Implications for the Mechanics of Slow-spreading Ridges," *Journal of Geophysical Research* v. 96, pp. 21789-21806.
- 2-134. Daz, S. and Scholz, C.H. (1983), "Why Large Earthquakes do not Nucleate at Shallow Depths," *Nature*, 305, 621-623.
- 2-135. Mori, J., C. McKee, I. Itikarai, P. Lowenstein, P. de Saint Ours, and B. Tali (1989), "Earthquakes of the Rabaul Seismo-Deformational Crisis September 1983 to July 1985: Seismicity on a Caldera Ring Fault," in J.H. Latter, ed., *Volcanic Hazards: IAVCEI Proceedings in Volcanology* 1, pp. 429-462.
- 2-136. Stickney, M.C., and D.R. Lageson (1999). *The 1999 Red Rock Valley, Montana, Earthquake: Seismological Constraints and Structural Model*, EOS, Transactions, American Geophysics Union, v. 80, No. 66, p. F725.
- 2-137. Shenon, P.J. (1936), "The Utah Earthquake of March 12, 1934 (extracts from unpublished report)," in Neumann, F., *United States Earthquakes, 1934*, U. S. Coast and Geodetic Survey, Serial 593, pp. 43-48.
- 2-138. dePolo, C.M., D.G. Clark, D.B. Slemmons, and W.H. Aymard (1989), "Historical Basin and Range Province Surface Faulting and Fault Segmentation," in *Fault Segmentation and Controls*

- of Rupture Initiation and Termination*, D.P. Schwartz and R.H. Sibson, eds., Proceedings Conference XLV, Palm Springs, U.S. Geological Survey Open File Report. 89-315, pp. 131-162.
- 2-139. Doser, D. I. (1989), "Extensional Tectonics in Northern Utah-Southern Idaho, U.S.A., and the 1934 Hansel Valley Sequence," *Physics of the Earth and Planetary Interiors*, v. 54, pp. 12-134.
- 2-140. Westaway, R. and R.B. Smith (1989), "Source Parameters of the Cache Valley (Logan), Utah Earthquake of 30 August 1962," *Bulletin of the Seismological Society of America*, v. 79, number 5, pp. 1410-1425.
- 2-141. Smith, R.B., and M.L. Sbar (1970). *Seismicity and Tectonics of the Intermountain Seismic Western United States, Part II: Focal Mechanism of Major Earthquakes*; Geological Society of America, Abstracts from Programs v. 2, p. 657.
- 2-142. Bache, T.C., D.G. Lambert and T.G. Barker (1980). "A Source Model for the March 28, 1975, Pocatello Valley Earthquake from Time-domain Modeling of Teleseismic P Waves," *Bulletin of the Seismological Society of America*, v. 70, pp. 405-418.
- 2-143. Arabasz W.J., W.D. Richins, and C.J. Langer (1979), "The Pocatello Valley (Idaho-Utah border) Earthquake Sequence of March to April 1975," in *Earthquake Studies in Utah 1850 to 1978*, W.J. Arabasz, R.B. Smith, and W.D. Richins, editors, University of Utah Special Publication, pp. 339-374.
- 2-144. Pechmann, J.C., D.A. Brumbaugh, S.J. Nava, T.G. Skelton, G.P. Fivas, W.J. Arabasz, and S.M. Jackson (1997). *The 1994 Draney Peak, Idaho, Earthquake and Its Aftershocks*, Eos, Transactions, American Geophysical Union, 78, No. 46, p. F480.
- 2-145. Eppley, R.A. and W.K. Cloud (1961), *United States Earthquakes 1959*, U.S. Coast and Geodetic Survey, 115 pp.
- 2-146. Witkind, I.J. (1964), *Reactivated Faults North of Hebgen Lake*, U.S. Geological Survey Professional Paper 435, pp. 37-50.
- 2-147. Pitt, A.M., C.S. Weaver, and W. Spence (1979), "The Yellowstone Park Earthquake of June 30, 1975," *Bulletin of the Seismological Society of America*, 69, pp. 187-205.
- 2-148. Pardee, J.T. (1926), *The Montana Earthquake of June 27, 1925*, U.S. Geological Survey Professional Paper 147-B, 17 pp.
- 2-149. Doser, D. I. (1989), "Source Parameters of Montana Earthquakes (1925-1964) and Tectonic Deformation in the Northern Intermountain Seismic Belt," *Bulletin of the Seismological Society of America*, v. 79, No. 1, pp. 31-50.
- 2-150. Dewey, J.W., W.H. Dillinger, J. Taggart, and S.T. Algermissen (1973). *A Technique for Seismic Zoning: Analysis of Earthquake Locations and Mechanisms in Northern Utah, Wyoming, Idaho, and Montana*, in *Contributions to Seismic Zoning*, S.T. Harding, editor, NOAA Technical Rept, ERL 267-ESL 30, p.541-575.

- 2-151. Turko, J.M. (1988), *Quaternary Segmentation History of the Lemhi Fault, Idaho*, M.S. Thesis, State University of New York at Binghamton.
- 2-152. Baltzer, E.M., P.L.K. Knuefer, and M.J. Turko (1989), "Late Quaternary Slip Events Along the Central Lemhi Fault, Idaho (Abstract)," *Geological Society of America Abstract Program*, v.21, no. 5, p. 53.
- 2-153. Pierce, K.L. (1985), *Quaternary History of Faulting on the Arco Segment of the Lost River Fault, Central Idaho*, Proceedings of Conference XXVIII on the Borah Peak, Idaho, Earthquake, U.S. Geological Survey Open-File Report 85-290, pp. 195-206.
- 2-154. Crone, A.J., and K.M. Haller (1991), "Segmentation and Coseismic Behavior of Basin-and-Range Normal Faults; Examples from East-central Idaho and Southwestern Montana, USA," *Journal of Structural Geology*, v.13, pp. 151-164.
- 2-155. Wu, D. and R.L. Bruhn (1994), *Structural and Rupture Characteristics of the Southern Lost River Fault Zone, Idaho*, University of Utah, Report to Woodward-Clyde Federal Services, April, 33 pp.
- 2-156. Woodward-Clyde Federal Services (1995) *Paleoseismic Investigation of the Southern Lost River Fault Zone, Idaho*; Lockheed Idaho Technologies Company, Technical Report INEL-95/0508, 82p. plus figures, tables, and appendices.
- 2-157. Stickney, M.C., and M.J. Bartholomew (1987), "Seismicity and Late Quaternary Faulting of the Northern Basin and Range Province, Montana and Idaho," *Bulletin of the Seismological Society of America* v.77, 1602, 1625.
- 2-158. Smith, R.P., W.R. Hackett, and D.W. Rogers (1989), "Geological Aspects of seismic hazards assessments at the INEL, Southeastern Idaho," *Proceedings of the Second DOE Natural Hazards Mitigation Conference*, Knoxville, Tennessee, pp. 282-289.
- 2-159. Kuntz, M.A., D.E. Champion, E.C. Spiker, and R.H. Lefebvre (1986), "Contrasting Magma Types and Steady-state, Volume-predictable, Basaltic Volcanism Along the Great Rift, Idaho," *Geological Society of America Bulletin*, v. 97, p. 579-594.
- 2-160. Forman, S.L., R.P. Smith, W.R. Hackett, J.A. Tullis, and P.A. McDaniel (1993), "Timing of Late Quaternary Glaciations in the Western United States Based on the Age of Loess on the Eastern Snake River Plain, Idaho," *Quaternary Research*, v. 40, pp. 30-37.
- 2-161. Kuntz, M.A. (1978), *Geology of the Arco-Big Southern Butte Area, Eastern Snake River Plain, and Potential Volcanic Hazards to the Radioactive Waste Management Complex and other Waste Storage and Reactor Facilities at the Idaho National Engineering Laboratory, Idaho*, U.S. Geological Survey Open-File Report 78-691, 70 pp.
- 2-162. Doser, D.I. (1985). *The 1983 Borah Peak, Idaho, and 1959 Hebgen Lake, Montana, Earthquakes: Models for normal fault earthquakes in the Intermountain Seismic Belt*; in Proceedings of

- Conference XXVIII on the Borah Peak, Idaho, Earthquake, U.S. Geological Survey, Open File Report 85-290, pp. 368-384.
- 2-163. Singh, S. and R.B. Herrmann (1983), "Regionalization of Crustal Coda Q in the Continental U.S.," *Journal of Geophysical Research* 88, pp. 527-538.
- 2-164. Braile, L.W., R.B. Smith, J. Ansorge, M.R. Baker, M.A. Sparlin, C. Prodehl, M.M. Schilly, J.H. Healy, S.T. Mueller, and K.H. Olsen (1982). *The Yellowstone-Snake River Plain Seismic Profiling Experiment; Crustal Structure of the Eastern Snake River Plain*, *Journal of Geophysical Research*, v. 87, no. B4, pp. 2597-2610.
- 2-165. Title 10, Code of Federal Regulations, Part 100, *Reactor Site Criteria*, Washington, D.C.
- 2-166. DOE (2000), *DOE-ID Architectural Engineering Standards*, Rev. 27, U.S. Department of Energy, Idaho Falls, Idaho, April.
- 2-167. Agbabian Associates (1977), *Evaluation of Seismic Criteria Used in the Design of INEL Facilities, manuscript prepared for Idaho National Engineering Laboratory, Research and Development Administration*, Report R-7741d-4509, 151 pp.
- 2-168. Der Kiureghian, A. and A. H-S. Ang (1977), "A Fault-rupture Model for Seismic Risk Analysis," *Bulletin of the Seismological Society of America*, 67, pp. 1173-1194.
- 2-169. Tera Corporation (1978), *Influence of Seismic Modeling on Seismic Exposure Evaluation*, Tera Corporation, Berkeley, California.
- 2-170. Mortgat, C.P., T.C. Zsutty, H.C. Shah, and L. Lubetkin (1977), *A Study of Seismic Risk for Costa Rica*, John A. Blume Earthquake Engineering Center, Stanford University, California, Report 25.
- 2-171. Campbell, K.W. (1982), *A Preliminary Methodology for the Regional Zonation of Peak Ground Acceleration*, Proceedings of Third International Conference on Earthquake Microzonation 1, Seattle, Washington, pp. 365-376.
- 2-172. Tera Corporation (1984), *Seismic Hazard Analysis for Area 410, Nevada Test Site*, Tera Corporation, Berkeley, California.
- 2-173. Cornell, C.A. (1968), "Engineering Seismic Risk Analysis," *Bulletin of the Seismological Society of America* 58, pp. 1583-1606.
- 2-174. Youngs, R.R. and K.J. Coppersmith (1990), *Keeping Pace with the Science: Seismic Hazard Analysis in the Western U.S.*, Proceedings of the Second Natural Phenomena Hazards Mitigation Conference, pp. 262-270.
- 2-175. Campbell, K.W. and Y. Bozorgnia (1994), *Near-source Attenuation of Peak Horizontal Acceleration from Worldwide Accelerograms Recorded from 1957 to 1993*, Fifth U.S. International Conference on Earthquake Engineering, Chicago, Illinois.

- 2-176. URS Greiner Woodward-Clyde Federal Services, Geomatrix Consultants, and Pacific Engineering and Analysis (1999), *Development of Design Basis Earthquake Parameters for TMI-2 Independent Spent Fuel Storage Installation at the Idaho National Engineering and Environmental Laboratory*, Bechtel BWXT Idaho LLC External Report INEEL/EXT-99-00619, November.
- 2-177. URS Greiner Woodward-Clyde Federal Services, Geomatrix Consultants, and Pacific Engineering and Analysis (2000), *Recomputation of the Seismic Hazard at the Idaho National Engineering and Environmental Laboratory*, Bechtel BWXT Idaho LLC External Report INEEL/EXT-99-00786.
- 2-178. Stark, C.L., W.J. Silva, I.G. Wong, and S.M. Jackson (1992), *Assessment of Stress Drops of Normal Faulting Earthquakes in the Basin and Range Province*, Seismic Research Letters v. 63, No. 1, p. 39.
- 2-179. Spudich, P., J.B. Fletcher, M. Hellweg, J. Boatwright, C. Sullivan, W.B. Joyner, T.C. Hanks, D.M. Boore, A. McGarr, L.M. Baker, and A.G. Lindh (1996), *Earthquake Ground Motions in Extensional Tectonic Regimes*, U.S. Geological Survey Open File Report 96-292, 351 pp.
- 2-180. Spudich, P., J.B. Fletcher, M. Hellweg, J. Boatwright, C. Sullivan, W.B. Joyner, T.C. Hanks, D.M. Boore, A. McGarr, L.M. Baker, and A.G. Lindh (1997), SEA96- "A New Predictive Relation for Earthquake Ground Motions in Extensional Tectonic Regimes," *Seismic Research Letters*, v. 68, No. 1, pp. 190-198.
- 2-181. Spudich, P.M., W.B. Joyner, D.M. Boore, and B.M. Margaris, and J.B. Fletcher (1999), SEA99- "A Revised Ground Motion Predication Relation for use in Extensional Tectonic Regimes," *Bulletin of the Seismological Society of America*, v. 89, No. 5, pp. 1156-1170.
- 2-182. CRWMS M&O (1998), *Probabilistic Seismic Hazard Analysis for Fault Displacement and Vibratory Ground Motion at Yucca Mountain, Nevada*, in I.G. Wong and J.C. Stepp, coordinators of Final Report, prepared for U.S. Geological Survey and U.S. Department of Energy, three volumes.
- 2-183. Payne, S.J., V.W. Gorman, S.A. Jensen, M.E. Nitzel, M.J. Russel, and R.P. Smith (1999), *Development of Probabilistic Design Basis Earthquake (DBE) Parameters for Moderate and High Hazard Facilities at INEEL*, INEEL/EXT-99-00775, Bechtel BWXT Idaho, LLC.
- 2-184. U.S. Nuclear Regulatory Commission, NUREG-0800, *Standard Review Plan for the Review of Safety Analysis Reports for Nuclear Power Plants*. 1996
- 2-185. Shannon & Wilson (2001), *Final Report, Idaho Spent Fuel Project Seismic Design, INTEC Area, Idaho National Engineering and Environmental Laboratory*, Subcontract Number 027781, 21-1-09092-001, February.
- 2-186. Silva, W.J., RANPAR (random soil profile generation software), version 1.0., Pacific Engineering and Analysis, El Cerrito, California.

- 2-187. ProShake Ground Response Analysis Program, Version 1.10 (1999). EduPro Civil Systems, Inc., Redmond, Washington.
- 2-188. Silva, W.J. and K. Lee (1987), WES RASCAL Code for Synthesizing Earthquake Ground Motions: State-of-the-art for Assessing Earthquake Hazards in the United States: Army Corps of Engineers Waterways Experiment Station, Report 24, Miscellaneous Paper S-73-1, 120 pp.
- 2-189. BASECOR (program for baseline correction of time histories) (1994). Abrahamson, N.A.
- 2-190. U.S. Nuclear Regulatory Commission, NUREG/CR-5437, *Organization and Safety in Nuclear Power Plants*.
- 2-191. Golder Associates (1992), *High Level Waste Tank Farm Replacement Project Geotechnical Investigation*; prepared for Westinghouse Idaho Nuclear Company under Contract C90-132739.
- 2-192. Greely, R. (1982), "The Style of Basaltic Volcanism in the Eastern Snake River Plain, Idaho;" *Cenozoic Geology of Idaho*, Idaho Bureau of Mines and Geology Bulletin 26, pp. 407-422.
- 2-193. Kuntz, M.A. (1992), "A Model-based Perspective of Basaltic Volcanism, Eastern Snake River Plain, Idaho," *Regional Geology of Eastern Idaho and Western Wyoming*, Geological Society of America Memoir 179, pp. 289-304.
- 2-194. Kuntz, M.A., D.E. Champion, R.H. Lefebvre, and H.R. Covington (1988), *Geologic Map of the Craters of the Moon, Kings Bowl, Wapi Lava Fields and the Great Rift Volcanic Rift Zone, South-central Idaho*, U.S. Geological Survey Miscellaneous Investigations Series Map I-1632, scale 1:1000,000.
- 2-195. Humphreys, E.D. and K.G. Dueker (1994), "Western U.S. Upper Mantle Structure," *Journal of Geophysical Research*, v. 99, pp. 9615-9634.

Table 2.1-1
Typical Work Force at INEEL Facilities

Location	Number of Employees
Argonne National Laboratory West Area (ANL-W)	693
Central Facilities Area (CFA)	975
Idaho Nuclear Technology and Engineering Center (INTEC)	1080
Radioactive Waste Management Complex (RWMC)	280
Naval Reactor Facility (NRF)	858
Special Power Excursion Reactor Test (SPERT) and Power Burst Facility (PBF) and Waste Reduction Operations	142
Test Area North (TAN)	459
Test Reactor Area (TRA)	478
TOTAL	4965

2.1-T9001

THIS PAGE INTENTIONALLY LEFT BLANK.

**Table 2.3-1
Historical INEEL Daily Temperature Extremes**

Year	Highest Temperature (°F)	Lowest Temperature (°F)	Year	Highest Temperature (°F)	Lowest Temperature (°F)
1952	94	-23	1980	97	-27
1953	98	-15	1981	97	-25
1954	99	-17	1982	96	-32
1955	99	-24	1983	98	-47
1956	96	-30	1984	96	-34
1957	93	-29	1985	99	-36
1958	97	-15	1986	98	-16
1959	98	-31	1987	97	-17
1960	101	-32	1988	100	-28
1961	98	-13	1989	99	-27
1962	96	-40	1990	101	-38
1963	94	-35	1991	97	-20
1964	96	-33	1992	101	-28
1965	95	-10	1993	91	-26
1966	97	-14	1994	98	-13
1967	96	-23	1995	95	-14
1968	97	-29	1996	99	-31
1969	99	-14	1997	95	-12
1970	96	-23	1998	101	-28
1971	98	-28	1999	97	-15
1972	98	-40	2000	100	-13
1973	98	-32	Average⁽¹⁾	98	-26
1974	97	-29			
1975	98	-26			
1976	98	-18			
1977	97	-30			
1978	99	-37			
1979	98	-33			

(1) Averages have been rounded to the nearest whole number to yield conservative values.

SOURCE: Table based on NOAA data collected from Station 46W between 1952 and 2000.

T9006

Table 2.3-2
Mean and Maximum of Daily Temperature Range for INEEL

	Mean Range (°F)	Maximum Range (°F)
January	23	52
February	24	50
March	24	53
April	28	57
May	30	55
June	33	54
July	38	56
August	38	59
September	36	58
October	34	59
November	24	52
December	23	54

Table based on CFA data collected between January 1950 and December 1988 (Ref. 2-6).

TNEW3

Table 2.3-3
Historical Freeze and Thaw Cycles at the INEEL

	Average Number of Cycles (%)	Maximum Number of Cycles (%)	Minimum Number of Cycles (%)
January	33	74	3
February	58	100	0
March	82	100	39
April	75	97	53
May	31	65	3
June	6	17	0
July	0	3	0
August	2	16	0
September	26	57	0
October	76	97	39
November	76	97	27
December	43	81	6

Table based on CFA data collected between January 1950 December 1988 (Ref. 2-6).

TNEW4

Table 2.3-4
Historical INEEL Monthly Heating Degree Days and Extremes

	Total Accumulated Heating Degree Days			Daily Extreme Heating Degree Days	
	Mean	Highest	Lowest	Highest	Lowest
January	1517	1709	1086	85	22
February	1226	1623	865	88	21
March	1069	1446	764	71	11
April	702	889	471	43	2
May	428	610	234	35	0
June	183	299	44	25	0
July	29	90	1	16	0
August	54	192	4	20	0
September	291	493	142	36	0
October	652	832	433	44	2
November	1055	1342	860	74	14
December	1436	1726	1181	93	21

Table based on CFA data collected between January 1950 and December 1988 (Ref. 2-6).

T9191

Table 2.3-5
Historical INEEL Monthly Cooling Degree Days and Extremes

	Total Accumulated Cooling Degree Days			Daily Extreme Cooling Degree Days	
	Mean	Highest	Lowest	Highest	Lowest
January	0	0	0	0	0
February	0	0	0	0	0
March	0	0	0	0	0
April	0	0	0	0	0
May	1	24	0	0	0
June	31	137	3	6	0
July	123	224	58	18	0
August	85	174	32	18	0
September	6	32	0	0	0
October	0	0	0	9	0
November	0	0	0	0	0
December	0	0	0	0	0

Table based on CFA data collected between January 1950 and December 1988 (Ref. 2-6).

79192

Table 2.3-6
Historical INEEL Area Precipitation

	Lowest (inches)	Highest (inches)	Average (inches)
January	0.00	2.56	0.69
February	0.00	2.40	0.64
March	0.07	1.44	0.60
April	0.00	2.50	0.73
May	0.07	4.42	1.20
June	0.02	3.89	1.18
July	0.00	2.29	0.53
August	0.00	3.27	0.57
September	0.00	3.52	0.63
October	0.00	1.67	0.52
November	0.00	1.74	0.68
December	0.02	3.43	0.75
Annual Totals	0.18	33.13	8.72

Recorded precipitation in the CFA between January 1950 to December 1988 (Ref. 2-6).

T9003

Table 2.3-7
Historical Precipitation Extremes at INEEL

	During 1-Hour Period	During 24-Hour Period
January	0.18	0.79
February	0.16	0.79
March	0.17	0.61
April	0.18	1.51
May	0.43	0.95
June	0.54	1.64
July	0.20	1.25
August	0.40	0.80
September	0.37	1.55
October	0.34	0.74
November	0.16	0.71
December	0.23	1.07

Table based on CFA data reported between January 1950 and December 1988 (Ref. 2-6).

T8009

**Table 2.3-8
Historical INEEL Snowfall Amounts**

	Minimum (inches)	Maximum (inches)	Maximum in 24-hour Period (inches)	Average (inches)
January	0.0	18.1	8.5	6.1
February	0.0	15.0	7.5	4.7
March	0.0	10.2	8.6	3.5
April	0.0	16.5	6.7	2.3
May	0.0	8.3	4.4	0.7
June	0.0	0.0	0.0	0.0
July	0.0	0.0	0.0	0.0
August	0.0	0.0	0.0	0.0
September	0.0	1.0	1.0	0.1
October	0.0	7.2	4.5	0.6
November	0.0	12.3	6.5	3.3
December	0.0	22.3	7.0	6.4
Annual Totals	6.8	59.7	N/A	27.6

Table based on CFA data collected between January 1950 and December 1988 (Ref. 2-6).

T9004

**Table 2.3-9
Historical INEEL Dewpoint Temperatures**

	Average Air Temperature (°F)	Average Wet Bulb (°F)	Average Dew Point (°F)
January	16.5	14.7	7.4
February	22.0	19.6	12.5
March	31.5	26.4	16.1
April	41.9	33.0	19.0
May	52.3	41.0	27.8
June	61.3	46.2	31.0
July	69.0	47.9	33.5
August	66.4	47.9	29.3
September	56.2	41.7	23.8
October	44.1	34.4	19.7
November	27.9	23.7	14.0
December	22.0	19.2	10.8

Table based on CFA data collected between April 1955 and April 1961 (Ref. 2-6).

T9005

**Table 2.3-10
Historical INEEL Average Wind Speeds**

	Average Speed (mph)		Highest Hourly Average Speed (mph)			
			20-ft Level		250-ft Level	
	20-ft Level	250-ft Level	Speed	Direction	Speed	Direction
January	5.6	9.7	48	WSW	65	SW
February	6.9	11.3	36	SW	52	WSW
March	8.7	13.8	51	WSW	67	WSW
April	9.3	14.6	39	WSW	49	WSW-SW
May	9.3	14.3	41	SW	47	WSW-SW
June	8.9	14.2	36	SW	46	WSW-SW
July	8.0	13.5	35	WSW	47	WSW
August	7.7	13.1	40	WSW	54	SW
September	7.2	12.8	42	WSW	56	WSW
October	6.8	12.3	44	WSW	58	WSW
November	6.4	11.6	40	WSW	54	WSW
December	5.1	9.6	43	SW	56	SW

Table based on CFA data collected between April 1950 and October 1983 (Ref. 2-6).

TNEW1

**Table 2.3-11
Historical CFA Atmosphere Pressure**

	Average	Average Daily High	Average Daily Low	Station Pressure (in. of mercury)	
				Highest	Lowest
January	25.08	25.18	25.00	25.69	24.26
February	25.07	25.15	24.98	25.58	24.27
March	24.99	25.08	24.90	25.61	24.26
April	24.98	25.07	24.91	25.44	24.46
May	25.00	25.07	24.94	25.48	24.51
June	25.02	25.09	24.96	25.39	24.55
July	25.09	25.15	25.04	25.44	24.71
August	25.09	25.15	25.03	25.37	24.72
September	25.09	25.16	25.03	25.59	24.54
October	25.11	25.19	25.03	25.59	24.54
November	25.12	25.21	25.04	25.65	24.46
December	25.13	25.23	25.04	25.66	24.29
Average	25.06	25.14	24.99	25.69	24.26

Table based on data reported in TMI-2 ISFSI SAR (Ref. 2-1).

TNEW7

Table 2.3-12
DEQ-Estimated Planning-Level Ambient Concentrations INEEL Airshed

	1-hr	8-hr	24-hr	Quarterly	Annual
PM-10	NA	NA	86 ug/m ³	NA	32.7 ug/m ³
TSP	NA	NA	130 ug/m ³	NA	36.7 ug/m ³
Pb	NA	NA	NA	0.17 ug/m ³	NA
CO	10 ppm (11450 ug/m ³)	4.5 ppm (5153 ug/m ³)	NA	NA	NA
NO ₂	NA	NA	NA	NA	40
SO ₂	NA	0.208 ppm (544 ug/m ³)	0.055 ppm (114 ug/m ³)	NA	0.009 ppm (23.6 ug/m ³)
O ₃	40 ppb (78.5 ug/m ³)	NA	NA	NA	NA

Table based on data reported in TMI-2 ISFSI SAR (Ref. 2-1).

TNEWS6

Table 2.3-13
Historical INEEL Extremes of Daily Temperatures

	Highest Daily Maximum (°F)	Lowest Daily Minimum (°F)	Change in Temperature (°F)
January	51	-40	91
February	59	-36	95
March	70	-28	98
April	82	6	76
May	91	13	78
June	100	23	77
July	101	28	73
August	99	28	71
September	96	12	84
October	85	3	82
November	67	-24	91
December	55	-47	102

Table based on CFA data collected between January 1950 and September 1988
(Ref. 2-1).

T2.3-NEW2

Table 2.3-14
Expected INEEL Peak Wind Gusts

	20-ft Level		250-ft Level	
	Direction	Speed (mph)	Direction	Speed (mph)
January	SW	78	S	75
February	WSW	60	SW	66
March	WSW	78	SW	84
April	S	67	SW	62
May	SW	62	SSW	67
June	SSW	60	SSW	75
July	N	68	S	66
August	WSW	62	SW	72
September	WSW	61	WSW	70
October	WSW	66	WSW	76
November	WSW-SW	60	WSW	70
December	SW	64	SSW	80

Table based on CFA data collected between April 1950 and October 1964 (Ref. 2-6).

T9007

Table 2.3-15
Design Basis Tornado

	ISF Site
Maximum wind speed (mph)	200
Rotational speed (mph)	160
Maximum translational speed (mph)	40
Pressure drop (psi)	1.5
Rate of pressure drop (psi/sec)	0.6

T9008

Table 2.3-16
Predicted Maximum Storm Precipitation Amounts

	During 1-Hour Period	During 24-Hour Period
January	0.18	0.79
February	0.16	0.79
March	0.17	0.61
April	0.18	1.51
May	0.43	0.95
June	0.54	1.64
July	0.20	1.25
August	0.40	0.80
September	0.37	1.55
October	0.34	0.74
November	0.16	0.71
December	0.23	1.07

Table based on data reported in TMI-2 ISFSI SAR (Ref. 2-1).

T9176

Table 2.3-17
Average Number of Days (percent) with Specified Amounts of
Precipitation at the INEEL

	Trace or More (%)	0.01-Inch or More (%)	0.10-Inch or More (%)	0.50-Inch or More (%)	1.00-Inch or More (%)
January	40	24	7	0.7	0.0
February	35	21	8	0.7	0.0
March	32	20	7	0.2	0.0
April	31	20	8	0.6	0.1
May	35	25	13	1.4	0.0
June	34	23	11	1.9	0.3
July	17	12	5	0.7	0.1
August	21	12	5	1.0	0.0
September	19	12	6	0.9	0.2
October	20	12	6	0.7	0.0
November	27	19	8	0.6	0.0
December	35	23	9	0.3	0.1

Table based on CFA data collected between January 1950 and December 1988 (Ref. 2-6).

T9011

Table 2.3-18
Historical INEEL Average Number of Days (percent) with Specified Snowfall Amounts

	Snowfall Amounts		
	0.1-Inch or More (%)	1.0-Inch or More (%)	3.0-Inch or More (%)
January	20	7	1
February	14	6	2
March	11	4	1
April	6	2	1
May	1	1	0
June	0	0	0
July	0	0	0
August	0	0	0
September	0	0	0
October	2	1	1
November	9	4	2
December	19	8	1

Table based on CFA data collected between January 1950 and December 1988 (Ref. 2-6).

T9012

Table 2.3-19
Historical INEEL Maximum and Average Snow Depths
(in inches)

	Maximum	Average
January	18.1	6.1
February	15	4.7
March	10.2	3.5
April	16.5	2.3
May	8.3	0.7
June	0	0.0
July	0	0.0
August	0	0.0
September	1.0	0.1
October	7.2	0.6
November	12.3	3.3
December	22.3	6.4

Table based on CFA data collected between January 1950 and December 1988 (Ref. 2-6).

T9013

Table 2.3-20
XOQDOQ Input Data and Program Options Used in the INEEL INTEC Dispersion Analysis

Parameter	Available Option	INTEC Application ⁽¹⁾
Stability	Various	NRC (UT) Grid 3
Wind	Various	PBF (1982)
Release height	Elevated or ground level or mixed mod	Ground level
Stack effluent momentum, temperature	Momentum and/or buoyancy	None, surface release
Building wake effects	Dimensions, relation to release point	Not used
Transport level wind height	May be extrapolated through planetary boundary layer	Not adjusted, 15.2 M used
Topography	Input for modified effective plume height	Not used, flat terrain
Radioactive decay	Incorporate varied half lives	Not used
Dry disposition	Incorporate depletion factors	Not used
Recirculation or stagnation	Tune X/Q; D/Q values	Not used
Receptor grid	Standard or custom	Standard

(1) Table as reported in TMI-2 ISFSI SAR (Ref. 2-1).

T9014

Table 2.3-21
MESODIF Input Data and Program Options Used in the INEEL INTEC Dispersion Analysis

Parameter	Available Option	INTEC Application ⁽¹⁾
Stability	Various	NRC (UT) Grid 3
Wind	Various	All stations
Release height	As input	Ground level
Stack effluent momentum, temperature	As input	Ambient
Building wake effects	Dimensions, relation to release point	Not used
Topography	Option not available	Not used
Radioactive decay	Option not available	Not used
Deposition decay	Option not available	Not used
Recirculation or stagnation	Consider directly	In windfield

(1) Table as reported in TMI-2 ISFSI SAR (Ref. 2-1).

T9015

THIS PAGE INTENTIONALLY LEFT BLANK.

Table 2.4-1
Historical Monthly Big Lost River Discharge Near INTEC (Cubic Feet)

Year	Jan	Feb	Mar	Apr	May	Jun	Jul	Aug	Sep	Oct	Nov	Dec	Annual
1965	0	0	2380	10300	15400	29600	31100	16900	10900	0	0	0	116580
1966	0	0	0	3660	981	0	0	0	0	0	0	0	4641
1967	0	0	0	0	2030	20180	18376	4400	9050	8740	0	0	62776
1968	0	0	2280	3390	16	524	0	1053	1130	3290	4500		16183
1969	0	0	0	3960	33000	33500	21800	4780	9840	6710	3290	0	116880
1970	0	0	501	1650	793	13800	17700	1510	6080	5280	4750	8	52072
1971	0	0	0	10600	12300	17200	20800	7760	13400	14400	13100	0	109560
1972	0	0	1540	4920	504	1710	861	84	2990	3520	3099	0	19228
1973	0	0	0	2830	405	0	0	0	0	0	0	0	3235
1974	0	0	3240	5520	6940	16200	9390	1170	1160	3760	4200	0	51580
1975	0	0	0	3180	12000	12100	18700	3560	6520	8210	7990	0	72260
1976	0	0	333	1450	1660	1120	0	0	300	620	1100	76	6659
1977	0	0	0	0	0	0	0	0	0	0	0	0	0
1978	0	0	0	0	0	0	0	0	0	0	0	0	0
1979	0	0	0	0	0	0	0	0	0	0	0	0	0
1980	0	0	0	0	0	0	1140	0	0	0	0	0	1140
1981	0	0	0	1300	5092	7560	0	0	0	0	0	0	13952
1982	0	0	0	5930	17200	13400	15100	4820	8190	10500	5740	600	81480
1983	600	600	900	12800	15800	18900	18200	9780	7320	6200	5660	1200	97960
1984	1200	1200	1200	2200	2230	4550	3950	5790	5140	5980	8710	2120	44360
1985	3	0	0	7170	6430	0	0	0	9950	10707	1275	0	35535
1986	0	96	537	8370	14825	20315	2900	1016	14753	8220	1190	2	72224
1987	0	0	531	491	0	0	0	0	0	0	0	0	1022
1988	0	0	0	0	0	0	0	0	0	0	0	0	0
1989	0	6	0	0	0	0	0	0	0	0	0	0	0
1990	0	0	0	0	0	0	0	0	0	0	0	0	0
1991	0	0	0	0	0	0	0	0	0	0	0	0	0
1992	0	0	0	0	0	0	0	0	0	0	0	0	0
1993	0	0	0	0	0	5116	0	0	0	0	0	0	5116
1994	0	0	0	0	0	0	0	0	0	0	0	0	0

Data for table as reported in TMI-2 ISFSI SAR (Ref. 2-1).

T9017

**Table 2.4-2
Dam and Reservoir Characteristics**

Characteristic	Mackay Dam	INEEL Flood Diversion Facility
Dam crest elevation (ft)	6076	5064.7
Dam crest length (ft)	1430	500
Dam height (ft)	79	22
Spillway	Ungated overflow crest, 75 ft	None
Spillway crest elevation (ft)	6066.5	N/A
Gate Centerline Elevation (ft)	Upper 6036.6 Lower 6007.8	5045.6
Dam base elevation (ft)	5997	5042.6
Spillway maximum capacity (cfs)	6588	N/A
Gate maximum capacity (cfs)	2960	1121
Reservoir capacity ⁽¹⁾ (ac-ft)	55091 @ 6076 44500 @ 6066.5 8750 @ 6030 500 @ 6010	18200 @ 5040 58000 @ 5050

- (1) The TMI-2 ISFSI SAR stated that the Mackay Reservoir lost 22% of mid and late season irrigation capacity due to sedimentation of the reservoir. Reservoir capacity for the INEEL Flood Diversion Facility Dam is for the spreading areas; no water is held immediately behind the diversion dam (Ref. 2-1).

T9016

Table 2.4-3
Results of Probable Maximum Flood Induced Overtopping Failure of Mackay Dam⁽¹⁾

Location	Elevation (ft-msl)	Peak Surface Water Elevation (ft-msl)	Peak Flood Flow (cfs)	Peak Water Velocity (ft/sec)	Time of Wave Arrival (hrs)
Mackay Dam	6076	6,078	306,700	8.5	0.0
ARCO	5310	5,319	147,720	5.6	6.7
INEEL Diversion Facility	5065	5,073	71,850	1.0	10.0
CFA	4928	4,942	67,830	3.4	12.8
TRA	4920	4,924	67,170	2.8	13.2
INTEC ⁽²⁾	4914	4,917	66,830	2.7	13.5
NRF	4845	4,851	61,620	1.9	16.4
TAN	4780	4,786	34,810	1.1	34.5

(1) Document Datum for these numbers is 1986 Flood Study Elevation Datum.
Table developed from data presented in the TMI-2 SAR (Ref. 2-1)

(2) The ISF Facility site is adjacent to the INTEC and is at an elevation of 4913* feet (1986 Flood Study)

* Note: The 1986 Flood Study elevations can be converted to NAVD 88 datum values in the vicinity of the ISF Facility site by adding 3.71 feet to the 1986 Flood Study elevation.

T9018

Table 2.4-4
Results of Seismic Induced Failure of Mackay Dam During 25-Year Flood⁽¹⁾

Location	Elevation (ft-msl)	Peak Surface Water Elevation (ft-msl)	Peak Flood Flow (cfs)	Peak Water Velocity (ft/sec)	Time of Wave Arrival (hrs)
Mackay Dam	6076	6,067	107,480	5.8	0.0
ARCO	5310	5,317	74,240	4.8	8.3
INEEL Diversion Facility	5065	5,070	45,410	1.4	11.8
CFA	4928	4,942	40,520	3.0	14.8
TRA	4920	4,923	39,580	2.5	15.3
INTEC ⁽²⁾	4914	4,916	39,080	2.4	15.8
NRF	4845	4,850	31,690	1.5	18.9
TAN	4780	4,782	4,440	0.7	42.5

(1) 1986 Flood Study Elevation Datum.

(2) The ISF Facility site is adjacent to the INTEC and is at an elevation of 4913* feet (1986 Flood Study).

Note: The 1986 Flood Study elevations can be converted to NAVD 88 datum values in the vicinity of the ISF Facility site by adding 3.71 feet to the 1986 Flood Study elevation.

T9019

**Table 2.4-5
Dam Failure Characteristics**

Failure	Seismic	100-Yr Piping	500-Yr Piping	Overtopping PMF
Mackay Dam				
Breach type	Trapezoid	Triangle	Trapezoid	Trapezoid
Breach bottom width (ft)	31.6	0.0	31.6	140.0
Breach side slope (x/y)	0.6	0.6	0.6	0.6
Failure mode	Internal (seismic)	Internal (piping)	Internal (piping)	Hydrologic (overtopping)
Failure time (hr)	1.0	1.0	1.0	1.0
Reservoir inflow hydrograph	25-Yr Flood	100-Yr Flood	500-Yr Flood	PMF
Peak reservoir inflow (cfs)	4,030	4,870	5,760	82,100
Reservoir level at failure (ft-msl)	6,066	6,066	6,066	6,077
INEEL Flood Diversion Facility				
Breach type	Trapezoid	Trapezoid	Trapezoid	Trapezoid
Breach bottom width (ft)	60.0	60.0	60.0	60.0
Breach side slope (x/y)	0.6	0.6	0.6	0.6
Failure mode	Overtopping	Overtopping	Overtopping	Overtopping
Failure time (hr)	0.1	0.1	0.1	0.1
Initial water level (ft-msl)	5,060	5,060	5,060	5,060
Flow losses, percent of total flow	40	40	40	40

T9020

THIS PAGE INTENTIONALLY LEFT BLANK.

**Table 2.5-1
INEEL Production Wells and Annual Volume Pumped**

Well Name ⁽¹⁾	Depth of Well (ft bls) ⁽²⁾	Depth to Water (ft bls)	Annual Volume (gal)
ANP-01	360	208	2.561E+06
ANP-02	340	211	1.433E+06
ANP-08	309	218	3.908E+05
Badging Facility Well	644	489	5.76E+04
CFA-1	639	468	1.473E+07
CFA-2	681	471	1.448E+05
CPP-01	586	460	1.834E+08 ⁽³⁾
CPP-02	605	460	1.834E+08 ⁽³⁾
CPP-04	700	462	1.834E+08 ⁽³⁾
CPP-05	695	447	1.834E+08 ⁽³⁾
EBR-1	1075	596	4.491E+04
EBR II-1	745	632	2.767E+06 ⁽⁴⁾
EBR II-2	753	630	2.767E+06 ⁽⁴⁾
FET-1	330	199	1.427E+06
FET-2	455	200	5.067E+05
Fire Station Well	516	420	1.057E+04
NRF-1	535	363	2.594E+06
NRF-2	529	362	9.368E+06
NRF-3	546	363	9.802E+04
NRF-4	597	363	1.649E+07
Rifle Range Well	620	508	9.115E+04
RWMC Production	685	568	4.824E+05
SPERT-1	653	456	3.871E+05
SPERT-2	1217	463	3.450E+05
TRA-01	600	453	3.595E+07
TRA-03	602	456	2.074E+06
TRA-04	965	463	9.006E+07

(1) All wells withdraw water from the main body of the Snake River Plain Aquifer and are used for drinking water with the exception of wells ANP-08, Fire Station Well, and NRF-4 that are production wells for INEEL operations.

(2) Feet below land surface (ft bls).

(3) Annual volume data is the total for Wells CPP-1, CPP-2, CPP-4, and CPP-5.

(4) Annual volume data is the total for Wells EBR II-1 and EBR II-2.

T9021

THIS PAGE INTENTIONALLY LEFT BLANK.

Table 2.6-1
Time Periods of Earthquake Data Completeness

Magnitude Interval	Completeness Period
2.0 – 4.0	1975 – 1995
4.0 – 5.0	1963 – 1995
5.0 – 5.5	1950 – 1995
5.5 – 6.0	1925 – 1995
6.0 – 6.5	1900 – 1995
6.5 – 7.0	1875 – 1995
7.0+	1850 – 1995

Table developed from information reported in TMI-2 ISFSI SAR (Ref. 2-1).

TNEWS

Table 2.6-2
Earthquakes with Magnitudes Greater than 5.5 within 321 Kilometers of INEEL ⁽⁴⁾

Earthquake Date/Time ⁽¹⁾	Magnitude ⁽²⁾	Modified Mercalli Intensity ⁽³⁾		Geographical Location	Radial Distance (km)
		Epicenter	INTEC Area		
1884: November 10/ 08:50					
1905: November 11/ 21:26	5.5 M _L	VII	IV	Shoshone, ID	164
1909: October 6/ 02:50	6.3 M _L	VIII		Hansel Valley, UT	216
1914: May 13/ 17:15	5.7 M _L	VII		Ogden, UT	283
1925: June 28/ 01:21	6.8 M; 6.6 M _w	VI		Clarkston, MT	275
1925: June 29/ 01:12	6.3 M			Clarkston, MT	292
1930: June 12/ 09:15	5.8 M _L	VI		East of Soda Springs, ID	190
1934: March 12/ 15:05	6.6 M _L ; 6.6 M _w	IX		Hansel Valley, UT	222
1934: March 12/ 18:20	6.2 M _L ; 5.9 M _w	VII		Hansel Valley, UT	222
1934: April 14/ 21:26	5.6 M _L	VII		Hansel Valley, UT	245
1934: May 6/ 08:09	5.6 M _L	VI		Hansel Valley, UT	222
1944: July 12/ 19:30	6.1 M _B	VII		North of Stanley, ID	235
1945: February 14/ 03:01	6.0 M _L	VI		North of Stanley, ID	235
1947: November 23/ 00:46	6.3 M; 6.1 M _w			Virginia City, MT	138
1959: August 18/ 06:37	7.5 M _s ; 6.3 M _w 7.3 M _w	X	VI	Hebgen Lake, MT	187
1959: August 18/ 07:56	6.5 M			Hebgen Lake, MT	208
1959: August 18/ 08:41	6.0 M			Hebgen Lake, MT	208
1959: August 18/ 11:03	5.6 M			Hebgen Lake, MT	182
1959: August 18/ 15:26	6.5 M _B ; 6.3 M _w			Hebgen Lake, MT	209
1959: August 19/ 04:04	5.9 M _s ; 6.0 M _w			Hebgen Lake, MT	209
1962: August 30/ 13:35	5.7 M _s ; 5.9 M _w	VII		Cache Valley, UT	208
1964: October 21/ 07:38	5.8 M _B ; 5.6 M _w			Hebgen Lake, MT	154
1975: March 28/ 02:31	6.1 M _B ; 6.2 M _w	VIII	III	Pocatello Valley, UT	183
1975: June 30/ 18:54	6.1 M _L	VII	Not Felt	Yellowstone Park, WY	209
1976: December 8/ 14:40	5.5 M _B			Yellowstone Park, WY	198
1983: October 28/ 14:06	7.3 M _s ; 6.8 M _w	IX	VI	Northwest of Mackay, ID	93

Table 2.6-2
Earthquakes with Magnitudes Greater than 5.5 within 321 Kilometers of INEEL ⁽⁴⁾

Earthquake Date/Time ⁽¹⁾	Magnitude ⁽²⁾	Modified Mercalli Intensity ⁽³⁾		Geographical Location	Radial Distance (km)
		Epicenter	INTEC Area		
1983: October 28/ 19:51	5.8 M _L ; 5.4 M _w			Northwest of Mackay, ID	98
1983: October 29/ 23:29	5.8 M _L ; 5.5 M _w			Northwest of Mackay, ID	121
1984: August 22/ 09:46	5.8 M _L ; 5.6 M _w			Challis, ID	127
1994: February 3/ 09:05	5.9 M _w ; 5.7 M _w	V	Not Felt	West of Afton, WY	172

- (1) Universal Time Coordinated (Greenwich Mean Time)
- (2) Highest magnitude value is reported on this table. Moment magnitudes are included, if calculated.
- (3) Modified Mercalli intensity for epicenter is based on Wood and Neumann, 1931. Modified Mercalli intensity at the ISF site was obtained from available intensity maps.
- (4) Table as reported in TMI-2 ISFSI SAR (Ref. 2-1).

Magnitude Scales:

M _I	Conversion from Intensity
M _L	Local or Richter
M	Magnitude type not specified
M _B	Body-wave
M _S	Surface-wave
M _w	Moment

T9023

Table 2.6-3
Ground Motions Recorded During the Borah Peak Earthquake at CPP-601

Location		Acceleration (g)	Velocity (cm/sec)	Displacement (cm)
CPP-601 1 st Floor	L	0.043	1.38	0.25
	T	0.065	2.76	0.13
	V	0.033	1.28	0.16
CPP-601 2 nd Basement	L	0.038	1.32	0.12
	T	0.044	2.19	0.16
	V	0.038	1.46	0.11
CPP-601 Free Field	L	0.078	2.03	0.23
	T	0.058	2.80	0.34
	V	0.035	1.39	0.25

Table developed from information reported in TMI-2 ISFSI SAR (Ref. 2-1).

TNEWS

Table 2.6-4
Basin and Range Faults Around the Eastern Snake River Plain

Fault	Important Points
Sawtooth, White Cloud Peaks Area	Contemporary earthquake swarms, maximum magnitude = 6.1, several mapped normal faults.
Lost River Fault	<p>Arco Segment – MRE ~30 Ka, trenching, D~2-3 m, L~10 km, SR~0.12 mm/y, RI~30-40 Ka</p> <p>Pass Creek Segment – MRE~30-50 Ka, scarp morphology, ND, L~30 km, RI~30-50 Ka, scarp Morphology, ND, L~30 Km, R1~30-50 Ka?</p> <p>Mackay Segment – MRE~4.3-6.8 Ka, trenching, ND, L~22 km, SR~0.3 mm/yr, RI~4.7 Ka</p> <p>Thousand Springs Segment – MRE=1983, trenching/earthquake, D=2.7 m, L=36 km, SR=0.3 mm/yr, RI=6-7 Ka</p> <p>Warm Spring Segment – MRE.5-6.2 Ka, trenching, ND, L=15 km, SR=0.3 mm/yr, RI<15 Ka</p> <p>North Segment – MRE>Late Quaternary, scarp morphology, ND, L~20km., ND, ND, low structural relief</p>
Lemhi Fault	<p>Southern Segment (Howe and Fallert Springs segments) – MRE~15-24 Ka, trenching/scarp morphology, D~2-3 m, L~25 km, SR~0.1 mm/yr, RI=3.3 Ka (avg.)</p> <p>Sawmill Gulch Segment – MRE<10 Ka, trenching, D=1.7 m, L=43 km, ND, ND</p> <p>Goldburg Segment – MRE~10-15 Ka, scarp morphology, ND, L=12 km, ND, ND</p> <p>Patterson Segment – MRE<10 Ka?, scarp morphology, ND, L~23 km, ND, ND</p> <p>May Segment – MRE~15-30 Ka?, scarp morphology, ND, L~23 km, ND, ND</p>
Beaverhead Fault	<p>Blue Dome Segment – MRE>30 Ka, scarp morphology, ND, L~25 km, ND, ND</p> <p>Nicholia Segment – MRE~10-15 Ka, scarp morphology, ND, L~42 km, ND, ND</p> <p>Badly Mountain Segment – MRE>30 Ka, scarp morphology, ND, L~21 km, ND, ND</p> <p>Leadore Segment – MRE<10 Ka, scarp morphology, ND, L~23 km, ND, ND.</p> <p>Mollie Gulch Segment – MRE~10-15 Ka?, scarp morphology, ND, L~20 km, ND, ND</p> <p>Lemhi Segment – MRE>30 Ka, scarp morphology, ND, L~20 km, ND, ND</p>
Red Rock Fault	<p>Sheep Creek Segment – MRE<10 Ka, scarp morphology, ND, L~16 km, ND, ND</p> <p>Timber Butte Segment – MRE~10-15 Ka, scarp morphology, ND, L~11 km, ND, ND</p>
Centennial Fault	<p>Western Centennial Valley Segment – MRE<10 Ka, scarp morphology, ND, L~23 km, ND, ND</p> <p>Red Rocks Lake Segment – MRE>20 Ka?, scarp morphology, ND, L~24 km, ND, ND</p> <p>Henrys Lake Segment – MRE<10 Ka, scarp morphology, ND, L~1 km, ND, ND</p>
Madison Fault	<p>Madison Canyon Segment – MRE~Late Holocene (1947?, 1959?), scarp morphology, ND, L~34 km (total fault length = 117 km)</p> <p>Additional scarps exist but no segments have been delineated (a short segment of this fault ruptured in 1959).</p>

Table 2.6-4
Basin and Range Faults Around the Eastern Snake River Plain

Fault	Important Points
Hebgen Fault and Red Canyon Fault	Hebgen Fault – MRE=1959, scarp morphology, D=6.7m, L~13 km (+14 km on R.C. Fault), ND, ND Red Canyon Fault – MRE=1959, scarp morphology, D=6.7 m, L~45 km, SR~1.2 – 1.5 mm/yr (pre-1959), RI=4.3 Ka
Yellowstone Area	Numerous north-trending normal faults around Yellowstone Caldera with Quaternary movement. Contemporary seismicity, maximum magnitude = 6.1. RI = 700-750 years for M7 earthquakes based on seismic moment rates.
Teton Fault	South Segment – MRE~7 Ka, trenching and scarp morphology, D=4.1m, L~24 km, SR~1.7-2.2 mm/yr, RI~1.4-2.3 Ka Middle Segment – MRE<11-14 Ka, scarp morphology, D~3m, L~20 km, SR~1.7-2.2 mm/yr, RI~1.4-2.3 Ka North Segment – MRE<11-14 Ka, scarp morphology, D~3m, L~20 km, SR~1.7-2.2 mm/yr, RI~1.4-2.3 Ka
Grand Valley Fault	Grand Valley Fault – MRE>15-30 Ka, scarp morphology, ND, L~72 km, SR~0.02-0.04 mm/yr, ND
Snake River Fault	Snake River Fault – MRE>15-30 Ka, scarp morphology, ND, L~50 km, SR~0.001 mm/yr, ND
Star Valley Fault	Northern Segment – MRE<9 Ka, scarp morphology, D~3.6-6.3, L~30 km, SR~0.8-1.2 mm/yr, RI~5-7 Ka Southern Segment – MRE<9 Ka, trenching and scarp morphology, D~5.0-6.3 m, L~28 km, SR~0.6-1.1 mm/yr, RI~5-7 Ka
Northern Wasatch Fault Segments	Collinston Segment – MRE>13 Ka, scarp morphology, ND, L~25 km, ND, ND Brigham City Segment – MRE=3400 yrs, trenching, ND, L~40 km, ND, ND Weber Segment – MRE~500 years, 1.7-3.7 m, trenching, D~1.7-3.7m, L~50 km, SR~1.2-2.8 mm/yr, RI~1 Ka?

For each segment or fault, the information under IMPORTANT POINTS is presented as follows: Most recent event (MRE); in thousands of years ago (Ka); type of study, displacement per last event (D); length (L); slip rate (SR); and recurrence interval (RI). ND – no data available.

TNEW7

Table 2.6-5
Earthquakes within 200 Miles that have Occurred on Tectonic Structures

Earthquake Date and Time (Hr/Min - UTC)	Seismic Moment ($\times 10^{25}$ dyne-cm)	Focal Mechanism Strike/Dip/Rake (Degrees)	Tectonic Structure, Source Parameters and Dimensions and References
1925 June 28 01:21	10 ± 2 B	30 80 -175 FM 250 56 -38 BW	Associated with a fault oriented in an oblique manner north of the Clarkston Valley Fault north of Bozeman, Montana. Z= 9 ± 5 km (LP); RL= 25 ± 5 km (BW), 59 ± 5 km (SF); SD= 2.0 ± 1.0 m (v).
1934 March 12 15:05	0.95 G 8.6 ± 2 B	7 80 -70 FM 40 87 -11 BW 0 73 -110 SF	Caused a fault scarp along an unnamed fault in Hansel Valley, Utah. Z= 8 ± 2 km (LP); RL= 11 ± 3 km (BW), 6 ± 2 km (SF); BWD= 2.1 ± 0.1 m (h), 0.2 ± 0.05 m (v); SD= 0.2 (h), 2.0 ± 1.0 m (v) GD= 0.4 ± 0.1 m (v)
1934 March 12 18:20	0.77 ± 0.3 B	25 85 -20 BW	Aftershock to March 12, 1934 earthquake Z= 8 ± 7 km (LP); RL= 7 ± 3 km (BW); BW= -0.5 ± 0.1 m (h).
1947 November 23 09:46	1.8 ± 0.5 B	120 60 -120 FM 104 48 -170 BW	Possibly associated with the Madison Fault northwest of Hebgen Lake, Montana Z= 8 ± 2 km (LP); RL= 9 ± 2 km (BW); BWD= -0.7 ± 0.2 m (h).
1959 August 18 06:37 (Ms 7.5)	41 G 150 L 120 S	102 60 -90 SW 120 70 -90 SF 132 45 -90 GE	Caused a fault scarp along the Hebgen and Red Canyon faults near Hebgen Lake, Montana. No distinction between subevents: Z= 11 ± 2 km (LP); RL= 24 ± 4 km (SF), 40 ± 4 km (GE) SD= 4.4 m (v); GD= 7.4 ± 0.4 m (v).
1959 August 18 06:37 (Mw 6.3)	2.8 B	102 60 -90 FM 95 42 -90 BW	Subevent 1: Z= 10 ± 2 km (LP); RL= 7 ± 1 km (BW); BWD= 0.95 m (v).
1959 August 18 06:37 (Mw 7.3)	92 B	100 54 -90 FM 95 42 -90 BW	Subevent 2: Z= 15 ± 3 km (LP); RL= 21 ± 5 km (BW); BWD= 6.8 m (v)
1959 August 18 07:56	nd	70 55 -45 FM	Aftershock to August 18, 1959 earthquake. nd.
1959 August 18 08:41	nd	70 65 -15 FM	Aftershock to August 18, 1959 earthquake. nd.

Table 2.6-5
Earthquakes within 200 Miles that have Occurred on Tectonic Structures

Earthquake Date and Time (Hr/Min – UTC)	Seismic Moment (x10 ²⁵ dyne-cm)	Focal Mechanism Strike/Dip/Rake (Degrees)	Tectonic Structure, Source Parameters and Dimensions and References
1959 August 18 11:03	nd	50 64 31 FM	Aftershock to August 18, 1959 earthquake. nd.
1959 August 18 15:26	3.10 B 5.5 S	90 60 -70 FM 83 50 -90 BW	Aftershock to August 18, 1959 earthquake. Z= 10±2 km (LP); RL= 9±1 km (BW).
1959 August 19 04:04	1.1 ± 0.3 B 4.8 S	60 75 -155 FM 57 80 -161 BW	Aftershock to August 18, 1959 earthquake. Z= 8±2 km (LP); RL= 11±2 km (BW)
1962 August 30 13:35	0.52 ± 0.2 B	185 58 -85 FM 201 49 -108 BW	Associated with the Temple Ridge fault, Cache Valley, Utah. Z= 12±2 km (LP); RL= 3±1 km (BW); BWD= 0.55 ± 0.2 m (h).
1964 October 21 07:38	1.10 ± 0.3 B	310 60 18 FM 307 56 14 BW	Aftershock to August 18, 1959 earthquake. RL= 3±1 km (BW).
1975 March 28 02:31	123 ± 0.6 B 2.4 L 1.2 S	225 39 -53 FM 200 38 -70 BW 210 60 -90 GE	Associated with an unnamed fault in Pocatello Valley, Utah. Z= 9±2 km (LP), 5±2 km (SP), 12 km (GE); R= 12±2 km (BW), 18±2 km (GE); BWD= 0.75 ± 0.25 m (v); GD = 0.50 m (v).
1975 June 30 18:54	0.75 S	302 71 -129 FM	Associated with an unnamed fault near the north-central boundary of the Yellowstone Caldera, Wyoming. Z= 6±1 km (SP); GD= 0.12 m (v).
1983 October 28 14:06	28 G 21 B 29L	138 45 -60 FM 155 50 -65 BW 160 70 -70 SF 152 49 nd GE	Caused a fault scarp along the Thousand Springs segment of the Lost River Fault in central Idaho. Z= 16±4 km (LP), 12±2 km (SP), 14 km (GE); RL= 21±2 km (BW), 19±2 km (SF), 20±2 km (GE); BWD= -0.20 m(h), 1.30 m (v); SD= -0.30 m (h), 1.50 m (v); GD= 2.10 m (v).
1983 October 28 19:51	0.13 B 0.24 S	287 58 -165 FM 282 48 -159 BW 286 70 -155 SF	Aftershock to October 28, 1983 earthquake. Z= 10 km (LP), 10 km (SP), 10 km (GE); RL= 6±2 km (BW).
1983 October 29 23:29	0.20 B	309 51 -65 FM 317 45 -90 BW	Aftershock to October 28, 1983 earthquake. Z= 19±9 km (LP), 10 km (SP); RL= 8±1 km (BW)
1984 August 22 09:46	0.24 B	170 70 -5 FM 348 85 -160 BW	Aftershock to October 28, 1983 earthquake. Associated with the Challis segment of the Lost River fault and possibly caused slip (M 5.0) on an antithetic fault, the

Table 2.6-5
Earthquakes within 200 Miles that have Occurred on Tectonic Structures

Earthquake Date and Time (Hr/Min – UTC)	Seismic Moment (x10 ²⁵ dyne-cm)	Focal Mechanism Strike/Dip/Rake (Degrees)	Tectonic Structure, Source Parameters and Dimensions and References
			Lone Pine fault, central Idaho. Z= 10 km (LP), 10 km (SP); RL= 7±1 km (BW)
1994 February 3 09:05	0.51 W	355 41 -91 WI	Mainshock associated with unknown fault located 18 km west of the west-dipping Star Valley normal fault Z= 8 km
1999 August 20 13:50	0.02 W	108 55 - 85WI	The earthquake and aftershocks are interpreted to be associated with a cross-over structural zone between the east-dipping Red Rock normal fault and the west-dipping Monument Hill fault, range-bounding faults with late Quaternary displacements

Events through February 3, 1994 documented in TMI-2 ISFSI SAR (Ref. 2.1).

TNEWS

Table 2.6-6
Historical Earthquakes Possibly Located within the Eastern Snake River Plain

Date	Origin Time (UTC)	Intensity	Magnitude	Location Error (km)
11 November 1905	22:29	MM VII	M _L 5.5	±100 – 200
20 February 1909	01:nd	MM II	nd	±50 – 100
6 December 1925	16:16	Felt	nd	±50 – 100
7 August 1927	nd	Felt	nd	±50 – 100
5 September 1928	05:36	Felt	M _L 5.2	>±100
6 June 1932	11:00	MM II	nd	±50 – 100
21 December 1932	08:00	MM II	nd	±50 – 100
28 April 1934	09:30	MM IV	nd	±100 – 200
28 April 1934	10:00	MM III	nd	±100 – 200
29 April 1934	06:10	MM III	nd	±100 – 200
18 November 1937	23:50	nd	M _L 5.4	nd
1 February 1954	03:33:19	nd	nd	±50 – 100
20 January 1964	10:09:39.7	nd	nd	±22 – 56
28 February 1969	15:30:24.4	nd	nd	±22 - 56

Table developed from information reported in TMI-2 ISFSI SAR (Ref. 2-1).

TNEW9

Table 2.6-7
Maximum Magnitudes and Focal Depths of Earthquakes Associated with Dike Injection^(a)

Location	Volcanic Event ^(c) (Year)	Maximum Magnitude ^(d)	Focal Depth(s) ^(e) (km)
Iceland			
Krafla	1975 - 75	5.0 ^(f)	0 - 4
Krafla	1977	3.8 ^(f)	0 - 6
Krafla	1978	4.1 ^(f)	1 - 4
Hawaii, USA			
Kilauea Rift Zones			
East	1965	4.4 (M)	0 - 8
East	1968, Aug.	3.3	<5
East	1968, Oct.	3.1	<6
East	1969	4.7	<7
Southwest	1975	3.0	nd
East	1976-77	4.0	<10
East	1980, Aug.	3.0 (M) ^(g)	0.5 - 3
East	1980, Nov.	3.1 (Mc) ^(g)	0.7 - 4
Southwest	1981	3.4 (M) ^(g)	1 - 2
East	1982	3.0 (M) ^(g)	0.5 - 3
Japan			
Izu Peninsula ^(h)	1989	5.5 (M)	<8
Africa			
Asal. Afar	1978	5.3 (m)	0 - 6
New Zealand			
Taupo Volcano Zone ⁽ⁱ⁾	1964 - 65	4.6	4 - 8
Taupo Volcano Zone ⁽ⁱ⁾	1983	4.3	6 - 10
California, USA			
Mono Craters ^(k)	1325 + 20 AD	>5.5 (M)	nd
Italy			
Mt. Etna	1989	3.3 (M)	<4
Mt. Etna	1991	3.3 (M)	<6
Mean ± sigma; n = 19 ^(l)	3.9 ± 0.8		

(a) Modified from Hackett et al. (1995)

(b) Worldwide dike-injection events associated with mafic magma except Mono craters which is associated with silicic magma and for Mt. Etna which is associated with intermediate magma. Composition of magma for New Zealand episodes are unknown.

(c) An episode of dike-injection and associated seismicity having a known beginning and end.

Table 2.6-7

Maximum Magnitudes and Focal Depths of Earthquakes Associated with Dike Injection^(a)

- (d) Maximum magnitude reported for the dike-injection event. Magnitudes: M_L – Local or Richter; M_c – Coda; M_{JMA} – Japan Meteorological Agency; m_b – Body-wave; M_s – Surface-wave. No definition of magnitude scale was reported for values without magnitude designation.
- (e) Depth range of volcanic seismicity and maximum magnitude earthquake associated with the dike-injection event.
- (f) Einarsson (1991) reports earthquakes of magnitude ≥ 5.0 are usually associated with caldera deflation events and magnitude ≤ 4.0 with dike injection at Krafla
- (g) Code magnitudes greater than amplitude magnitudes for these events (Nakata et al., 1982; Tanigawa et al., 1981, 1983).
- (h) This earthquake is interpreted to have triggered magma movement, but was part of an earthquake swarm that began about 10 days prior to a dike-fed submarine eruption (10, 11, 12).
- (i) Associated with or triggered by dike intrusion, or possibly associated with tectonic subsidence of the basin (15).
- (j) Minimum estimate of the largest of five historic earthquakes based on liquefaction deposits produced by earthquakes equivocally associated with dike intrusion or tectonic faults (16).
- (k) Mean and one standard deviation computed based on magnitudes as presented without Mono Craters because it's a minimum estimate.

nd No data obtained

Table developed from information reported in TMI-2 ISFSI SAR (Ref. 2-1)

Table 2.6-8
Maximum Magnitudes Based on Rupture Areas of Normal Faults
and Fissures in Eastern Snake River Plain Volcanic Rift Zones

Normal Faults or Fissures	Surface Length – SL (km)	Fault Widths		Rupture Areas		Moment Magnitudes ^(c)	
		Depth to Dike Top ^(a) – DDT (km)	Level of Neutral Buoyancy ^(b) – LNB (km)	SI x DDT (km ²)	SL x LNB (km ²)	M	M
Kings Bowl, Fissures ^(d)	11.5 E	0.6	4.0	6.9	46.0	4.9	5.7
	14.0 M			8.4	56.0	5.0	5.8
South of New Butte, Fissures ^(d)	19.0 E	1.0	4.0	19.0	76.0	5.3	5.9
	22.0 M			22.0	88.0	5.4	6.0
Southeast of New Butte, Fissures ^(d)	11.0	1.0	4.0	11.0	44.0	5.1	5.7
Railroad Monocline, Fault ^(e)	5.0	0.2	4.0	1.0	20.0	4.1	5.3
Jaylin Monocline Fault ^(e)	3.2	nc	4.0	nc	12.8	nc	6.4
Box Canyon, Fault ^(e)	3.0	0.2	4.0	6.0	12.0	4.8	5.6
East-West, Fault ^(e)	0.7	nc	4.0	nc	2.8	nc	5.6
Southeast Butte City, Fissure ^(e)	0.7	nc	4.0	nc	2.8	nc	5.6
Northwest of Tea Kettle Butte, Fissure ^(e)	2.3	nc	4.0	nc	9.2	nc	6.2
Northeast of Sixmile Butte, Fissure ^(e)	1.2	nc	4.0	nc	4.8	nc	5.9
Northeast of Tea Kettle Butte, Fissure ^(e)	0.3	nc	4.0	nc	1.2	nc	5.2
East of Tea Kettle Butte, Fissure ^(e)	0.5	nc	4.0	nc	2.0	nc	5.4
Northwest of Sixmile Butte, Fissure ^(e)	1.1	nc	4.0	nc	4.4	nc	5.8
Kath Fissure ^(e)	0.6	nc	4.0	nc	2.4	nc	5.5
NRF Fissure ^(e)	1.5	nc	4.0	nc	6.0	nc	6.0
Hells Half Acre, Fissures ^(e)	4.0 E	0.8	4.0	3.2	16.0	4.5	5.3
	15.0 M		4.0	12.0	60.0	5.1	5.8
Lapoint Monocline, Fissure ^(e)	1.4	nc	4.0	nc	5.6	nc	5.9
East of Morgan Crater, Fault ^(f)	11.7	0.5	4.0	5.9	46.8	4.8	5.7
North of Morgan Crater, Fault ^(f)	9.2	1.3	4.0	12.0	36.8	5.1	5.6
West of High Point Butte, Fault ^(f)	10.0	1.0	4.0	10.0	40.0	5.1	5.6
Antelope Flat, Fault ^(f)	11.0	1.7	4.0	18.7	44.0	5.3	5.7
South of Antelope Flat, Fault ^(f)	3.7	0.3	4.0	1.1	14.8	4.1	5.2
Mean ±1 sigma; n = 11; n = 22						4.9±0.4	5.7±0.3

E – Exposed surface length; corresponding magnitude not used to estimate the mean value.

M – Maximum surface length estimated from extrapolation of fissures beneath younger lava flows.

nc – Not calculated because only one fissure or fault exposed, and therefore the depth to the dike top could not be estimated.

(a) Maximum depth calculated using: $d=1/2W$; where d=depth to dike top; W=width of graben (Pollard et al., 1983; Mastin and Pollard, 1988).

(b) Depth extent based on Ryan (1987) and Rubin (1992)

(c) Magnitudes calculated using $M=4.07+0.98*\text{Log}(RA)$; where M=moment magnitude; RA=rupture area. Magnitudes are extrapolated if less the constant in the equation (Wells and Coppersmith, 1994).

(d) Surface lengths obtained from Kuntz et al. (1988)

(e) Surface lengths obtained from Bolder Associates (1992a).

(f) Surface lengths obtained from aerial photographs and topographic maps.

Table 2.6-9
Probabilistic Seismic Hazard Studies Applicable to the INTEC

Seismic Hazard Study	Methodology	Input Parameters	Peak Horizontal Acceleration (g)	
			Bedrock	Soil
Agbabian Associates 1977 (2.178)	Calculated the probability of experiencing the design earthquake during the service life of the facility. Calculation procedure uses the mathematical model by Der-Kiureghian and Ang (1977). Evaluation performed for the NWCF site at the ICPP located 320 m from the ISFSI site.	Three source areas located around the Eastern Snake River Plain having maximum magnitudes (6.75-7.5) corresponding to Modified Mercalli Intensities (MMI) IX-X, recurrence intervals based on the historical earthquake record, and intensity attenuation relationships developed from five regional earthquakes.	0.4/MMI VIII-IX (0.01% chance of exceedance in 100 years)	None
Tera Corporation 1984	Calculated probabilities of peak horizontal accelerations with return periods of 100, 1,000, and 10,000 yrs. Procedure uses the Tera (1978) model based on the work of Mortgat et al. (1977) and Mortgat and Shah (1979). Analysis done for Argonne National Laboratory site, but hazard maps include the ICPP.	Nine source regions, three are the major range-bounding faults northwest of the Eastern Snake River Plain. Magnitudes range 6.5-7.75 and recurrence based on 17 years of earthquake data. Attenuation based on Campbell (1982) and Tera (1984) with $Q_0=450$, $\eta=0.2$ outside the Eastern Snake River Plain; $Q_0=150$, $\eta=0.55$ inside the Eastern Snake River Plain.	0.18 (1,000 yrs) 0.30 (10,000 yrs)	None
Woodward-Clyde Federal Services 1996	Calculated annual exceedance probabilities (500, 1,000, 2,000, and 10,000) for peak horizontal accelerations. Procedures are based on Cornell (1968) and Youngs and Coppersmith (1990). Results are in the form of mean peak horizontal acceleration and uniform hazard spectra for rock. Evaluation performed for the ICPP.	Source zones: basin and range faults, M6.5-7.75 volcanic rift zones, M4.5-5.5; Eastern Snake River Plain background seismicity, M5-6; northern basin and range background seismicity, M6.25-6.75. Recurrence based on earthquake catalog 1884-1992. Attenuation includes four empirical relationships unmodified for style of Faulting factors and stochastic numerical modeling ($\Delta\sigma=75$ bars; $V_s=3.55$ km/sec; $\rho_s=2.7$ gm/cm ³ ; $Q_0=150$; and $\eta=0.6$. Site response V_s and V_p measured in boreholes drilled at ICPP and INEEL)	0.10 (1,000 yrs) 0.13 (2,000 yrs) 0.22 (10,000 yrs)	None

Table 2.6-9
Probabilistic Seismic Hazard Studies Applicable to the INTEC

Seismic Hazard Study	Methodology	Input Parameters	Peak Horizontal Acceleration (g)	
			Bedrock	Soil
Woodward-Clyde Federal Services 1999 (Ref. 2-171)	Developed seismic design parameters for the ISFSI site. Procedures include: deaggregation of mean uniform hazard spectra and adjustment of the normalized spectral shapes to produce bedrock response spectra; soil response analysis using a frequency-domain equivalent-linear formulation (Silva et al.); and development of acceleration time histories by combining a Fourier amplitude spectrum with a phase spectrum from an observed strong ground motion record based on (Silva and Lee, 1987). Results in the form of peak horizontal and vertical accelerations for soil, smoothed response spectra and time histories.	Recomputed the seismic hazard using extensional empirical attenuation relationships and stochastic numerical modeling ($\Delta\sigma=50$ bars; $V_s=3.55$ km/sec; $P_s=2.7$ gm/cm ³ ; $Q_0=150$; and $\eta=0.6$. Site response V_s and V_p measured in boreholes drilled at TMI-2 ISFSI and INTEC. Soil analysis includes depths ranging 20m and shear wave velocities consistent with Table 2.6-11 obtained from boreholes drilled at the TMI-2 ISFI site.	0.09 (1,000 yrs) 0.11 (2,000 yrs) 0.18 (10,000 yrs)	0.18 ^(a) (1,000 yrs) 0.22 (2,000 yrs) 0.36 (10,000 yrs)
Payne et al. (Ref. 2-178)	Developed horizontal and vertical design basis earthquake (DBE) response spectra based on the URSG-WCFS [2.179] rock UHS. The rock UHS was adjusted for a 2,500-yr return period. The DBE response spectral shapes incorporate broadened regions of the peak accelerations, velocities, and displacements defined by the rock UHS.	Smoothed horizontal rock UHS and vertical to horizontal (V/H) ratio developed by URSG-WCFS (Ref. 1-179).	0.12 ^(b) (2500 yrs) 0.19 (10,000 yrs)	

Table developed from information presented in TMI-2 ISFSI SAR (Ref. 2-1).

- (a) Peak vertical accelerations for soil are 0.14g (1,000 yrs), 0.17 g (2,000 yrs), and 0.28g (10,000 yrs).
(b) Peak vertical accelerations for rock are 0.09g (2,500 yrs) and 0.14g (10,000 yrs).

TNEW10

Table 2.6-10
Estimated Volcanic-Recurrence Intervals and Corresponding Annual Eruption
Probabilities (in parentheses) for Volcanic Zones and Boreholes of the INEEL Area

Volcanic Zone or Borehole	Data Sources	Time Interval of Volcanism (yrs before present)	Number of Vents, Fissures or Flow Groups	Comments	Estimated Recurrence Interval
Great Rift (25 km southwest of INEEL)	Kuntz et al., 1986, 1988	2,100 - 15,000 yrs (radiocarbon dating)	> 100 vents 8 Holocene eruptive periods (each lasting a few decades or centuries, and each including multiple flows and cones).	No impact on INEEL; Most recently and frequently active of all ESRP rift zones; thus provides minimum-recurrence for entire ESRP; most probable area of future ESRP volcanism could affect much of southern INEEL; most recently and frequently active of all volcanic zones that could impact INEEL	2,000 yrs (5×10^{-4} / yr)
Axial Volcanic Zone (southern INEEL)	Kuntz et al., 1986, 1994	5,000 - 730,000 yrs (K-Ar dating; radiocarbon; paleomagnetic data)	73 vents & fissure sets 4 Holocene lava fields 3 of them shared by volcanic rift zones 45 cogenetic vent/fiss gps		16,000 yrs (6.2×10^{-5} / yr)
Arco Volcanic Rift Zone (southwestern INEEL)	Kuntz, 1978; Smith et al., 1989; Kuntz et al., 1994	10,000 - 600,000 yrs (radiocarbon, K-Ar and TL dating; paleomagnetic data)	83 vents & fissure sets 2 Holocene lava fields 35 cogenetic vent/fiss gps	Volcanism could affect southwestern INEEL	17,000 yrs (5.9×10^{-5} / yr)
Lava Ridge-Hells Half Acre Volcanic Rift Zone (includes Circ Butte/Kettle Butte volcanic rift zone)(north & eastern INEEL) Howe-East Butte Volcanic Rift Zone (central INEEL)	Kuntz et al., 1986, 1994	5,000 - 1,200,000 yrs (K-Ar dating; radiocarbon; paleomagnetic data)	48 vents & fissure sets 1 Holocene lava field: Hells Half Acre 30 cogenetic vent/fiss gps	Could affect northern and eastern INEEL: extremely long eruptive history; includes oldest and youngest basalts in the INEEL area	40,000 yrs (2.5×10^{-5} / yr)
	Kuntz, 1978, 1992; Golder Associates, 1992a	230,000 - 730,000 yrs (K-Ar dating; paleomagnetic data)	7 vents & fissure sets; no Holocene features 5 cogenetic vent/fissure groups	Old, poorly exposed and sediment-covered; identified in part by subsurface geophysical anomalies	100,000 yrs (1.0×10^{-5} / yr)
Borehole (NPR Site E (south-central INEEL)	Champion et al., 1988	230,000 - 640,000 yrs (K-Ar dating; paleomagnetic data)	9 lava-flow groups (each group contains multiple flows, erupted over a short time)	Dates from 600-foot interval of subsurface lavas give recurrence estimate consistent with surficial geology of the area	45,000 yrs (2.2×10^{-5} / yr)
Borehole RWMC 77-1 (southwestern INEEL)	Kuntz, 1978; Anderson & Lewis, 1989	100,000 - 565,000 yrs (K-Ar and TL dating; paleomagnetic data)	11 lava-flow groups (each group contains multiple flows, erupted over a short time)	Dates from 660-foot interval of subsurface lavas give longer recurrence interval than nearby Arco & Axial zones, reflecting flow-group (subsurface) vs. vent-counting (surface geology) approaches	45,000 yrs (2.2×10^{-5} / yr)

T9029

Table 2.6-11
Strain-Iterated Dynamic Soil Properties

	Depth (ft)	Mean - σ Strain-Iterated Profile				Mean Strain-Iterated Profile				Mean + σ Strain-Iterated Profile				Unit Weight (pcf)
		G (ksf)	Vs (ft/s)	Vp* (ft/s)	Damping (%)	G (ksf)	Vs (ft/s)	Vp* (ft/s)	Damping (%)	G (ksf)	Vs (ft/s)	Vp* (ft/s)	Damping (%)	
Soil	0-2.5	1696	675	1339	1.88	3097	912	1810	1.65	5655	1232	2445	1.44	120
Soil	2.5-5.5	4973	1132	2247	1.97	7566	1396	2772	1.74	11512	1722	3419	1.54	125
Soil	5.5-8.5	4781	1110	2203	2.43	7375	1378	2736	2.06	11376	1712	3398	1.75	125
Soil	8.5-11.5	4606	1089	2162	2.86	7188	1361	2701	2.35	11216	1700	3375	1.94	125
Soil	11.5-14.5	4432	1068	2121	3.31	7006	1343	2667	2.63	11075	1689	3353	2.10	125
Soil	14.5-17.5	4274	1049	2083	3.72	6833	1327	2634	2.90	10925	1678	3330	2.26	125
Soil	17.5-20.5	4145	1033	2051	4.08	6685	1312	2605	3.14	10781	1666	3308	2.41	125
Soil	20.5-23.5	4378	1062	2108	3.05	6942	1337	2655	2.40	11008	1684	3343	1.89	125
Soil	23.5-27	4404	1065	2115	3.24	6999	1343	2666	2.53	11123	1693	3360	1.97	125
Rock	> 27	28808	2671	5192	3.10	50926	3552	6903	3.09	90025	4722	9178	3.07	130

* For soil, based on Poisson's ratio=0.33

For rock, based on Poisson's ratio=0.32

TNEW2

Table 2.6-12
Properties of Soil (Sediments) and Bedrock at INTEC

Unit of Depth of Occurrence	Classification (USGS)	Dry Density (lbs/ft ³)	Moisture Content (%)	Relative Density (%)	Porosity (%)	Strength Characteristics	V _p Ft/s (m/s)	V _s Ft/s (m/s)	Damping
Upper Alluvial Soils (0-20 ft)	Sandy Gravel (GW)	110-123	1-8	36-98	29	C=0; F=43	2000(610)	1000 (300)	0.5%@10 ⁻⁴ % strain 15%@10 ⁻¹ % strain
		131.5 – 133	6		29	C=0; F=38-43	2000 (610)- 2300 (700)	1000 (300)- 1150 (350)	
		117-142	2-20	13-100		C=0; F=38°	3300 (1000)	1400(425)	1%@10 ⁻⁴ % strain
		98-135					1600 (490)- 1700 (520)	500 (150) 900 (275)	
							3665 (1120)- 5600 (1700)	650 (200) 1700 (520)	
Lower Alluvial Soils (20-40 ft)	Sandy Gravel (GW) and Poorly Graded Sand (SP)	112-123	1-8	49-98	29	C=0; F=43 (gravel); F=35 (sand)	2300(700)	1150 (350)	10 ⁻⁴ %@0.5% strain 10 ⁻¹ %@15% strain
		131.5 – 133	6		29	C=0; F=38-43	2000 (610)- 2300 (700)	1000 (300)- 1150 (350)	
		117-142				C=0, F=38°; (compacted gravel)	3300 (1000)	1400 (425)	1%@10 ⁻⁴ % strain
							2500 (760)- 3000 (910)	1400 (425)- 1600 (490)	
Clay Soils (0-14 ft) (variable just above bedrock)	Sandy Clay Silty Clay (CL) Sandy Silt to Clayey Sand (ML-SC)	92-110	17-23		39	C=650-5000 psf; F=0-25°	2600 (790)	1150 (350)	Similar to lower alluvial soils
		109	17		39	C=0-1500 psf; F=25-38°	2600 (790)	1150 (350)	
Basalt Bedrock (>40 ft)	Vesicular olivine basalt	136-163				6-17x10 ⁵ psf; Uniax. Comp. Strength	6800 (2070)	3500 (1070)	
		140-165				1.3-1.7x10 ⁶ psf; Uniax. Comp. Strength	6800 (2070)	3500 (1070)	
							9000 (2740)- 10000 (3050)	4000 (1200)- 5500 (1670)	
							7500 (2300)	4000 (1200)	
						5-16 x 10 ⁵ psf	9200 (2800)	3900 (1200)	1%

**Table 2.6-12
(continued)**

Unit and Depth of Occurrence	Shear Modulus (G)	Poissons Ratio (n)	Static Modulus of Elasticity (E)	Bulk Modulus (K)	Consolidation Characteristics	Location
Upper Alluvial Soils (0-20 ft)	2.2 x 10 ⁶ psf 5.5 x 10 ⁵ psf	0.32	1.8x10 ⁶ psf @ 5000 psf load 2.5x10 ⁶ psf @ 10000 psf load	1.7x10 ⁶ psf @ 5000 psf 2.3x10 ⁶ psf @ 10000 psf	Elastic-Dependent on E	New Waste Calcining Faci.
	6.8x10 ⁵ psf @ 5000 psf 0.32 9.5x10 ⁵ psf @ 10000 psf		1.8x10 ⁶ psf @ 5000 psf load 2.5x10 ⁶ psf @ 10000 psf load		Cv=0.012; Cc=0.015	7th Bin Set & FPR
	8.2 x 10 ⁶ psf	0.39	2.2x10 ⁷ psf		Slightly compressible	SIS
	1.1x10 ⁶ to 3.1x10 ⁶ psf dynamic max. (Gmax)	0.27 - 0.30 (dynamic)	2.9x10 ⁶ to 8.1x10 ⁶ psf (dynamic)			HLWTF Replacement
		0.41 - 0.45				FFTF
Lower Alluvial Soils (20-40 ft)		0.32	1.8x10 ⁶ psf @ 5000 psf load 2.5x10 ⁶ psf @ 10000 psf load	1.7x10 ⁶ psf @ 5000 psf 2.3x10 ⁶ psf @ 10000 psf	Elastic – Dependent on E	New Waste Calcining Faci.
	6.8x10 ⁵ psf @ 5000 psf 0.32 9.5x10 ⁵ psf @ 10000 psf		1.8x10 ⁶ psf @ 5000 psf load 2.5x10 ⁶ psf @ 10000 psf load		Cv=0.012; Cc=0.015	7th Bin Set & FPR
	8.2 x 10 ⁶ psf	0.39	1x10 ⁸ to 3x10 ⁸ psf		Slightly compressible	SIS
	7.6x10 ⁶ to 9.9x10 ⁶ psf dynamic max. (Gmax)	0.27 - 0.30 (dynamic)	1.9x10 ⁷ to 2.57x10 ⁷ psf (dynamic)			HLWTF Replacement
		0.41 - 0.45				FFTF
Clay Soils (0-14 ft) (variable just above bedrock)	Similar to lower Alluvial soils	0.38			Cv=0.037 @ 0-5000 psf load Cv=0.065 @ 5000-10000 psf	New Waste Calcining Faci.
	4.3x10 ⁵ psf @ 8000 psf		1.2x10 ⁶ psf @ 8000 psf	1.6x10 ⁶ psf; @ 8000 psf	Cv=0.001; Cc=0.016	7th Bin Set & FPR
Basalt Bedrock (>40 ft)		0.18-0.25 (calc)	1.3-3.1 x 10 ⁸ psf 1.9-4.5x10 ⁸ psf	1.6-3.7x10 ⁸ psf	Relatively incompressible	New Waste Calcining Faci.
	0.99-2.2x10 ⁸ psf 0.73-1.7x10 ⁸ psf	0.115-0.136	2.1-5.9 x 10 ⁸ psf	1.6-3.7x10 ⁸ psf	Relatively incompressible	7th Bin Set & FPR
	7.4x10 ⁷ to 1.41x10 ⁸ psf	0.28-0.38 (dynamic)	2.1-3.6 x 10 ⁸ psf (dynamic)			HLWTF replacement
		0.25-0.30				FFTF
	7.1x10 ⁷ psf	0.39	2.0x10 ⁸ psf		Incompressible	SIS

T9022

THIS PAGE INTENTIONALLY LEFT BLANK.

Table 2.6-13
Hazards Associated with Basaltic Volcanism on the Eastern Snake River Plain

Phenomenon	Frequency	Area	Comments
Lava flow	Common	0.1 km ² to 400 km ² in area, up to 25 km length based on sizes of ESRP lava flows of the past 400,000 years	Significant hazard; typical basaltic phenomenon; lava from fissures or shield volcanoes may inundate large areas downslope of vents
Ground deformation: fissuring, faulting and uplift	Common; associated with virtually all shallow magma intrusion and eruption	Fissuring could affect areas to 2 x 10 km; minor tilting & broad uplift in areas to 5 x 20 km	Significant hazard; due to shallow dike intrusion; "dry" intrusion may occur without lava flows; affects smaller areas than for lava inundation
Volcanic earthquakes	Common; associated with magma intrusion before and during eruption	Maximum M = 5.5 and most events M < 4; ground vibration may affect facilities within 25 km	Low to moderate hazard; swarms of shallow earthquakes (<4 km focal depth) occur as dikes propagate underground
Gas release(toxic and corrosive vapors)	Common; associated with fissuring and lava eruption	Restricted to near-vent areas; may affect several-square-km area downwind	Low hazard; local plume of corrosive vapor, downwind from eruptive vent or fissure; cooled vapors may collect in local topographic depressions
Tephra fall (volcanic ash and bombs)	Uncommon	As per gas release	Low hazard; basaltic eruptions are inherently nonexplosive and may form small tephra cones but little fine ash to be carried downwind
Base surge(ground-hugging blast of steam and tephra)	Rare	Effects limited to radius of several km from vent; < 10 km ² area	Low hazard; steam explosions due to interaction between ascending magma and shallow groundwater; water table too deep under most of INEEL
Tephra flow (ground-hugging flow of hot, pyroclastic material)	Extremely rare	Near vent; may affect area < 1 km ²	Low hazard; as per tephra fall but affecting even smaller areas

T9028

THIS PAGE INTENTIONALLY LEFT BLANK.

**Figure 2.1-1
Location Map of the INEEL**



Figure 2.1-2
INEEL Vicinity Map (with 50-mile radius line)

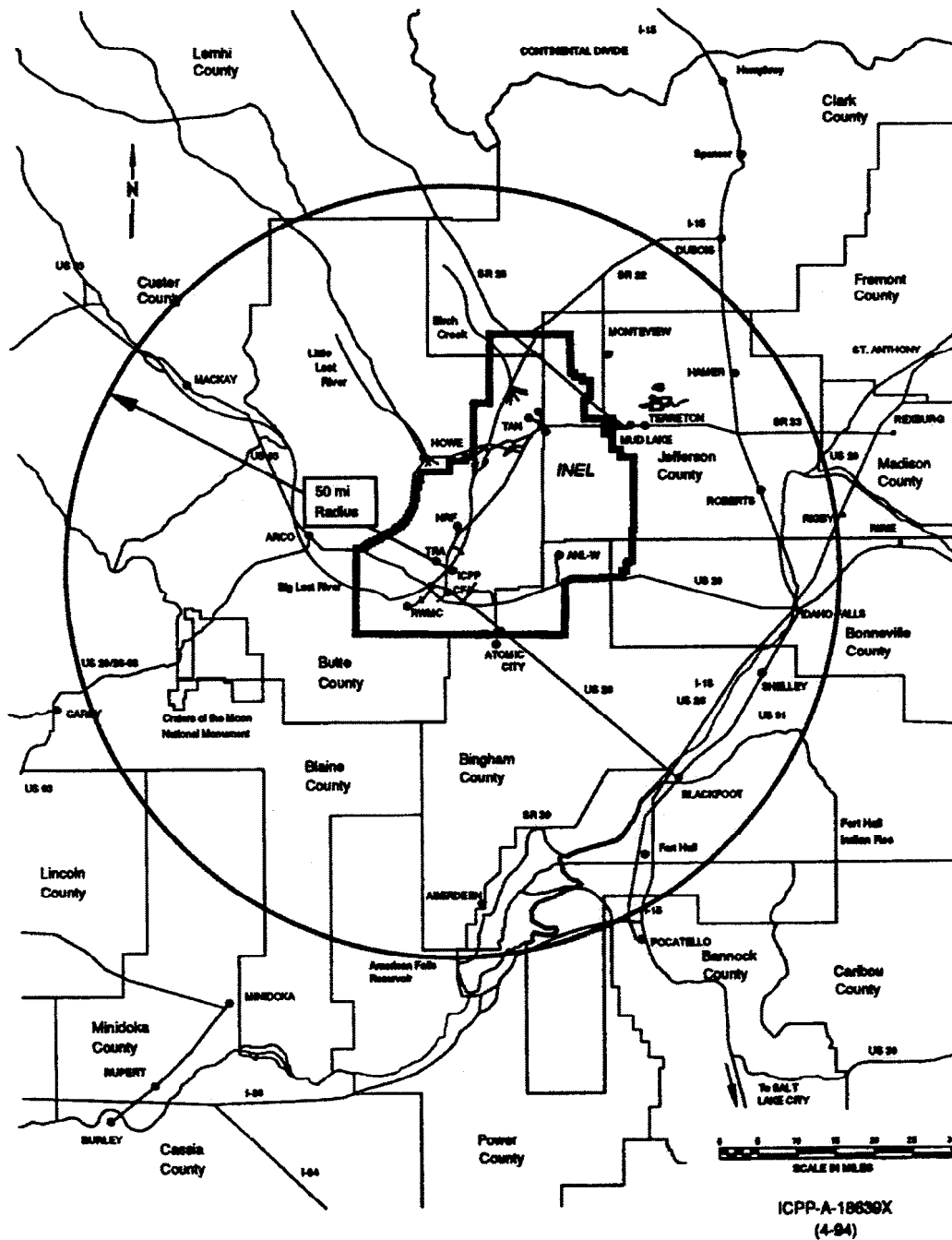


Figure is adapted from the TMI-2 ISFSI SAR (Ref. 2-1). The ICPP is an earlier name for the INTEC, which is adjacent to the ISF Facility site.

Figure 2.1-3
Map of INEEL

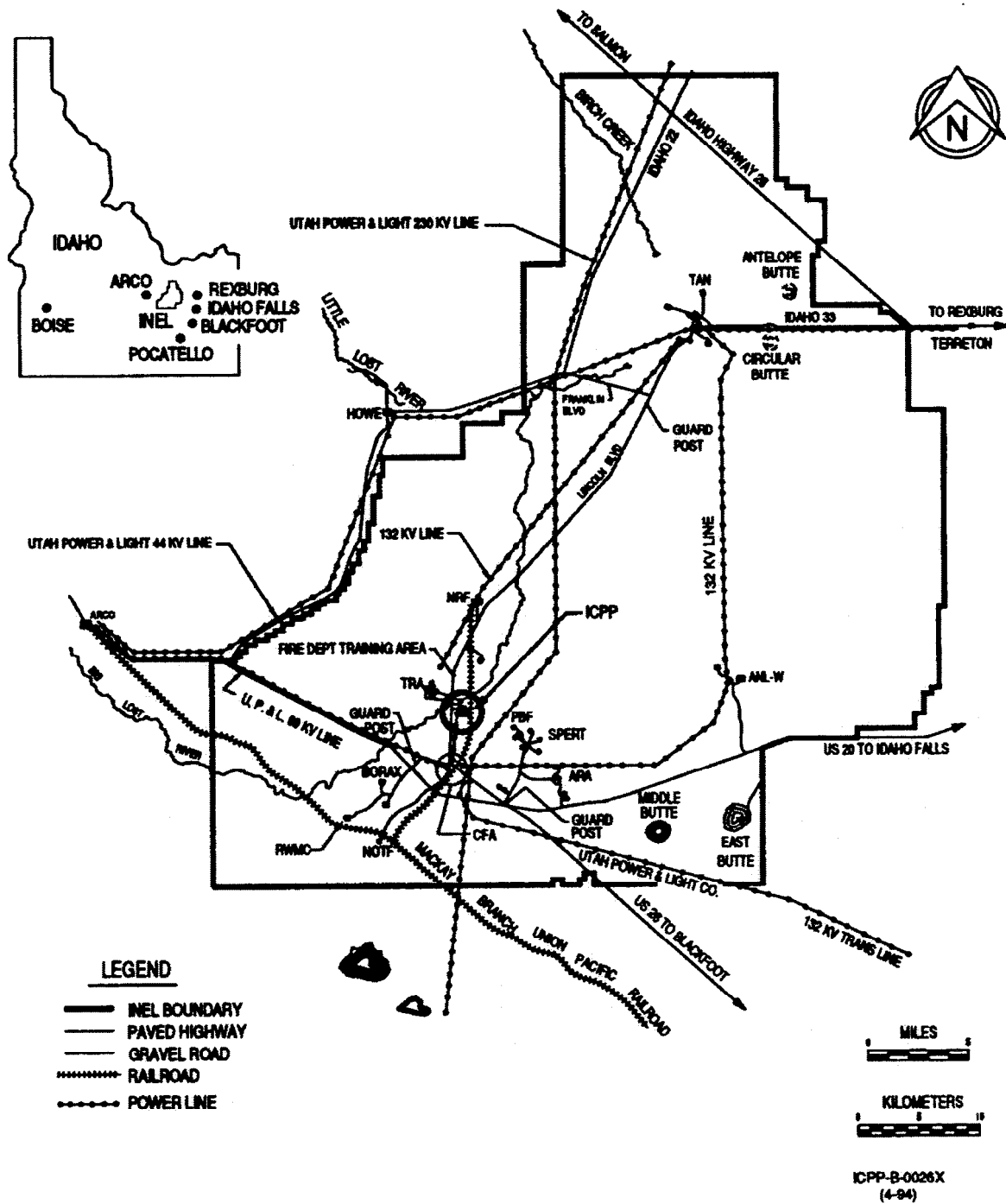


Figure is adapted from the TMI-2 ISFSI SAR (Ref. 2-1). The ICPP is an earlier name for the INTEC, which is adjacent to the ISF Facility site.

Figure 2.1-4
Aerial View of INTEC Showing ISF Site (looking north)

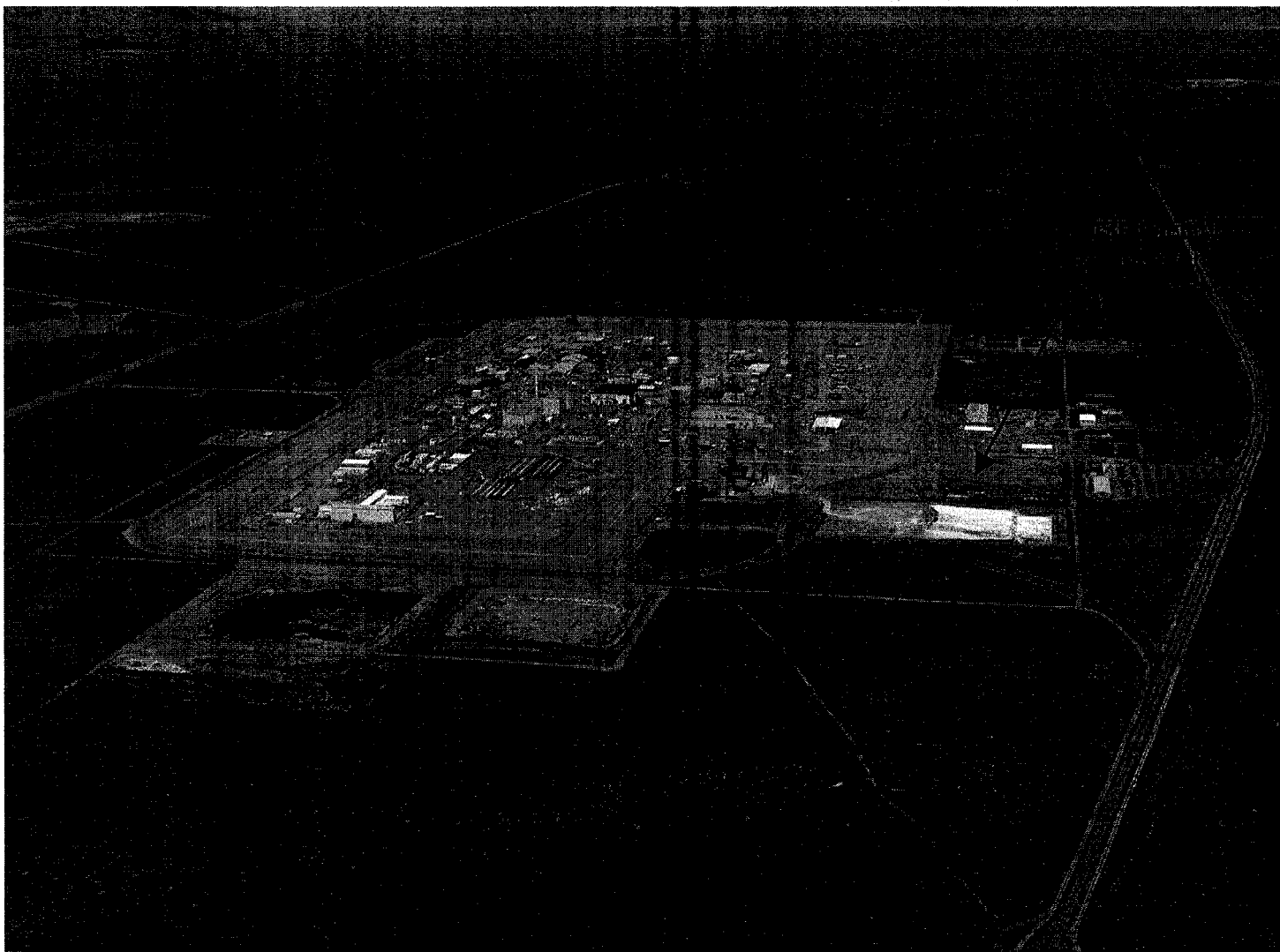


Figure 2.1-5
INTEC Area Plot and Location of ISF Site

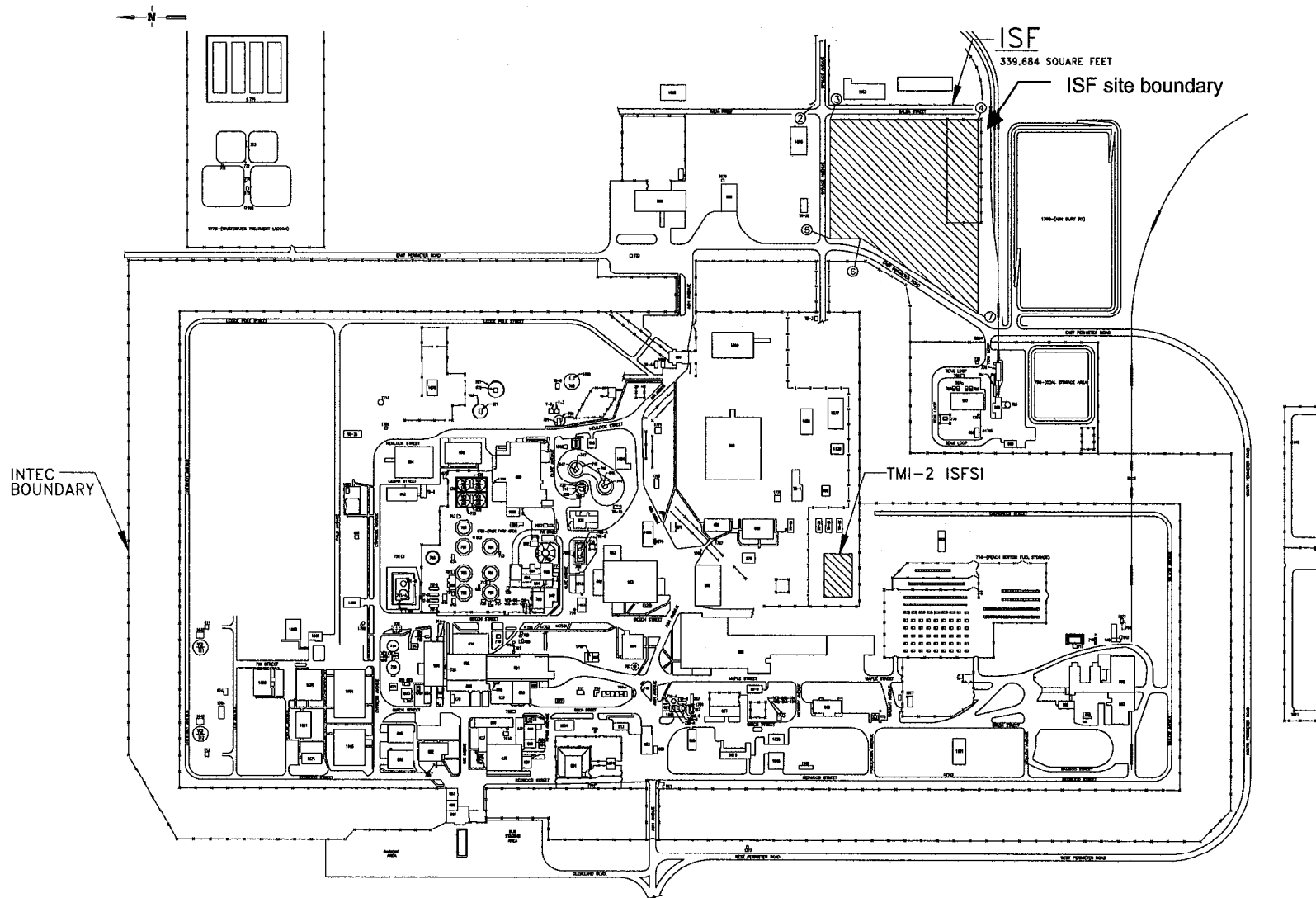
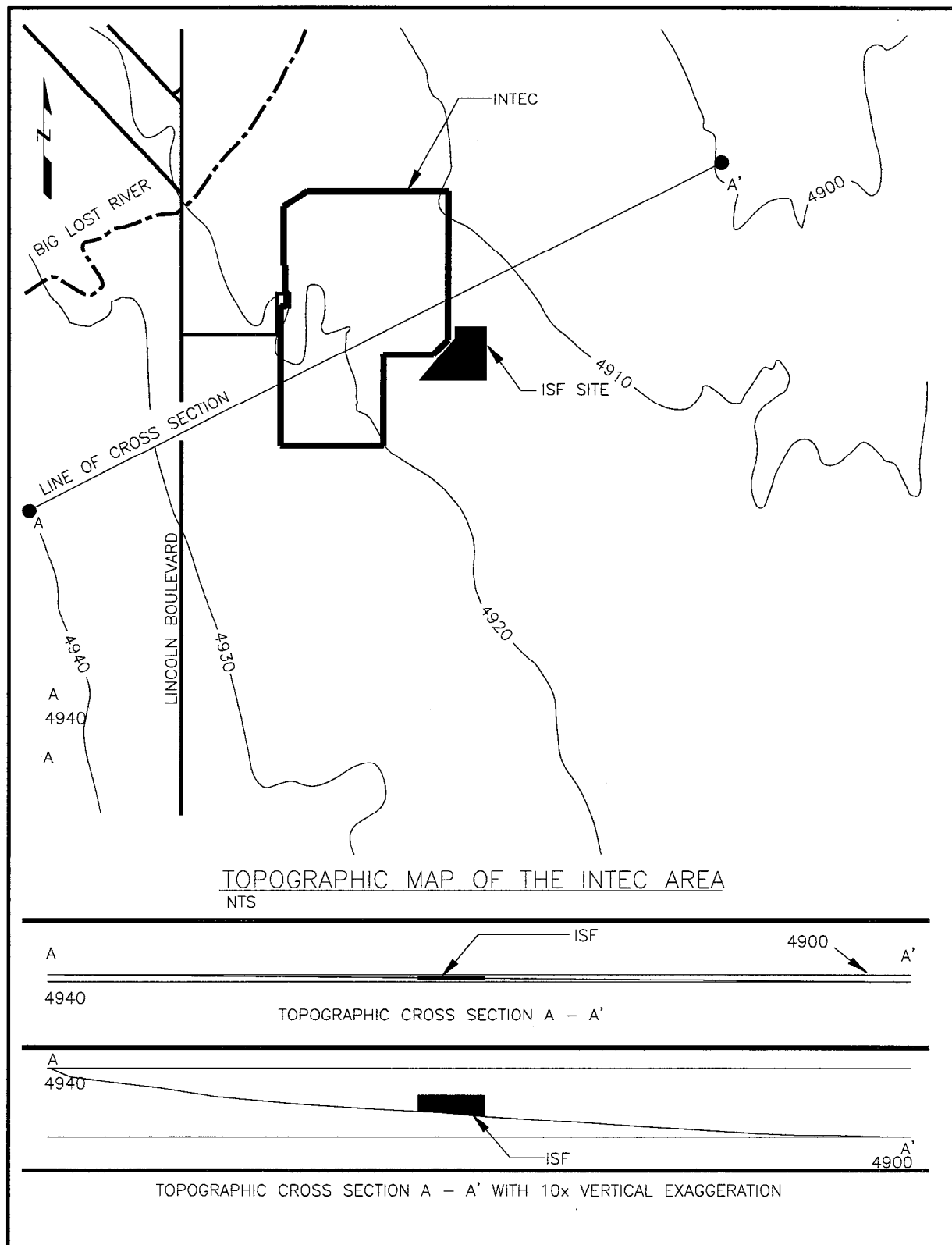
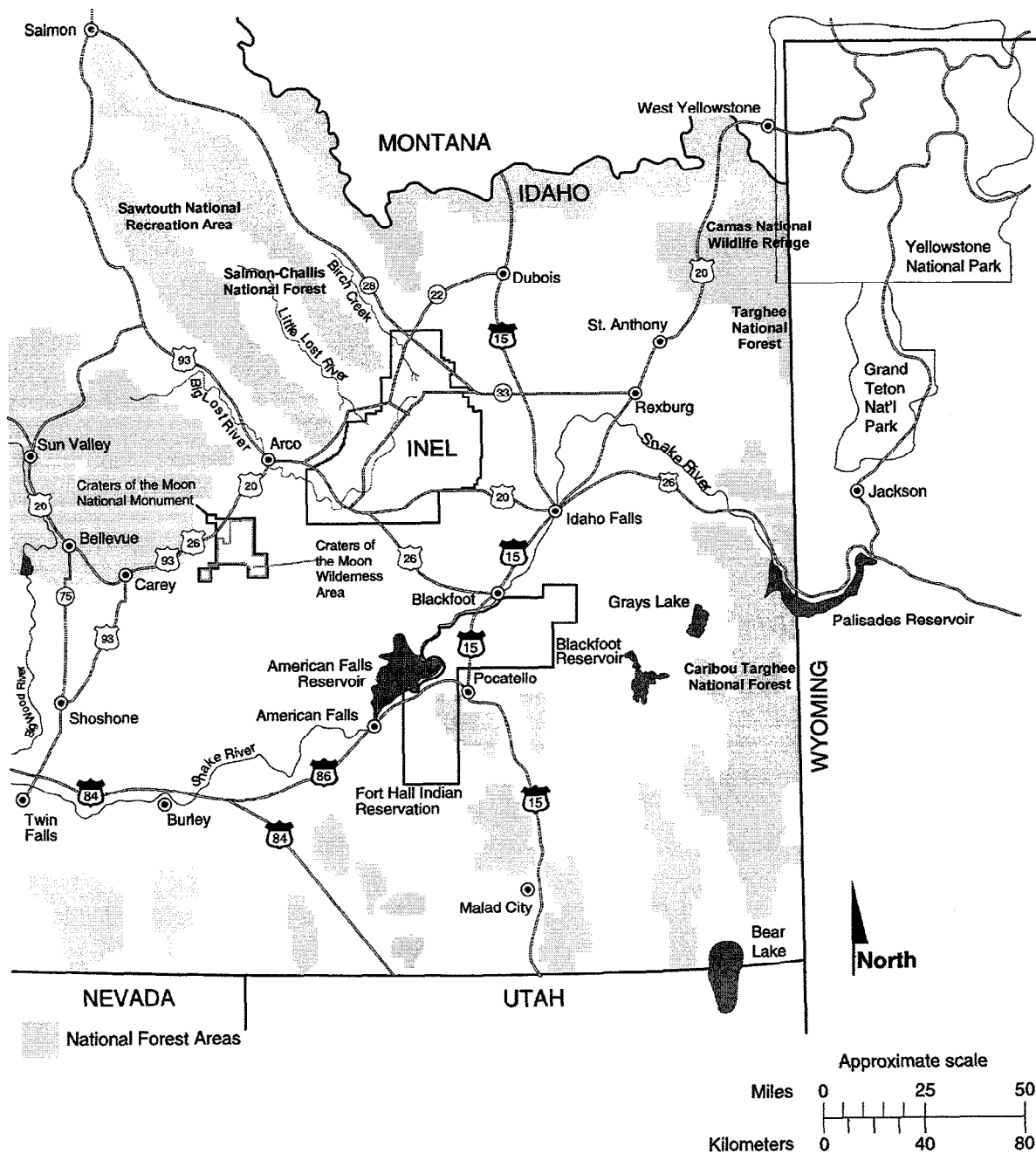


Figure 2.1-6
INTEC Area Topographical Map



*Elevation from 1986 flood study datum.

Figure 2.1-7
Location of the INEL in Southeastern Idaho



SAA0044

**Figure 2.1-8
INEEL Map with Major Drainages**

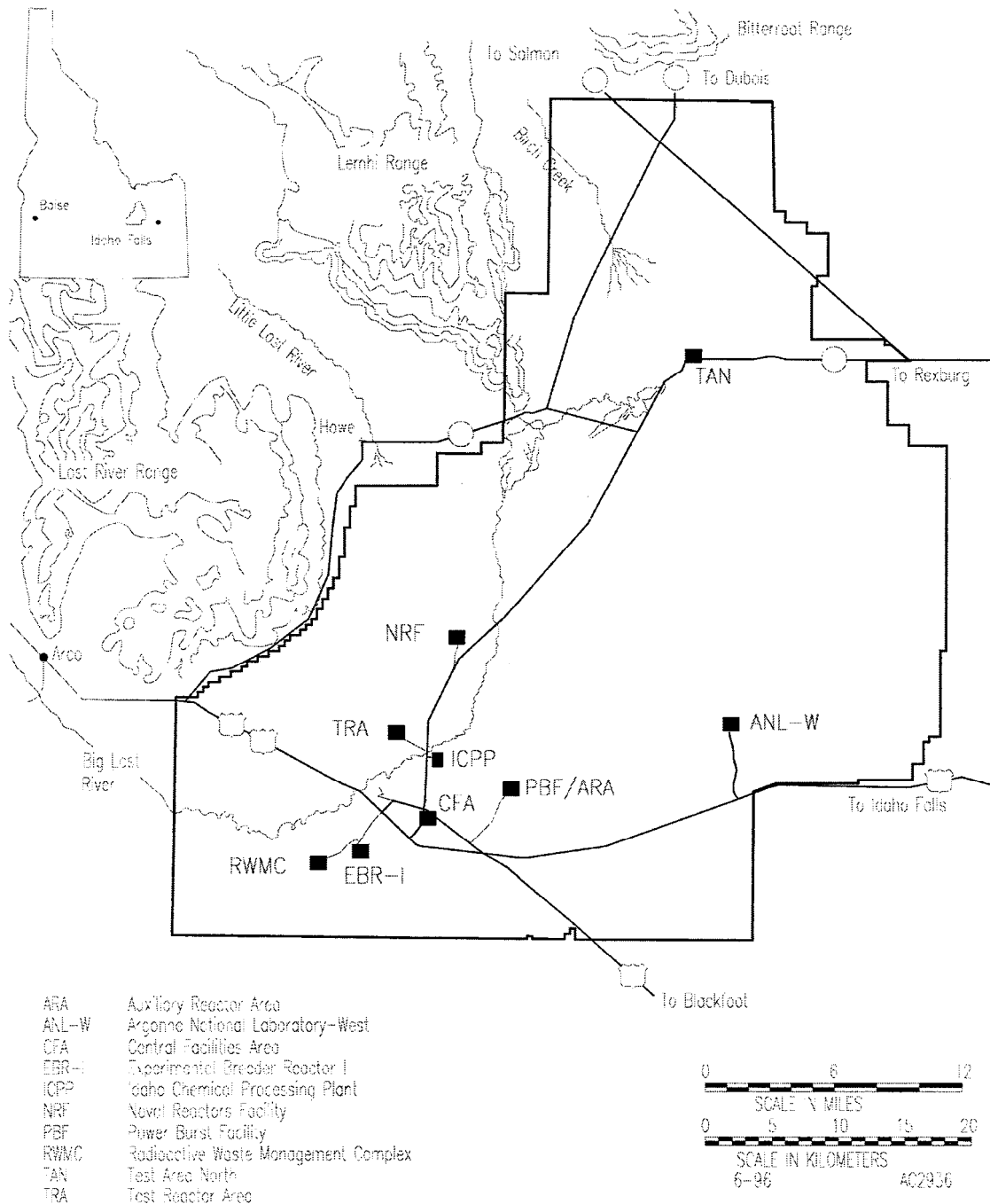
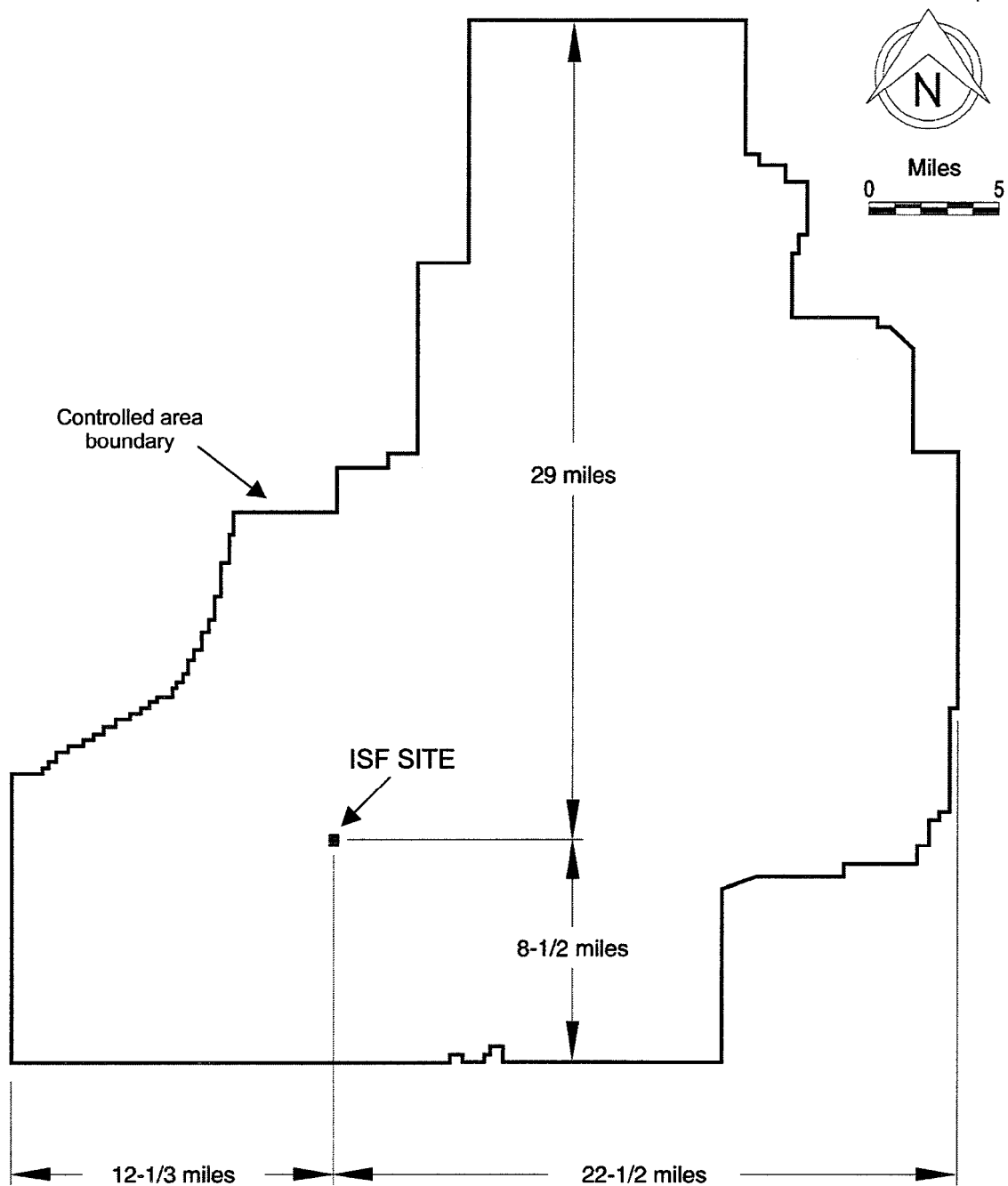


Figure is adapted from the TMI-2 ISFSI SAR (Ref. 2-1). The ICPP is an earlier name for the INTEC, which is adjacent to the ISF Facility site.

Figure 2.1-9
Distances from the ISF Site to the INEEL Boundary



ICPP-A-1804X
(5-90)

Figure 2.1-10
Approximate Distribution of Vegetation at the INEEL

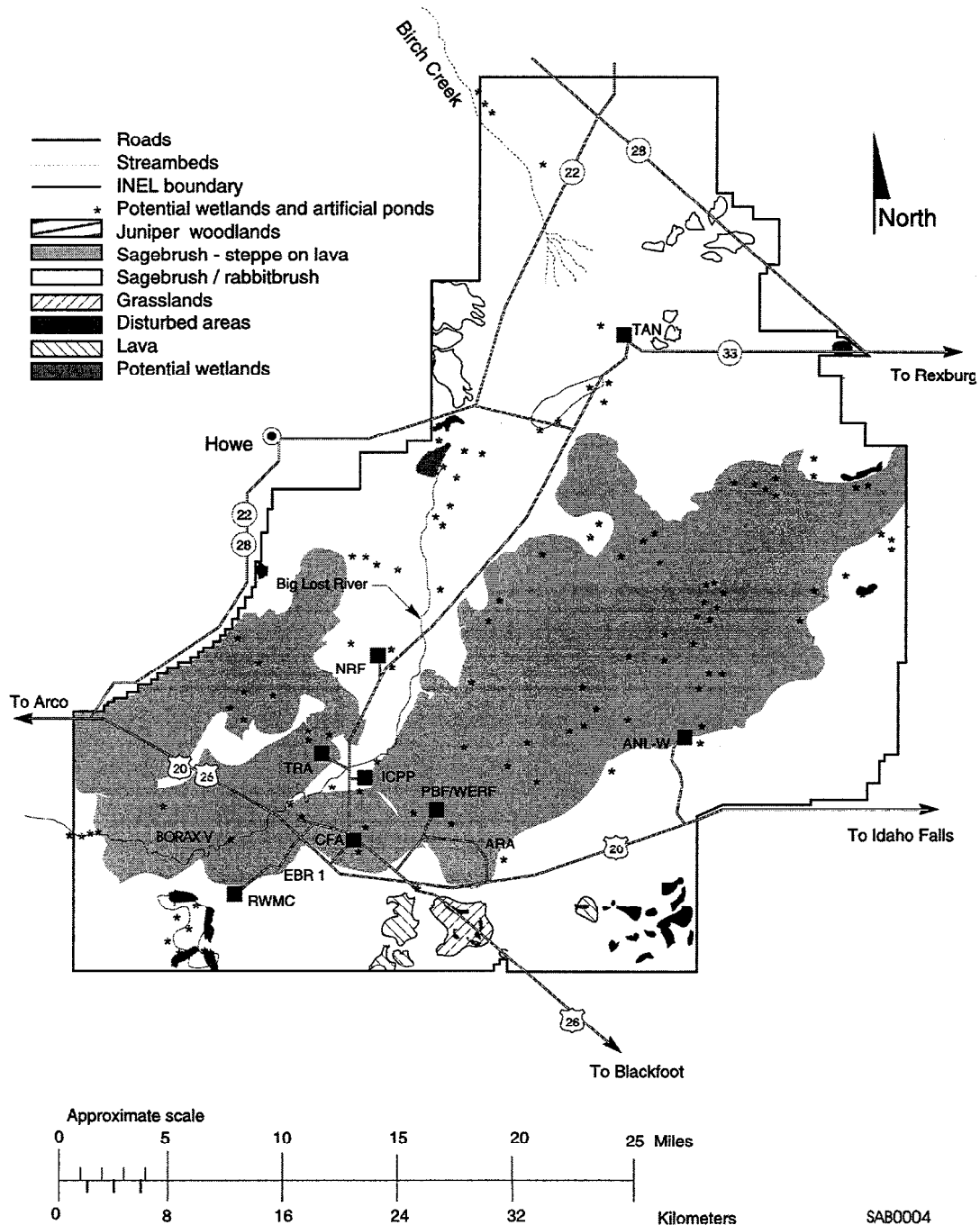


Figure is adapted from the TMI-2 ISFSI SAR (Ref. 2-1). The ICPP is an earlier name for the INTEC, which is adjacent to the ISF Facility site.

Figure 2.1-11
ISF Site Plan

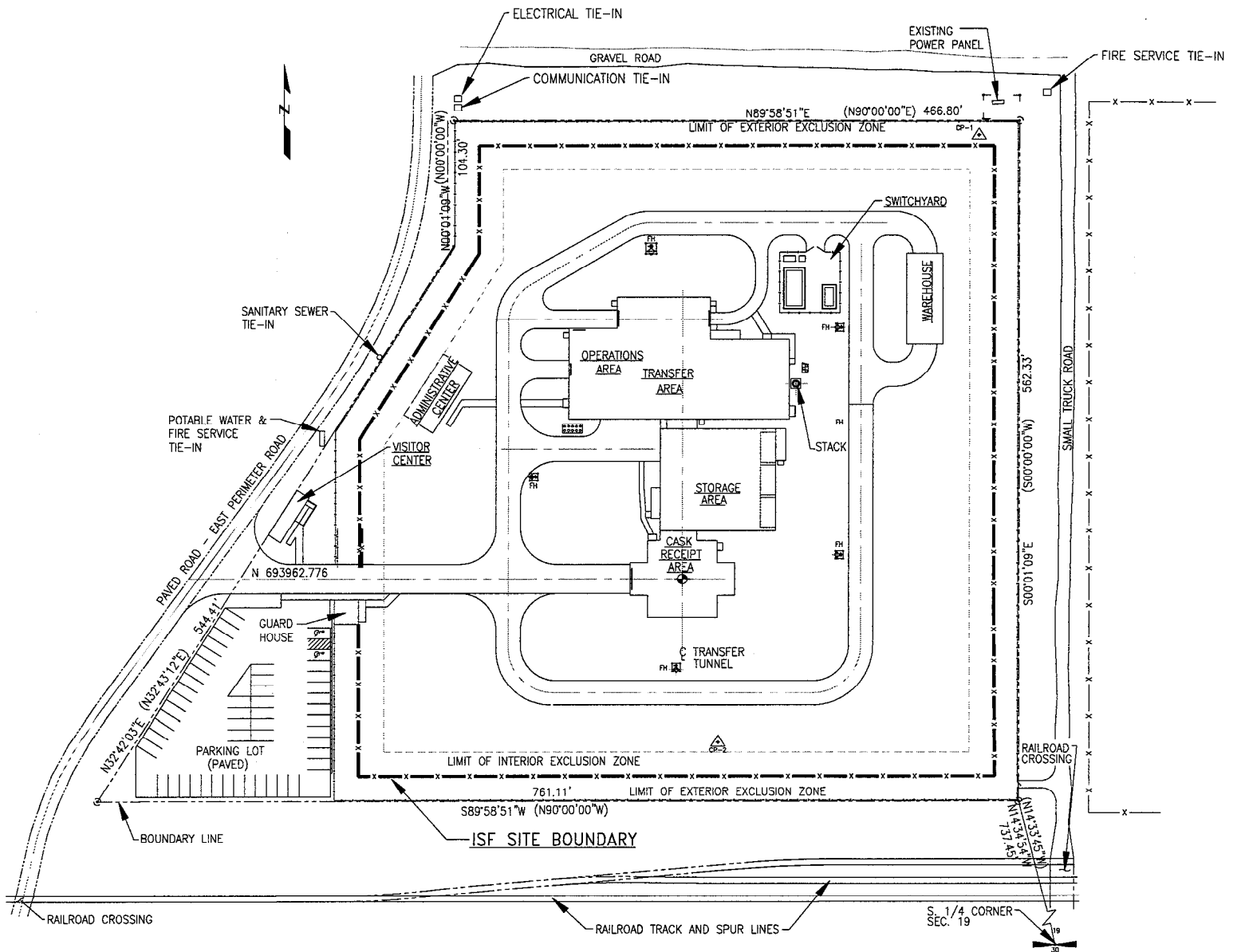
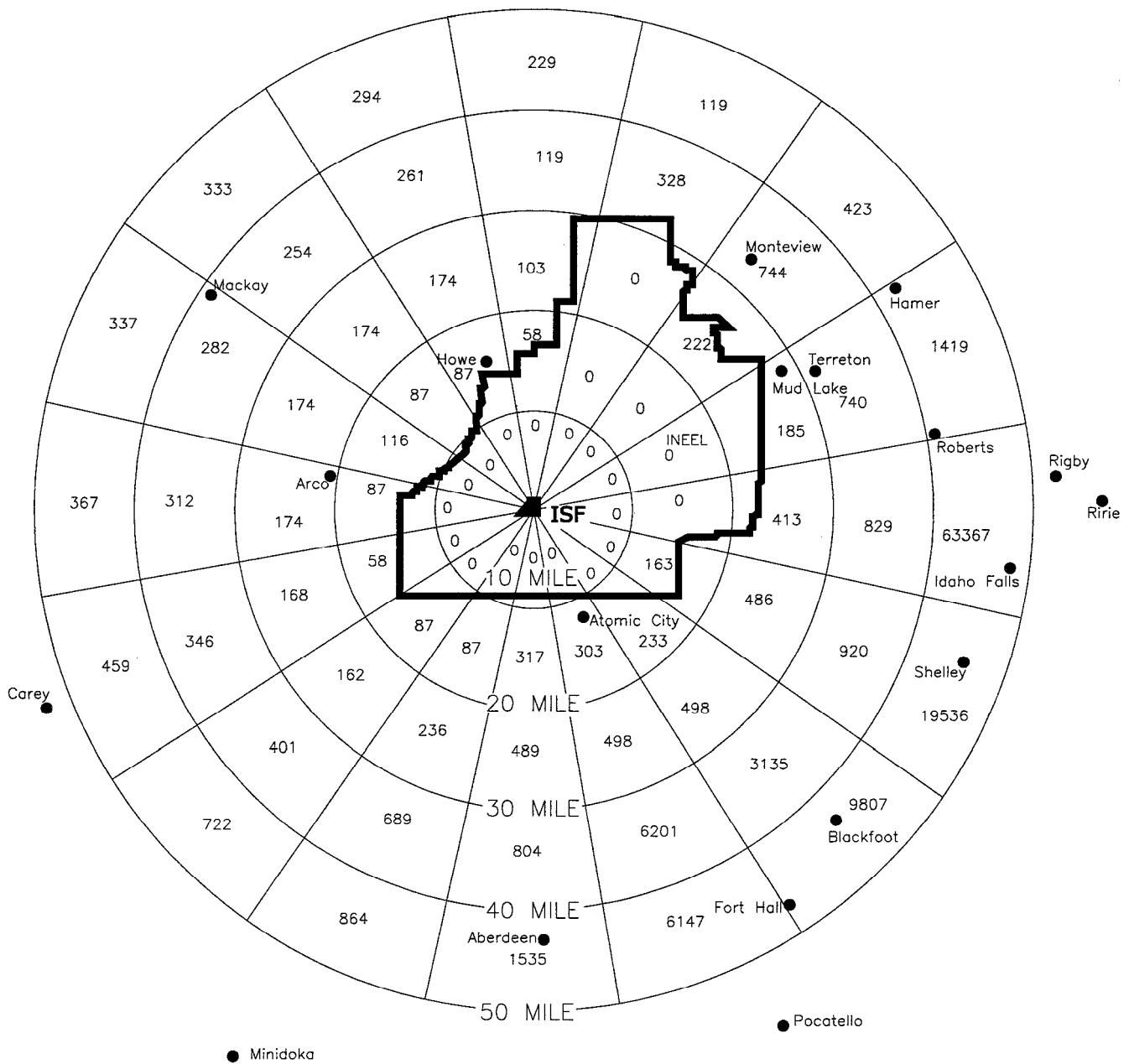


Figure 2.1-12
2000 Census Population Distribution Within 50 Miles of the ISF Facility



TOTAL = 128162

Figure 2.1-13
Selected Land Uses at the INEEL Site and Surrounding Region

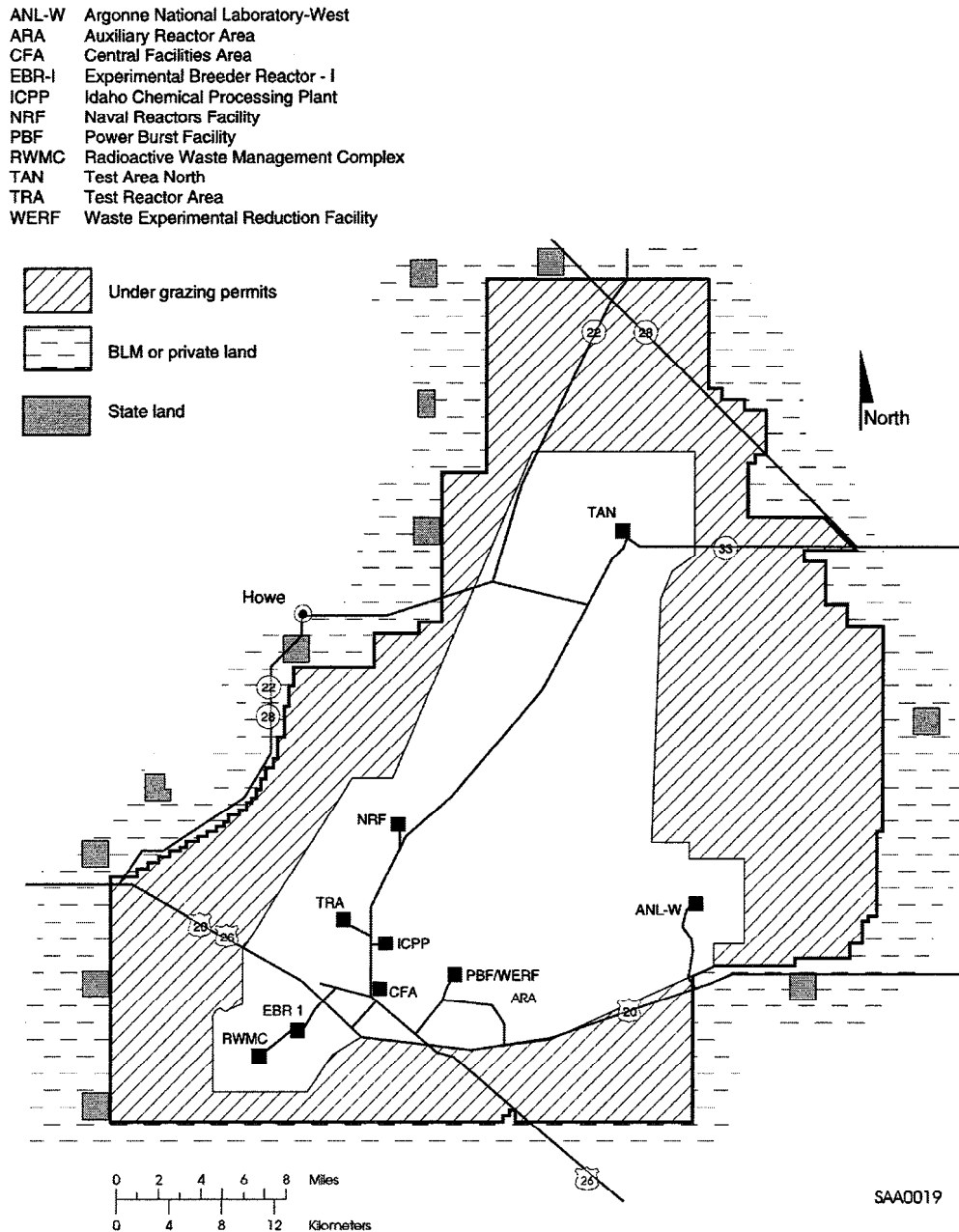
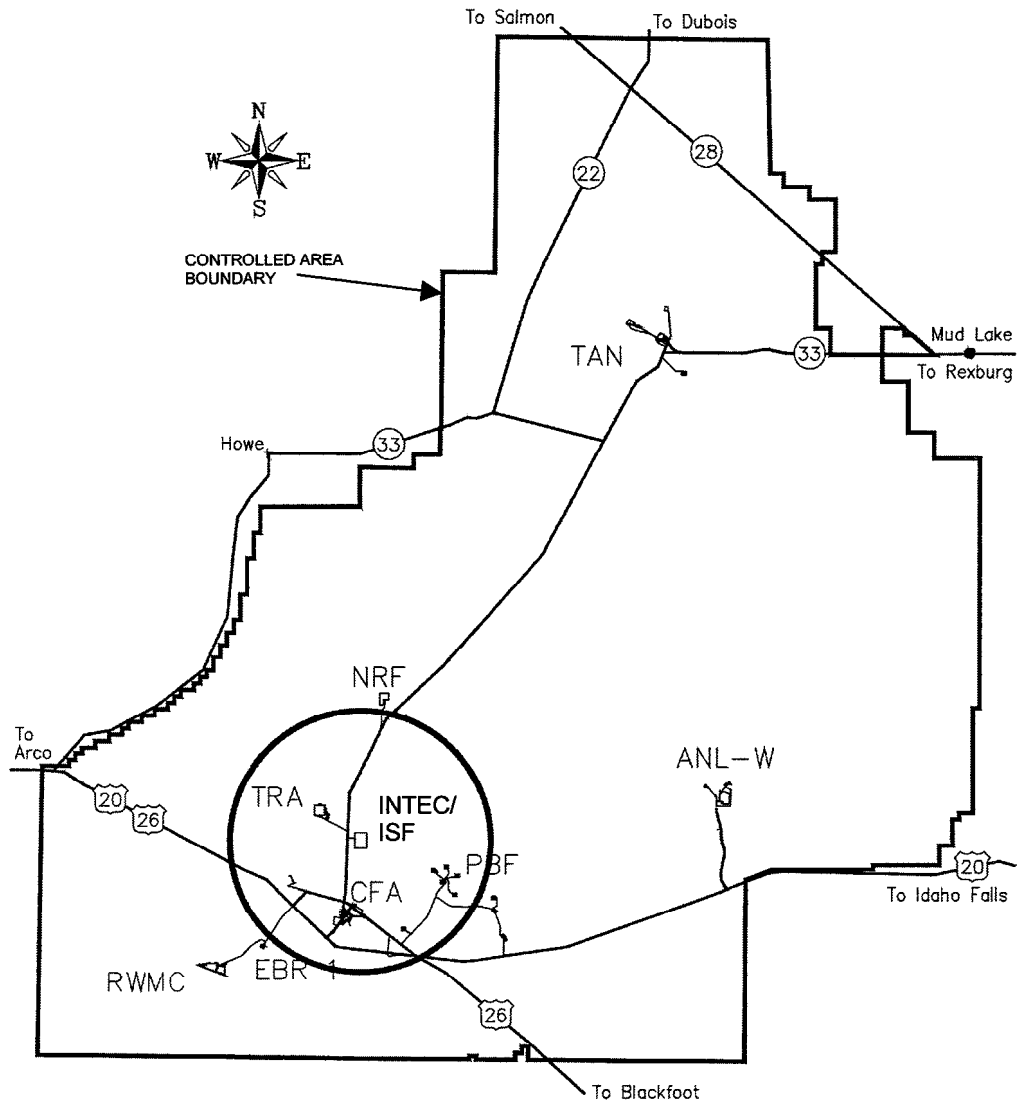


Figure is adapted from the TMI-2 ISFSI SAR (Ref. 2-1). The ICPP is an earlier name for the INTEC, which is adjacent to the ISF Facility site.

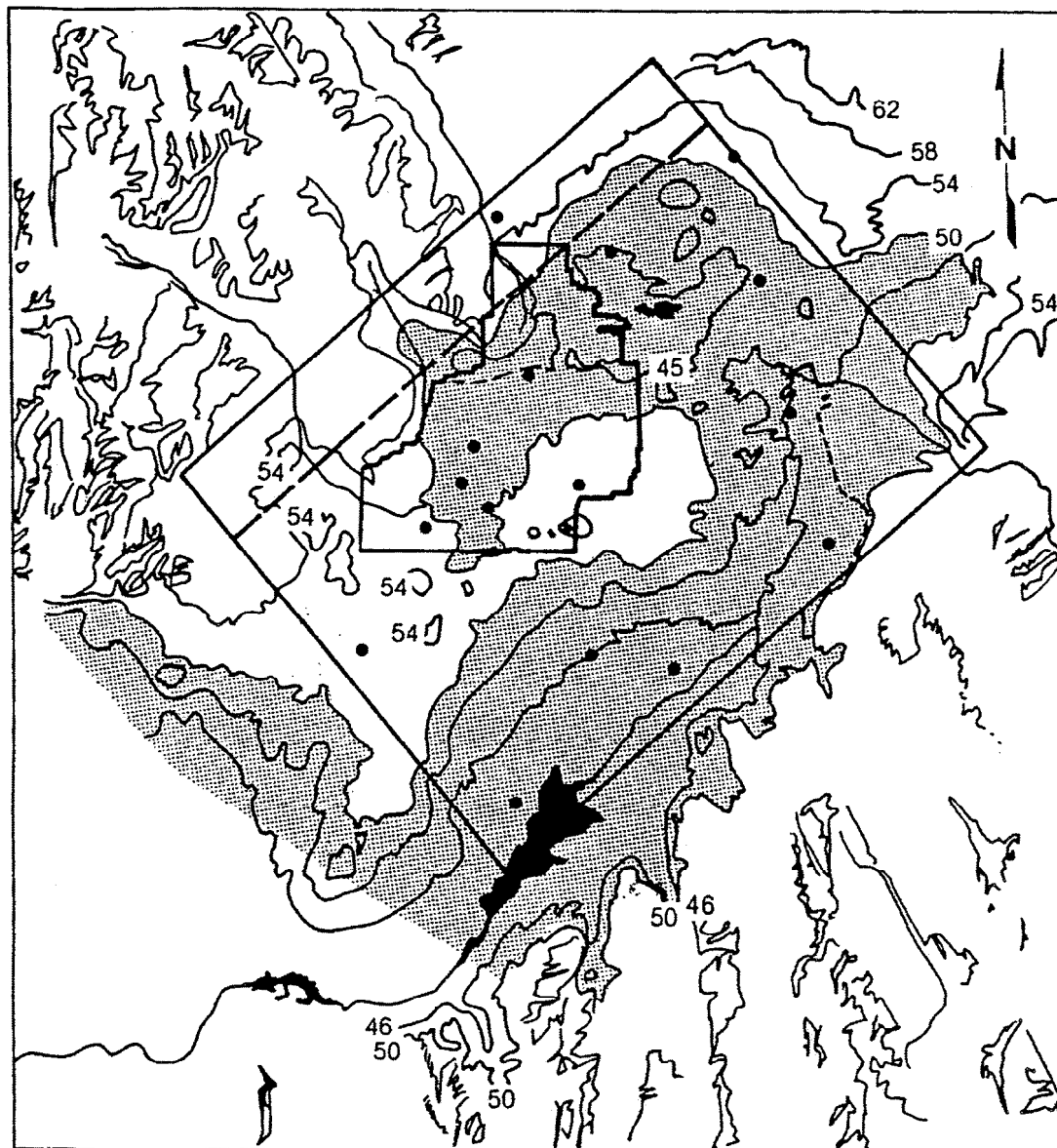
Figure 2.2-1
INEEL Primary Facility Areas
(showing 5-mile radius from ISF site)



Central Facilities Area (CFA)
Argonne National Laboratory West (ANL-W)
Experimental Breeder Reactor-1 (EBR-1)
Idaho Nuclear Technology and Engineering Center (INTEC)
Naval Reactor Facility (NRF)
Power Burst Facility (PBF)
Radioactive Waste Management Complex (RWMC)
Test Area North (TAN)
Test Reactor Area (TRA)

GT980173

Figure 2.3-1
Relief Map of the Eastern Snake River Plain



- 46-62 = Height values in hundreds of ft above mean sea level (msl)
[Shaded Area] = Below 5000 ft msl
Tick marks = 8.6 km (computational grid mesh size)
• = Tower-mounted wind sensors

Figure 2.3-2
Average Monthly Subsoil Temperatures (°F) Sandy Soil Surface

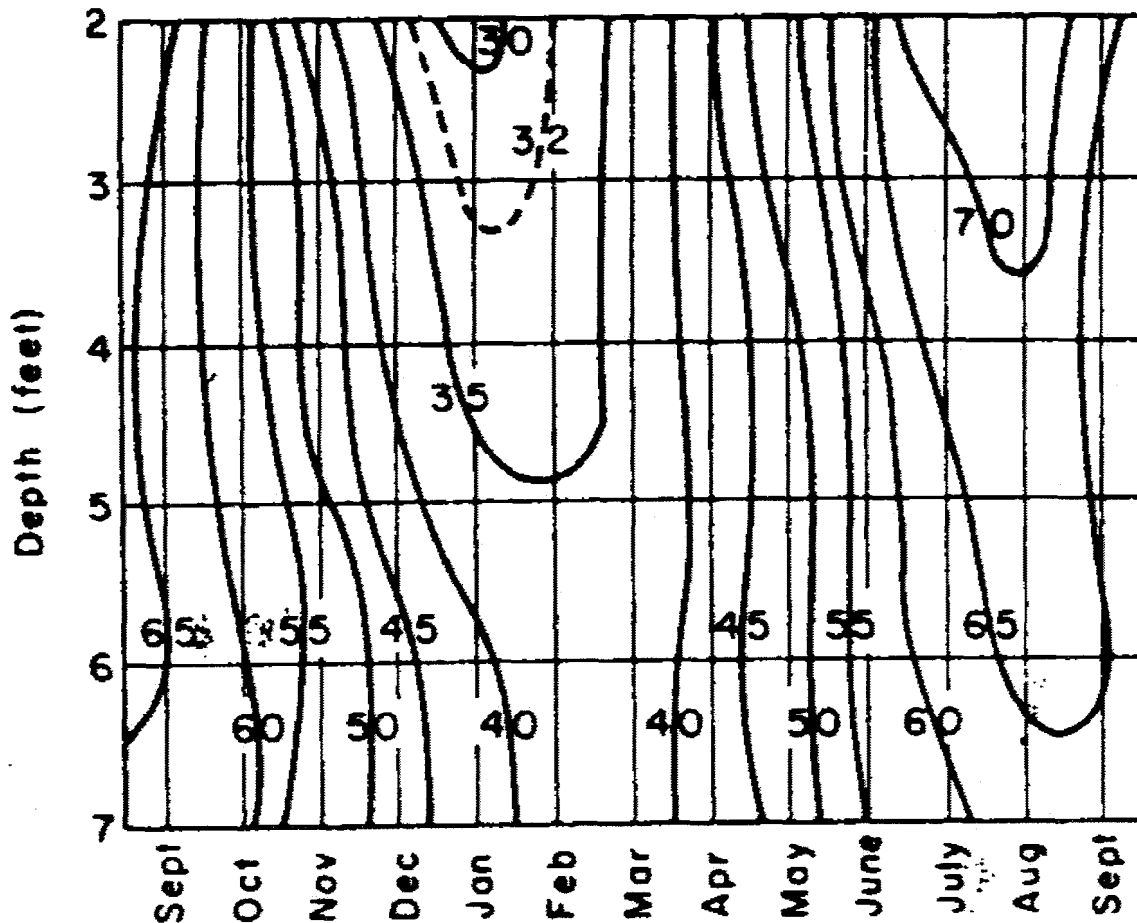
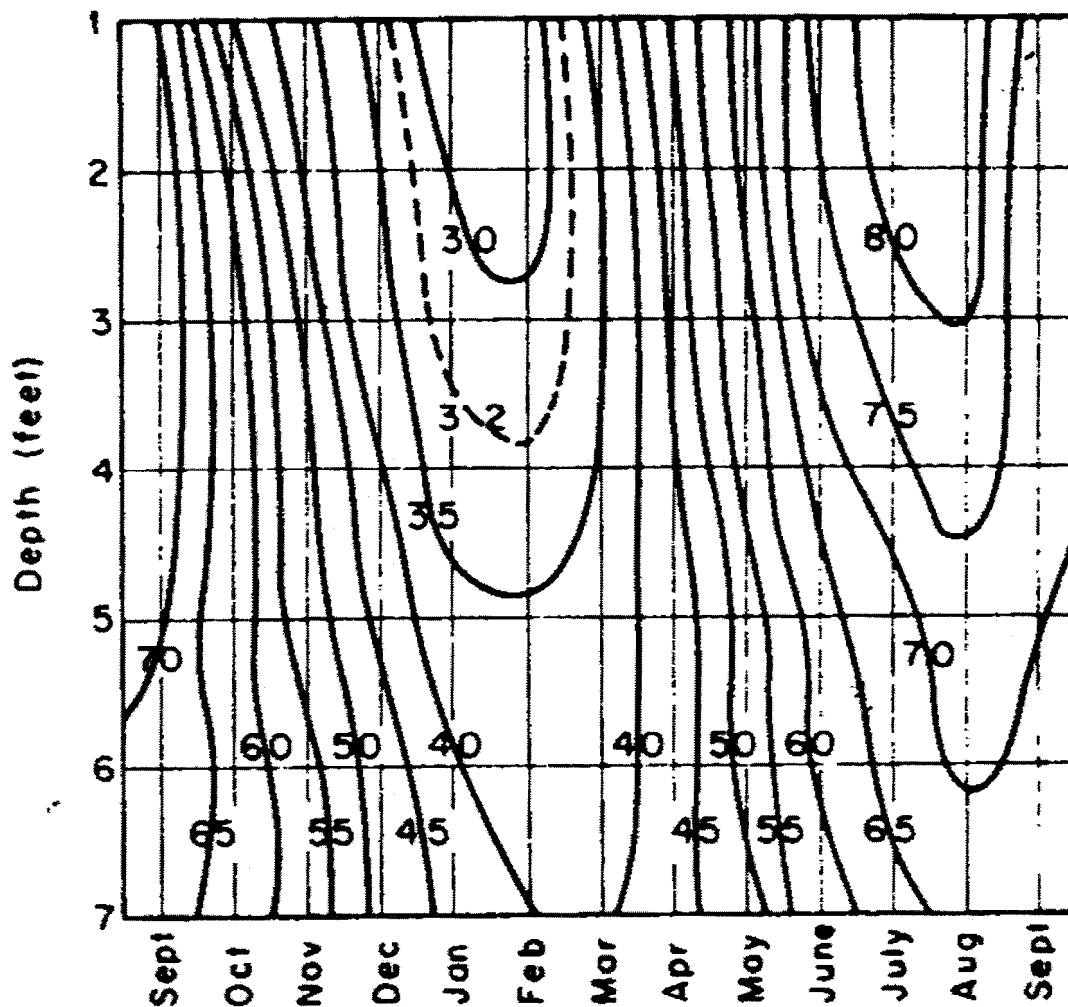


Figure 2.3-3
Average Monthly Subsoil Temperatures (°F) Asphalt Surface



INEL 4 4825

**Figure 2.3-4
Topographic Map of the INEEL Area**

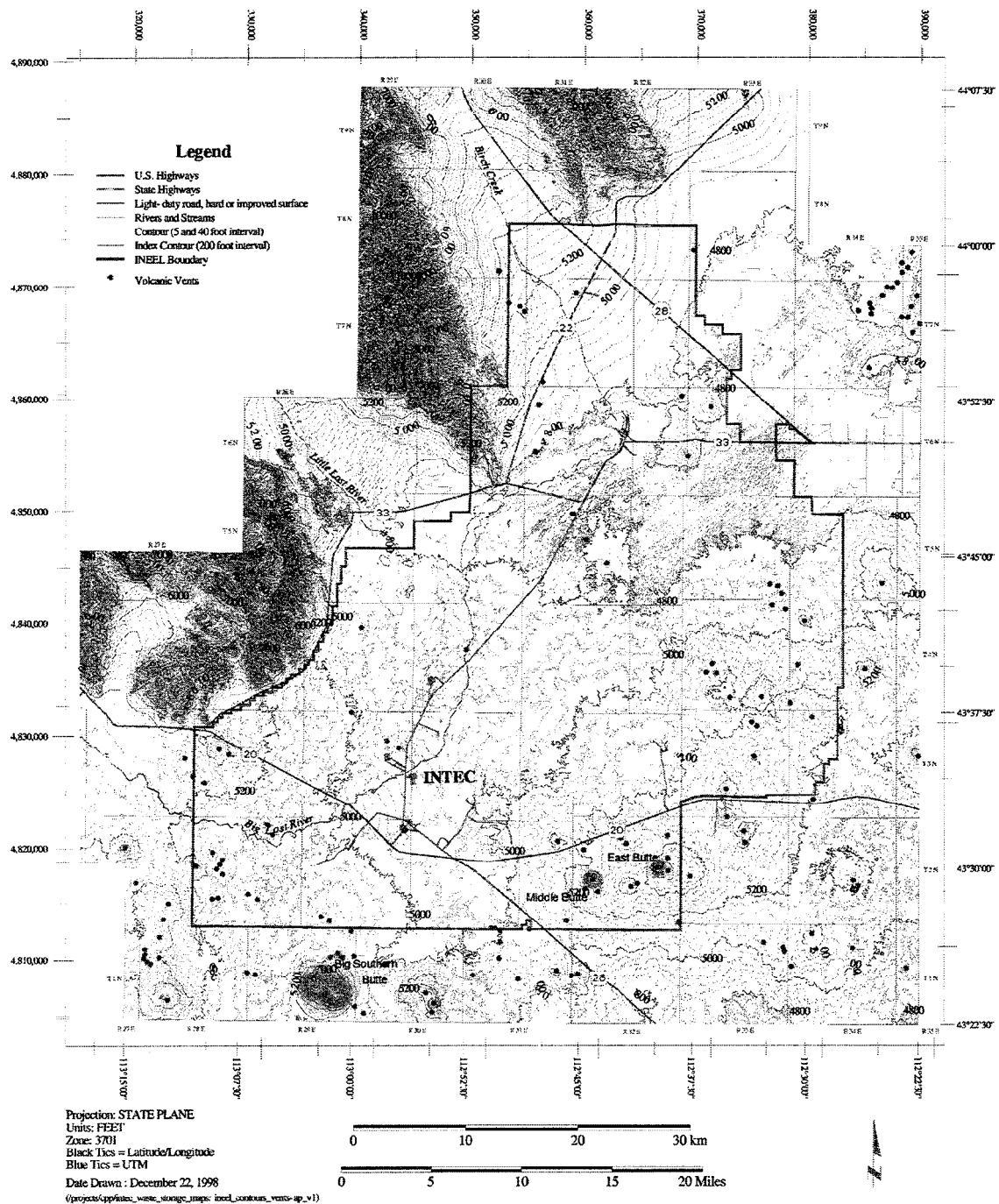


Figure is adapted from the TMI-2 ISFSI SAR (Ref. 2-1). The ISF Facility site is adjacent to the INTEC depicted on the figure.

Figure 2.3-5
Topographical Cross-Sections for TMI-2 ISFSI 50-Mile Radius, North and East Radials

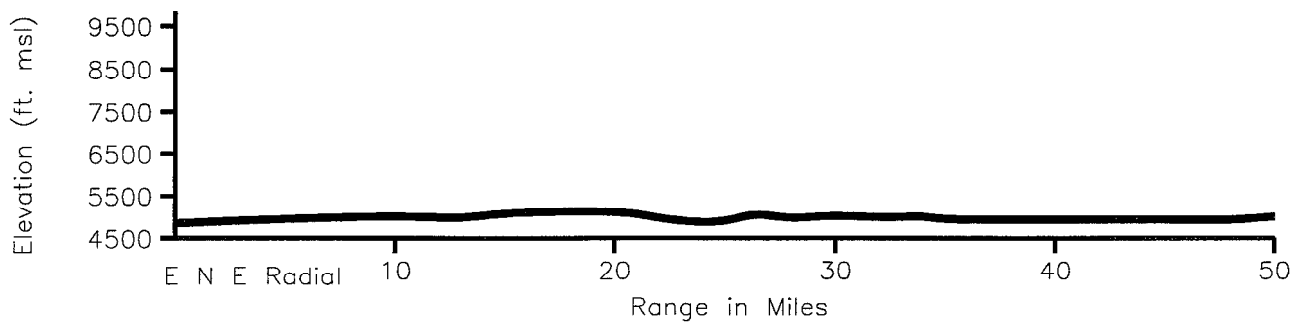
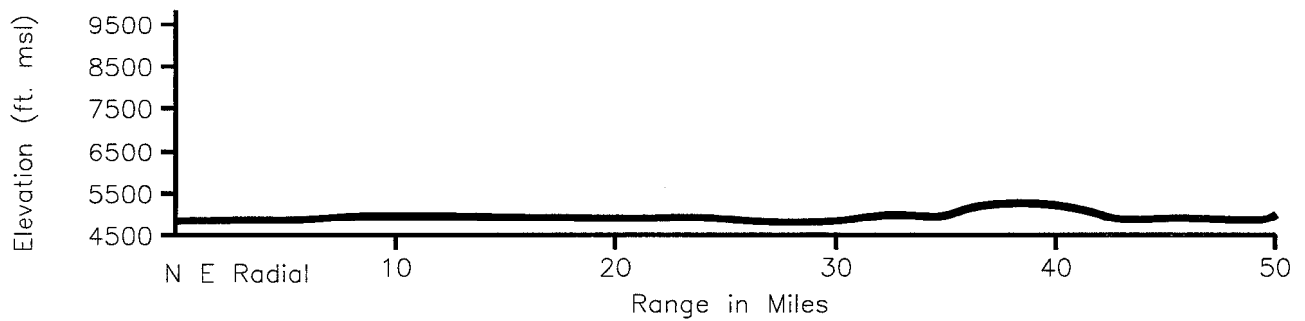
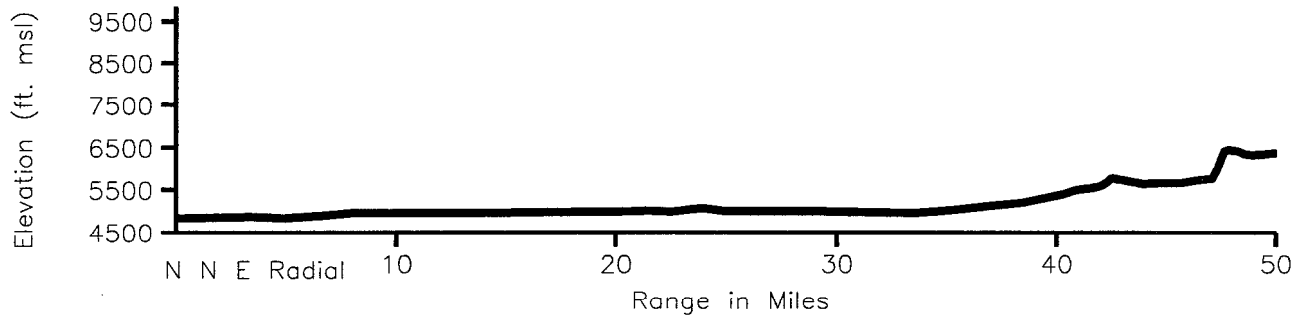
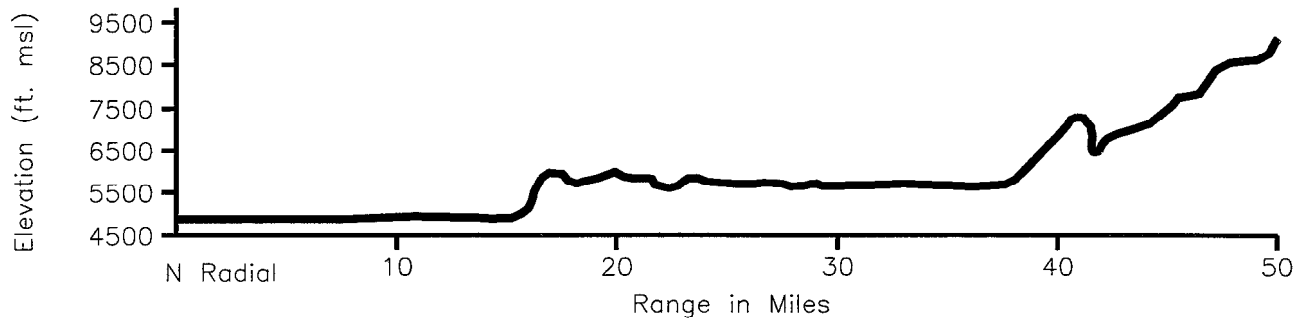


Figure 2.3-6
Topographical Cross-Sections for TMI-2 ISFSI 50-Mile Radius, South and East Radials

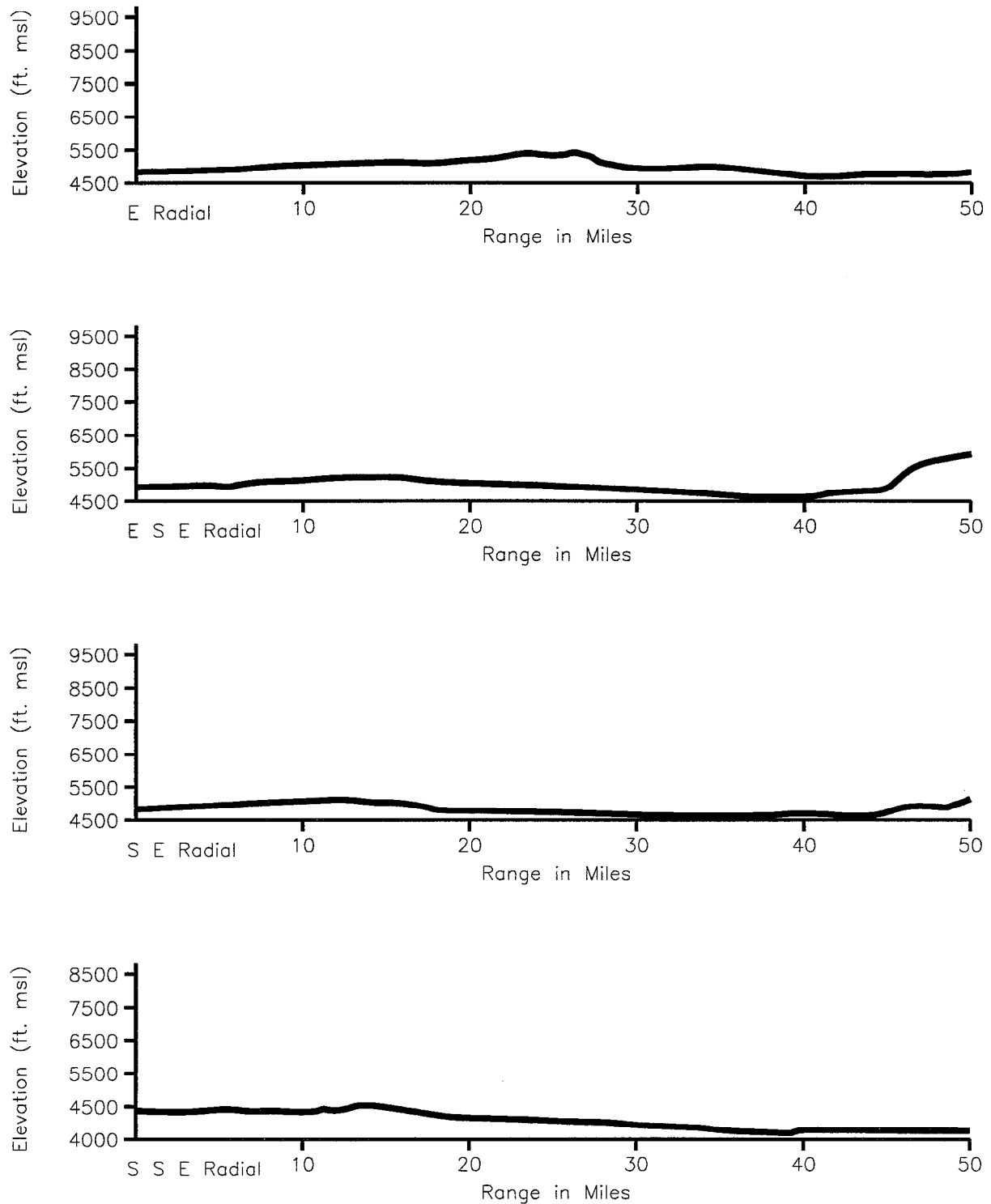


Figure 2.3-7
Topographical Cross-Sections for TMI-2 ISFSI Site
50-Mile Radius, South and West Radials

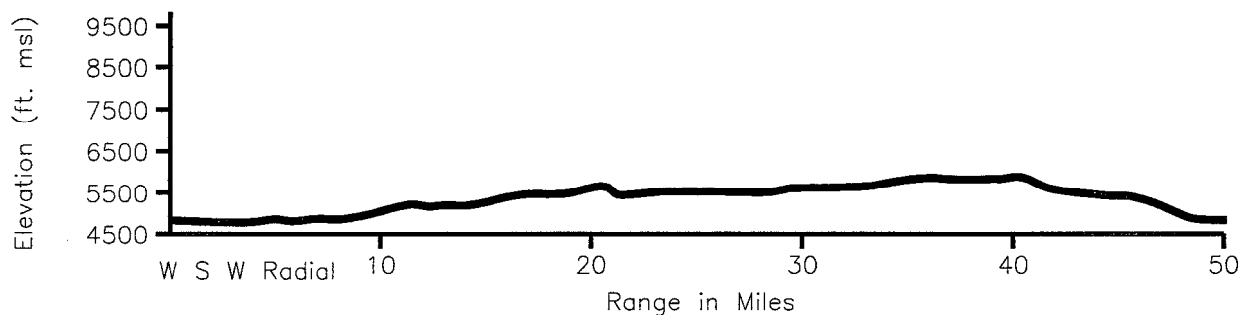
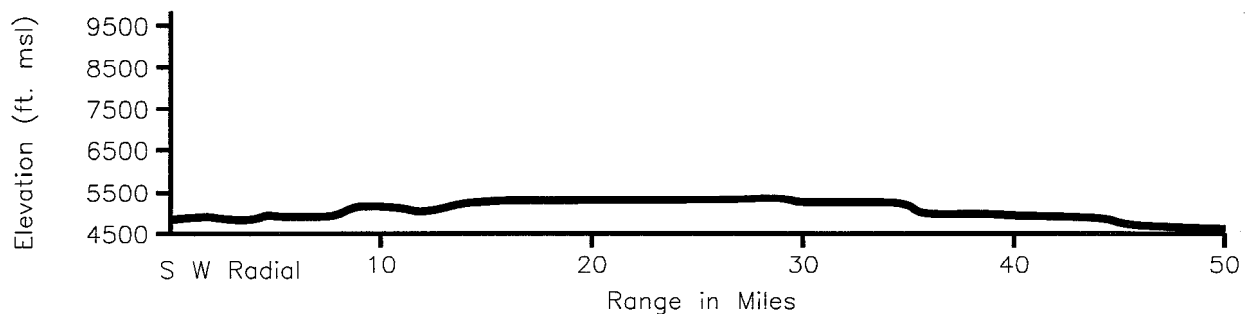
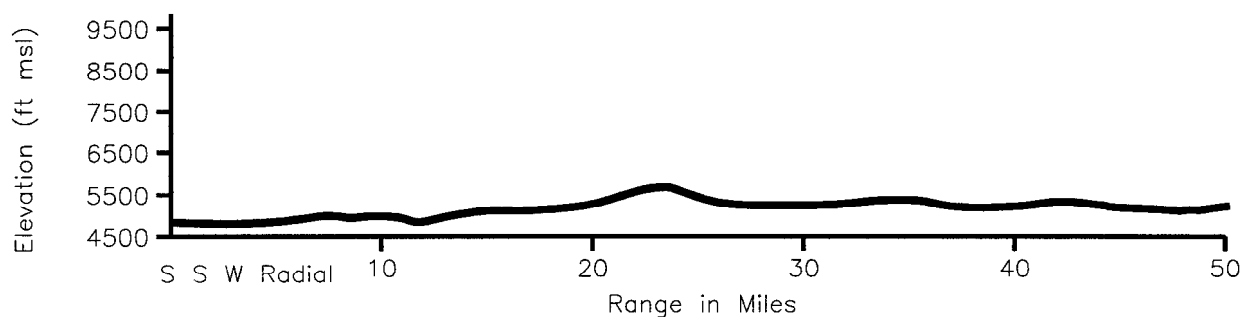
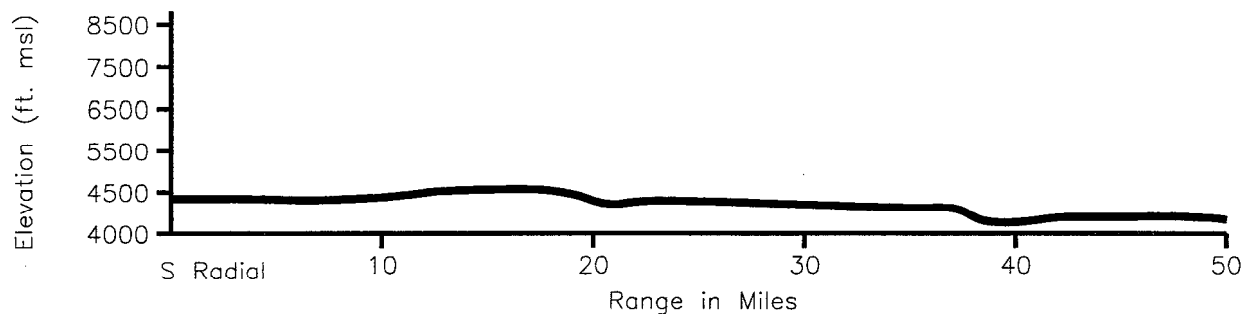


Figure 2.3-8
Topographical Cross-Sections for TMI-2 ISFSI
50-Mile Radius, North and West Radials

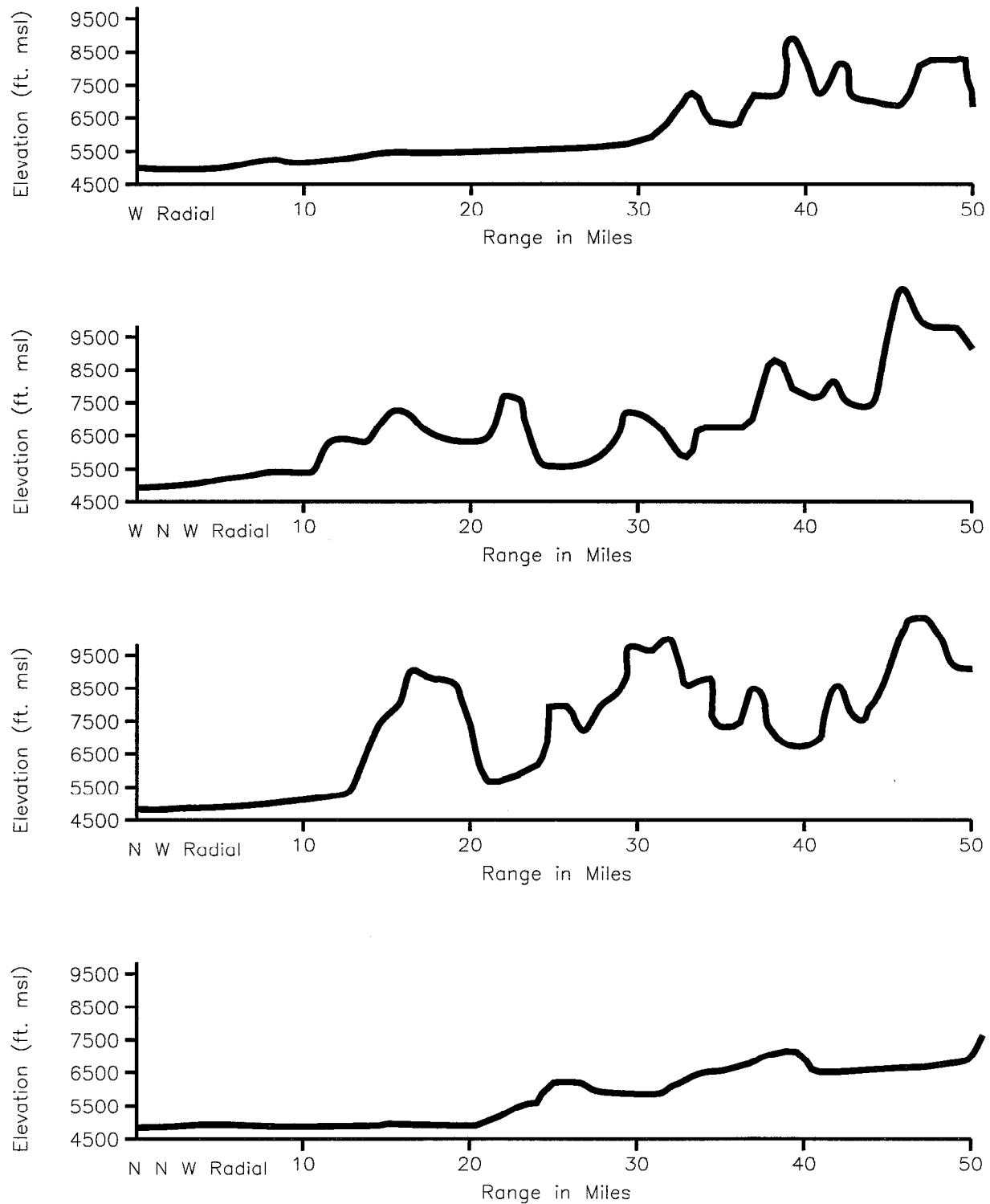


Figure 2.3-9
Topographical Cross-Sections for TMI-2 ISFSI Site
5-Mile Radius, North and East Radials

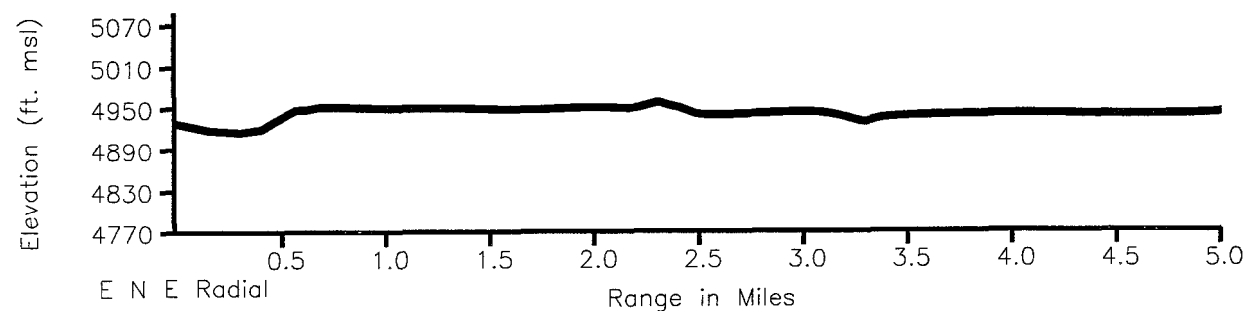
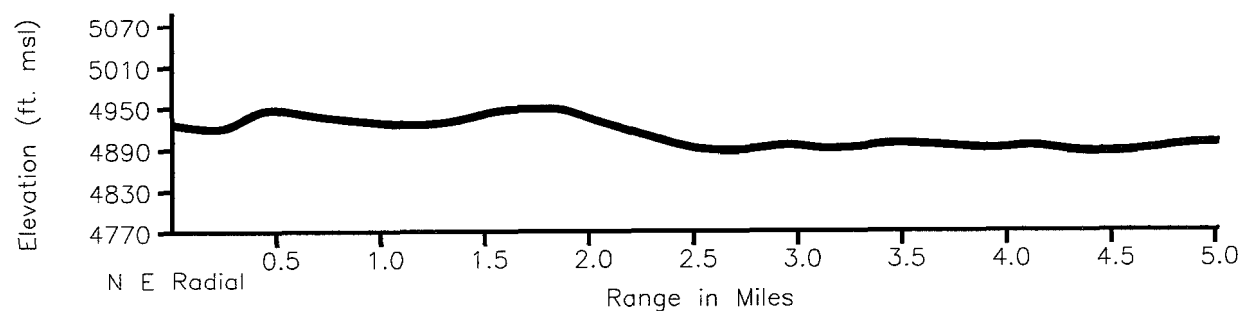
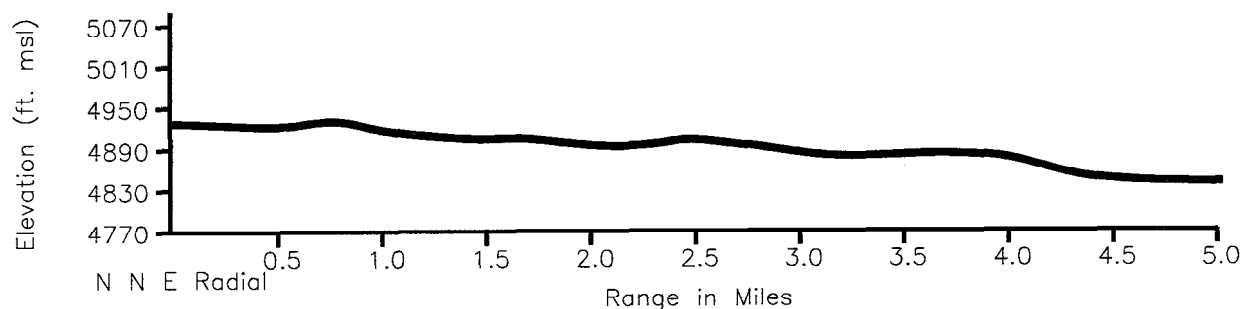
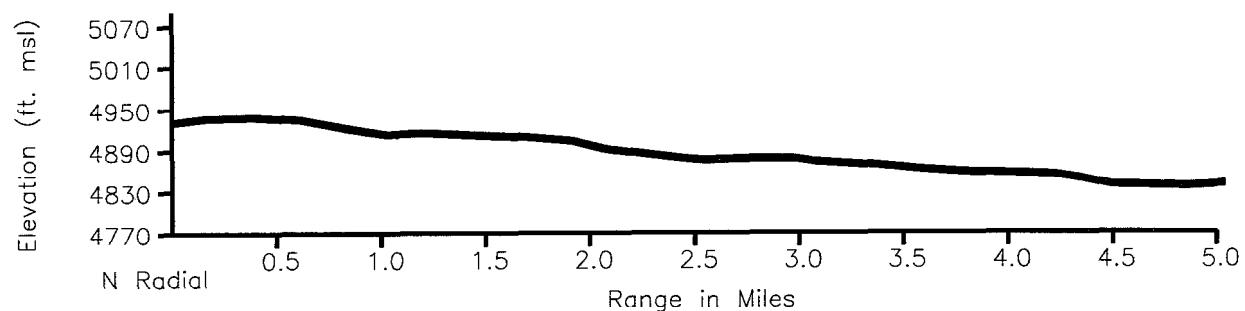


Figure 2.3-10
Topographical Cross-Sections for TMI-2 ISFSI Site
5-Mile Radius, South and East Radials

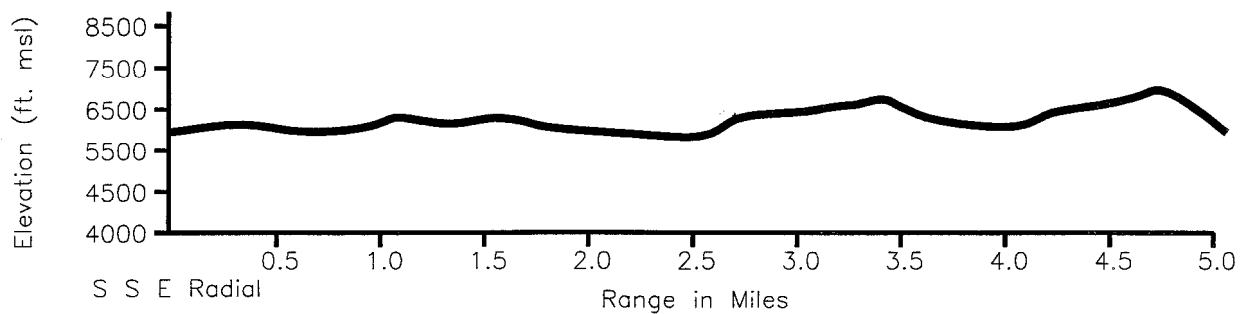
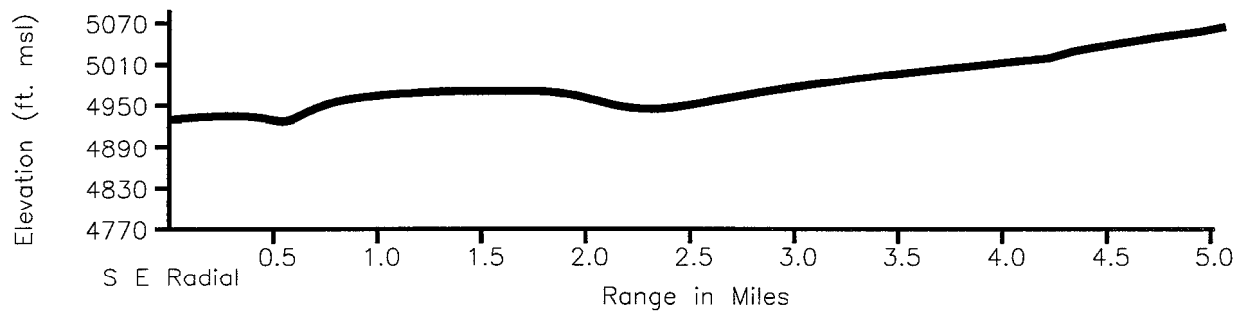
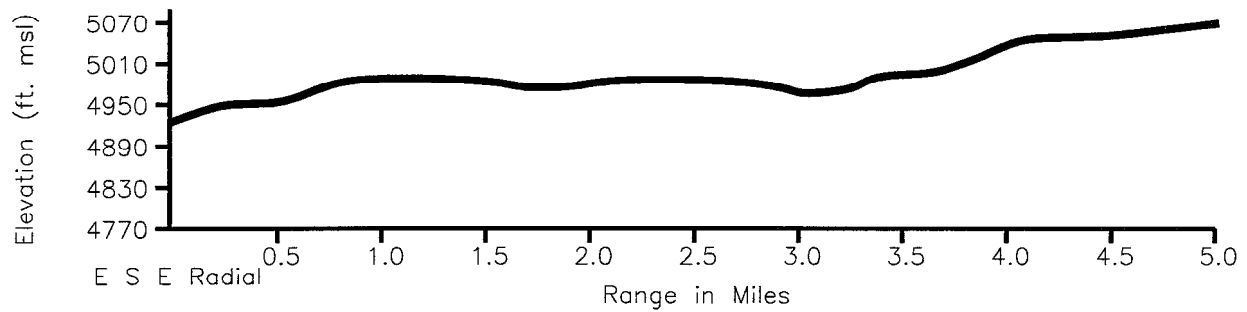
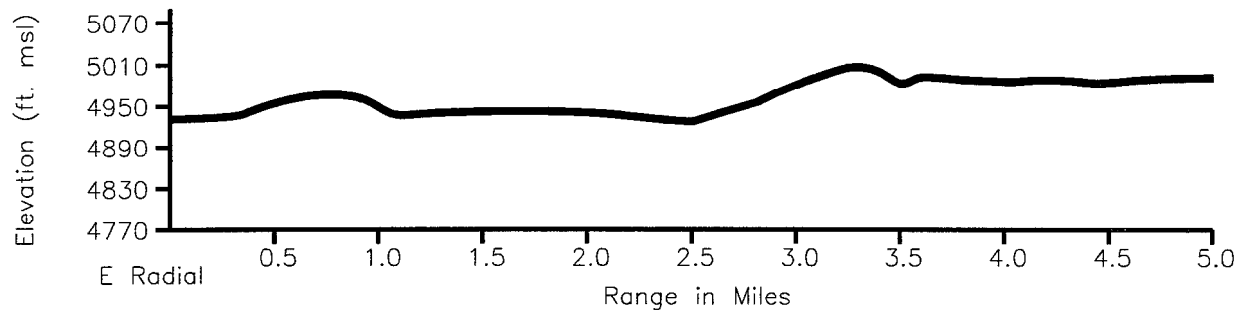


Figure 2.3-11
Topographical Cross-Sections For TMI-2 ISFSI Site
5-Mile Radius, South And West Radials

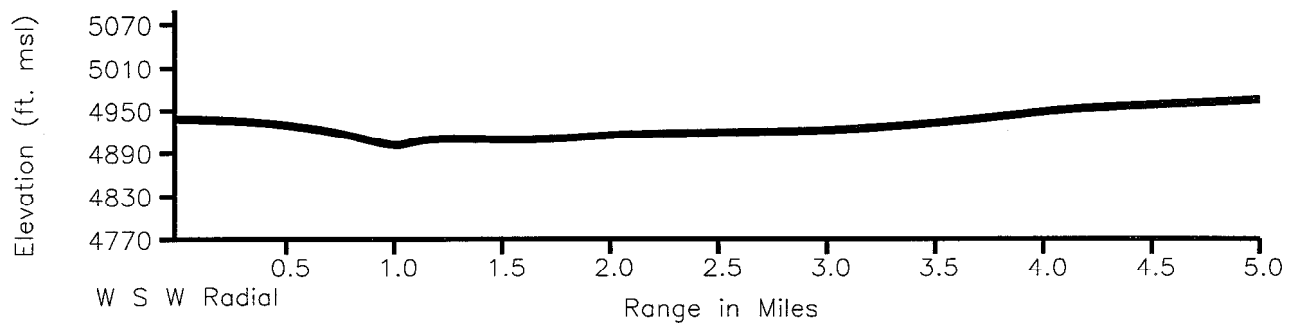
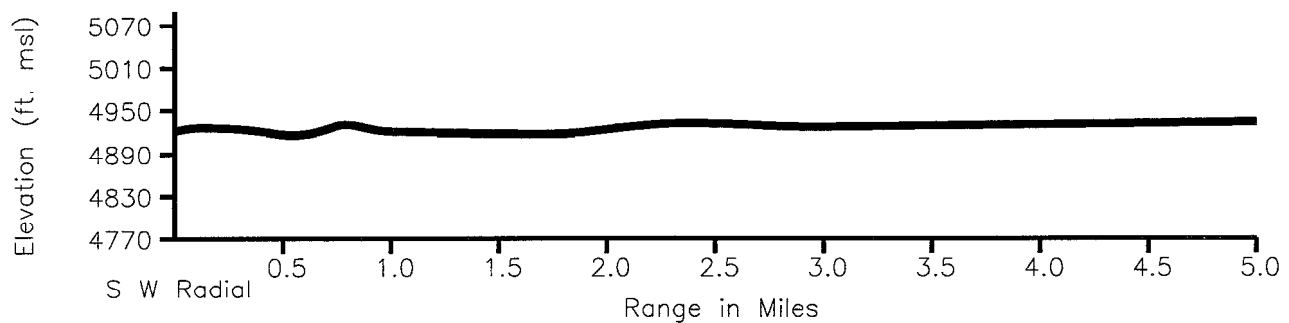
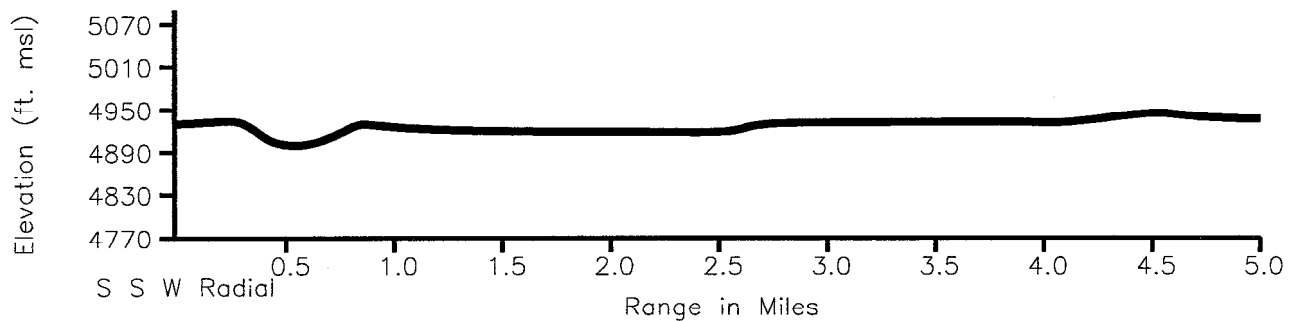
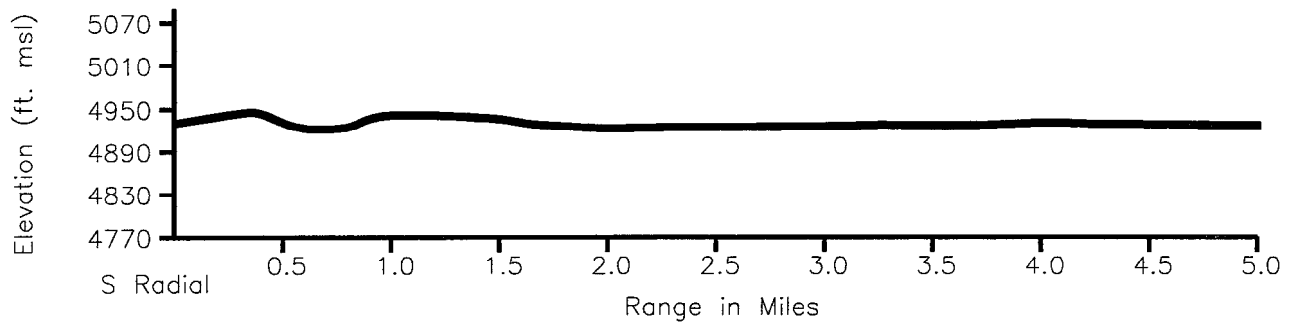


Figure 2.3-12
Topographical Cross-Sections for TMI-2 ISFSI Site
5-Mile Radius, North and West Radials

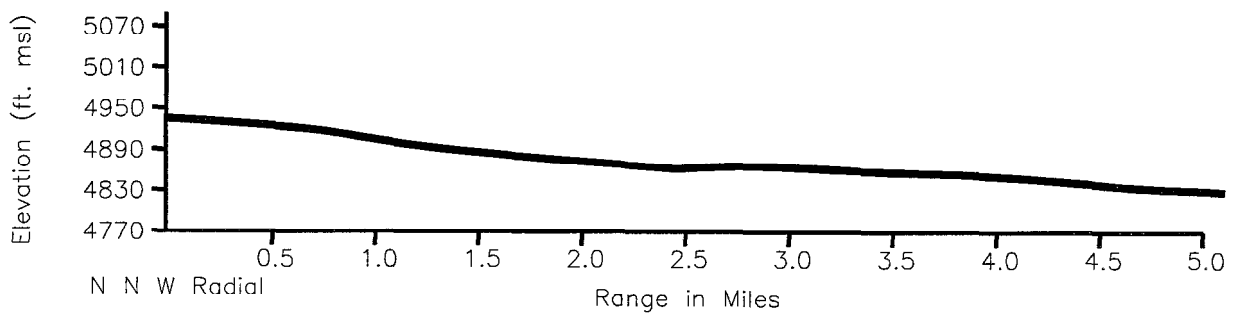
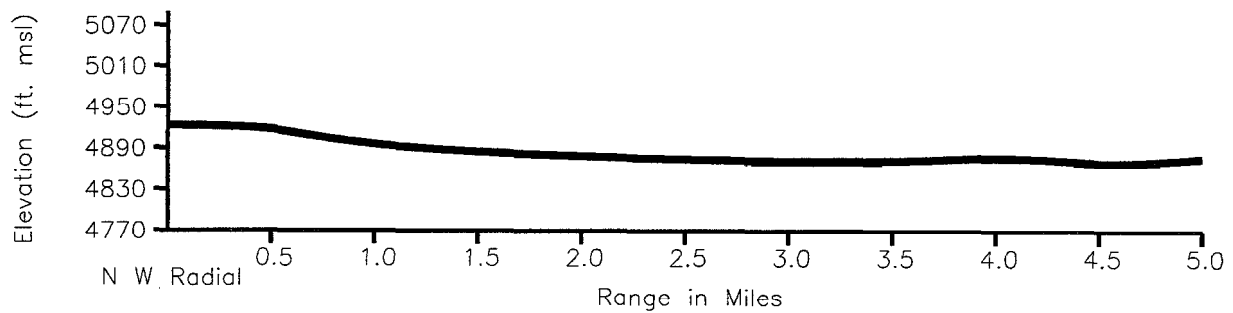
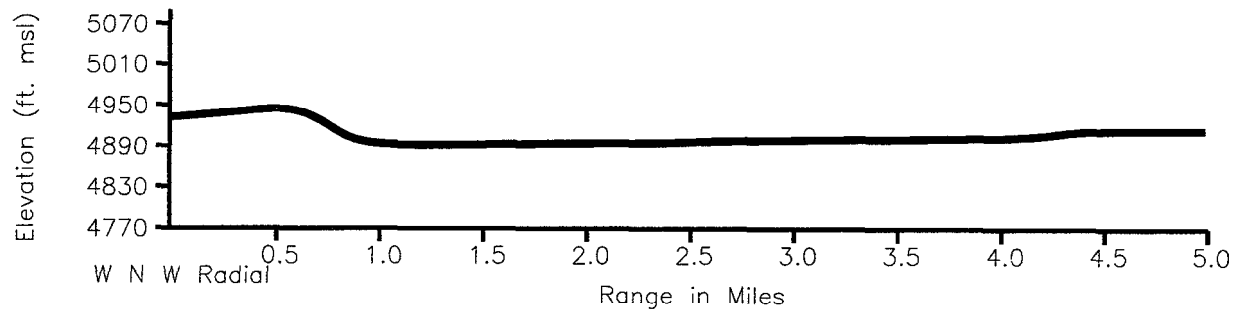
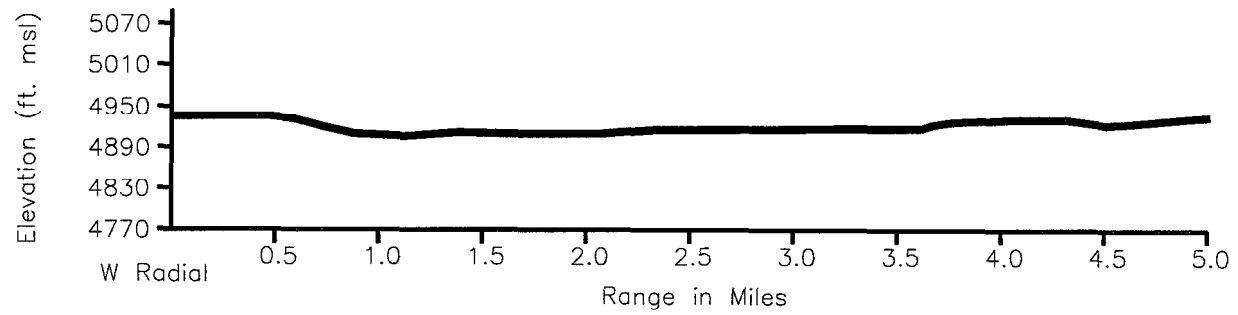


Figure 2.3-13
Grid 3 – 10 Meter Level Annual Wind Roses (1980-1982)

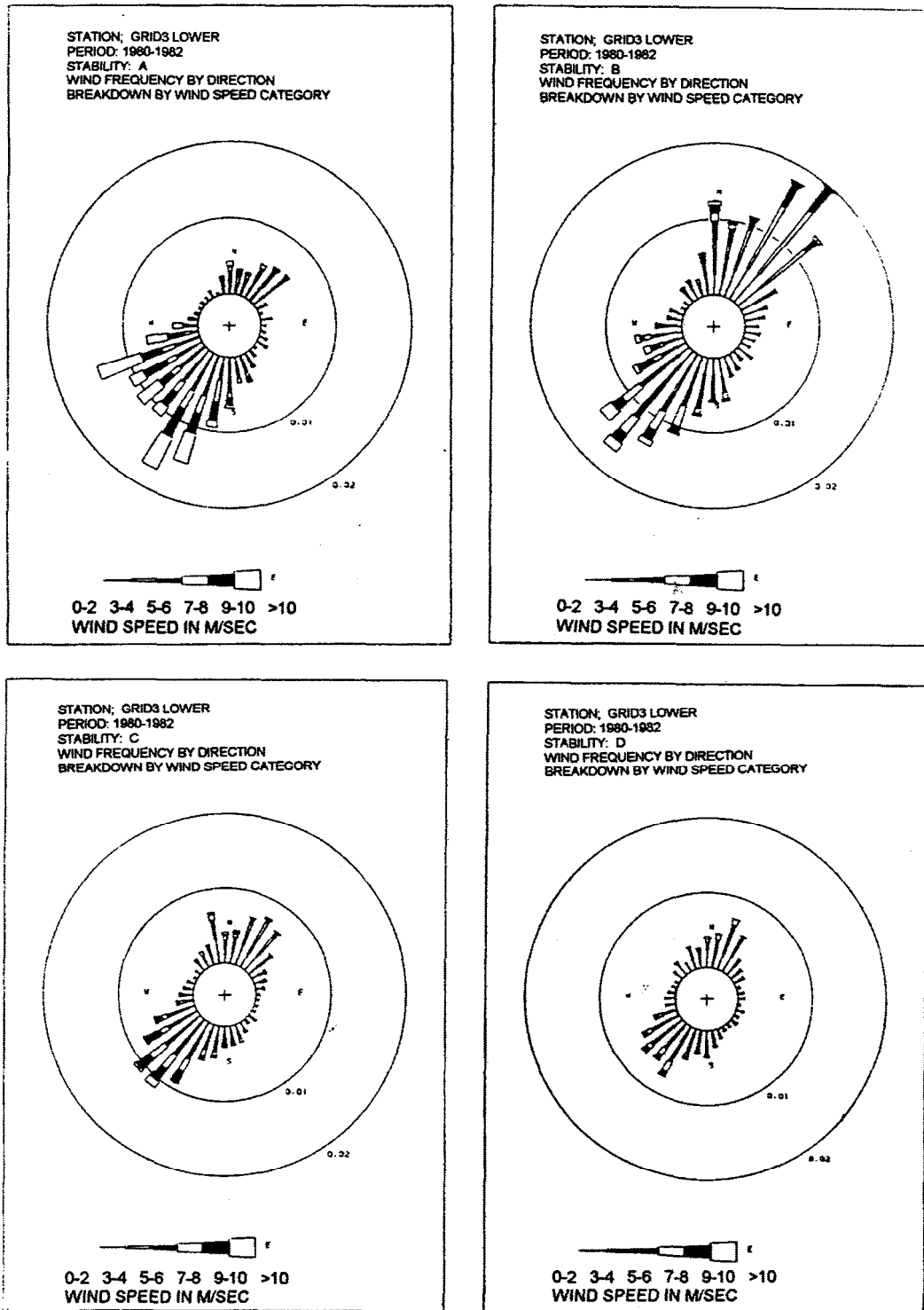
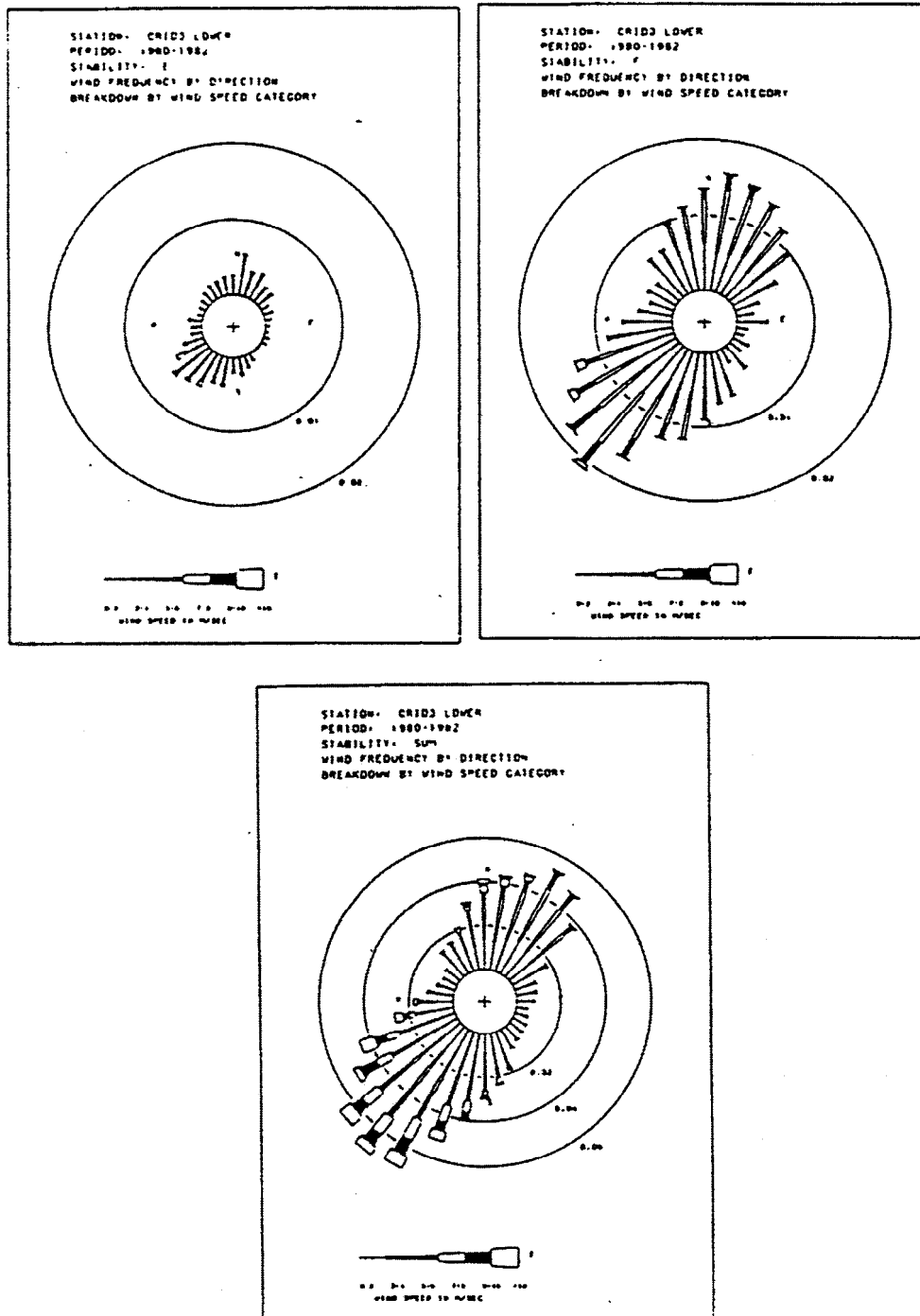
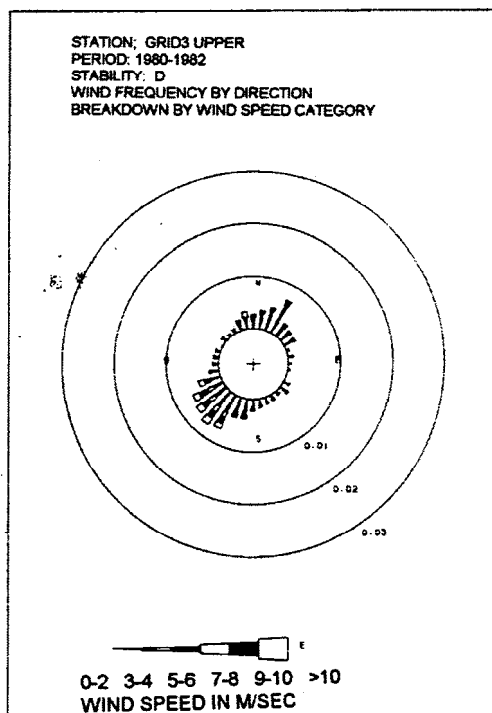
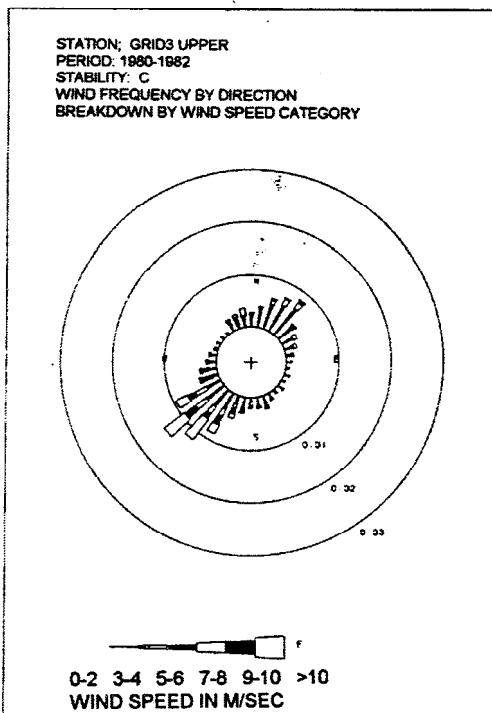
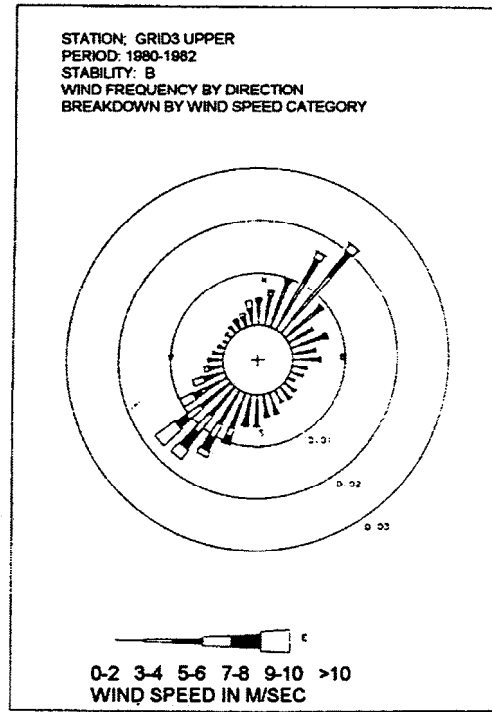
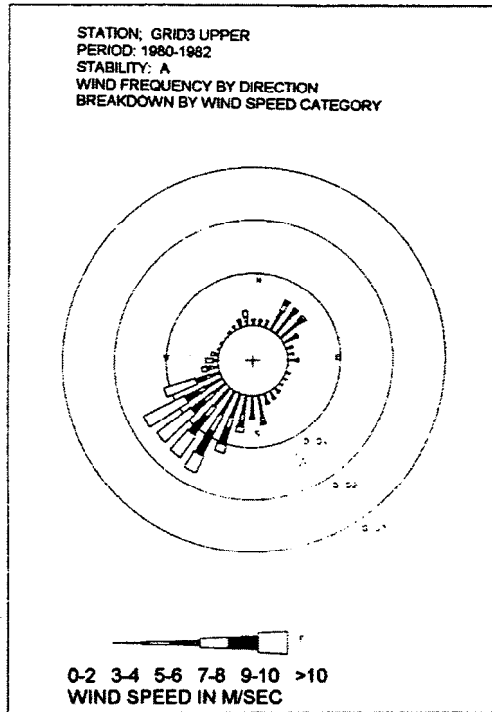


Figure 2.3-14
Grid 3 – 10- Meter Level Annual Wind Roses (1980-1982)



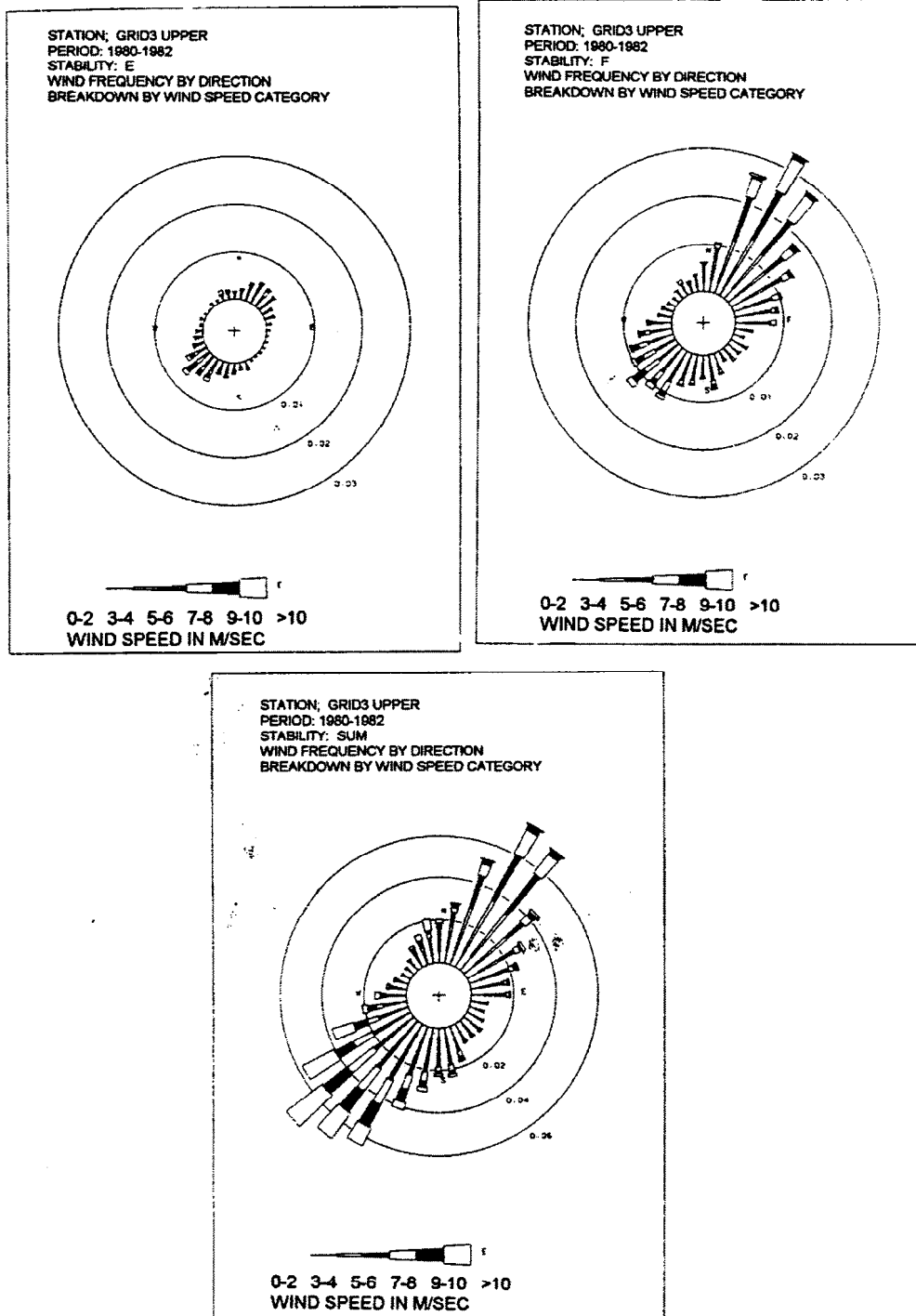
INEL 4 4850

Figure 2.3-15
Grid 3 – 61 Meter Level Annual Wind Roses (1980-1982)



INEL 4 4848

Figure 2.3-16
Grid 3 – 61 Meter Level Annual Wind Roses (1980-1982)



INEL 4 4845

Figure 2.3-17
Wind Observation Locations within a 50-Mile Radius of the ISF Site

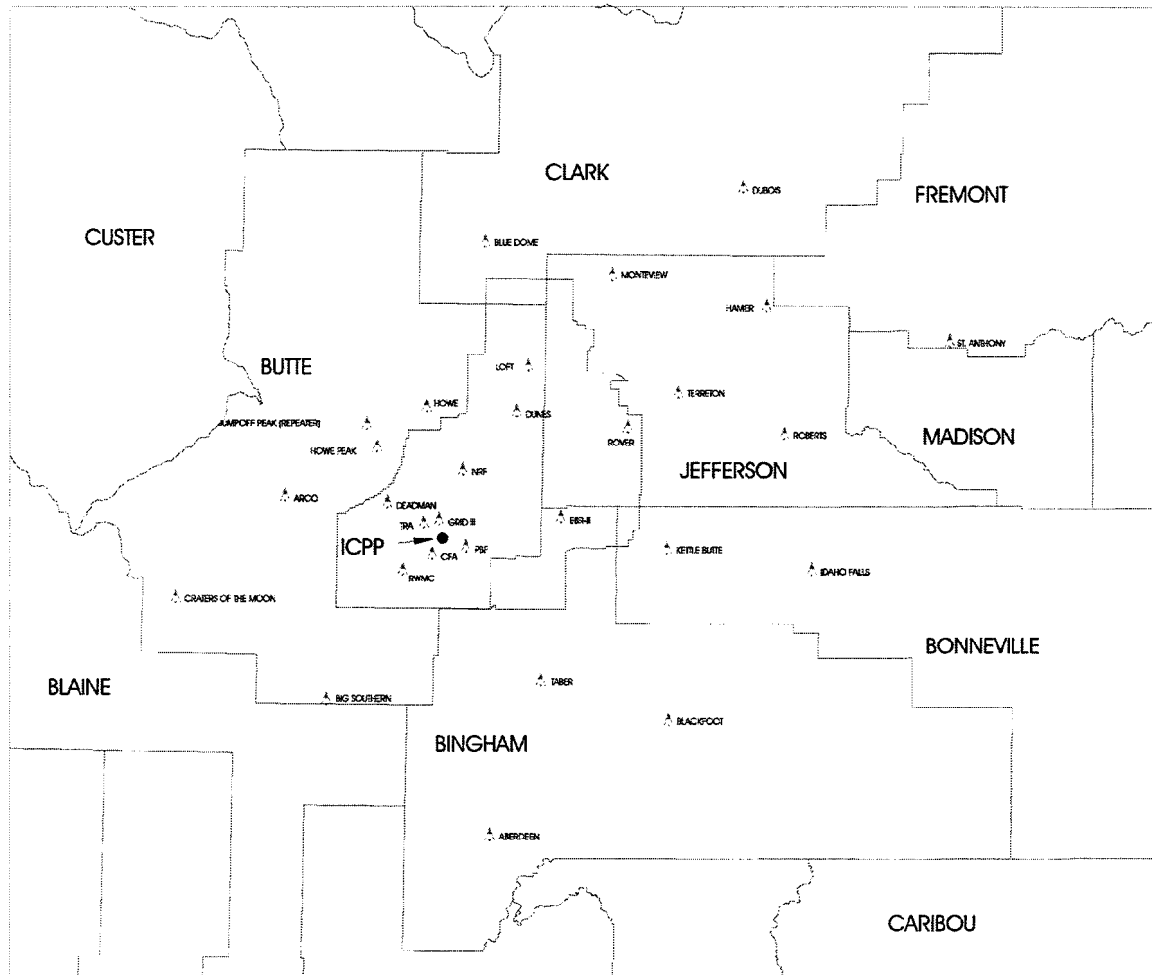


Figure is adapted from the TMI-2 ISFSI SAR (Ref. 2-1). The ICPP is an earlier name for the INTEL, which is adjacent to the ISF Facility site.

Figure 2.3-18
 σ_z versus Distance at INEEL

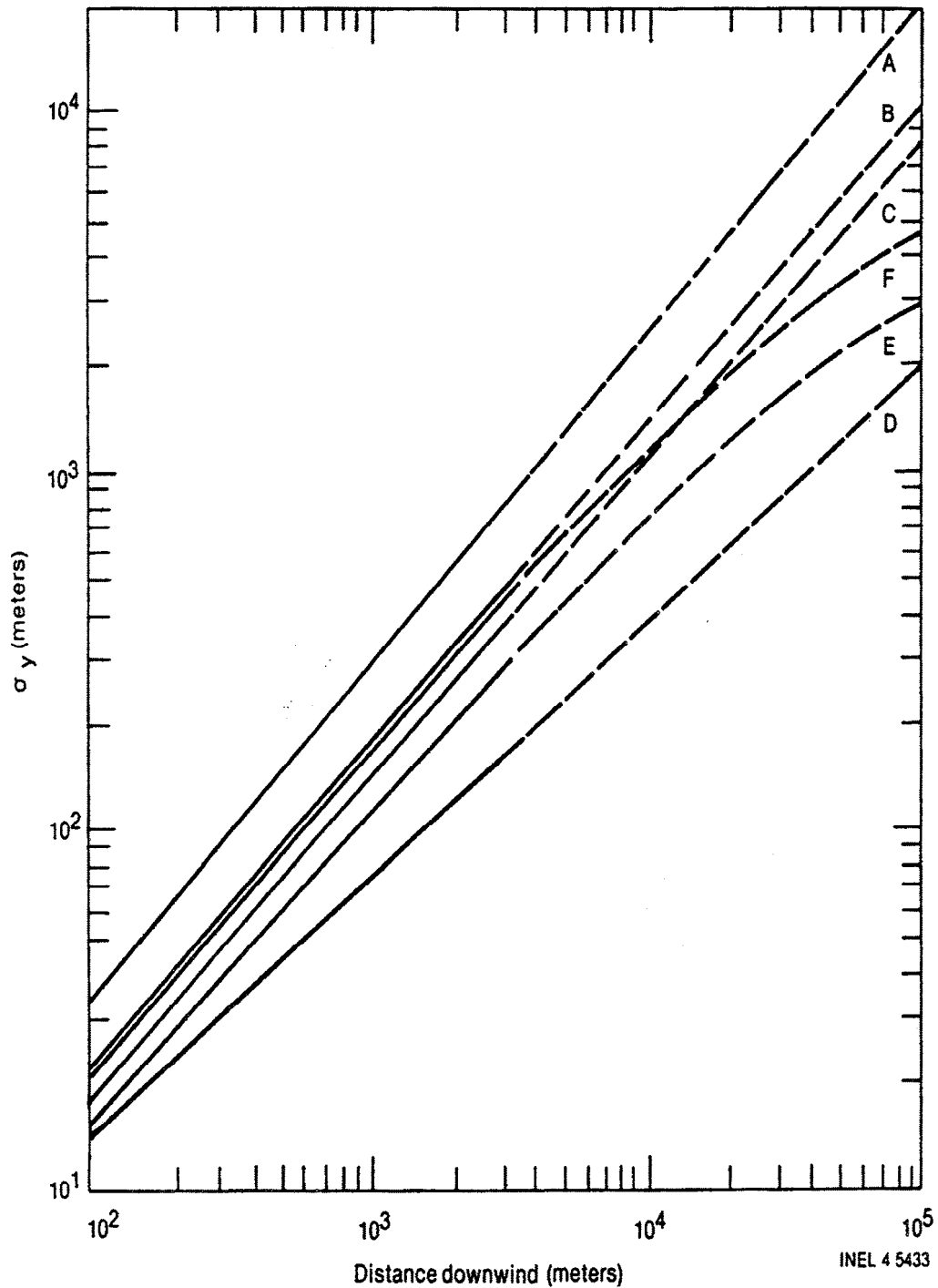


Figure developed from data presented in TMI-2 ISFSI SAR (Ref. 2-1)

Figure 2.3-19
 σ_y versus Distance at INEEL

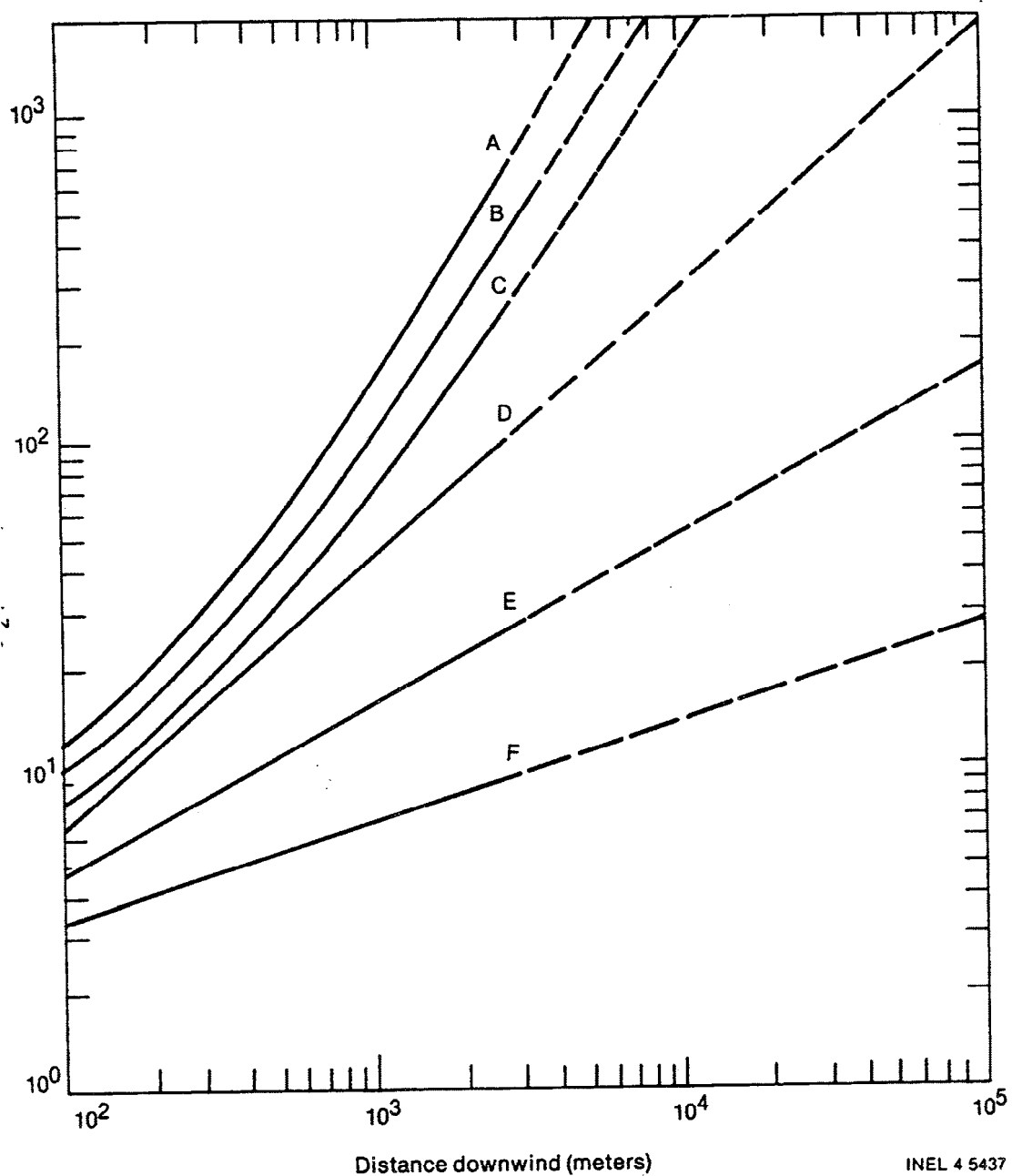


Figure developed from data presented in TMI-2 ISFSI SAR (Ref. 2-1)

Figure 2.3-20
Annual Normalized Concentration – 50-Mile Radius
(INTEC 1982)

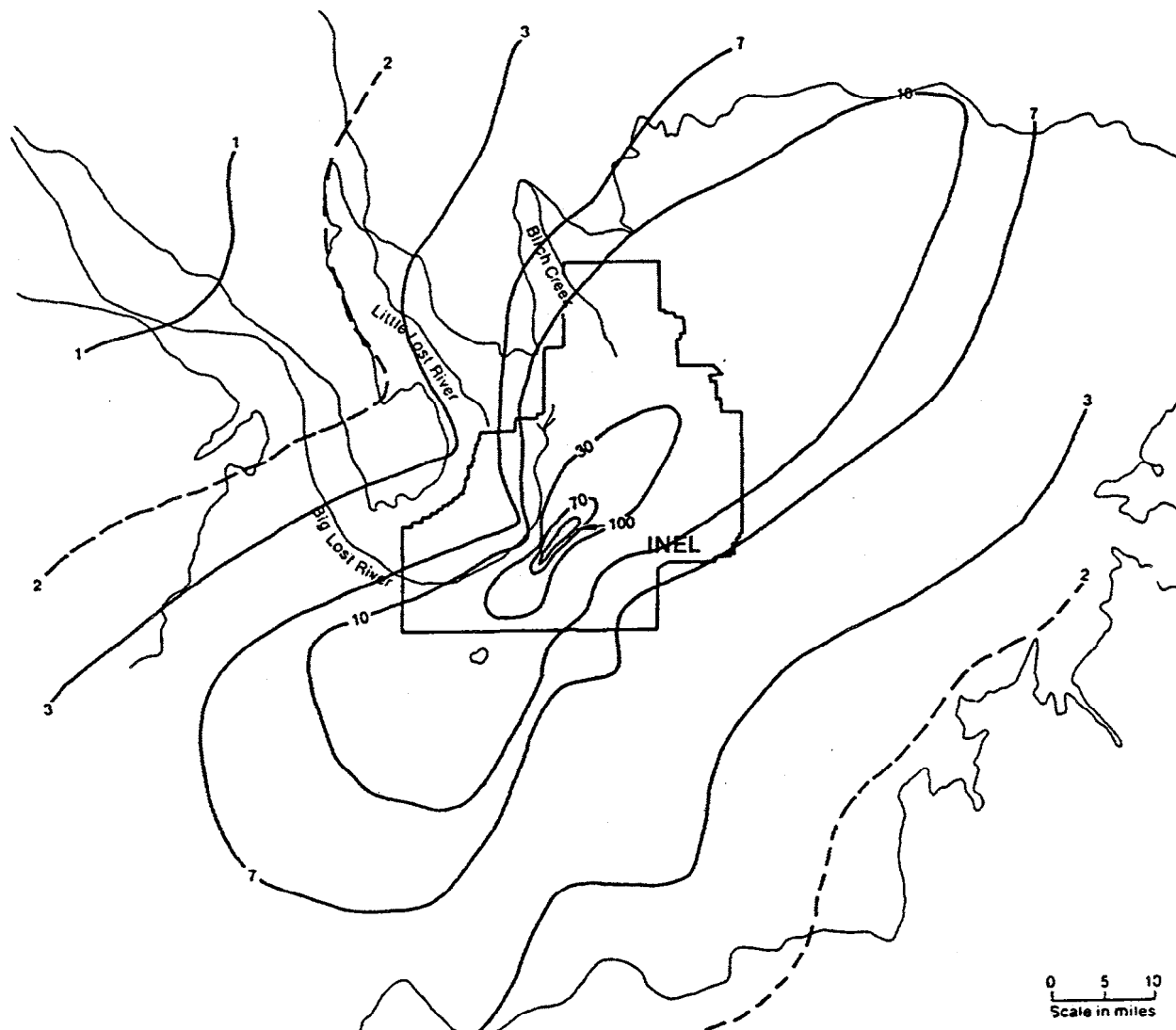


Figure developed from data presented in TMI-2 ISFSI SAR (Ref. 2-1)

Figure 2.3-21
Annual Normalized Concentration – 5-Mile Radius
(INTEC 1982)

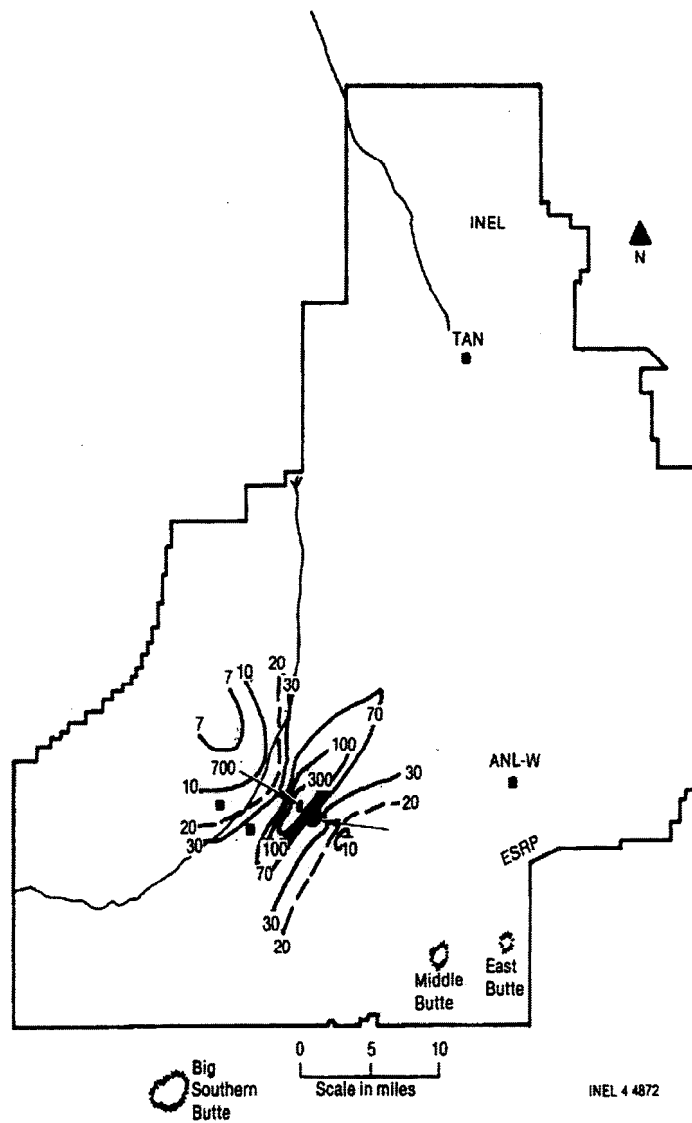


Figure developed from data presented in TMI-2 ISFSI SAR (Ref. 2-1)

Figure 2.3-22
Annual Normalized Total Integrated Concentration
(INTEC 1980)

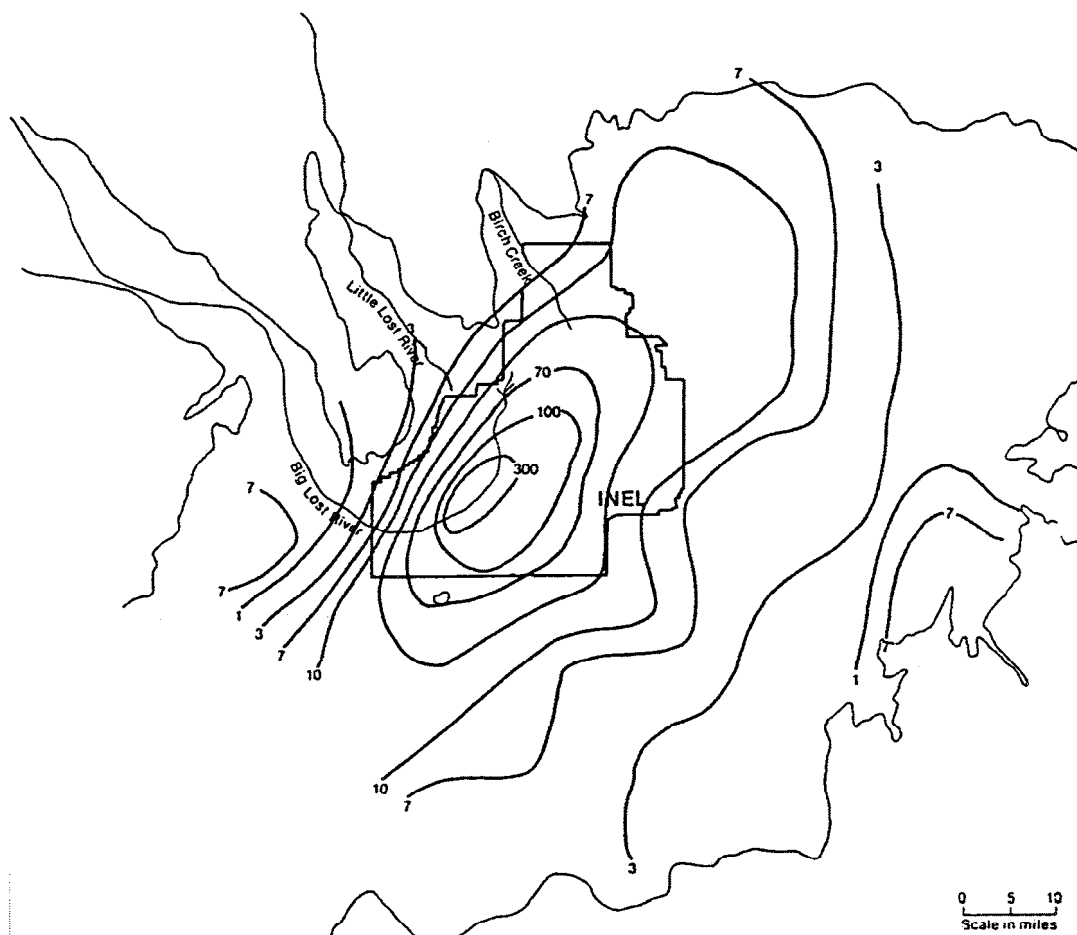


Figure developed from data presented in TMI-2 ISFSI SAR (Ref. 2-1)

Figure 2.3-23
Annual Normalized Total Integrated Concentration
(INTEC 1981)

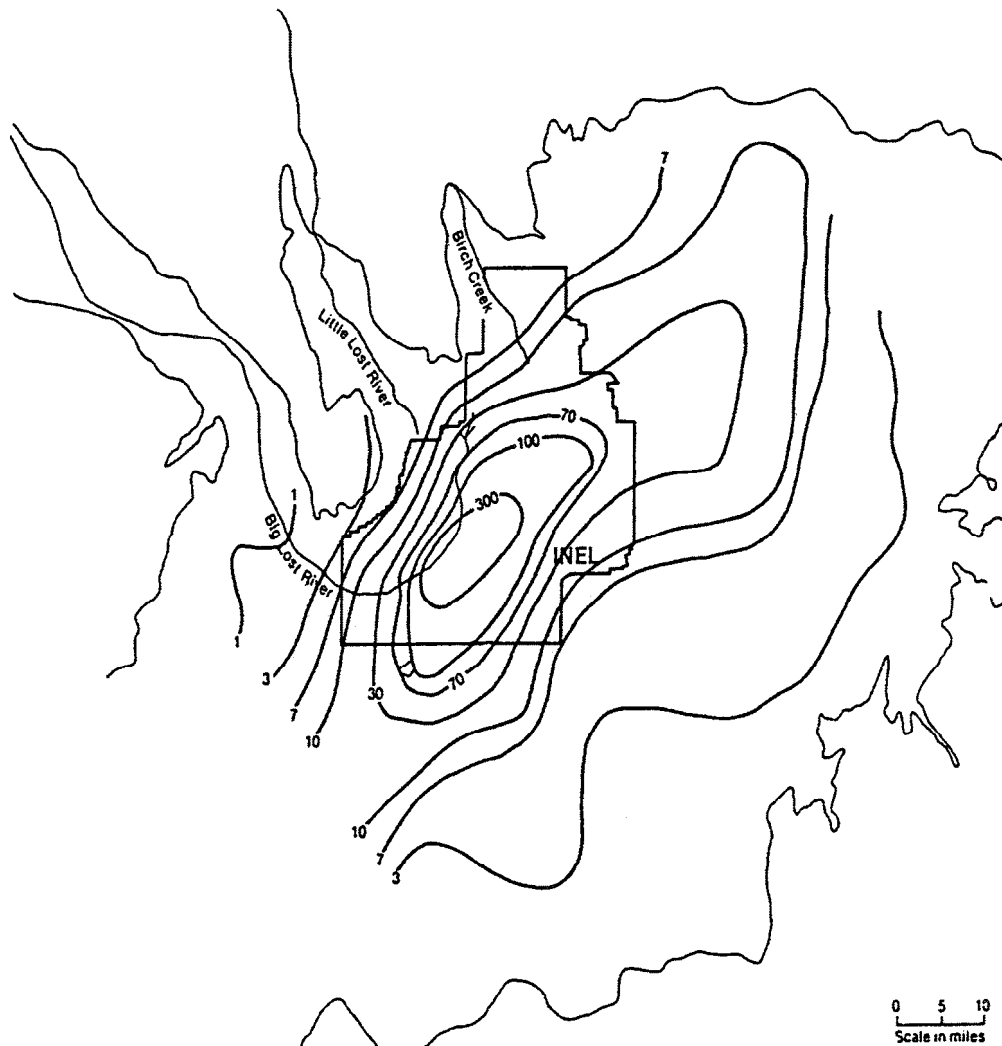


Figure developed from data presented in TMI-2 ISFSI SAR (Ref. 2-1)

Figure 2.3-24
Annual Normalized Total Integrated Concentration
(INTEC 1982)

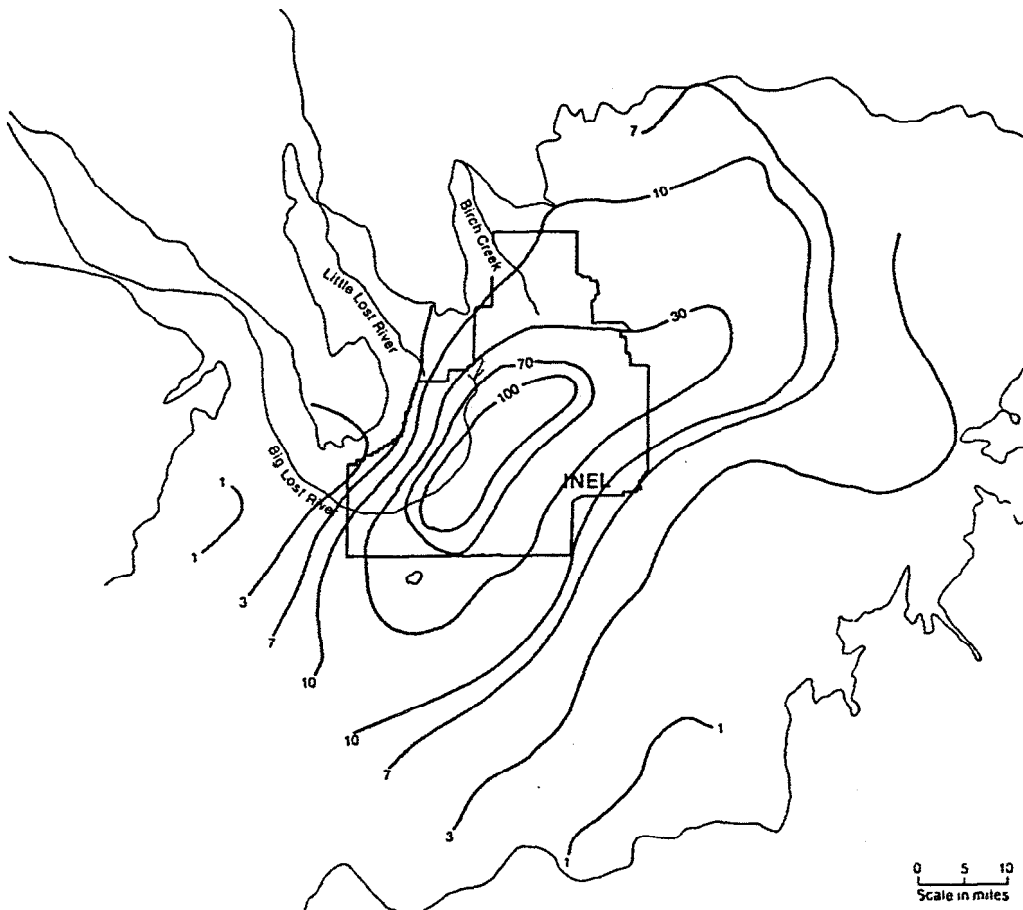


Figure developed from data presented in TMI-2 ISFSI SAR (Ref. 2-1)

Figure 2.3-25
Annual Normalized Total Integrated Concentration
(INTEC 1974-1983)

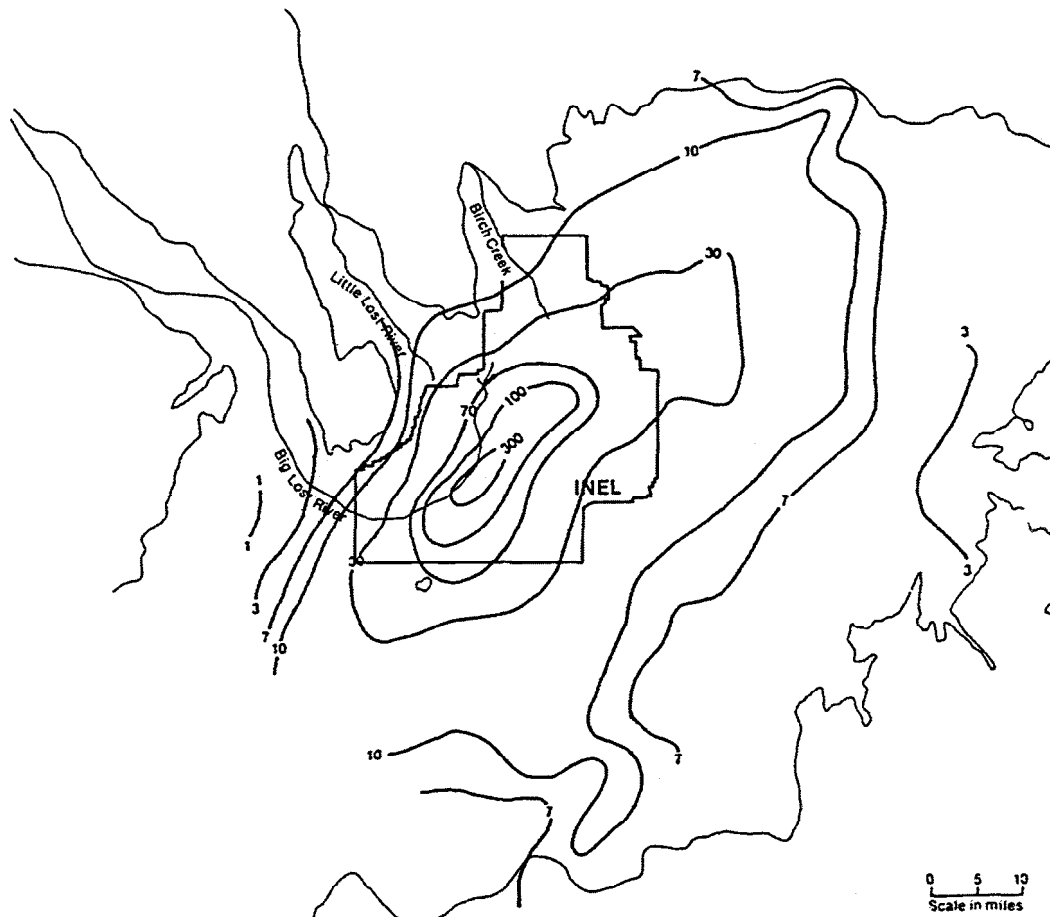


Figure developed from data presented in TMI-2 ISFSI SAR (Ref. 2-1)

Figure 2.4-1
Big Lost River System on the INEEL

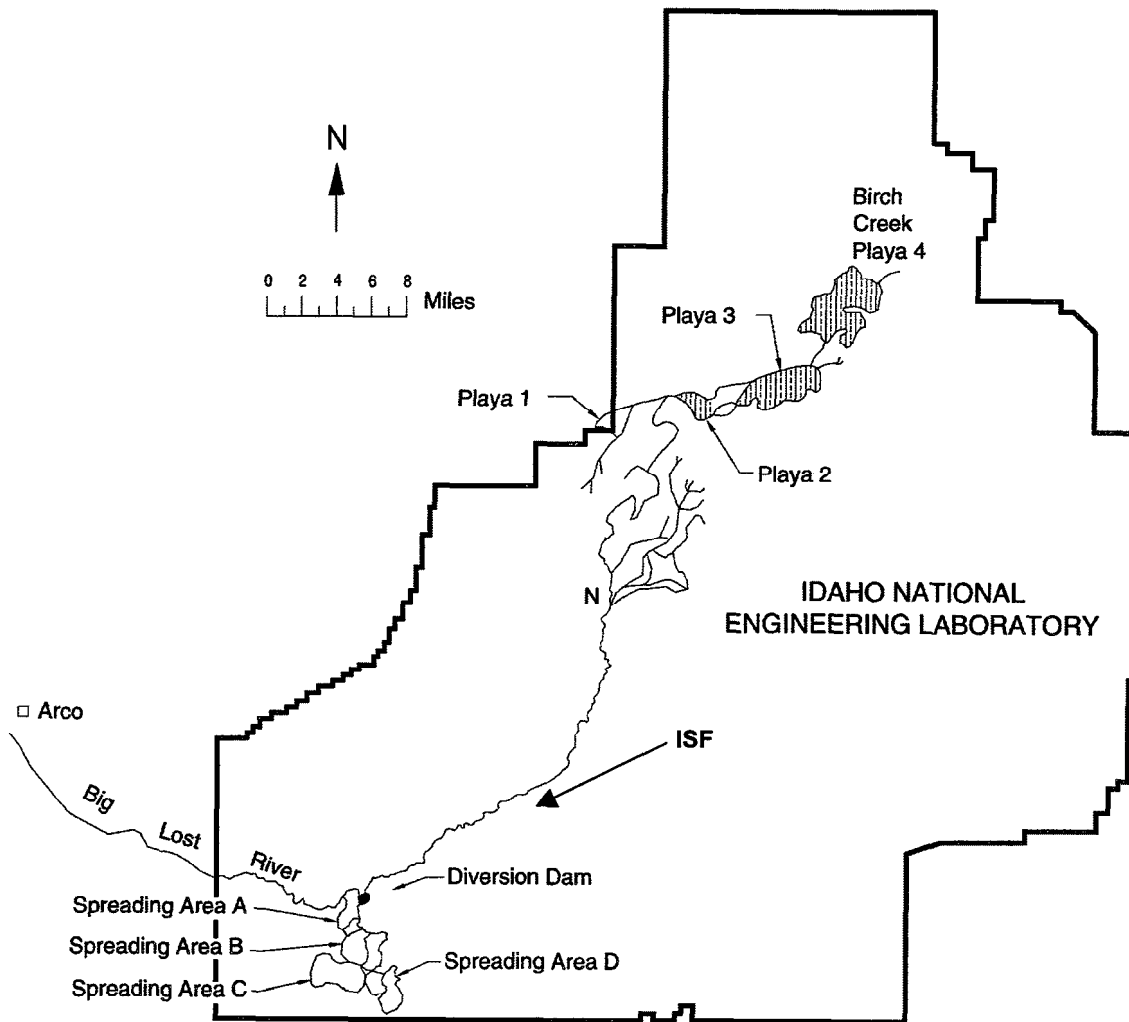
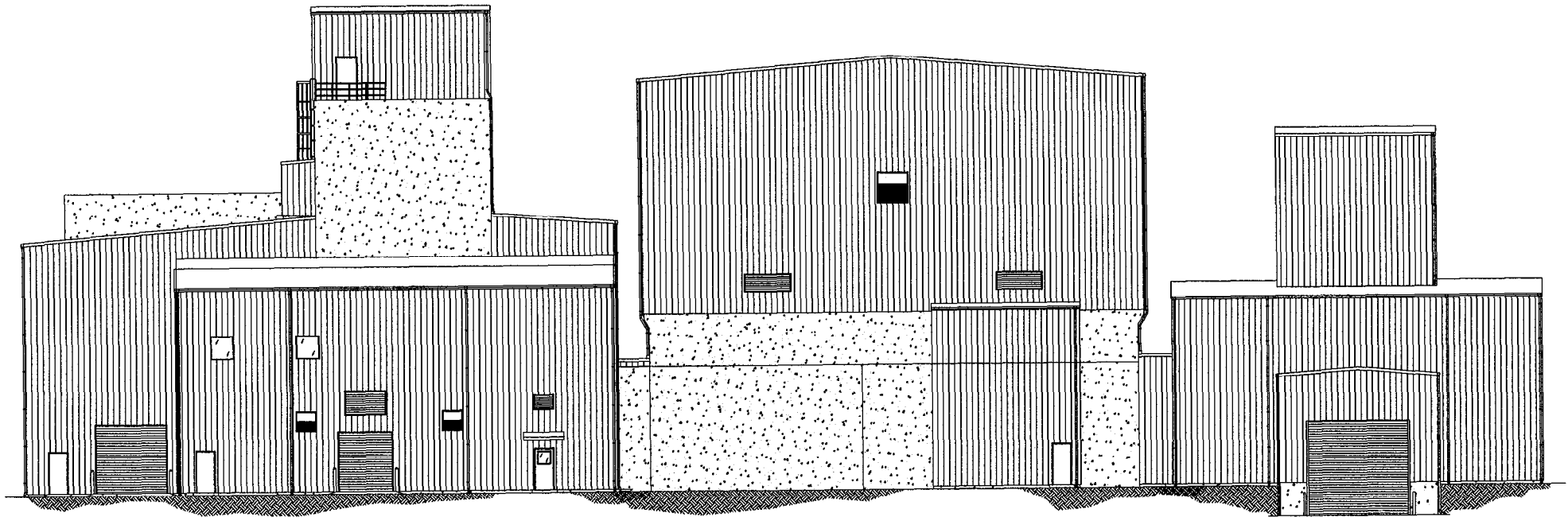


FIGURE 2.4-2
ISF Facility – Front View



ELEVATION LOOKING EAST

Grade elevation 4917 feet msl

Figure 2.4-3
Hydrograph for PMF-Induced Failure of the Mackay Dam
(Koslow and van Haften, 1986)

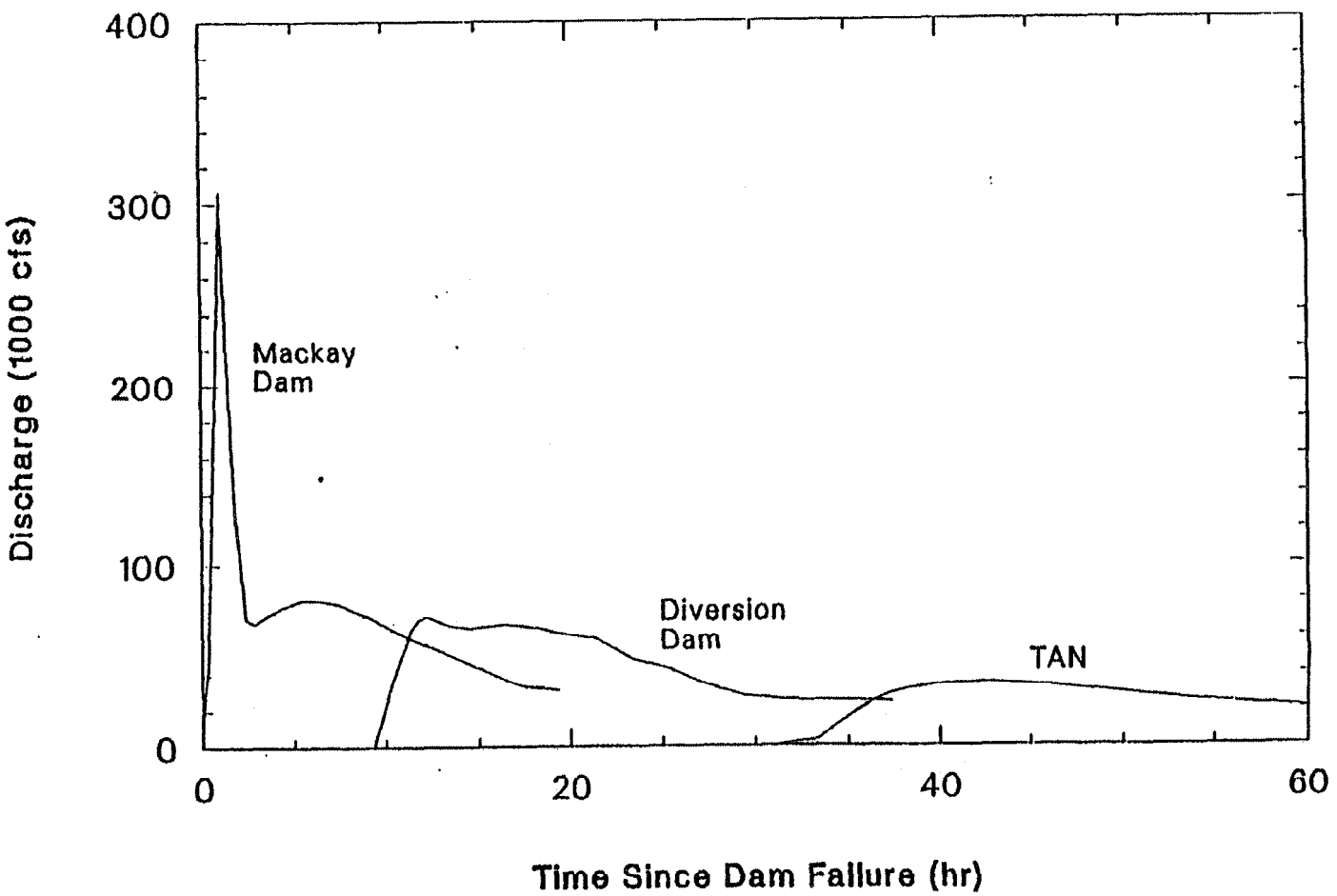
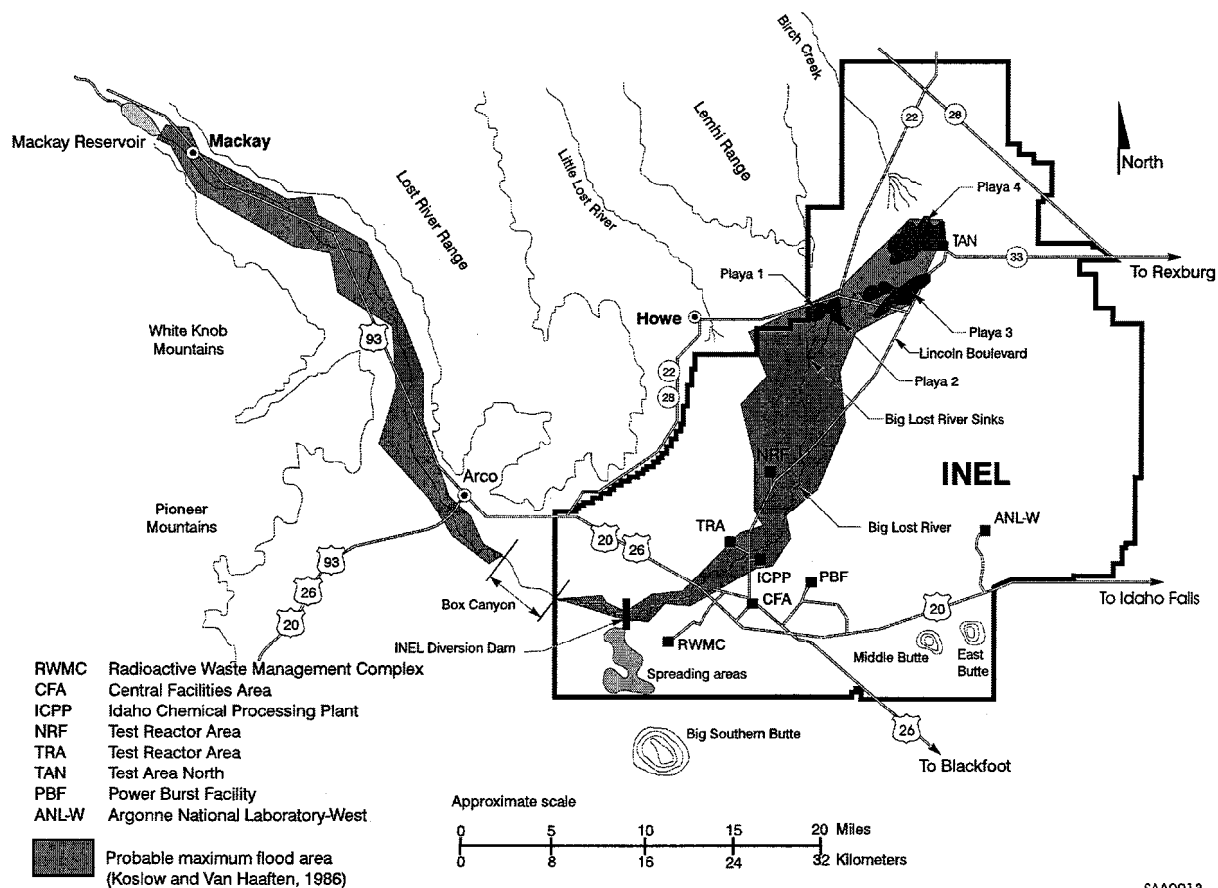


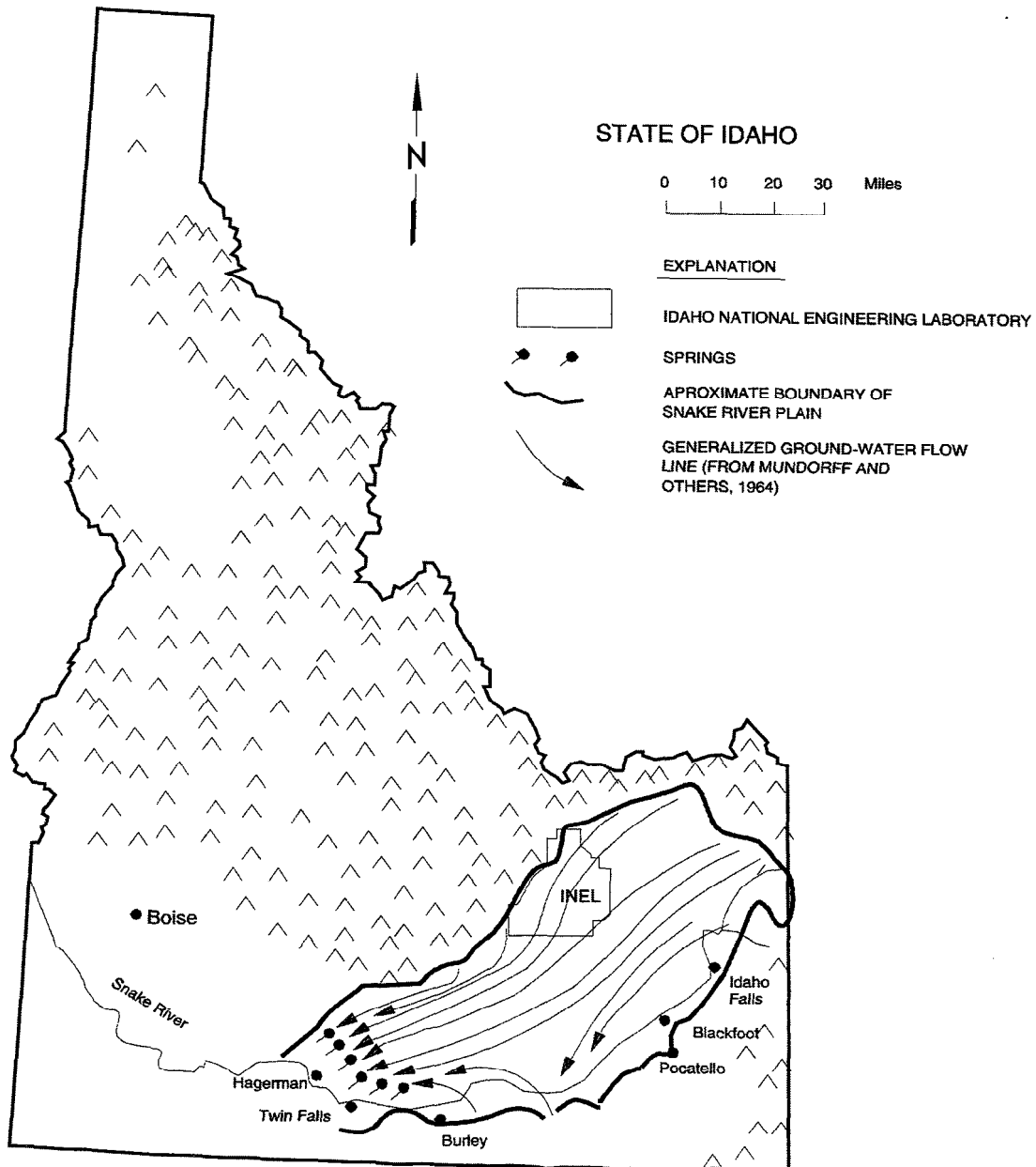
Figure 2.4-4
Predicted Inundation Area at INEEL for PMF-Induced Overtopping of Mackay Dam
(Bennett 1990)



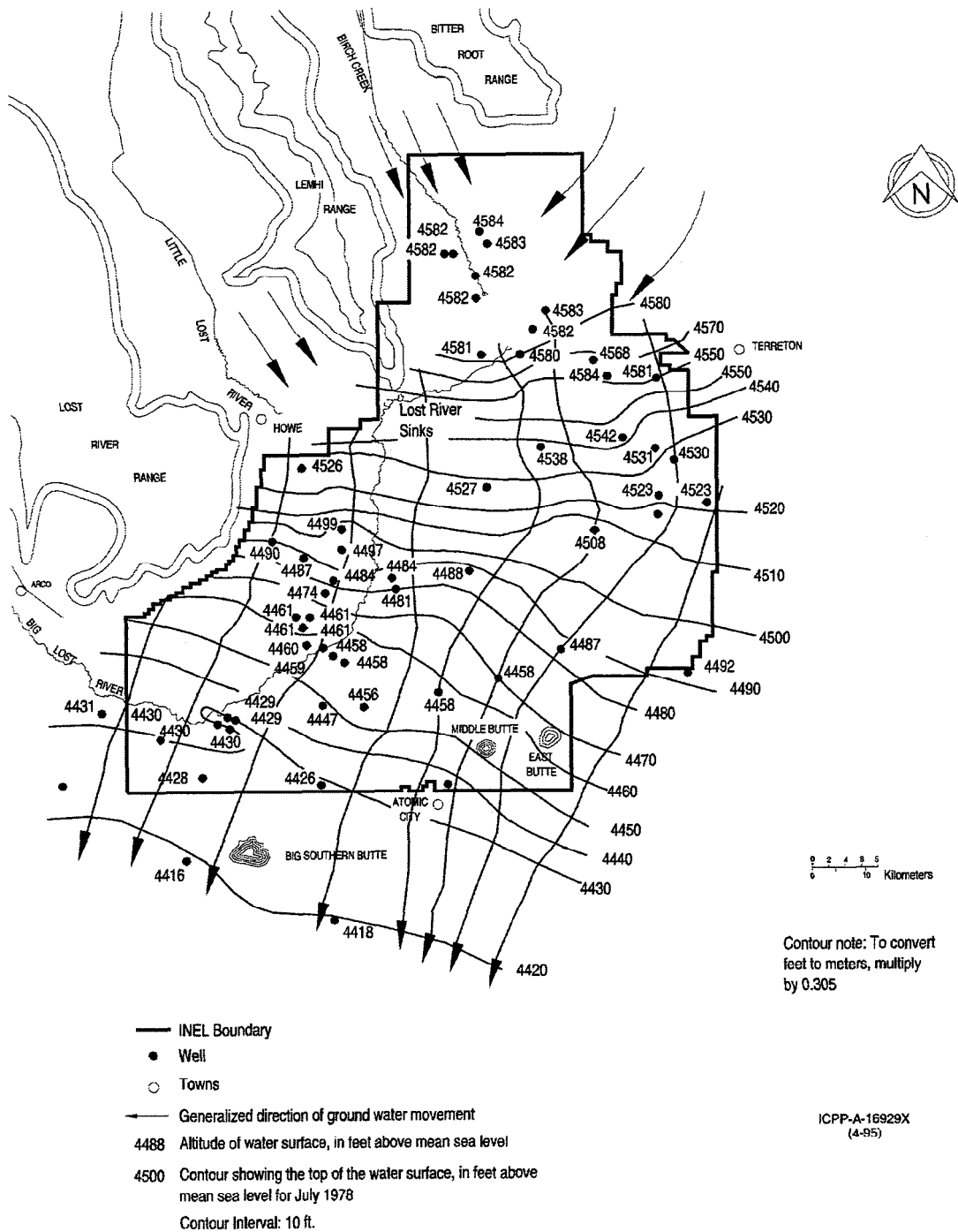
SAA0013

Figure is adapted from the TMI-2 ISFSI SAR (Ref. 2-1). The ICPP is an earlier name for the INTEC, which is adjacent to the ISF Facility site.

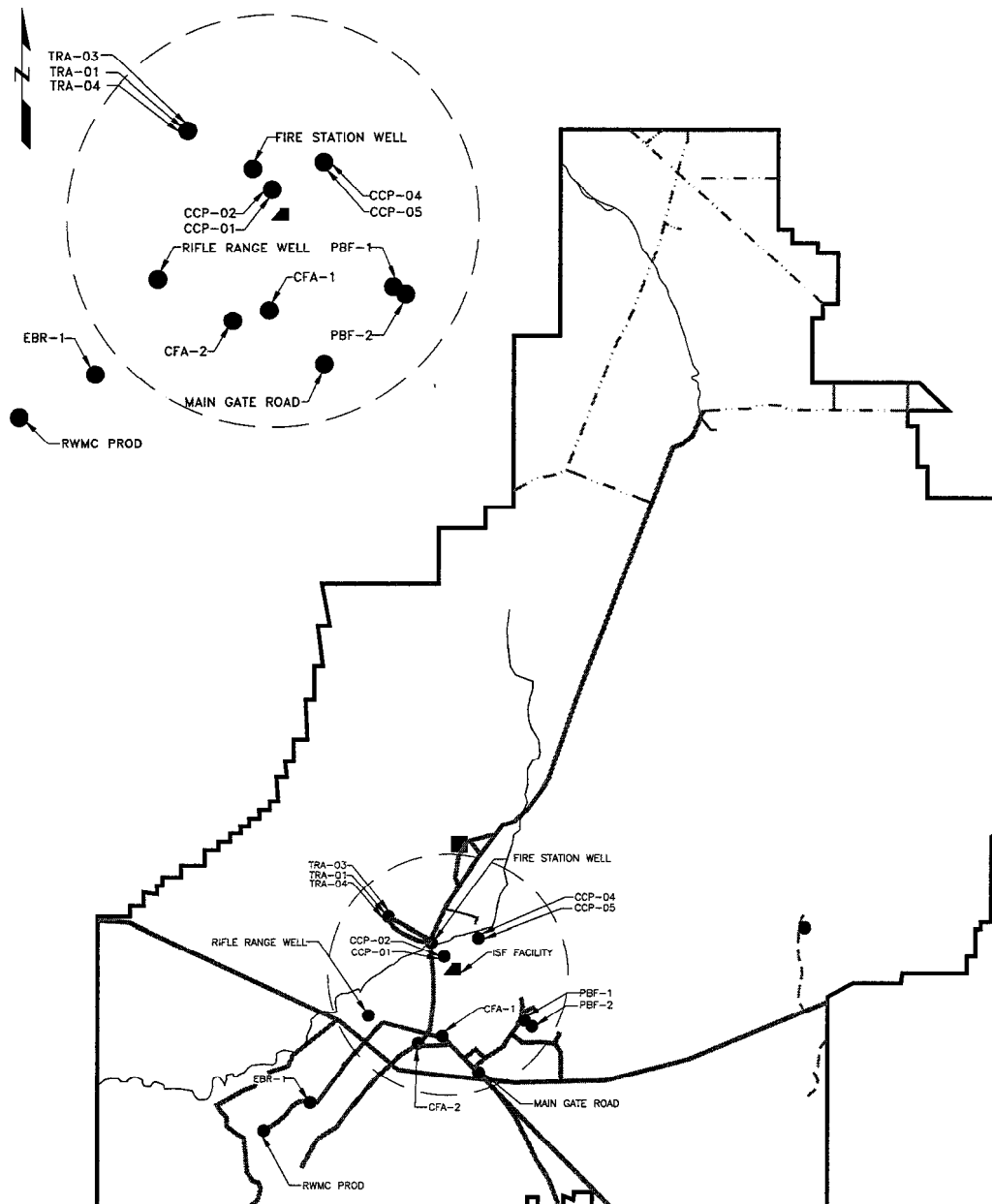
Figure 2.5-1
Relief Map of Idaho with Groundwater Flow Lines



**Figure 2.5-2
Groundwater Contours and Directions-INEEL**



**Figure 2.5-3
Map Showing Production Wells-INEEL**



LEGEND

- | | |
|---|---|
| — US HIGHWAY | — STREAM |
| - - - STATE HIGHWAY | — INEEL BOUNDARY |
| - - - LIGHT-DUTY ROAD, HARD OR IMPROVED SURFACE | — 5 MILE RADIUS AROUND INEEL-ISF BUILDING |
| ● PRODUCTION WELLS | ▲ LOCATION OF ISF FACILITY |

Figure 2.5-4
Depth to Water Table—INEEL

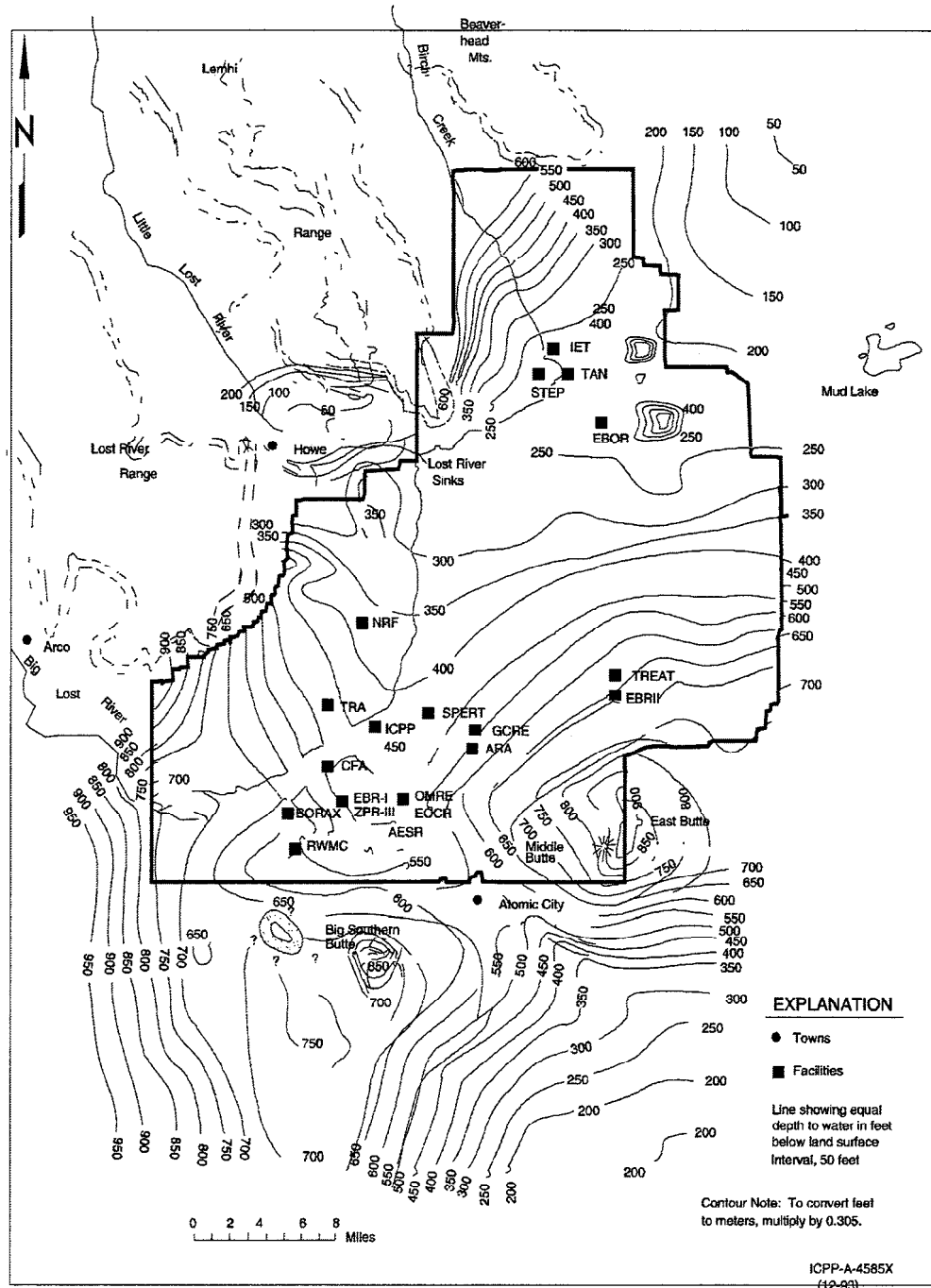


Figure is adapted from the TMI-2 ISFSI SAR (Ref. 2-1). The ICPP is an earlier name for the INTEC, which is adjacent to the ISF Facility site.

Figure 2.6-1
Physiographic Province Map of the Western United States

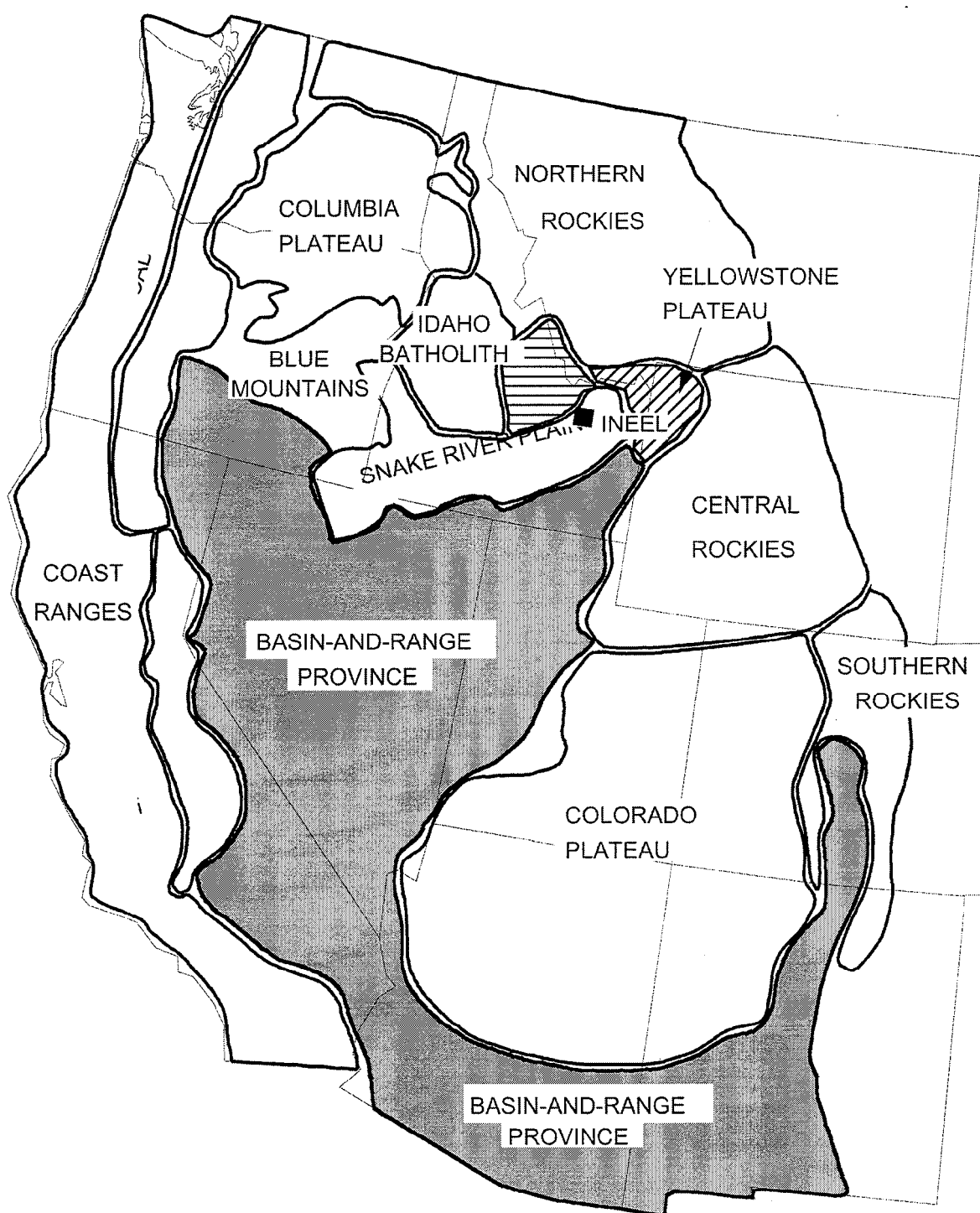
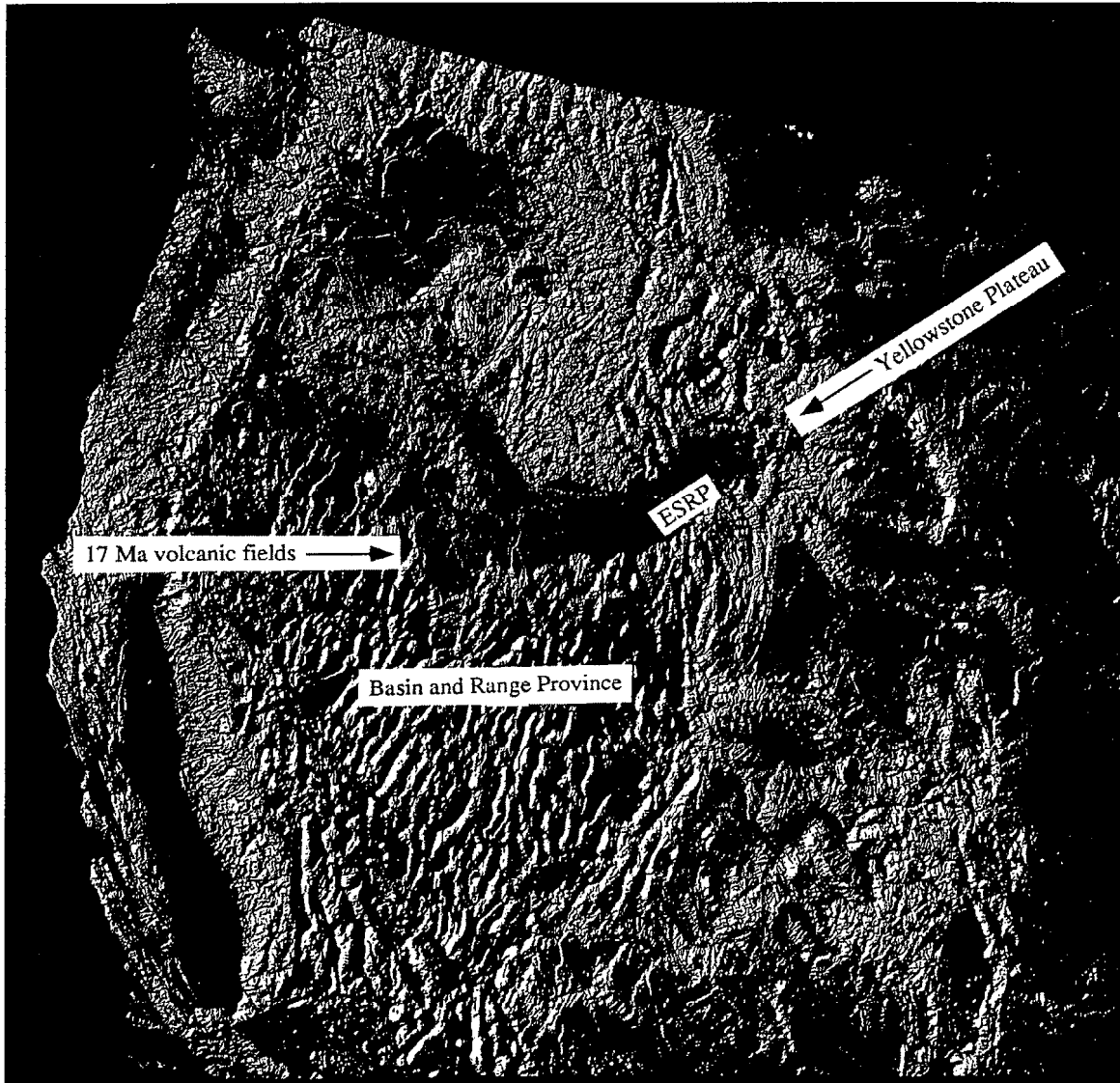
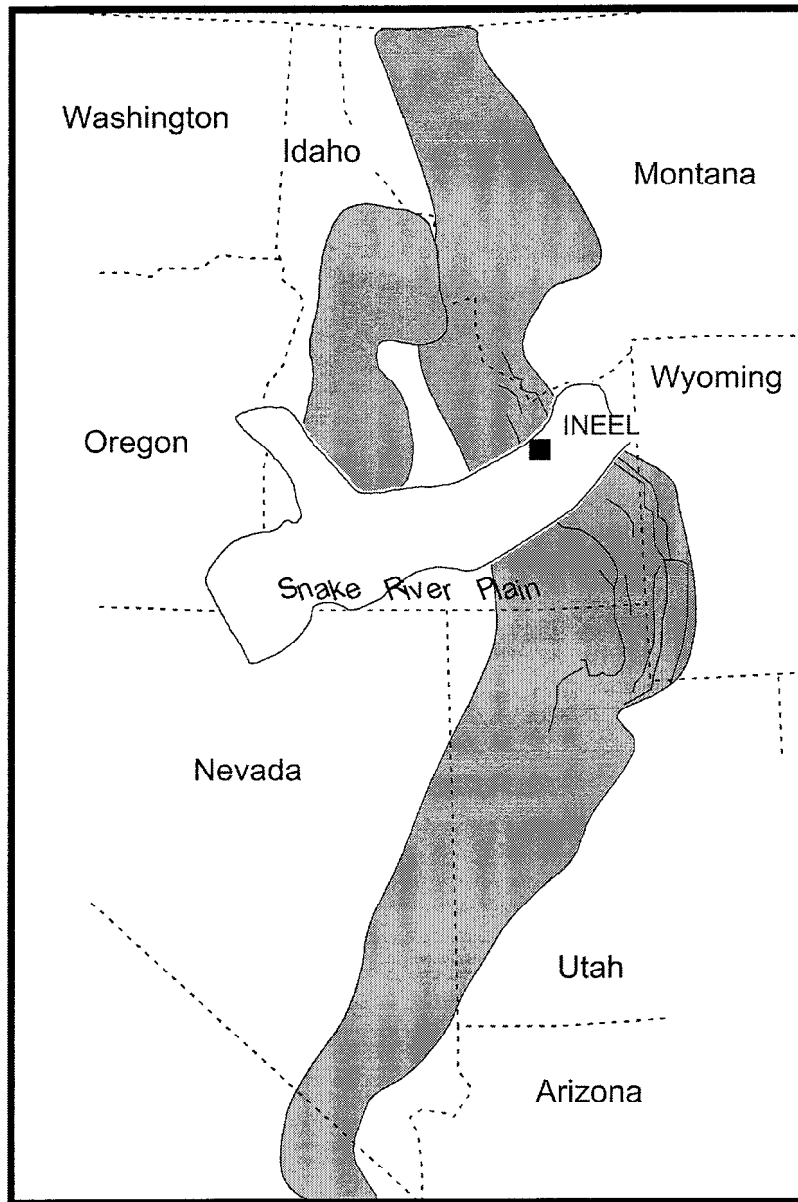


Figure 2.6-2
Shade Relief Map of Western United States



**Figure 2.6-3
Map of the Overthrust Belt**



Overthrust Belt (Late Cretaceous to
early Tertiary)



Idaho Batholith (Mesozoic to
Early Tertiary)



Thrust Faults

Figure 2.6-4
Map of Trans-Challis Fault Zone and Challis Volcanic Field

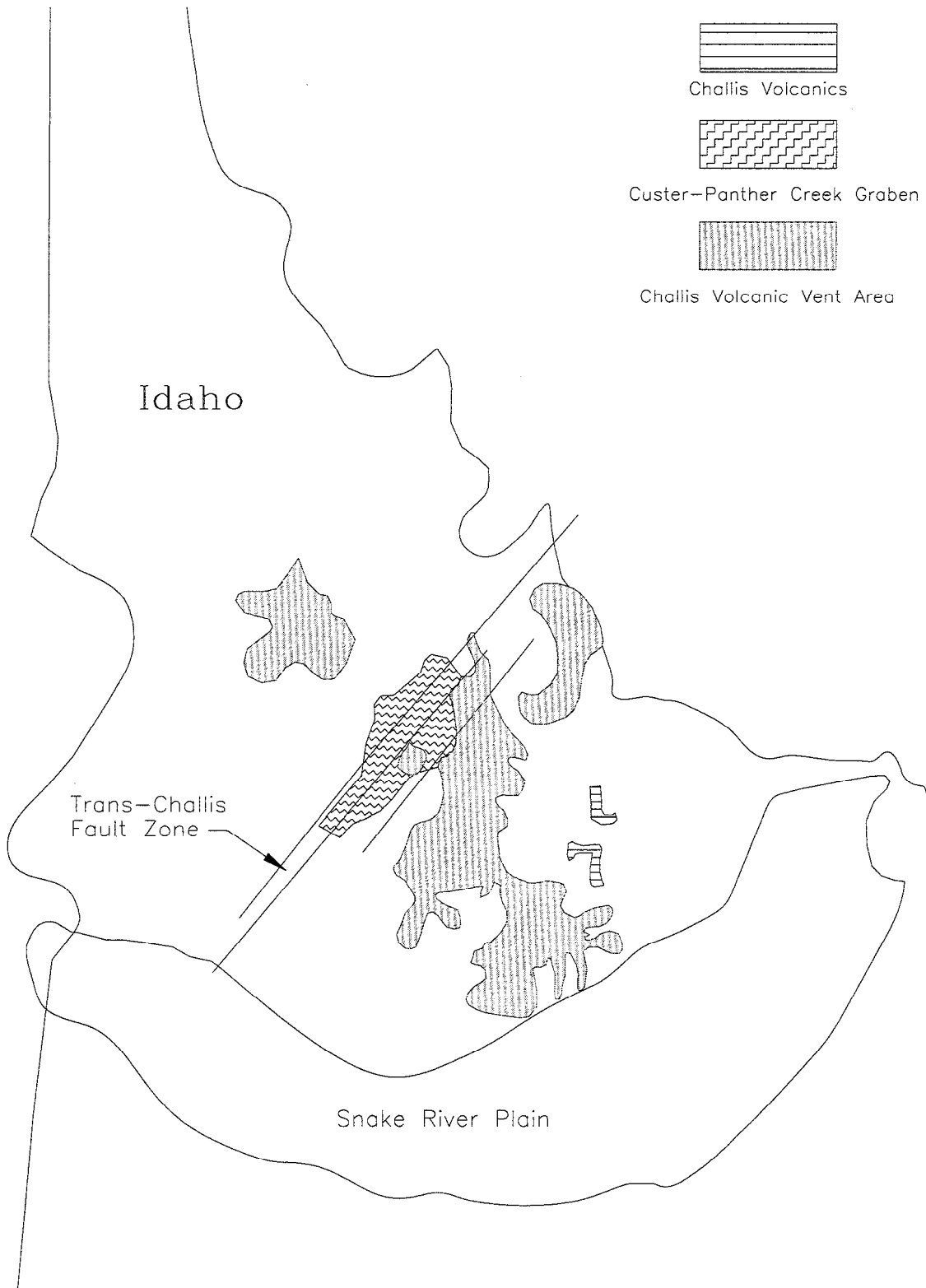


Figure 2.6-5
Calderas in the Track of the Yellowstone Hotspot
(Modified from Pierce and Morgan, 1992)

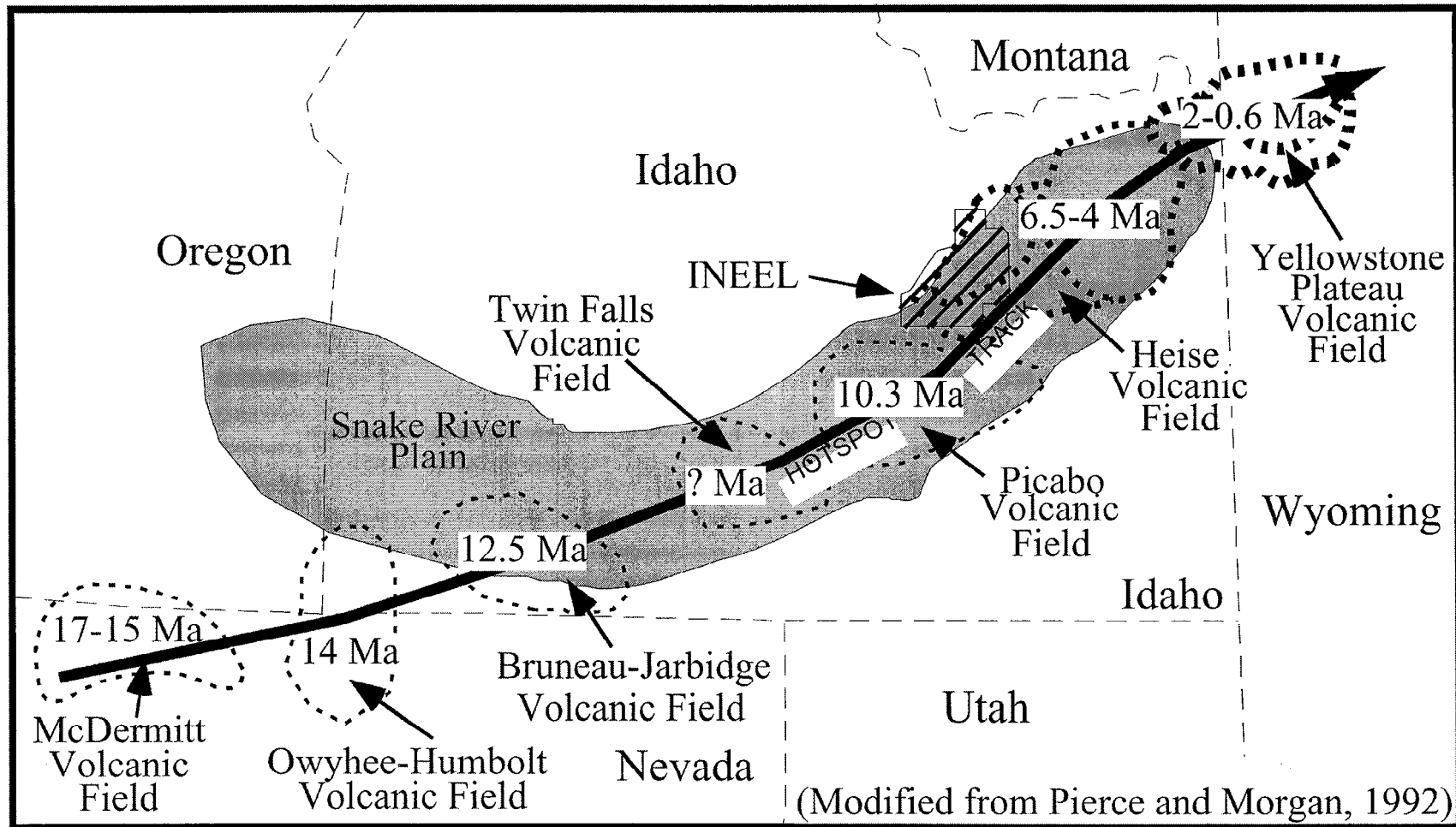


Figure 2.6-6
Volcanic Zones on the Eastern Snake River Plain

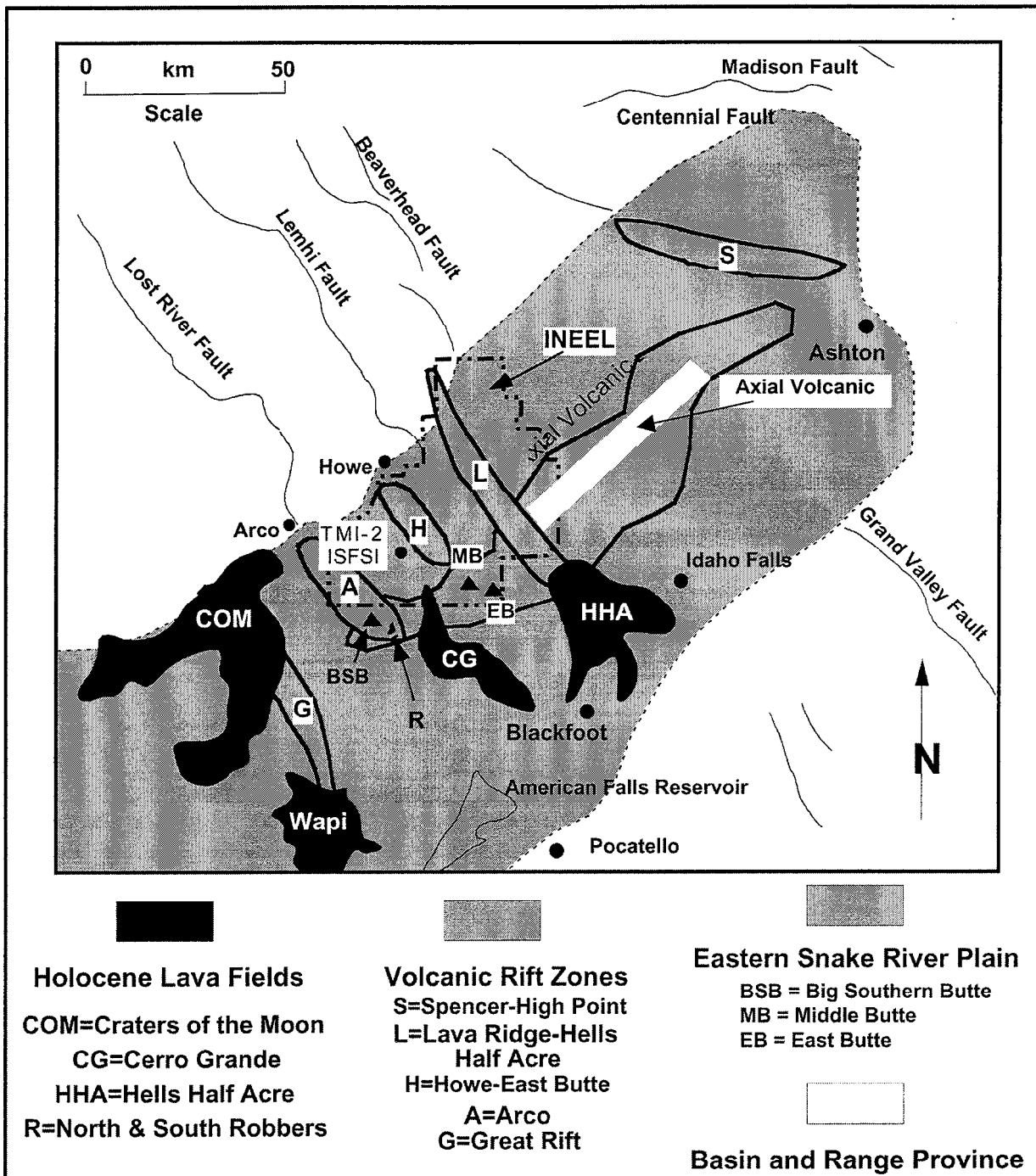


Figure adapted from TMI-2 ISFSI SAR (Ref. 2-1). The ISF Facility site is in the same area as the TMI-2 ISFSI depicted in the figure.

Figure 2.6-7
Lithographic Logs of the Four INEEL Deep Drill Holes

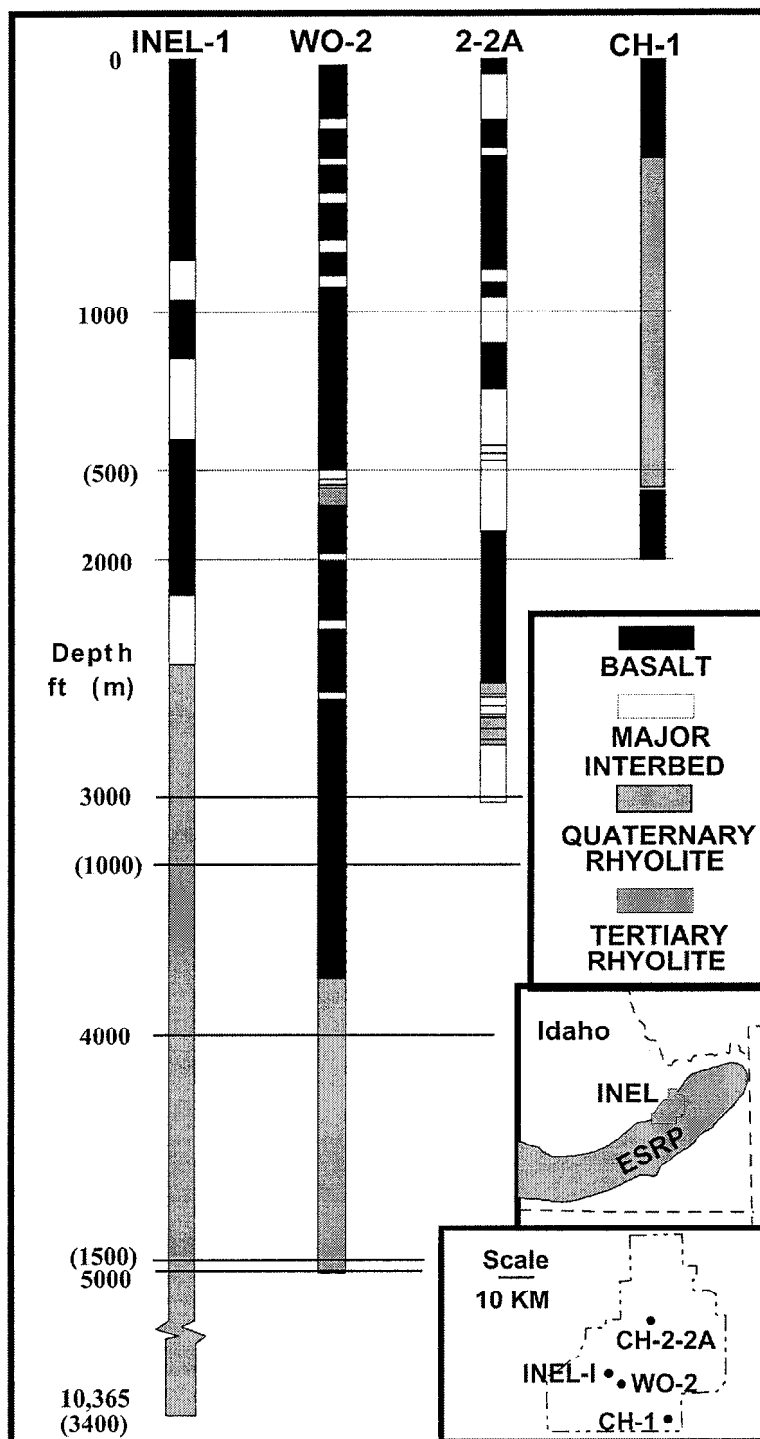


Figure 2.6-8
Idealized Longitudinal Section of an Eastern Snake River Plain Basalt Lava Flow

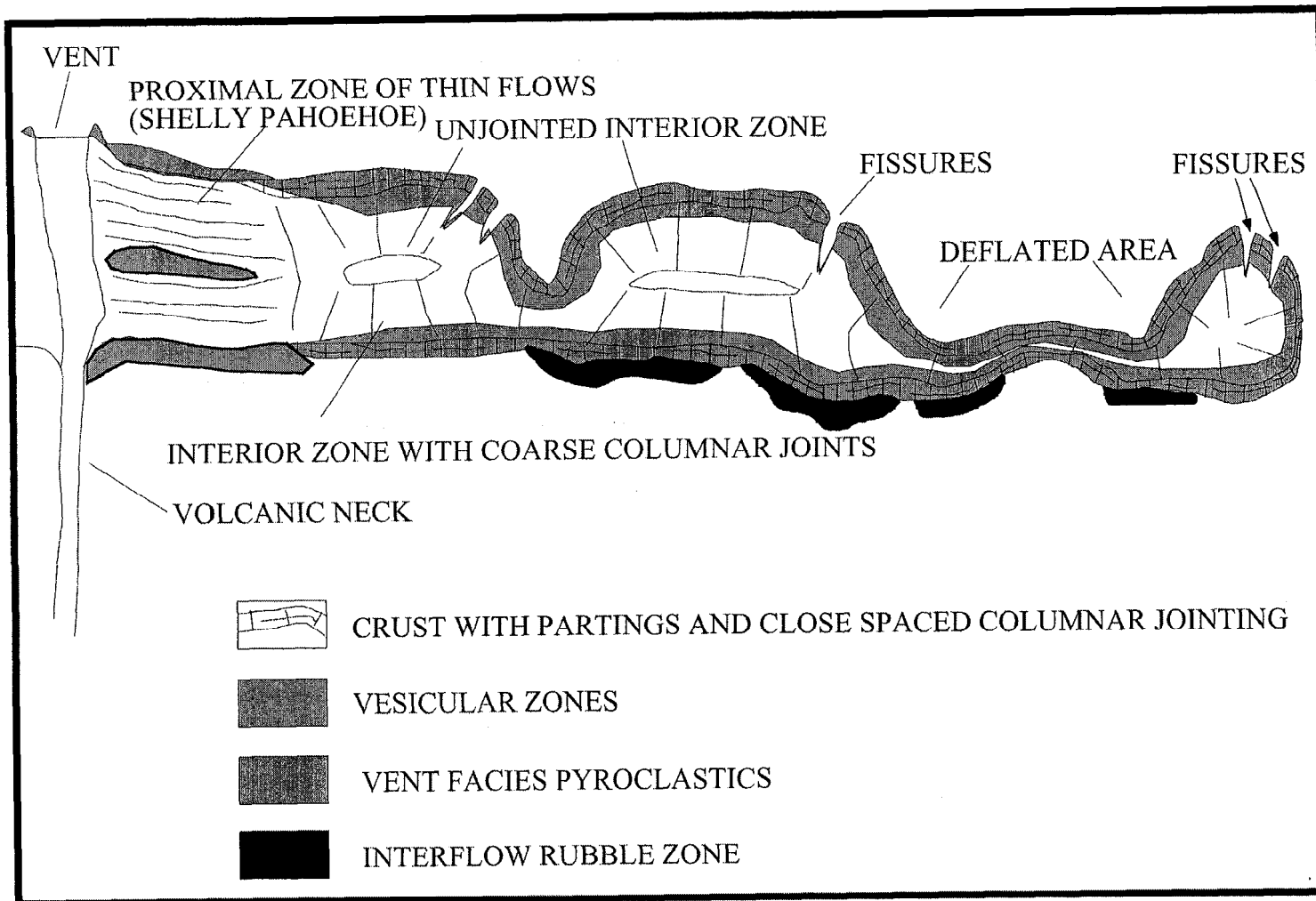


Figure 2.6-9
Generalized Geological Map of the INEEL with INTEC Located

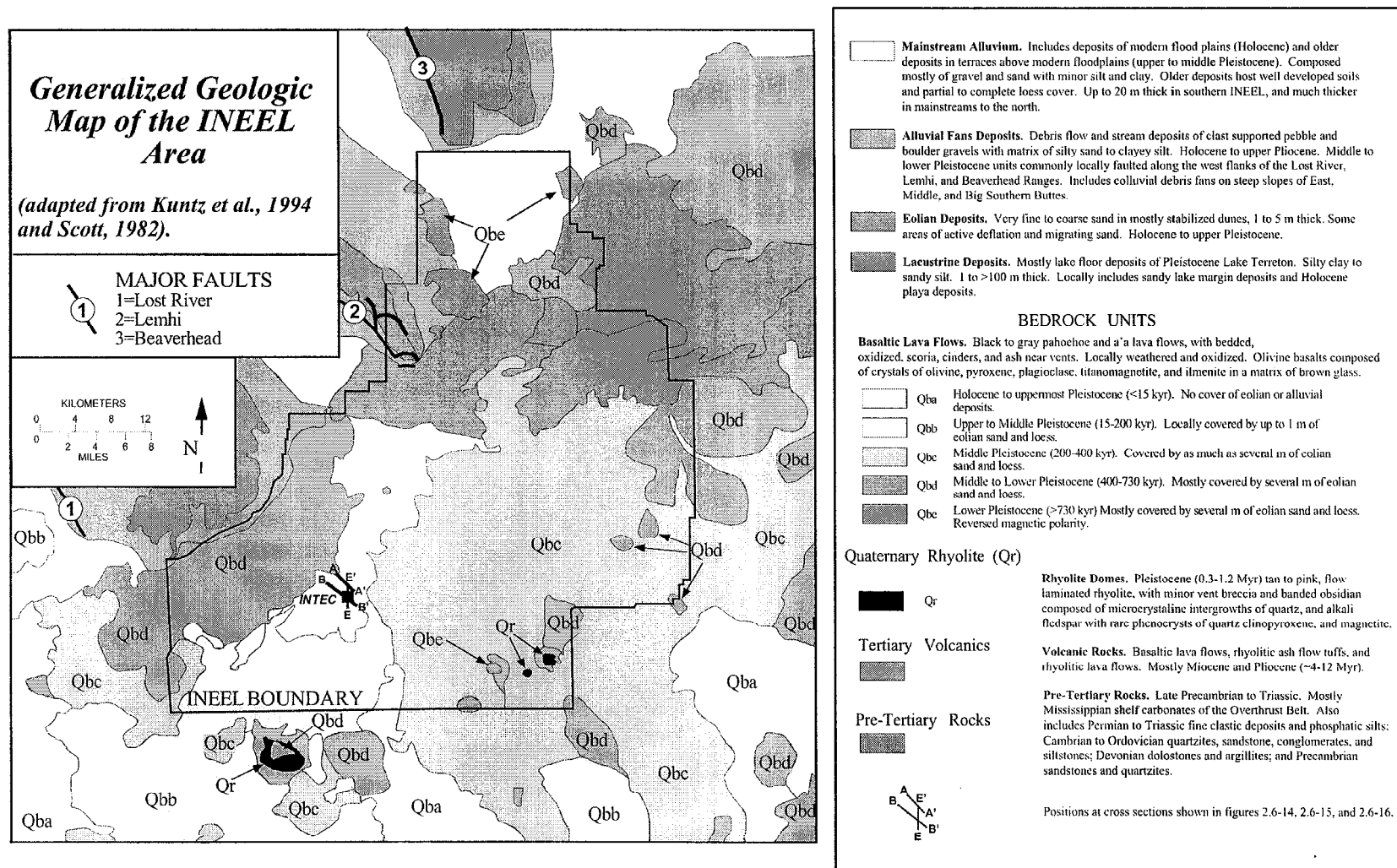


Figure is adapted from the TMI-2 ISFSI SAR (Ref. 2-1). The ISF Facility site is adjacent to the INTEC depicted in the figure.

Figure 2.6-10
Geologic Cross-Section Through the INTEC-TRA Area Showing Anderson's Interpreted Dome

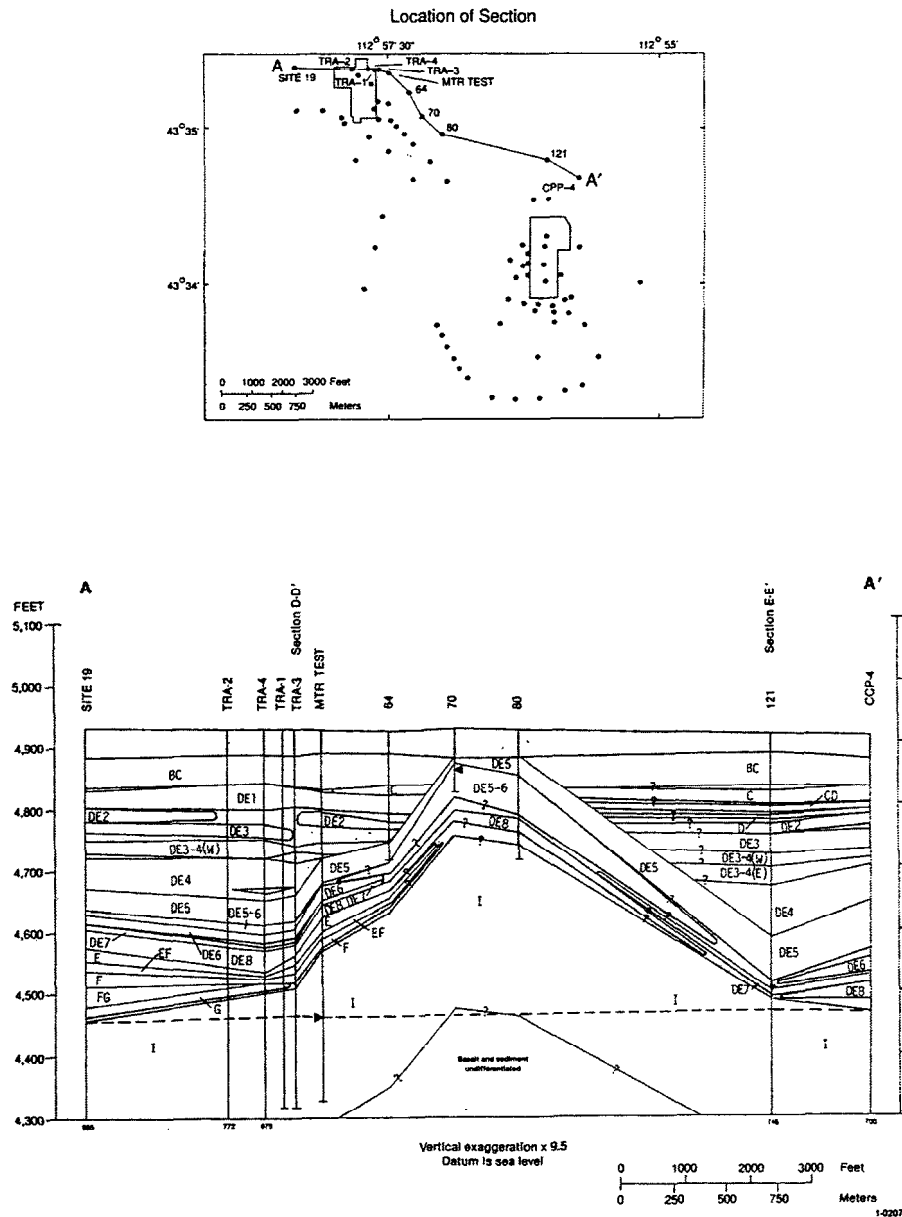


Figure 2.6-11
East-West Geologic Cross-Section Through the INTEC-TRA Area

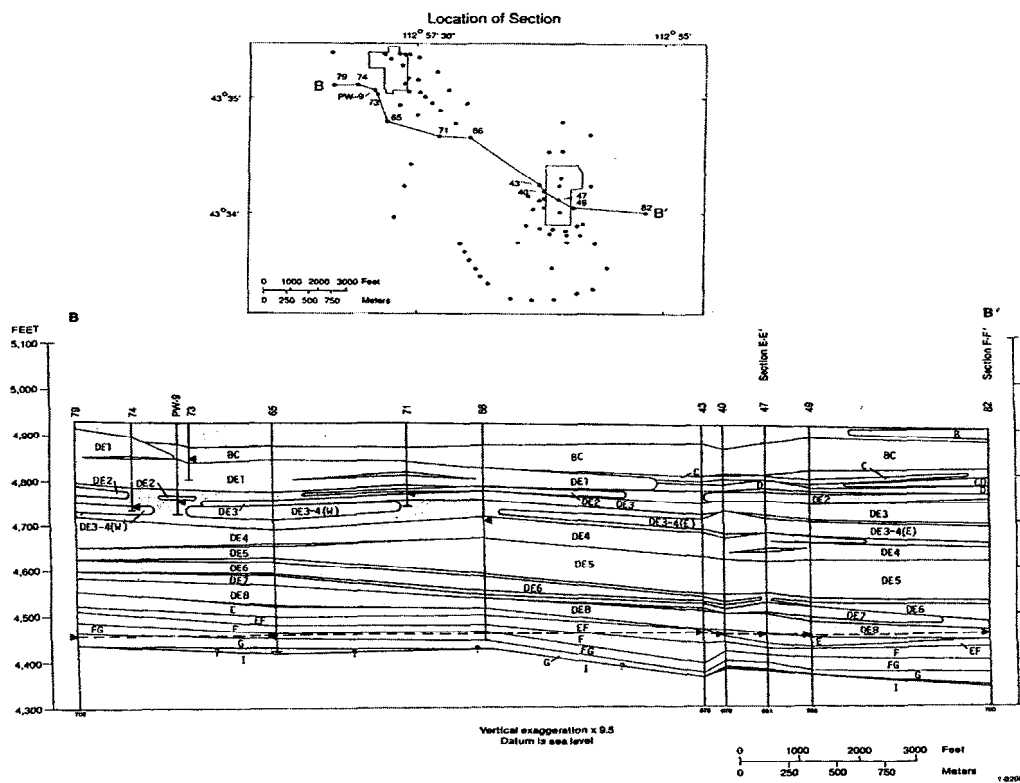


Figure 2.6-12
North-South Geologic Cross-Section Through the INTEC-TRA Area

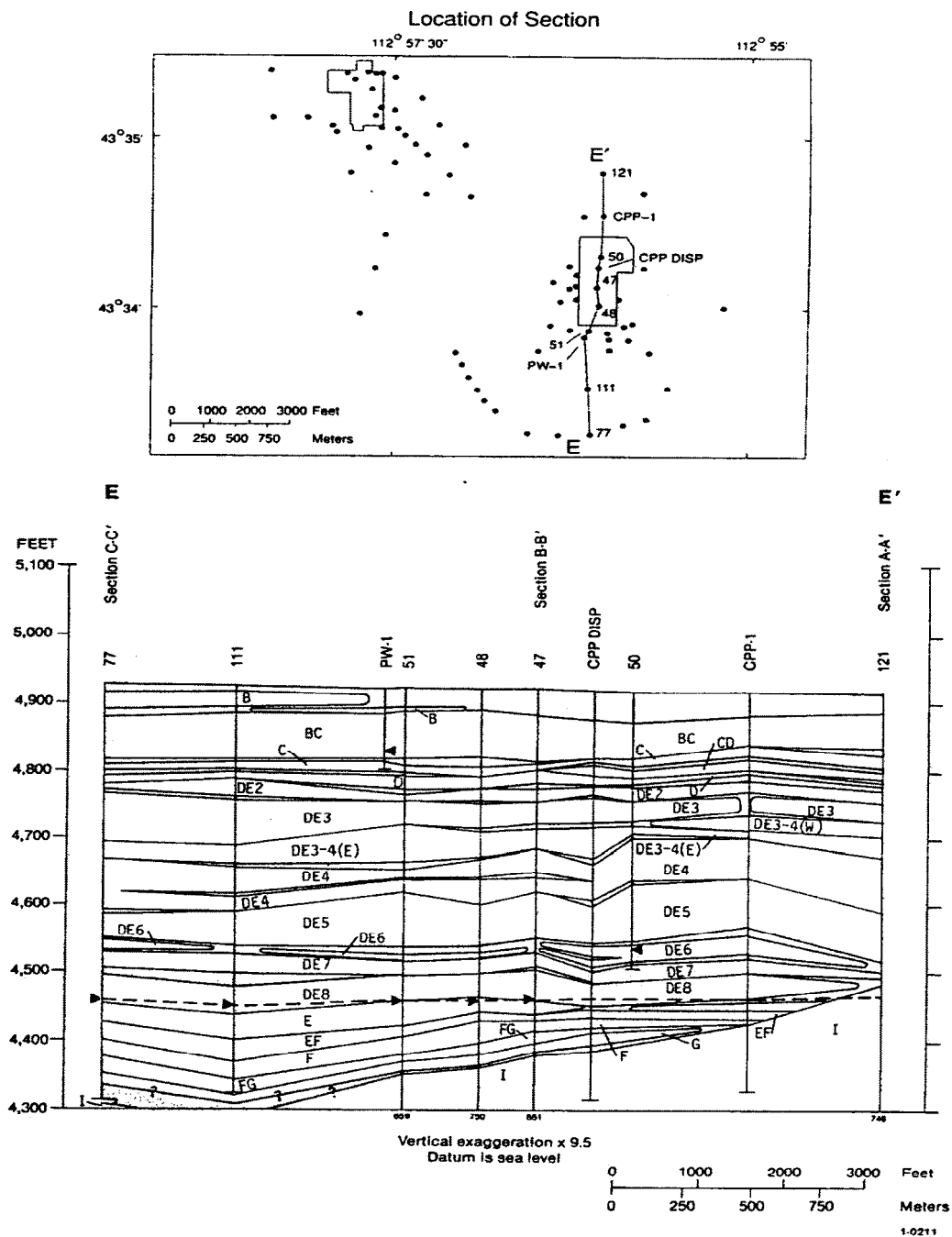


Figure 2.6-13
ISF Site Borehole Locations and Elevation Contours

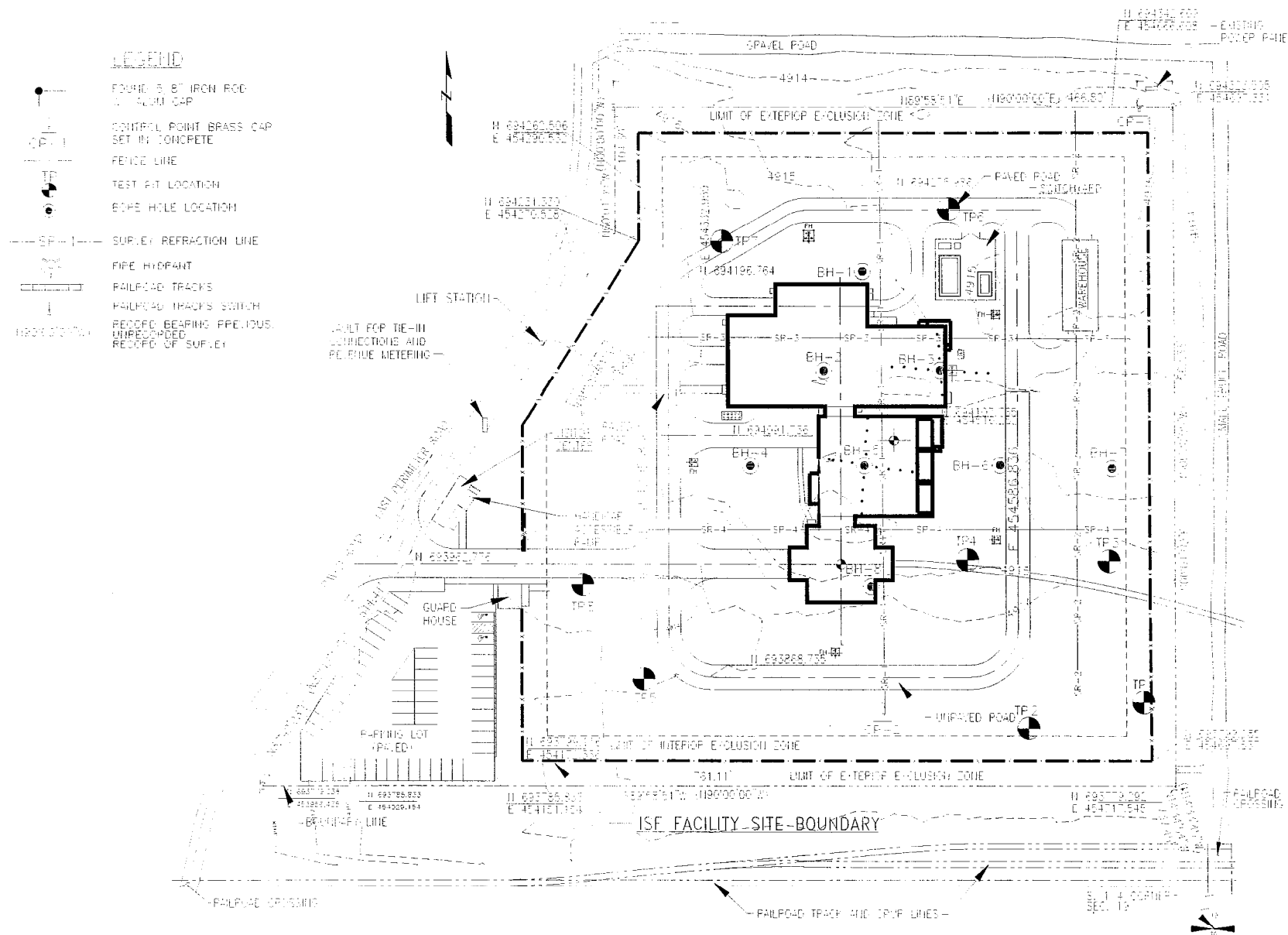


Figure 2.6-14
Boring B-1 Log

FOSTER WHEELER ENVIRONMENTAL							
LOGGED BY <u>D. L. Young</u> DRILL CONTRACTOR <u>Layne Christensen</u> DRILLER <u>Randy</u> TYPE DRILL <u>Speedstar 700</u> SIZE & TYPE OF CASING <u>8" O.D. Tube - X</u>				JOB <u>Idaho Spent Fuel / Project</u> BORING NUMBER <u>B-1</u> ELEV. <u>4916'</u> LOCATION <u>See Exploration Plan</u> DATE <u>6/27/00</u> WEATHER <u>Clear and Windy</u>			
SAMPLE NO. TYPE	DEPTH	SAMPLE DEPTH	DRIVING RESISTANCE BLOWS/1 FT.	RQD%	LENGTH NO. SAVED	GRAPHIC	GROUND WATER
	0						Ground Surface
	2						
	4						
S-1 SPT	6	X	32		0.5'-1bag		Encountered
	8						
S-2 SPT	10	X	83		1.0'-1bag		Not
	12						
	14						
S-3 SPT	16	X	50/5"		0.7'-1bag		
	18						
S-4 SPT	20	X	96		0.9'-1bag		
	22						
	24						
S-5 SPT	26	X	50/1"		0.4'-1bag		
	28						
S-6 Core	30						
	32			40	5.0'		
	34						
	36						Bottom of hole - 35 feet
	38						
	40						
	42						

Figure 2.6-15
Boring B-2 Log


FOSTER WHEELER ENVIRONMENTAL							
LOGGED BY <u>D. L. Young</u> DRILL CONTRACTOR <u>Layne Christensen</u> DRILLER <u>Randy</u> TYPE DRILL <u>Speedstar 700</u> SIZE & TYPE OF CASING <u>8" O.D. Tube - X</u>				JOB <u>Idaho Spent Fuel / Project</u> BORING NUMBER <u>B-2</u> ELEV. <u>4915'</u> LOCATION <u>See Exploration Plan</u> DATE <u>6/29/00</u> WEATHER <u>Clear and Windy</u>			
SAMPLE NO. TYPE	DEPTH	SAMPLE DEPTH	DRIVING RESISTANCE BLOWS/1 FT.	RQD%	LENGTH NO. SAVED	GRAPHIC	GROUND WATER
	0						Ground Surface
S-1 SPT	2	X	31		0.5'-1bag		Encountered
	4						
S-2 SPT	8	X	77		0.8'-1bag		
	10						
S-3 SPT	12	X	58		0.9'-1bag		
	14						Not
S-4 SPT	18	X	50		0.9'-1bag		
	20						
S-5 SPT	22	X	50/5"		0.4'-1bag		
	24						
S-6 Core	28						
	30			96	5.0'		
	32						Bottom of hole - 32 feet.
	34						
	36						
	38						
	40						
	42						

Figure 2.6-16
Boring B-3 Log

FOSTER WHEELER ENVIRONMENTAL							
LOGGED BY <u>D.L. Young</u> DRILL CONTRACTOR <u>Layne Christensen</u> DRILLER <u>Randy</u> TYPE DRILL <u>Speedstar 700</u> SIZE & TYPE OF CASING <u>8" O.D. Tube-X</u>				JOB <u>Idaho Spent Fuel Project</u> BORING NUMBER <u>B-3</u> ELEV. <u>4916'</u> LOCATION <u>See exploration plan</u> DATE <u>7/8/00-7/8/00</u> WEATHER <u>Clear and windy</u>			
SAMPLE NO. TYPE	DEPTH	SAMPLE DEPTH	DRIVING RESISTANCE BLOWS/1 FT.	RQD%	LENGTH NO. SAVED	GRAPHIC	GROUND WATER
	0						Ground Surface
	2						
	4						
S-1 3" SS	6	X	80				Very dense, grey-brown, poorly graded GRAVEL with sand, dry, trace of silt, round to sub-round grains.
	8						
S-2 3" SS	10	X	50/4"				Very dense, grey-brown, well to poorly graded GRAVEL with sand, traces of silt; dry; round to sub-round grains. (GP-GM/GW-GM)
	12						
	14						
S-3 3" SS	16	X	50/5"				Very dense, grey-brown, poorly graded GRAVEL with sand, dry, trace of silt, round to sub-round grains. (GP)
	18						
S-4 SPT	20	X	50/5"				Very dense, grey-brown, poorly graded GRAVEL with sand, dry, trace of silt, round to sub-round grains. (GP)
	22						
	24						
S-5 SPT	26	X	50/4"				Very dense, grey-brown, poorly graded GRAVEL with sand, dry, trace of silt, round to sub-round grains. (GP)
	28						BASALT: Low strength, grey, moderately vespicular, porphyritic-phaneritic, dry.
S-6 Core	30			68			
	32						
	34						
S-7 Core	36						BASALT: Low strength, grey, moderately vespicular, porphyritic-phaneritic, dry.
	38			88			
	40						BASALT: Low strength, grey, moderately vespicular, porphyritic-phaneritic, dry.
S-8 Core	42			79			
	44						Bottom of hole - 45 feet.
	46						

Figure 2.6-17
Boring B-4 Log

FOSTER WHEELER ENVIRONMENTAL								
LOGGED BY <u>D. L. Young</u> DRILL CONTRACTOR <u>Layne Christensen</u> DRILLER <u>Randy</u> TYPE DRILL <u>Speedstar 700</u> SIZE & TYPE OF CASING <u>8" O.D. Tube - X</u>					JOB <u>Idaho Spent Fuel / Project</u> BORING NUMBER <u>B-4</u> ELEV. <u>4916</u> LOCATION <u>See Exploration Plan</u> DATE <u>6/30/00</u> WEATHER <u>Clear</u>			
SAMPLE NO. TYPE	DEPTH	SAMPLE DEPTH	DRIVING RESISTANCE BLOWS/1 FT.	RQD%	LENGTH NO. SAVED	GRAPHIC	GROUND WATER	DESCRIPTION AND REMARKS
	0							Ground Surface
S-1 SPT	2						Encountered Not	
	4							
	6	X	37					Dense, grey-brown, well to poorly graded GRAVEL with silt and sand; dry, round to sub-round grains. (GP-GM/GW-GM)
S-2 SPT	8							
	10	X	50/5"					Very dense, grey-brown, well to poorly graded GRAVEL with silt and sand; dry, round to sub-round grains. (GP-GM/GW-GM)
	12							
S-3 SPT	14							
	16	X	68					Very dense, grey-brown, poorly graded GRAVEL with sand; traces of silt; dry; round to sub-round grains. (GP)
	18							
S-4 SPT	20	X	91					Very dense, grey-brown, poorly graded GRAVEL with sand; traces of silt; dry; round to sub-round grains. (GP)
	22							
S-5 Core	24							
	26	X						BASALT: Low strength, grey, moderately vassicular, porphyritic-phaneritic, dry.
	28	X		21				
	30	X						Bottom of hole - 30 feet.
	32							
	34							
	36							
	38							
	40							
	42							

Figure 2.6-18
Boring B-5 Log

FOSTER WHEELER ENVIRONMENTAL								
LOGGED BY <u>D.L. Young</u> DRILL CONTRACTOR <u>Layne Christensen</u> DRILLER <u>Randy</u> TYPE DRILL <u>Speedstar 700</u> SIZE & TYPE OF CASING <u>8" O.D. Tube-X</u>					JOB <u>Idaho Spent Fuel Project</u> BORING NUMBER <u>B-5</u> ELEV. <u>4915'</u> LOCATION <u>See exploration plan</u> DATE <u>7/7/00-7/8/00</u> WEATHER <u>Clear</u>			
SAMPLE NO. TYPE	DEPTH	SAMPLE DEPTH	DRIVING RESISTANCE BLOWS/H FT.	RQD%	LENGTH NO SAVED	GRAPHIC	GROUND WATER	DESCRIPTION AND REMARKS
	0							Ground Surface
S-1 SPT	2							
	4							
	6	X	40		0.3'-1bag			Dense, grey-brown, well to poorly graded GRAVEL with silt and sand; dry; round to sub-round grains. (GP-GM/GW-GM)
	8							
S-2 SPT	10	X	50/5"		0.8'-1bag			Very dense, grey-brown, well to poorly graded GRAVEL with silt and sand; dry; round to sub-round grains. (GP-GM/GW-GM)
	12							
	14							
S-3 SPT	18	X	63					Very dense, grey-brown, poorly graded GRAVEL with sand, dry, trace of silt, round to sub-round grains. (GP)
	20							
S-4 SPT	22	X	50/5"					Very dense, grey-brown, poorly graded GRAVEL with sand, dry, trace of silt, round to sub-round grains. (GP)
	24							
S-5 SPT	26	X	50/3"					Very dense, grey-brown, poorly graded GRAVEL with sand, dry, trace of silt, round to sub-round grains. (GP)
	28							BASALT: Low strength, grey, moderately vassicular, porphyritic-phaneritic, dry.
S-6 Core	30							BASALT: Low strength, grey, moderately vassicular, porphyritic-phaneritic, dry.
	32			30				
S-7 Core	34							BASALT: Low strength, grey, moderately vassicular, porphyritic-phaneritic, dry.
	36			84				
	38							
S-8 Core	40							BASALT: Low strength, grey, moderately vassicular, porphyritic-phaneritic, dry.
	42			99				
	44							
	46							Bottom of hole - 45 feet.

Figure 2.6-19
Boring B-6 Log

FOSTER WHEELER ENVIRONMENTAL								
LOGGED BY <u>D. L. Young</u> DRILL CONTRACTOR <u>Layne Christensen</u> DRILLER <u>Randy</u> TYPE DRILL <u>Speedstar 700</u> SIZE & TYPE OF CASING <u>8" O.D. Tube - X</u>					JOB <u>Idaho Spent Fuel / Project</u> BORING NUMBER <u>B-6</u> ELEV. <u>4915'</u> LOCATION <u>See Exploration Plan</u> DATE <u>7/5/00</u> WEATHER			
SAMPLE NO. TYPE	DEPTH	SAMPLE DEPTH	DRIVING RESISTANCE BLOWS/1 FT.	RQD%	LENGTH NO. SAVED	GRAPHIC	GROUND WATER	DESCRIPTION AND REMARKS
	0							Ground Surface
	2							
	4							
S-1 SPT	6	X	81				Encountered	Very dense, grey-brown, well to poorly graded GRAVEL with silt and sand; dry; round to sub-round grain shape. (GP-GM/GW-GM)
	8							
S-2 SPT	10	X	50/5"				Not	Very dense, grey-brown, well to poorly graded GRAVEL with silt and sand; dry; round to sub-round grain shape. (GP-GM/GW-GM)
	12							
	14							
S-3 SPT	16	X	100					Very dense, grey-brown, poorly graded GRAVEL with sand; dry; traces of silt. (GP)
	18							
S-4 SPT	20	X	50/5"					Very dense, grey-brown, poorly graded GRAVEL with sand; dry; traces of silt. (GP)
	22							
	24							
S-5 SPT	26	X	50/5"					
S-6 Core	28							BASALT: Low strength, grey, moderately vossicular, porphyritic-phaneritic, dry.
	30							
	32							Bottom of hole - 31 feet.
	34							
	36							
	38							
	40							
	42							

Figure 2.6-20
Boring B-7 Log

FOSTER WHEELER ENVIRONMENTAL								
LOGGED BY <u>D. L. Young</u> DRILL CONTRACTOR <u>Layne Christensen</u> DRILLER <u>Randy</u> TYPE DRILL <u>Speedstar 700</u> SIZE & TYPE OF CASING <u>8" O.D. Tube - X</u>					JOB <u>Idaho Spent Fuel / Project</u> BORING NUMBER <u>B-7</u> ELEV. <u>4815'</u> LOCATION <u>See Exploration Plan</u> DATE <u>7/6/00</u> WEATHER <u>Clear</u>			
SAMPLE NO. TYPE	DEPTH	SAMPLE DEPTH	DRIVING RESISTANCE BLOWS/1 FT.	RQD%	LENGTH NO. SAVED	GRAPHIC	GROUND WATER	DESCRIPTION AND REMARKS
	0							Ground Surface
S-1 SPT	2						Encountered	
	4							
	6	X	63		0.4'-1bag			Very dense, grey-brown, well to poorly graded GRAVEL with silt and sand; dry; round to subround grains. (GP-GM/GW-GM)
	8							
S-2 SPT	10	X	80		0.9'-1bag			Very dense, grey-brown, well to poorly graded GRAVEL with silt and sand; dry; round to subround grains. (GP-GM/GW-GM)
	12						Not	
	14							
S-3 SPT	16	X	85					Very dense, grey-brown, poorly graded GRAVEL with sand, traces of silt, dry, round to subround grains. (GP)
	18							
S-4 SPT	20	X	50/5"					Very dense, grey-brown, poorly graded GRAVEL with sand, traces of silt, dry, round to subround grains. (GP)
	22							
	24							
S-5 SPT	26	X	77					Very dense, grey-brown, poorly graded GRAVEL with sand, traces of silt, dry, round to subround grains. (GP)
	28							BASALT: Low strength, grey, moderately vesiicular, porphyritic-phaneritic, dry.
	30							Bottom of hole - 27 feet.
	32							
	34							
	36							
	38							
	40							
	42							

Figure 2.6-21
Boring B-8 Log

FOSTER WHEELER ENVIRONMENTAL								
LOGGED BY <u>D. L. Young</u> DRILL CONTRACTOR <u>Layne Christensen</u> DRILLER <u>Randy</u> TYPE DRILL <u>Speedstar 700</u> SIZE & TYPE OF CASING <u>8" O.D. Tube - X</u>					JOB <u>Idaho Spent Fuel / Project</u> BORING NUMBER <u>B-8</u> ELEV. <u>4913'</u> LOCATION <u>See Exploration Plan</u> DATE <u>7/5/00</u> WEATHER			
SAMPLE NO. TYPE	DEPTH	SAMPLE DEPTH	DRIVING RESISTANCE BLOWS/1 FT.	RQD%	LENGTH NO. SAVED	GRAPHIC	GROUND WATER	DESCRIPTION AND REMARKS
	0							Ground Surface
	2							
	4							
S-1 SPT	6	X	46				Encountered	Dense, grey-brown, well to poorly graded GRAVEL with silt and sand; dry; round to sub-round grain shape. (GP-GM/GW-GM)
	8							
S-2 SPT	10	X	42				Not	Dense, grey-brown, well to poorly graded GRAVEL with silt and sand; dry; round to sub-round grain shape. (GP-GM/GW-GM)
	12							
	14							
S-3 SPT	16	X	50/5"					Dense, grey-brown, poorly graded GRAVEL with sand, traces of silt; dry. (GP)
	18							
S-4 SPT	20	X	50/4"					Dense, grey-brown, poorly graded GRAVEL with sand, traces of silt; dry. (GP)
	22							
	24							
S-5 SPT	26	X	50/4"					Dense, grey-brown, poorly graded GRAVEL with sand, traces of silt; dry. (GP)
	28							BASALT: Low strength, grey, moderately vespicular, porphyritic-phaneritic, dry.
	30							
	32							Bottom of hole - 31 feet.
	34							
	36							
	38							
	40							
	42							

Figure 2.6-22
Faults, Volcanic Zones, and Historic Earthquakes in the INEEL Region

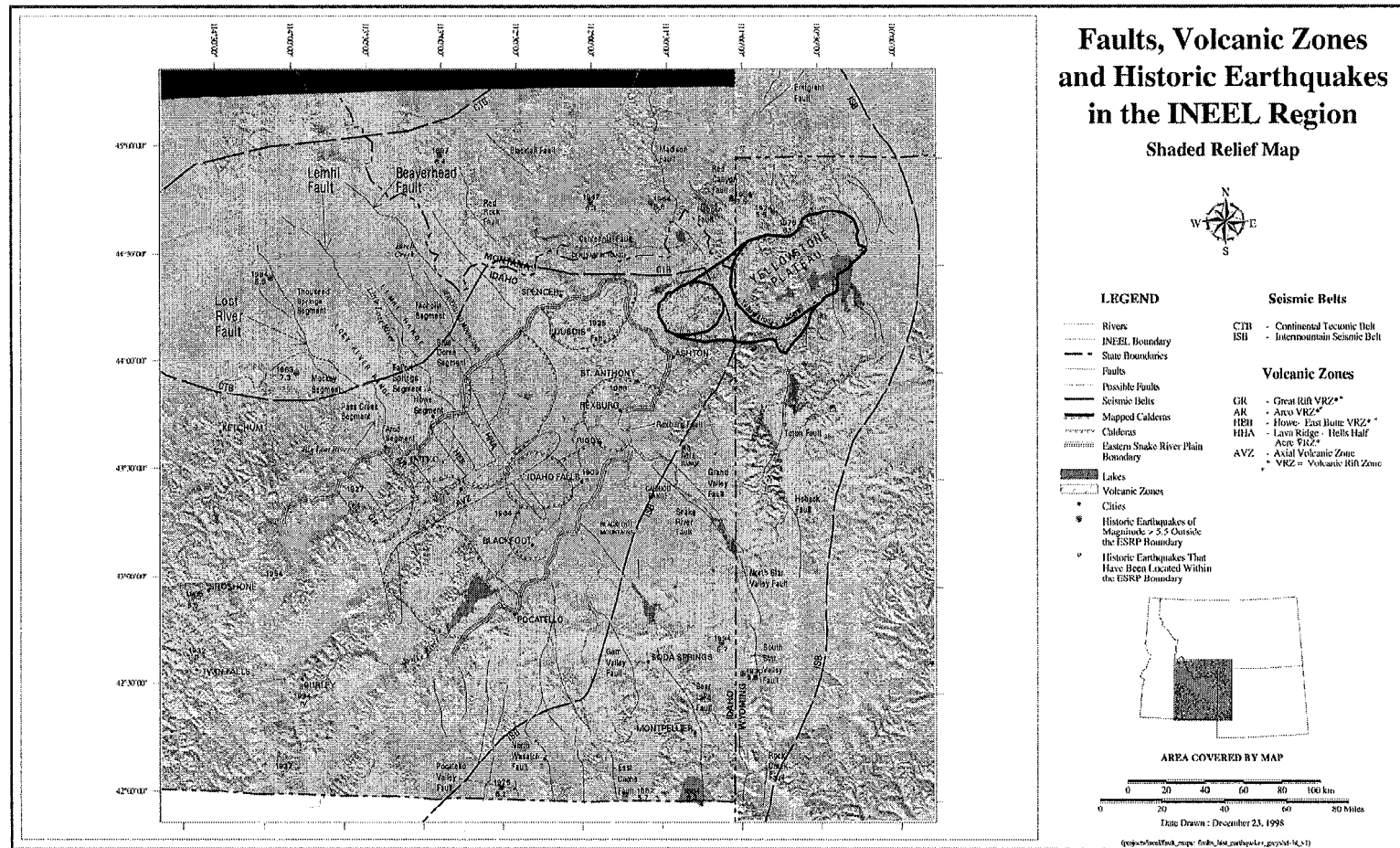


Figure 2.6-23
Seismic Source Zones in the INEEL Region

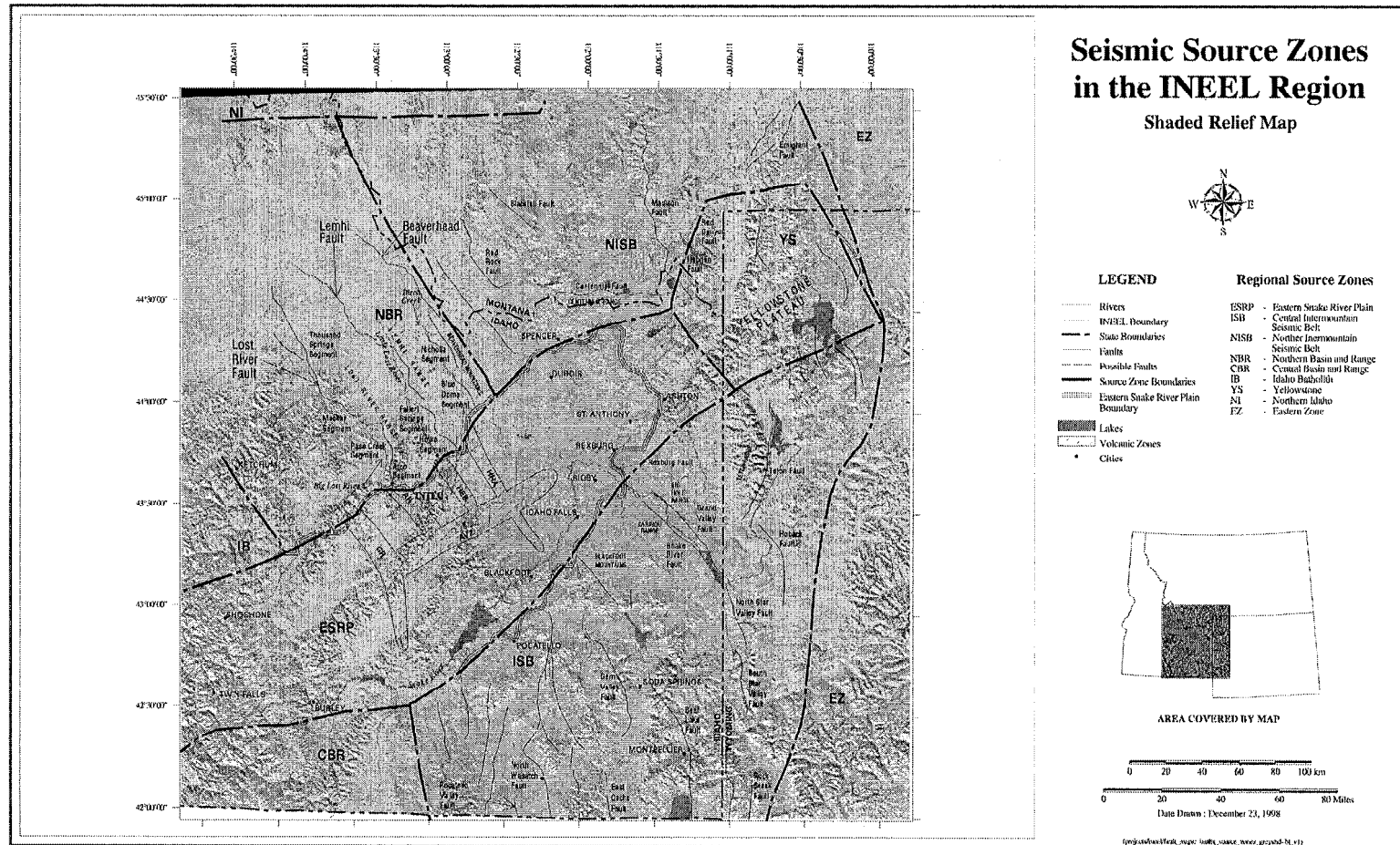


Figure 2.6-24
Principle Stress Orientations Affecting the Eastern Snake River Plain

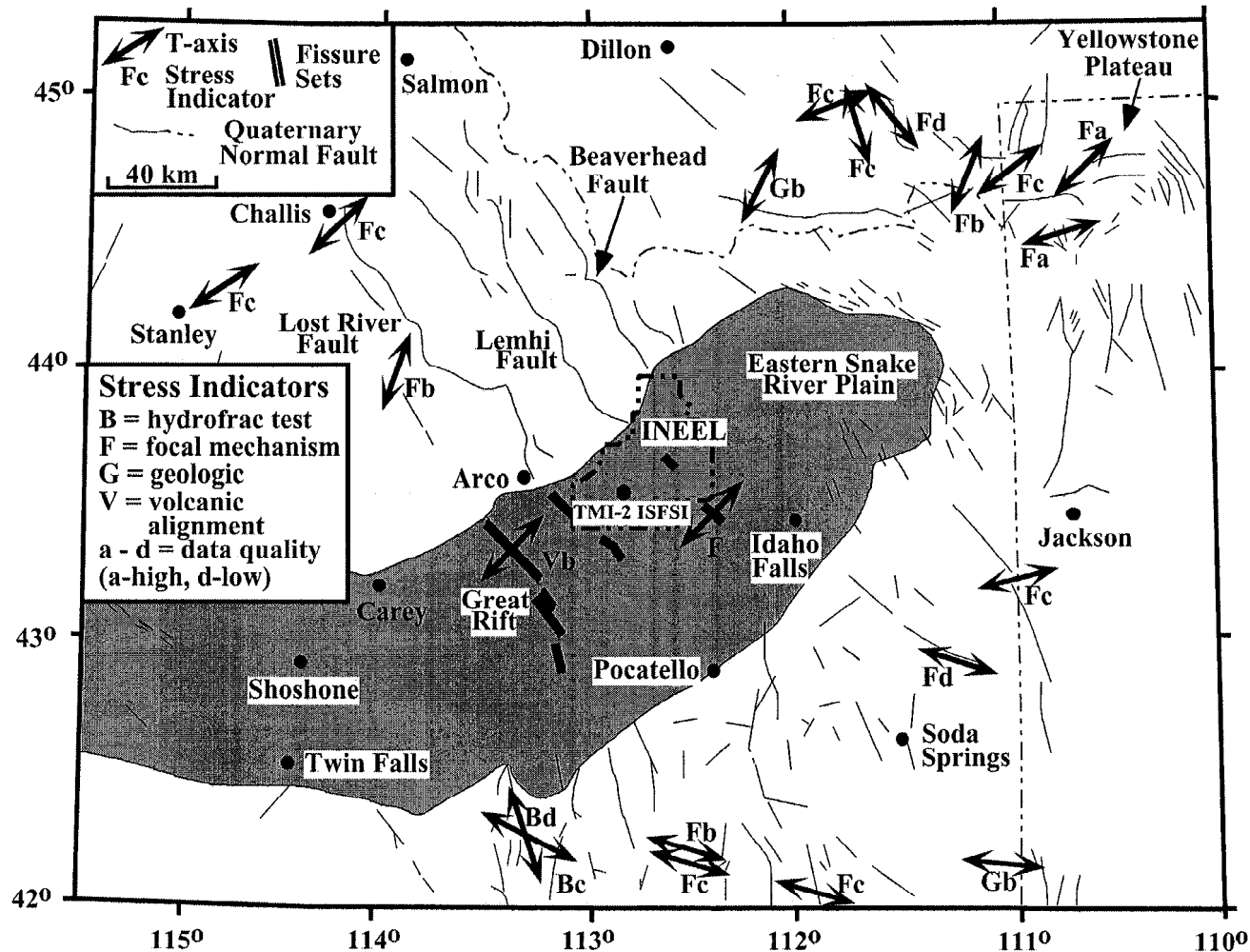


Figure is adapted from the TMI-2 ISFSI SAR (Ref. 2-1). The ISF Facility site is in the same area as the TMI-2 ISFSI depicted in the figure.

Figure 2.6-25
Strain Rates in the Eastern Snake River Plain and Adjacent Areas

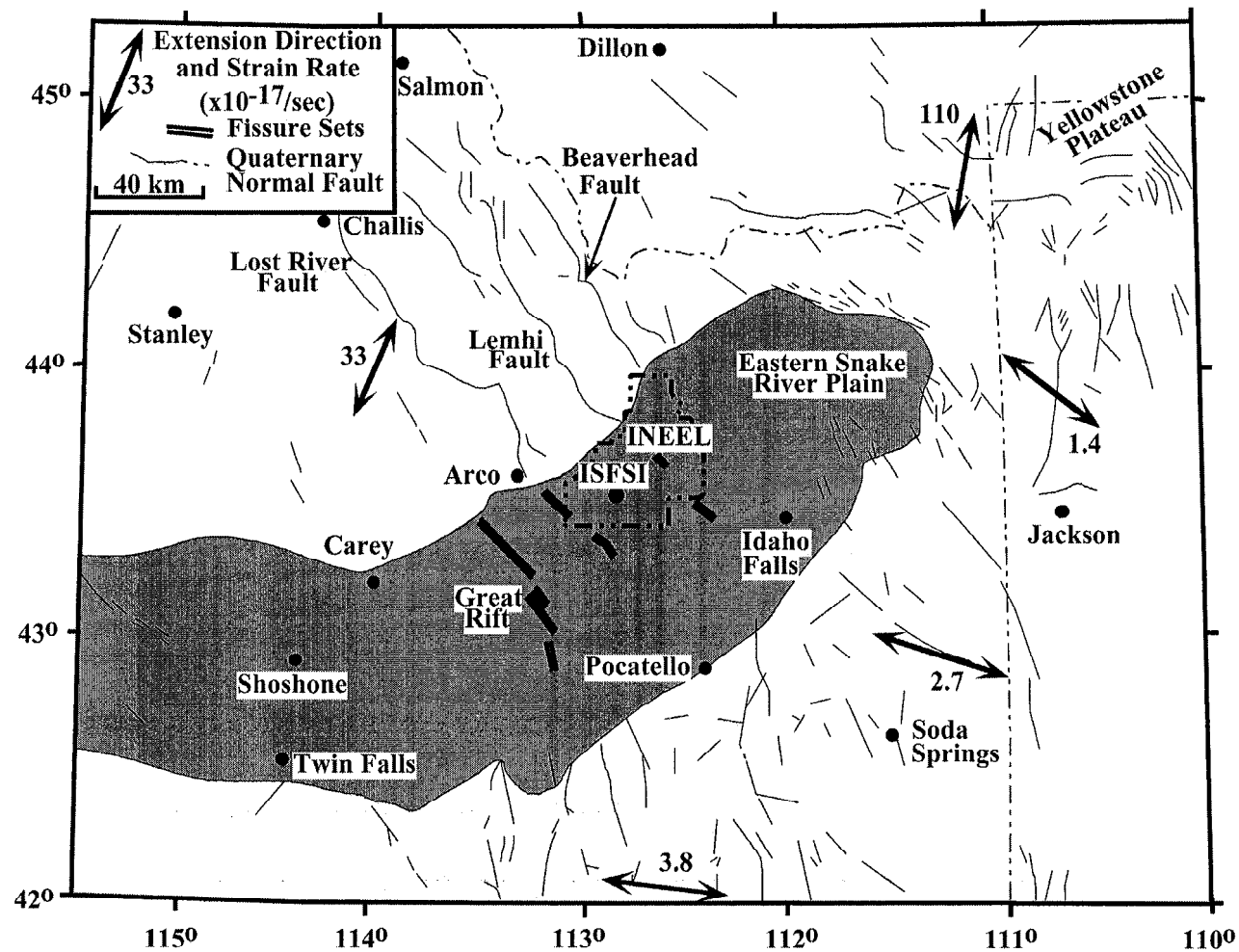


Figure is adapted from the TMI-2 ISFSI SAR (Ref. 2-1). The ISF Facility site is in the same area as the TMI-2 ISFSI depicted in the figure.

Figure 2.6-26
Intermountain Seismic Belt and Centennial Tectonic Belt Seismicity Map

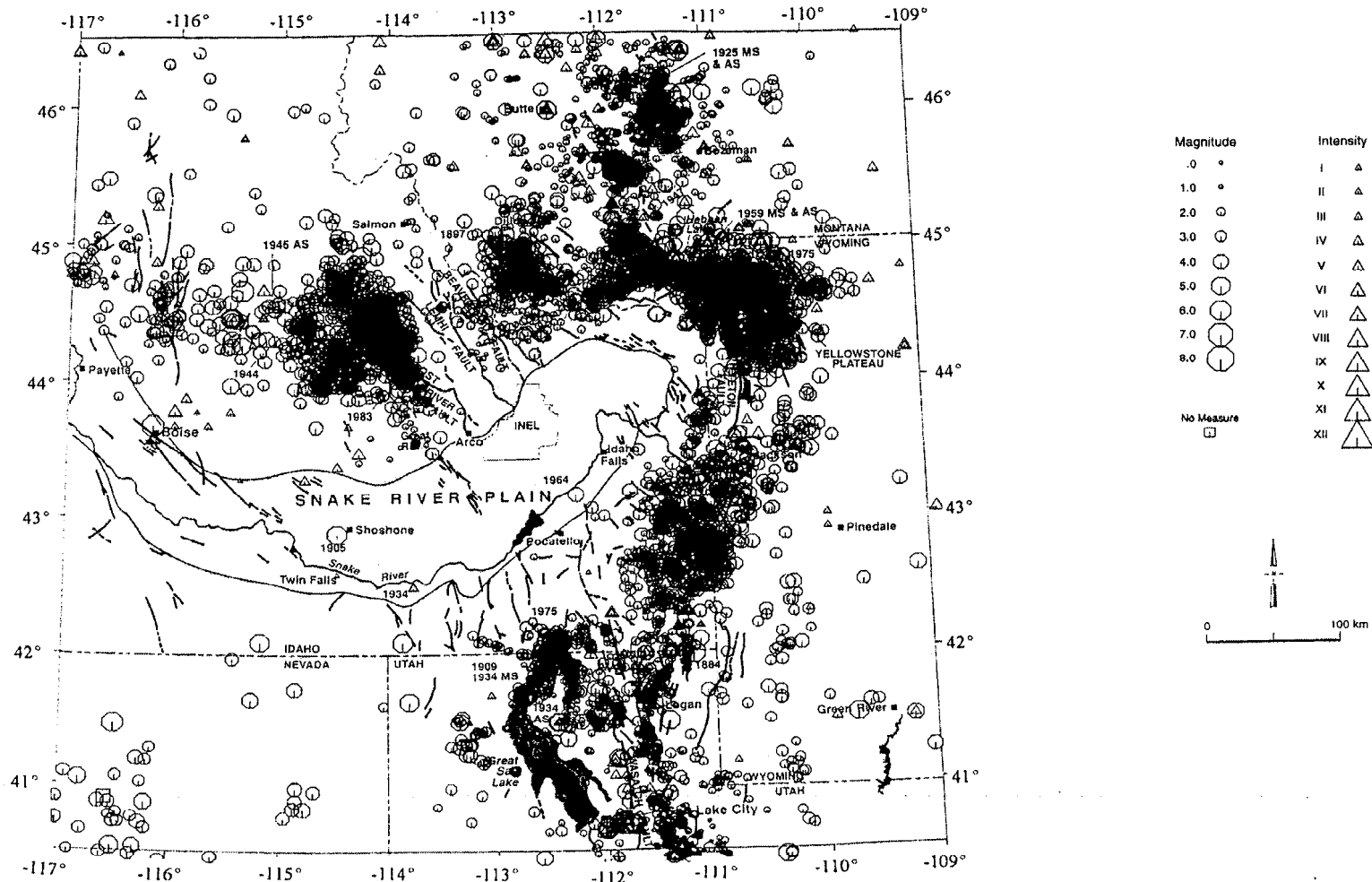


Figure 2.6-27
Earthquake Epicenters in the INEEL Region, 1850-1995

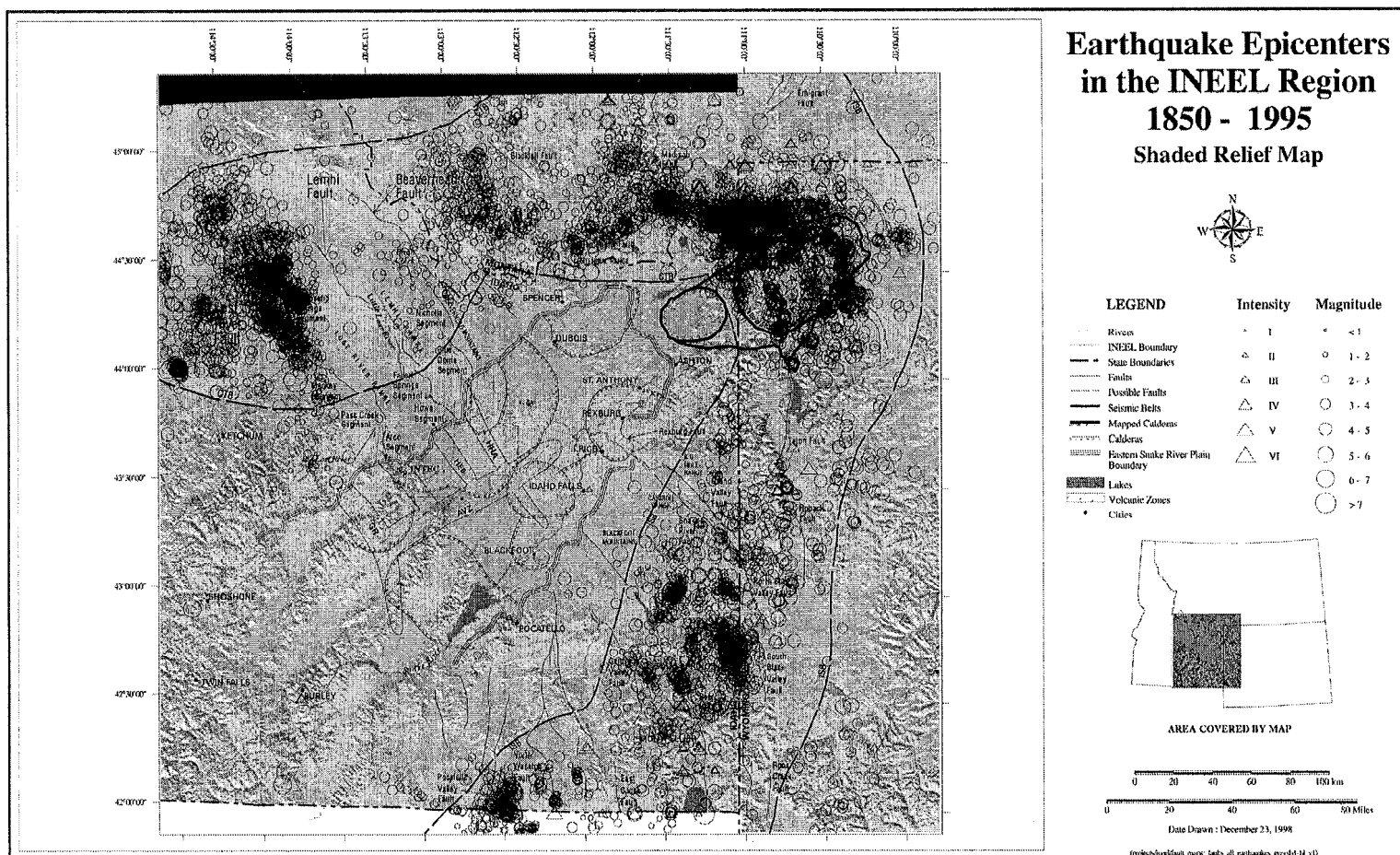


Figure 2.6-28
Map of INEEL Seismic Network Stations and Epicenters of Earthquake
(Within 100 Mile radius of Center of INEEL, 1972-1995)

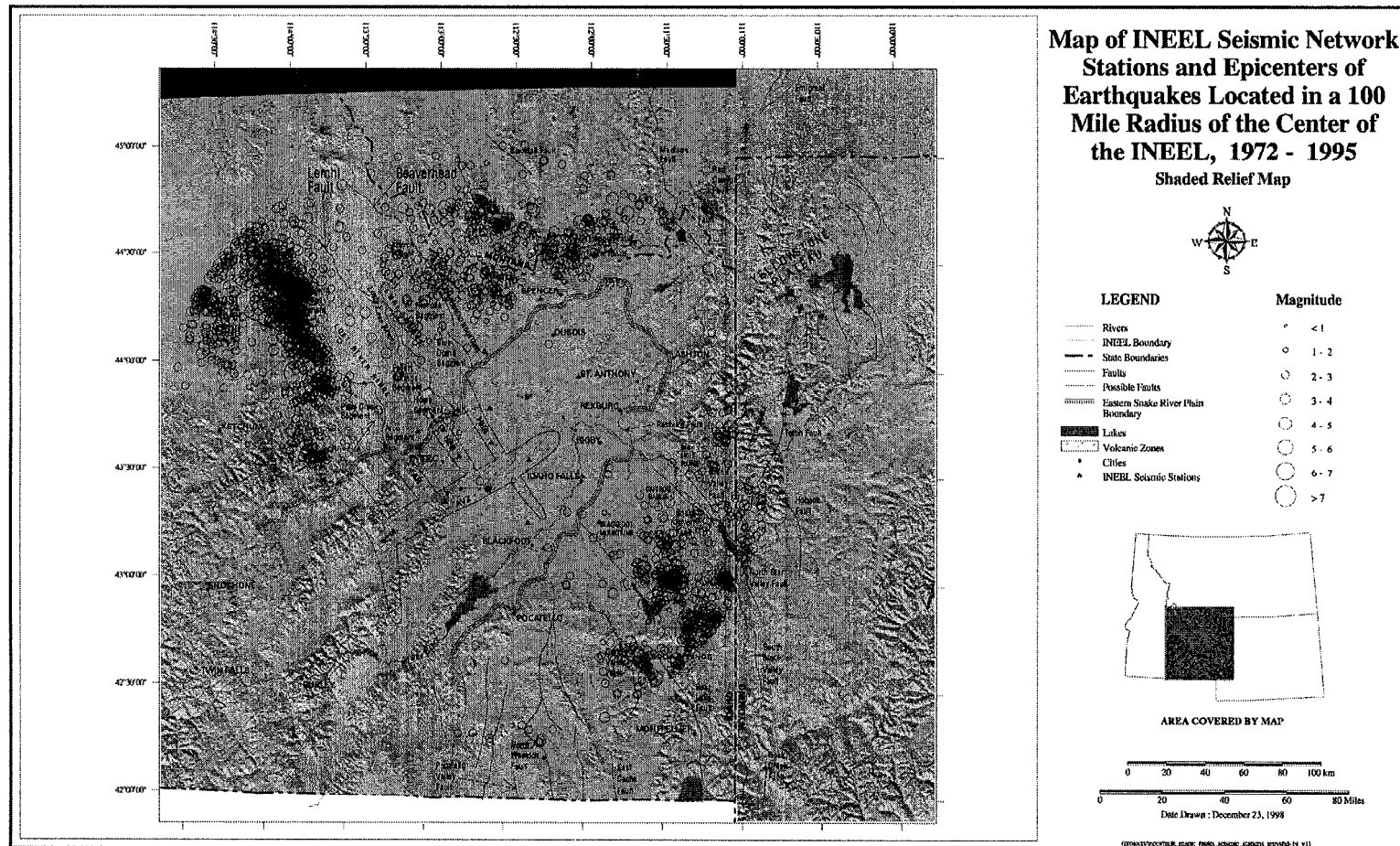


Figure Developed From Data Presented in TMI-2 ISFSI Sar (Ref 2-1)

Figure 2.6-29
Isoseismal Map for the 1959 Hebgen Lake Earthquake

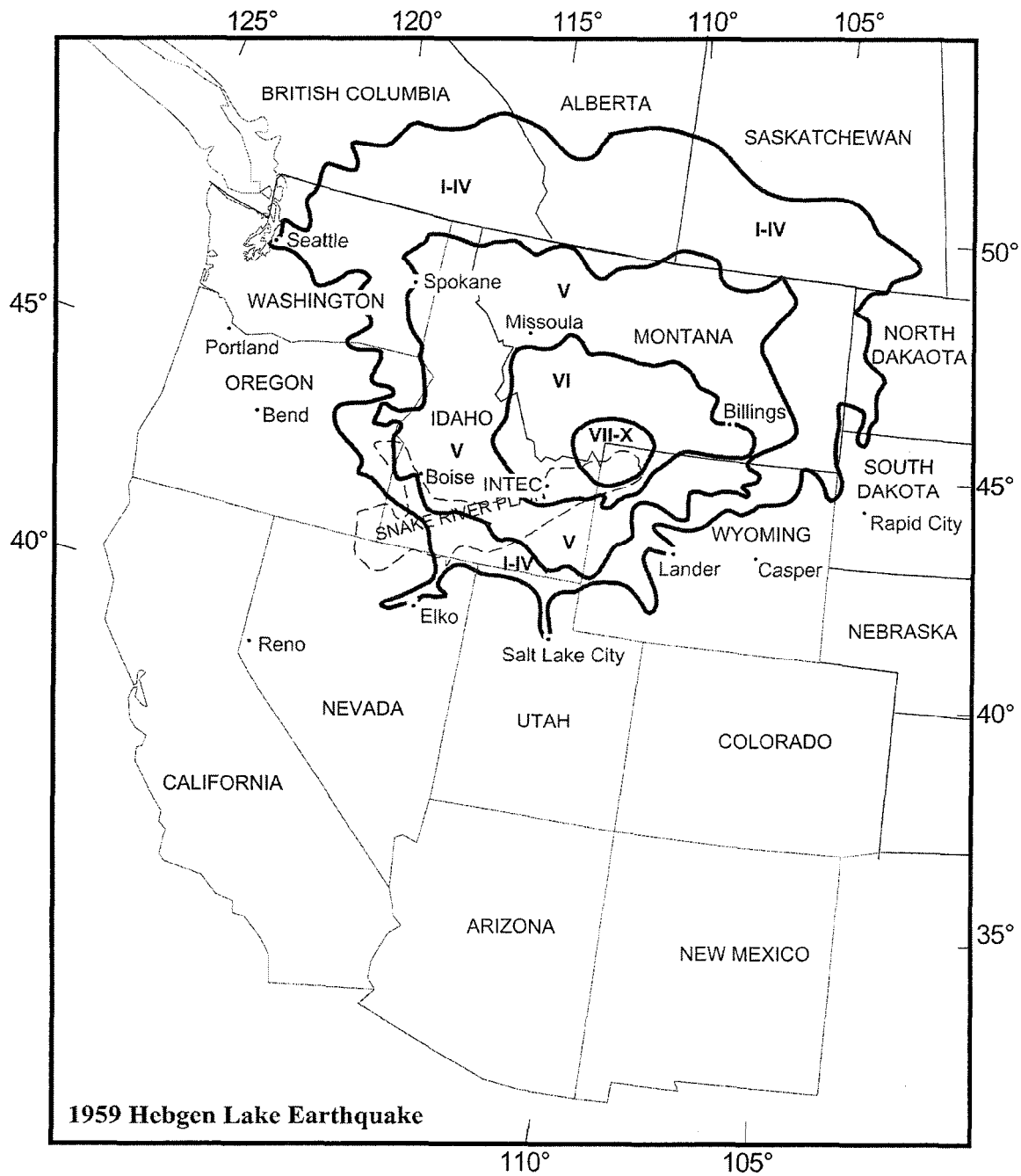


Figure 2.6-30
Isoseismal Map for the 1983 Borah Peak Earthquake

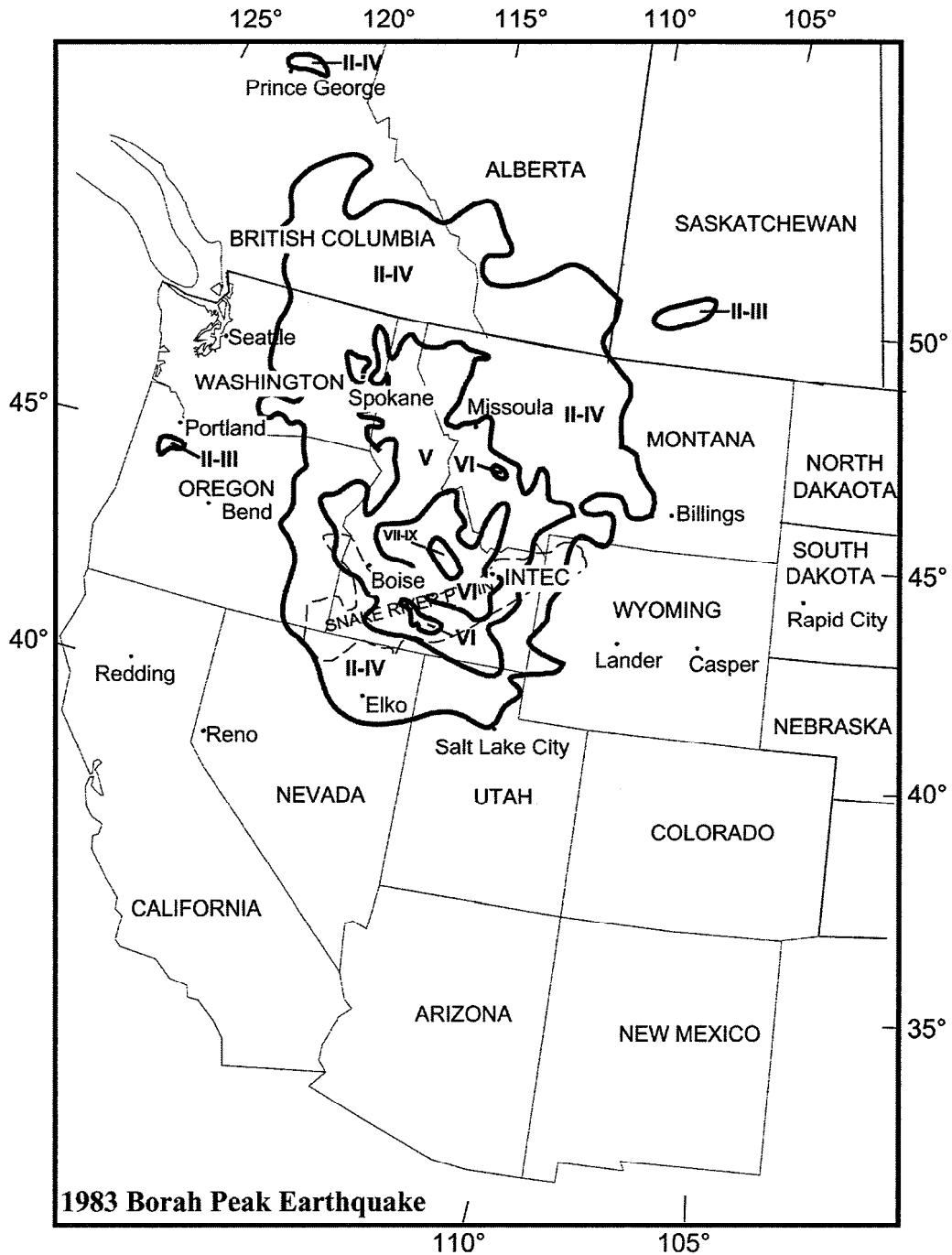


Figure Developed From Data Presented in TMI-2 ISFSI Sar (Ref 2-1)

Figure 2.6-31
Isoseismal Map for the 1905 Shoshone Earthquake

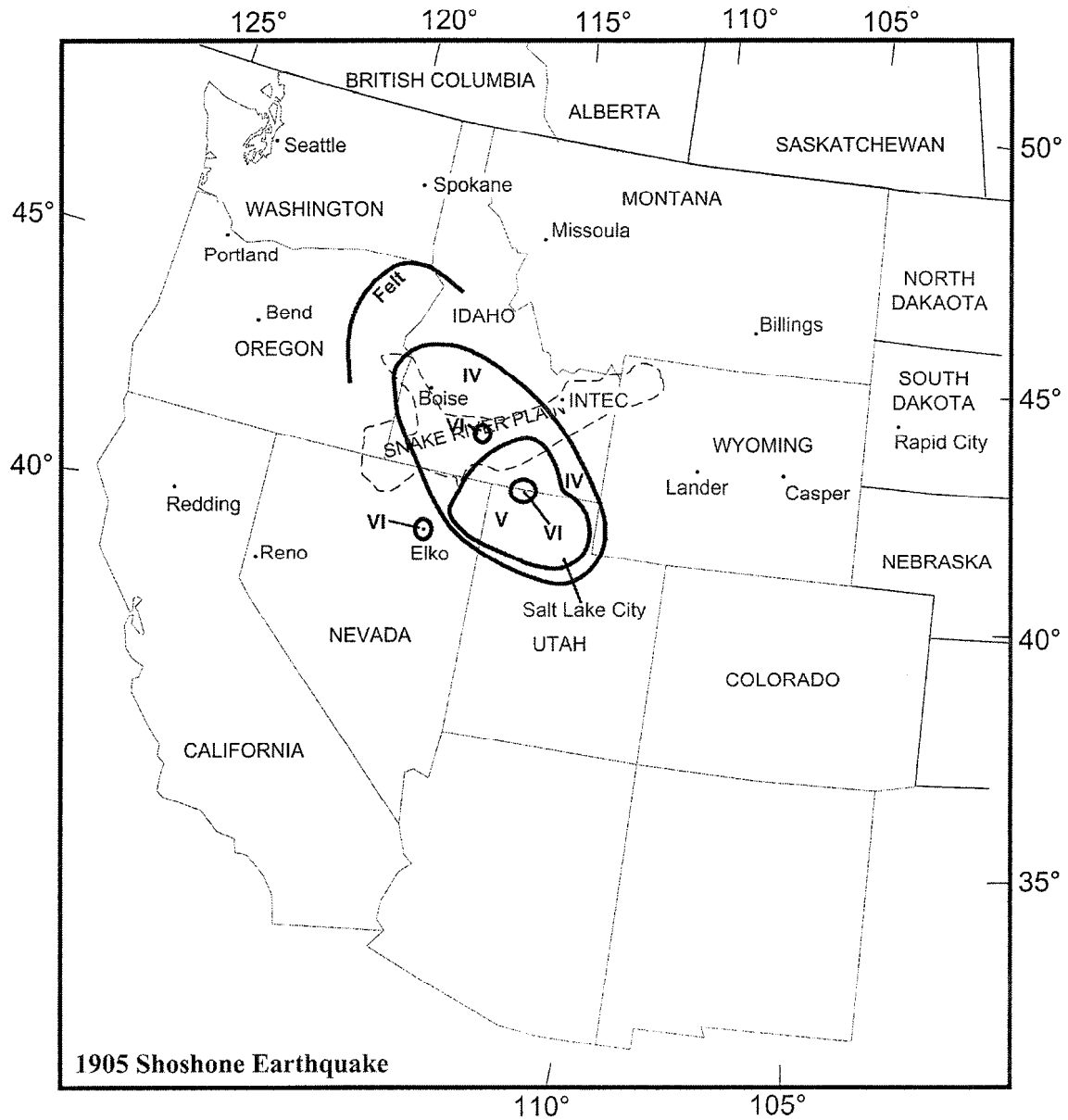


Figure Developed From Data Presented in TMI-2 ISFSI Sar (Ref 2-1)

Figure 2.6-32
Isoseismal Map for the 1975 Pocatello Valley Earthquake

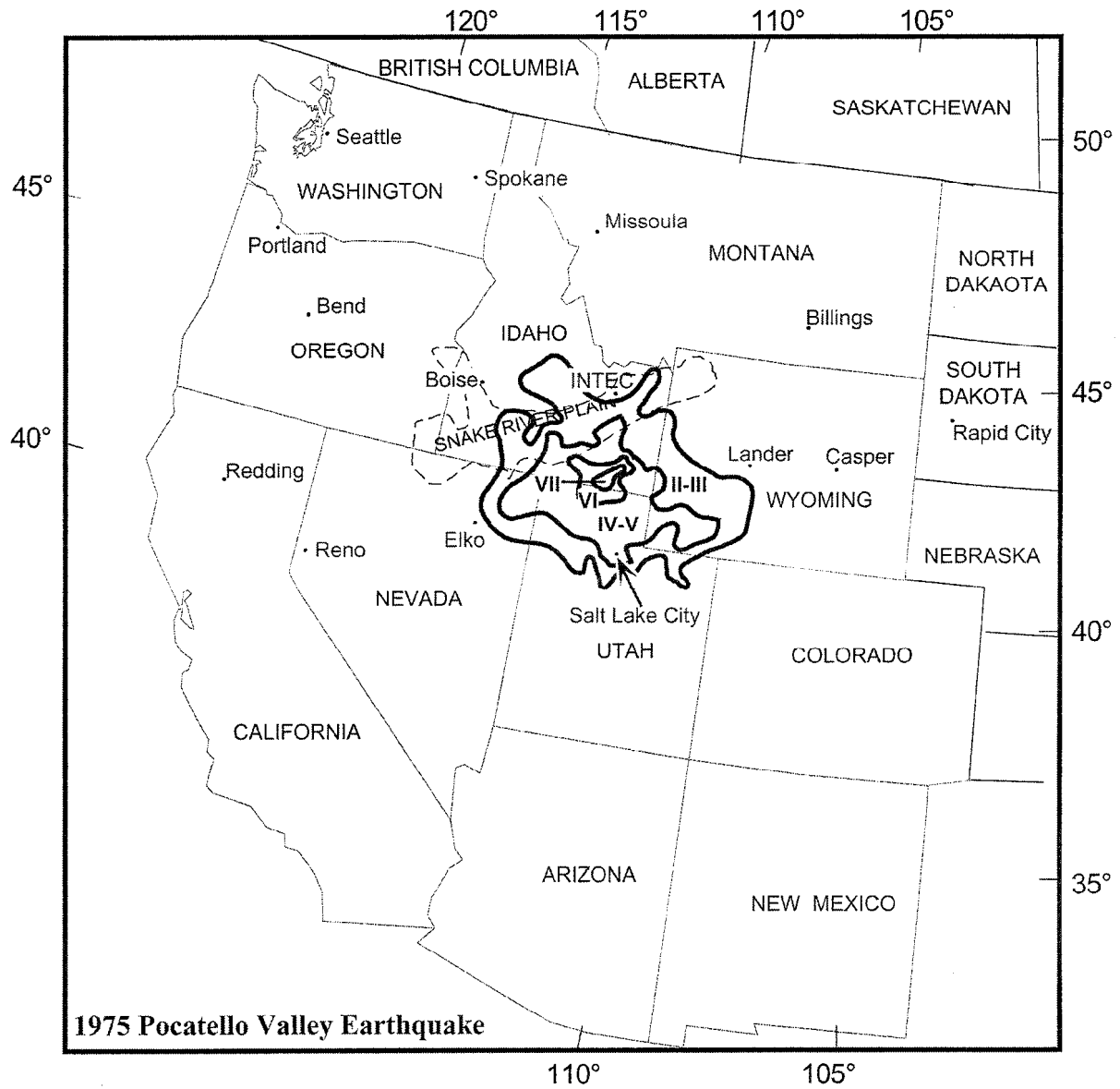


Figure developed from data presented in TMI-2 ISFSI SAR (Ref 2-1)

Figure 2.6-33
Isoseismal Map for the 1975 Yellowstone Earthquake

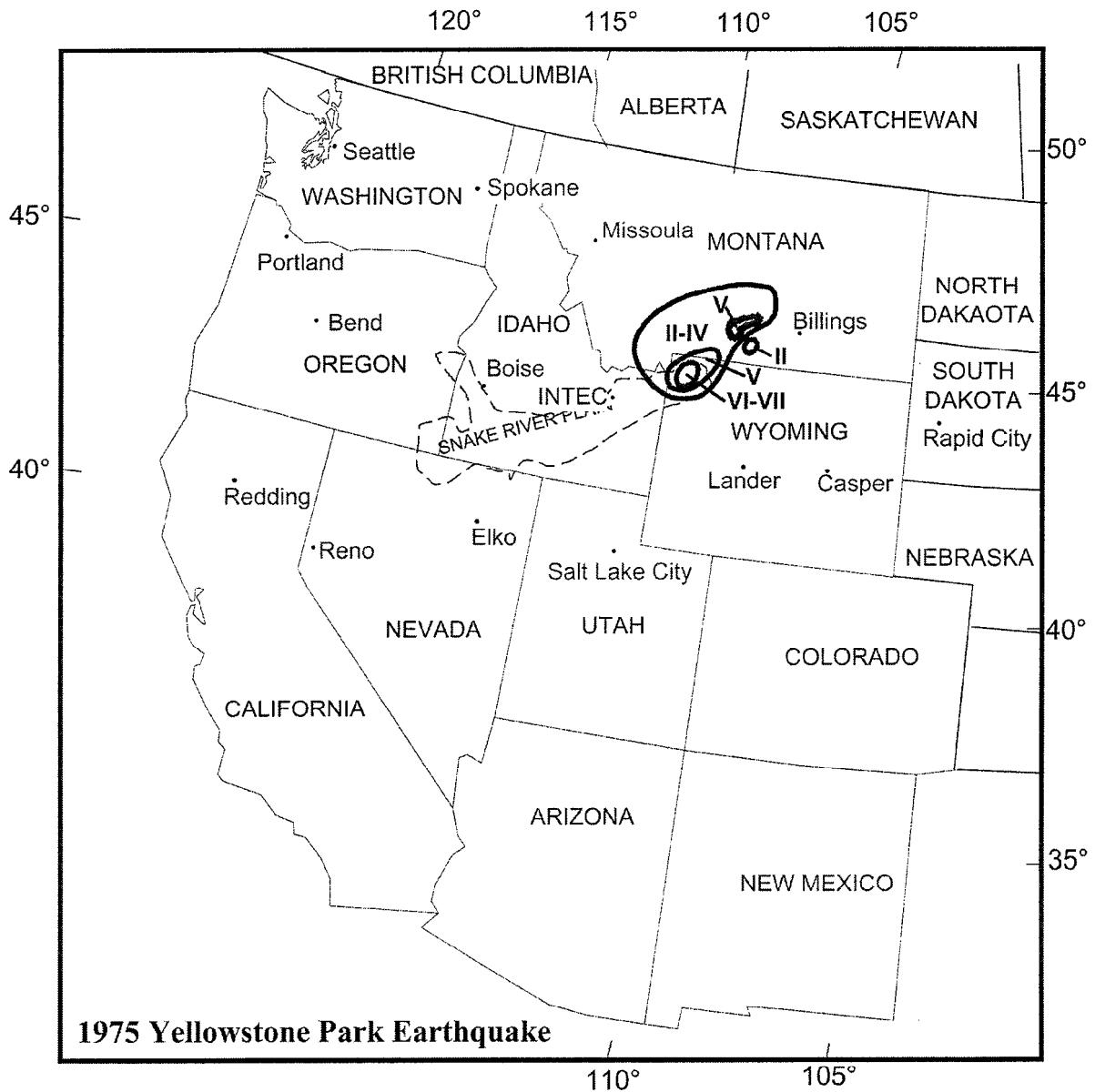


Figure 2.6-34
Isoseismal Map for the 1994 Draney Peak Earthquake

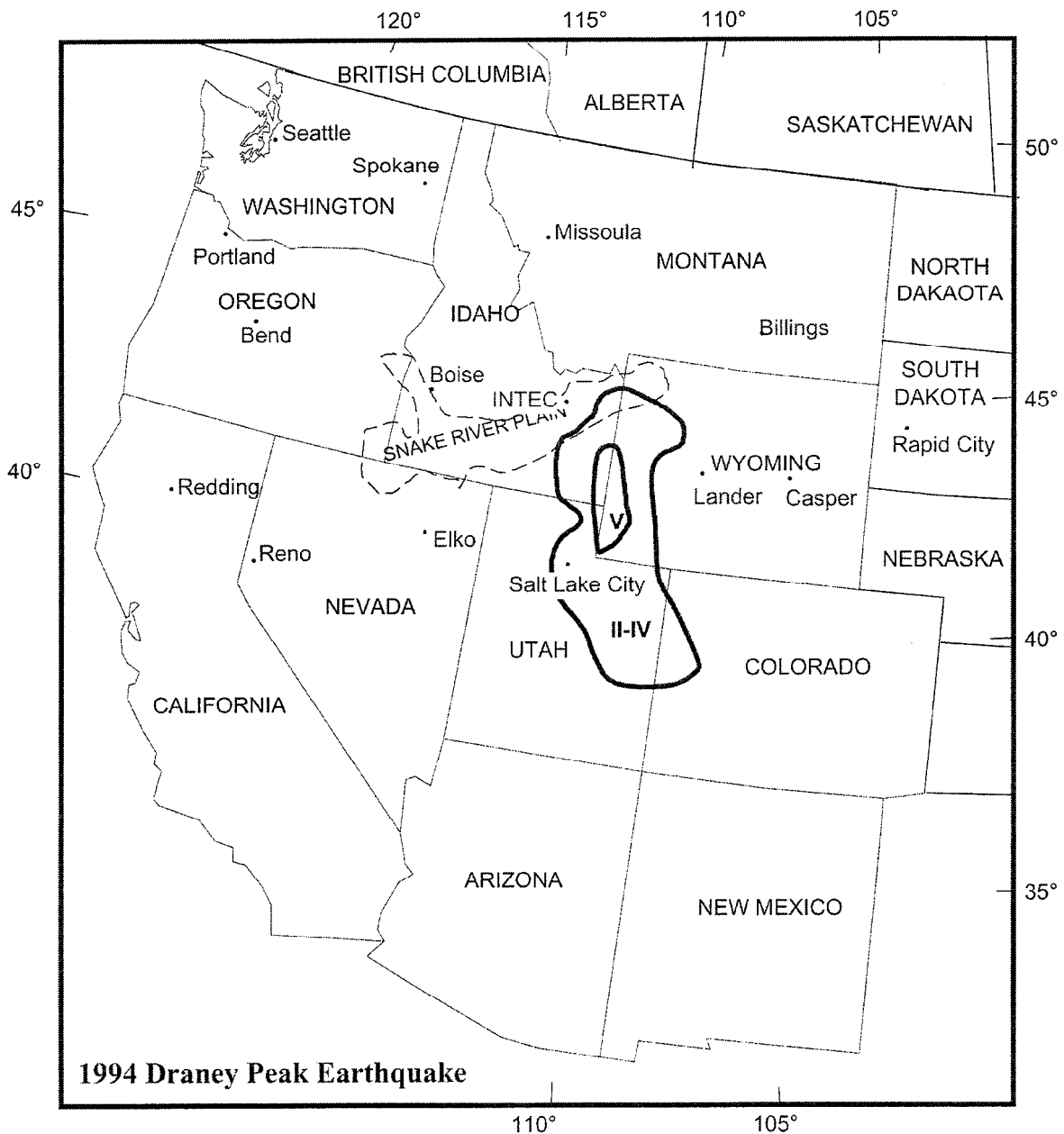


Figure developed from data presented in TMI-2 ISFSI SAR (Ref 2-1)

Figure 2.6-35
Map of the Southern Lemhi Fault

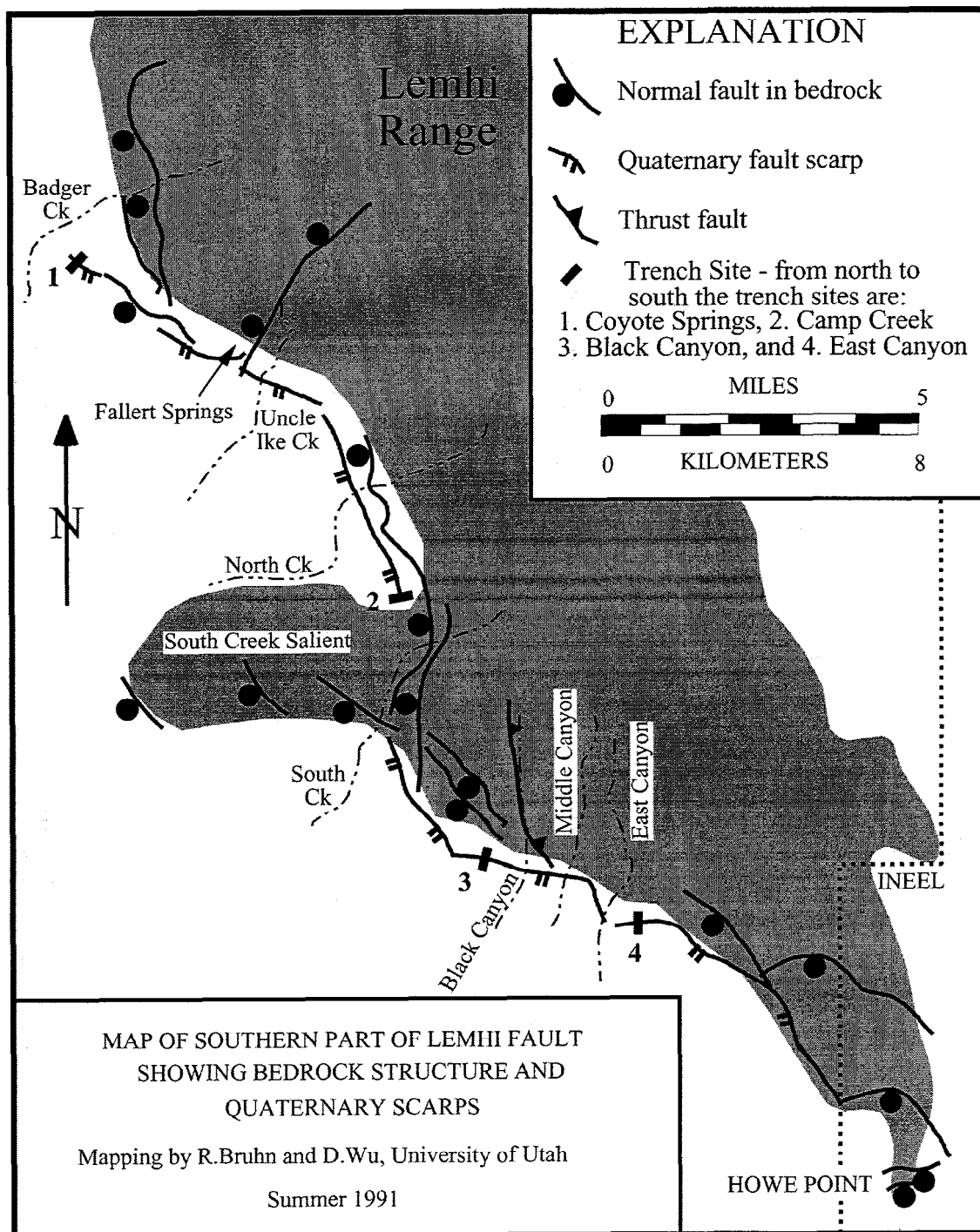


FIGURE 2.6-36
Summary of Paleoseismic Results for the Lemhi Fault (Four Trenches)

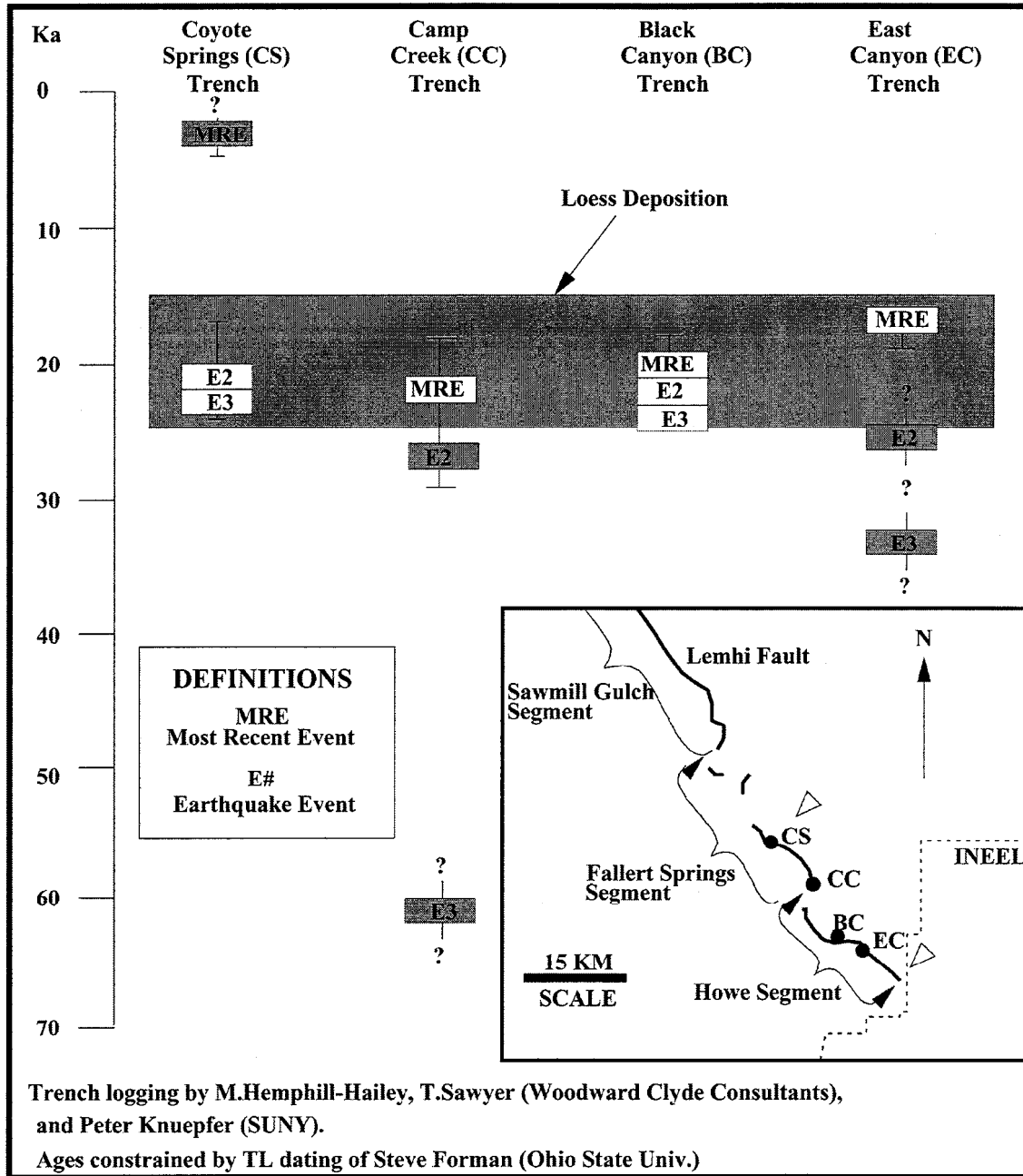


Figure developed from data presented in TMI-2 ISFSI SAR (Ref 2-1)

Figure 2.6-37
Comparison of Surface Area of the Howe Segment of the Lemhi Fault to the
Surface Area of Dike-Induced Normal Faults

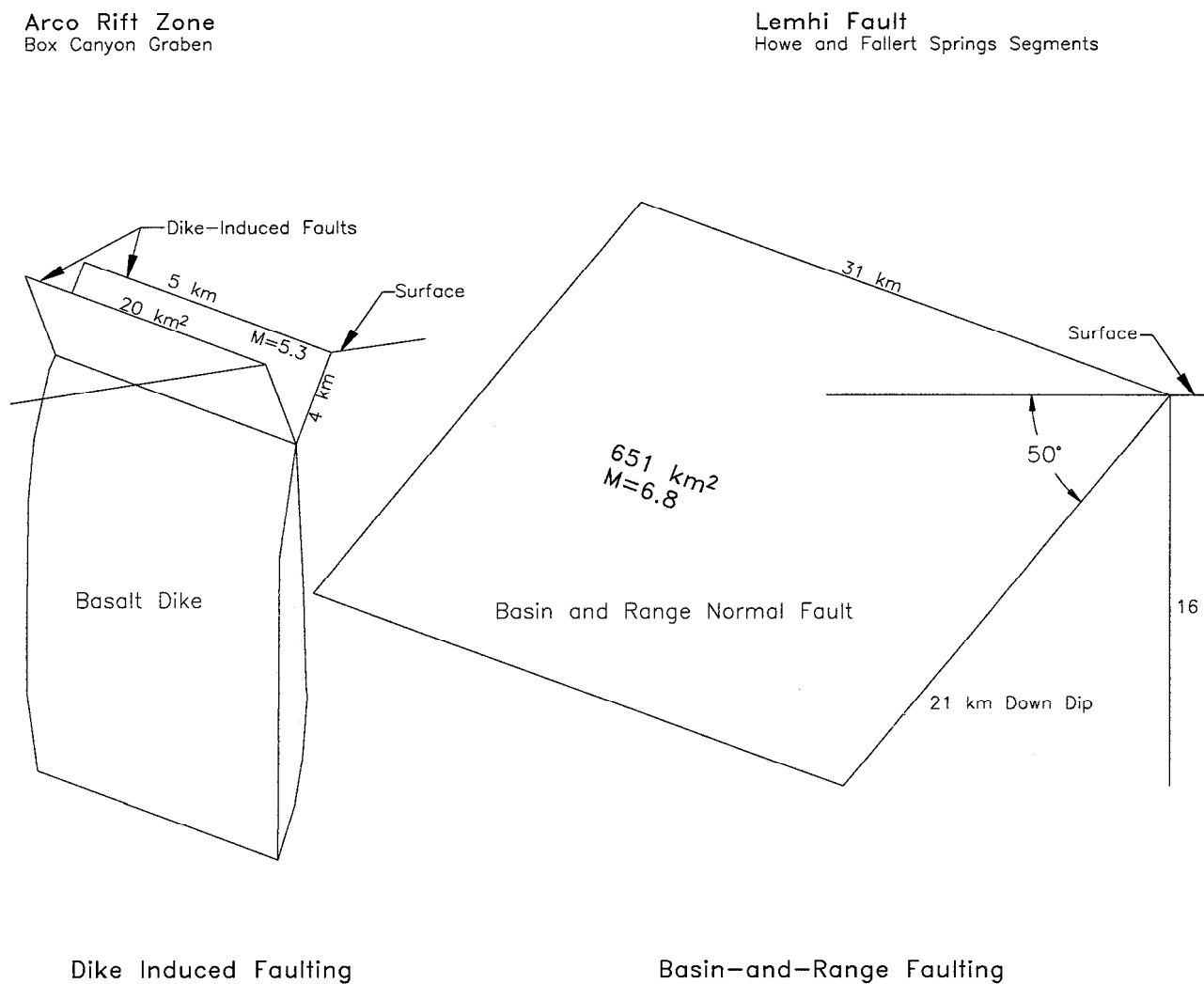


Figure 2.6-38
Deep Bore Hole Shear Wave Velocity

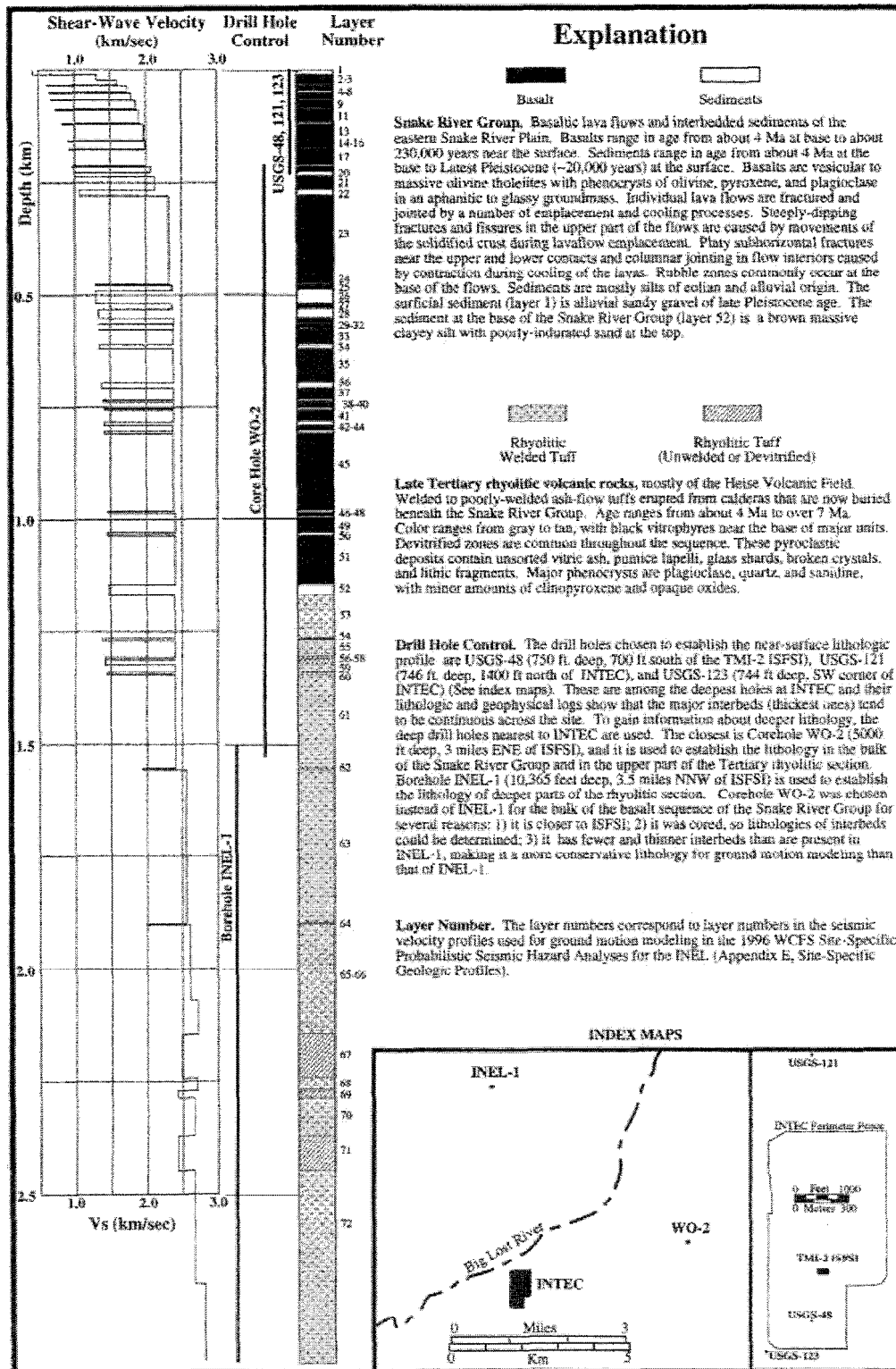


Figure 2.6-39
Comparison of the PC 3 (2500 years) Horizontal Rock DBE 5% Damped Response Spectra with the Adjusted UHS for INTEC, TRA, RWMC, and PBF

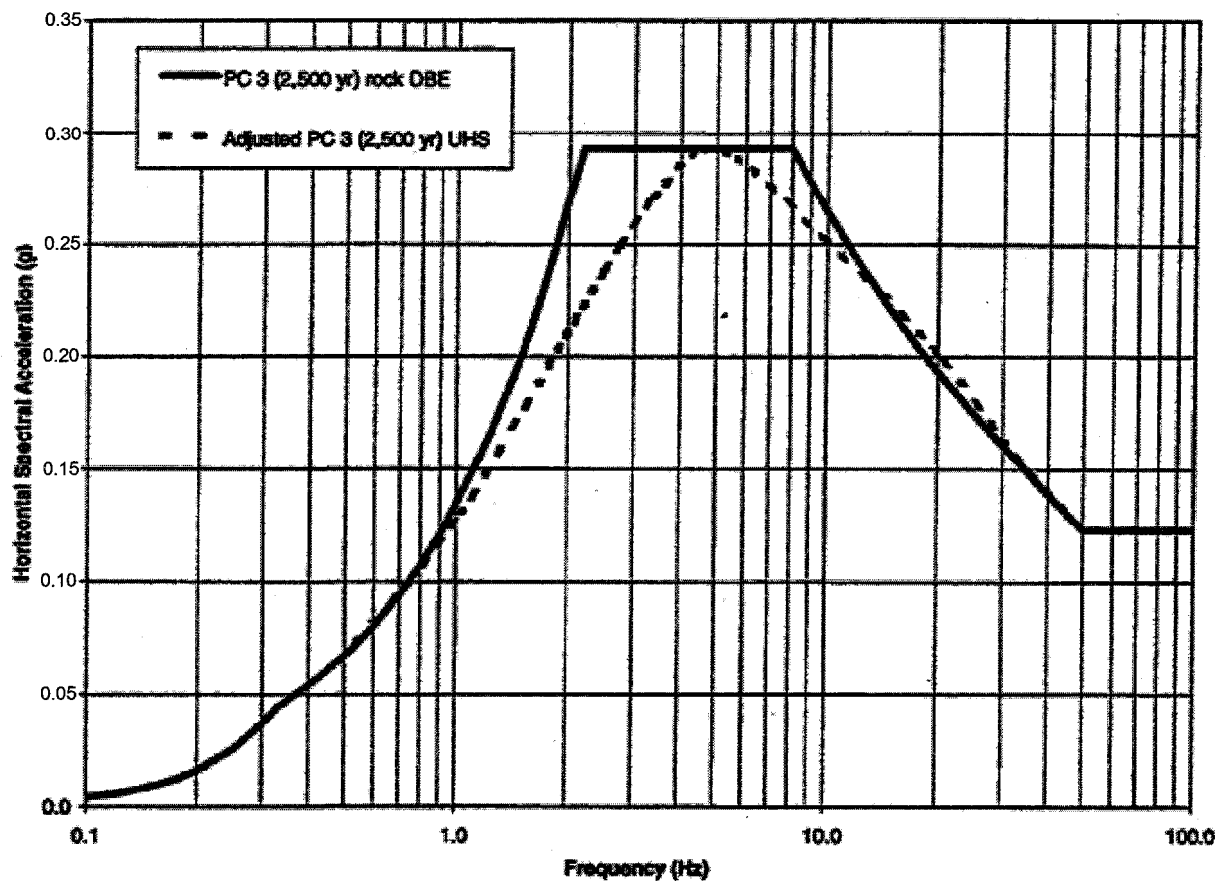


Figure 2.6-40
Plots of the Acceleration, Velocity, and Displacement Time Histories for One Horizontal Component of the PC 3 (2,500 years) Rock DBE Response Spectrum at INTEC, TRA, RWMC, and PBF.

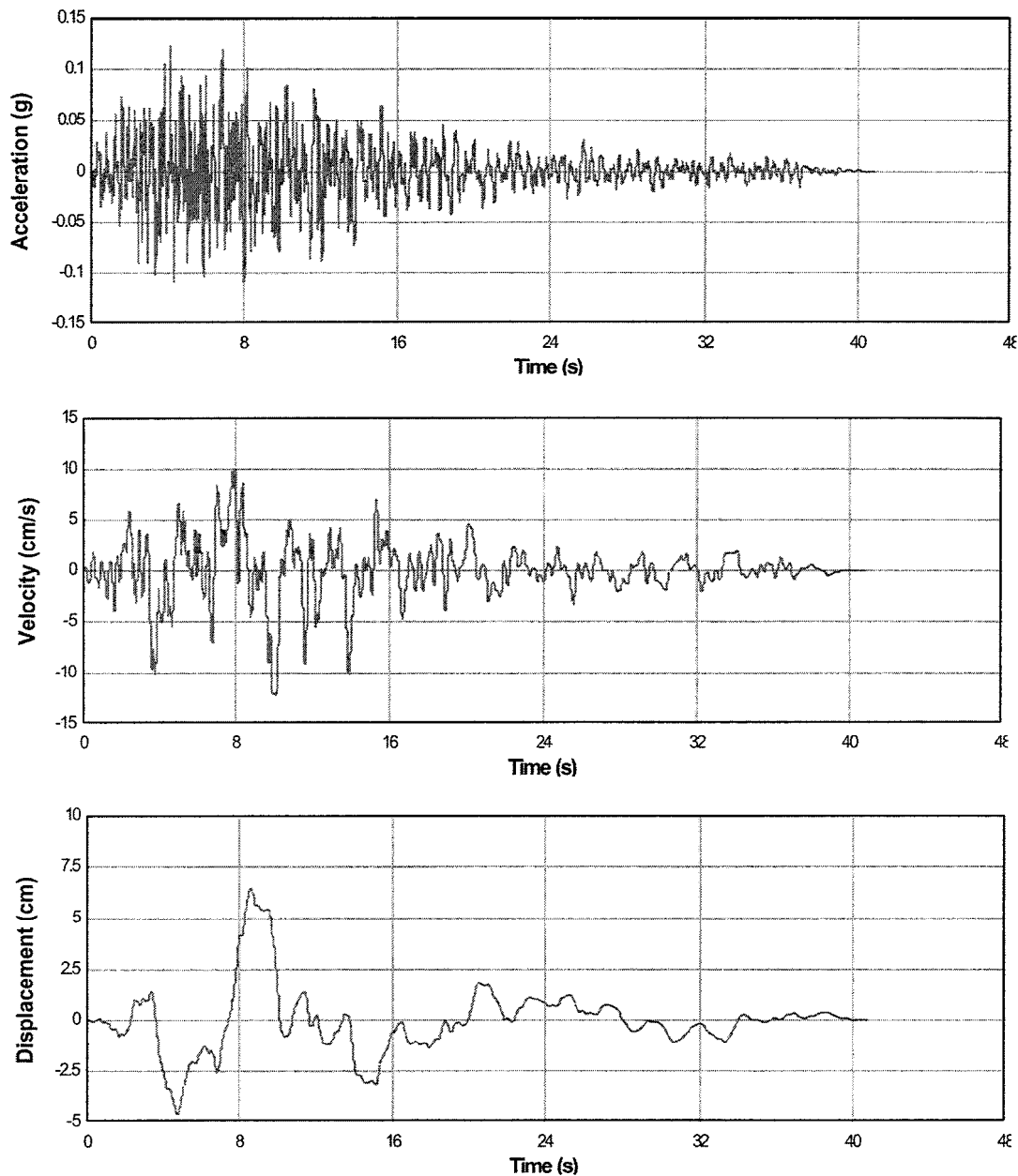


Figure 2.6-41
Plots of the Acceleration, Velocity, and Displacement Time Histories for the Second Horizontal Component of the PC 3 (2,500 years) Rock DBE Response Spectrum at INTEC, TRA, RWMC, and PBF.

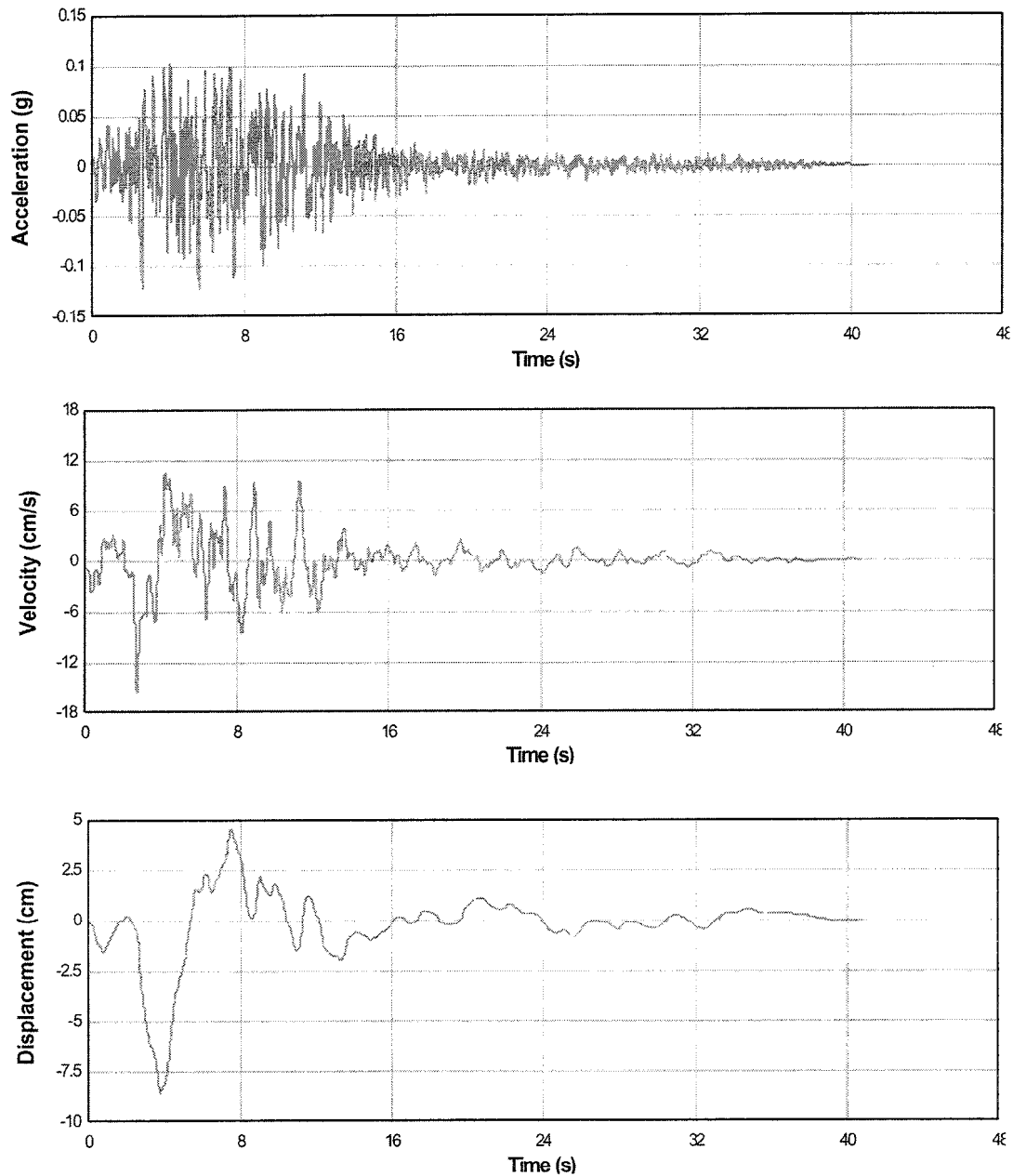


Figure 2.6-42
Measured Shear Wave Velocities and Basecase Profile

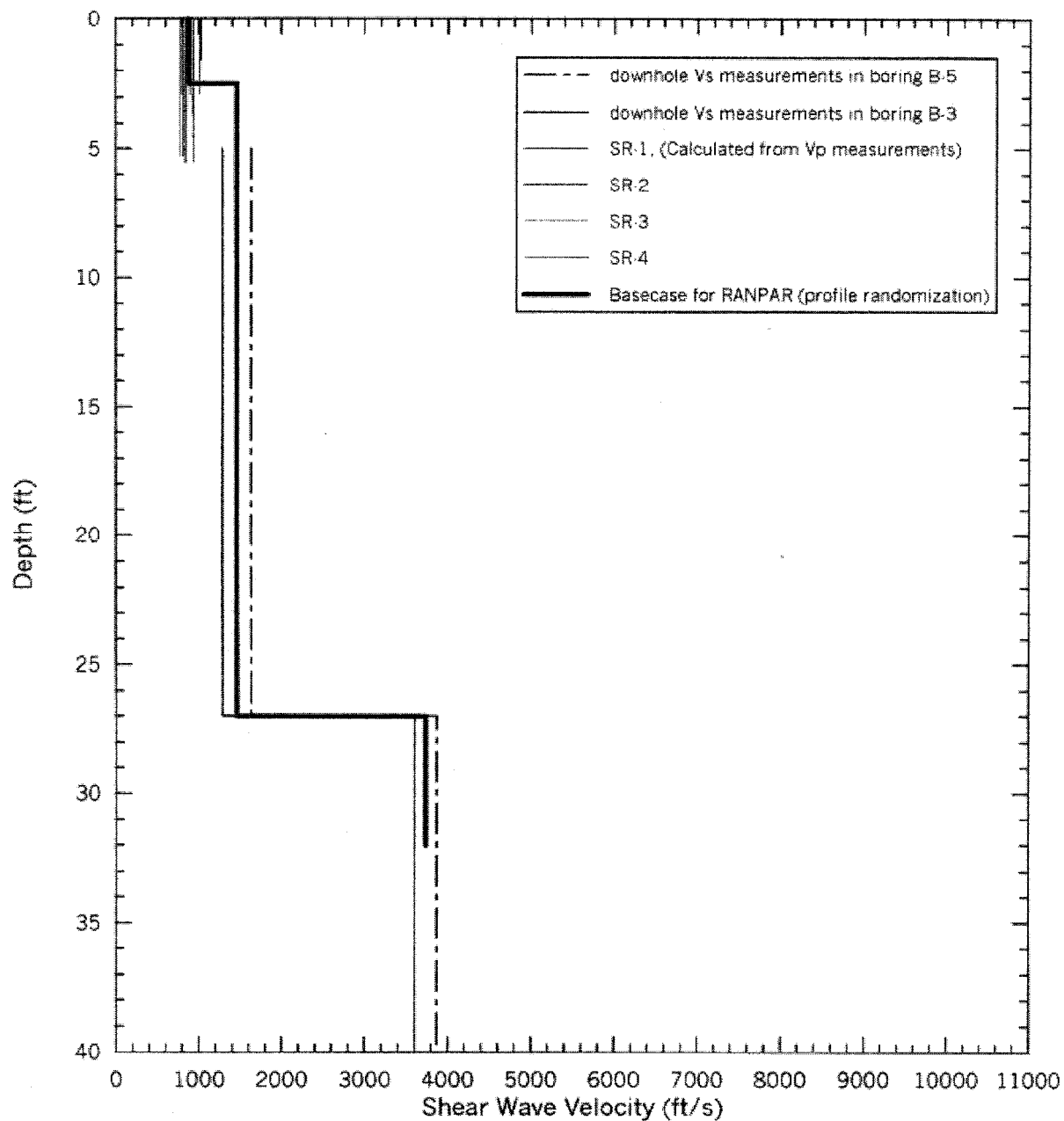


Figure 2.6-43
Randomized Shear Wave Velocity Profiles

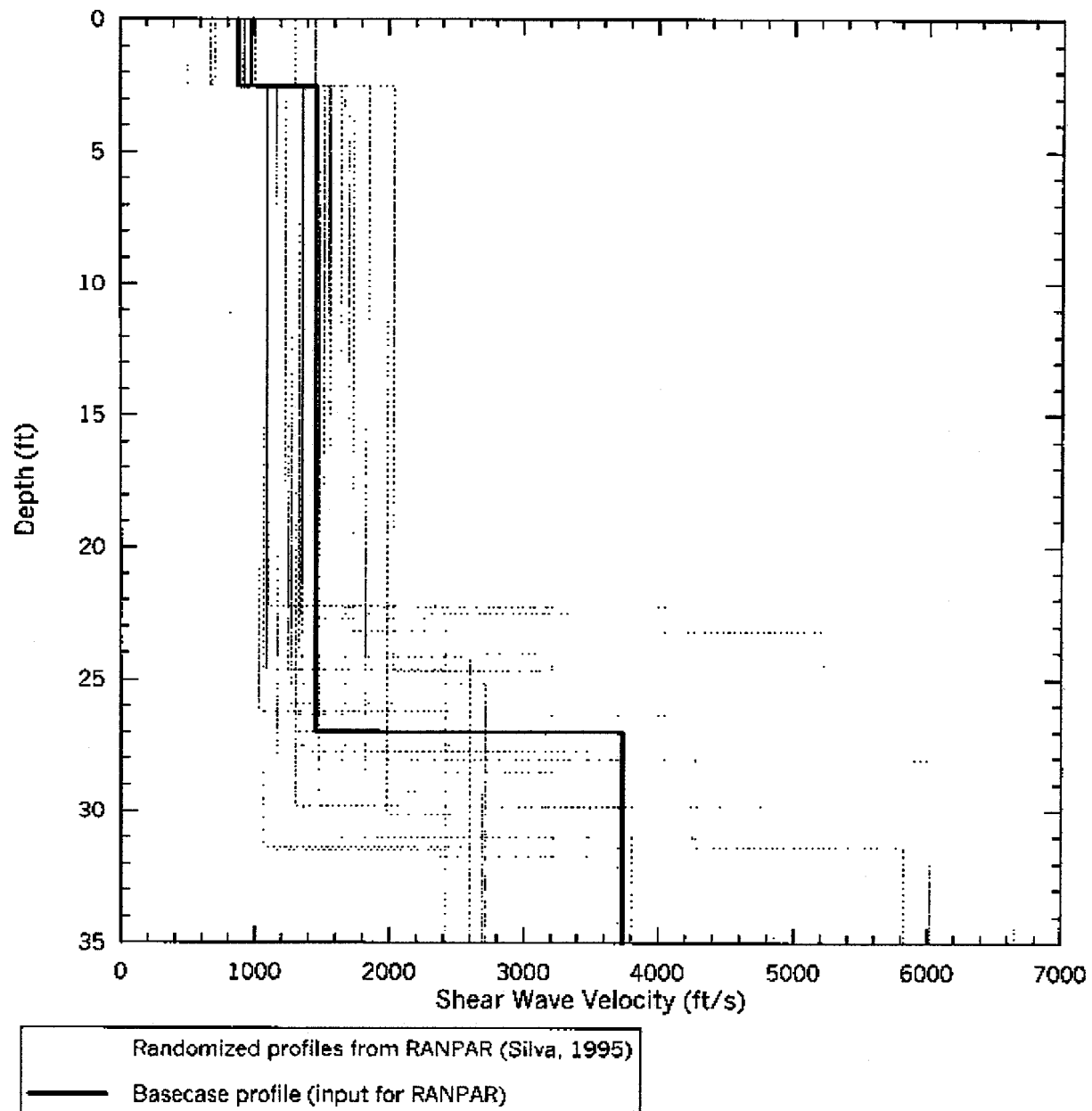


Figure 2.6-44
Response of 30 Profiles to 2500-Year Input Motion (Horizontal 1)

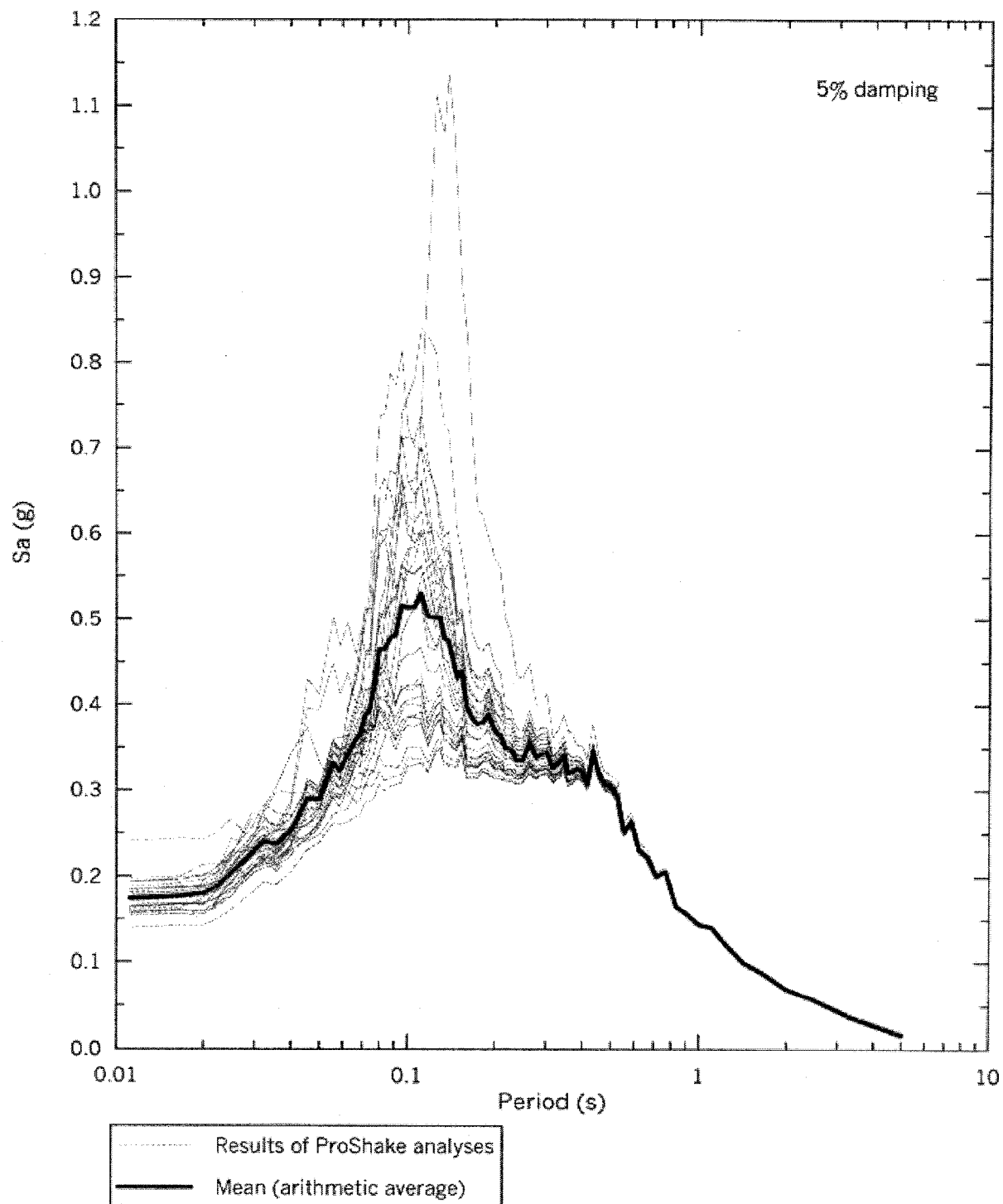


Figure 2.6-45
Response of 30 Profiles to 2500-Year Input Motion (Horizontal 2)

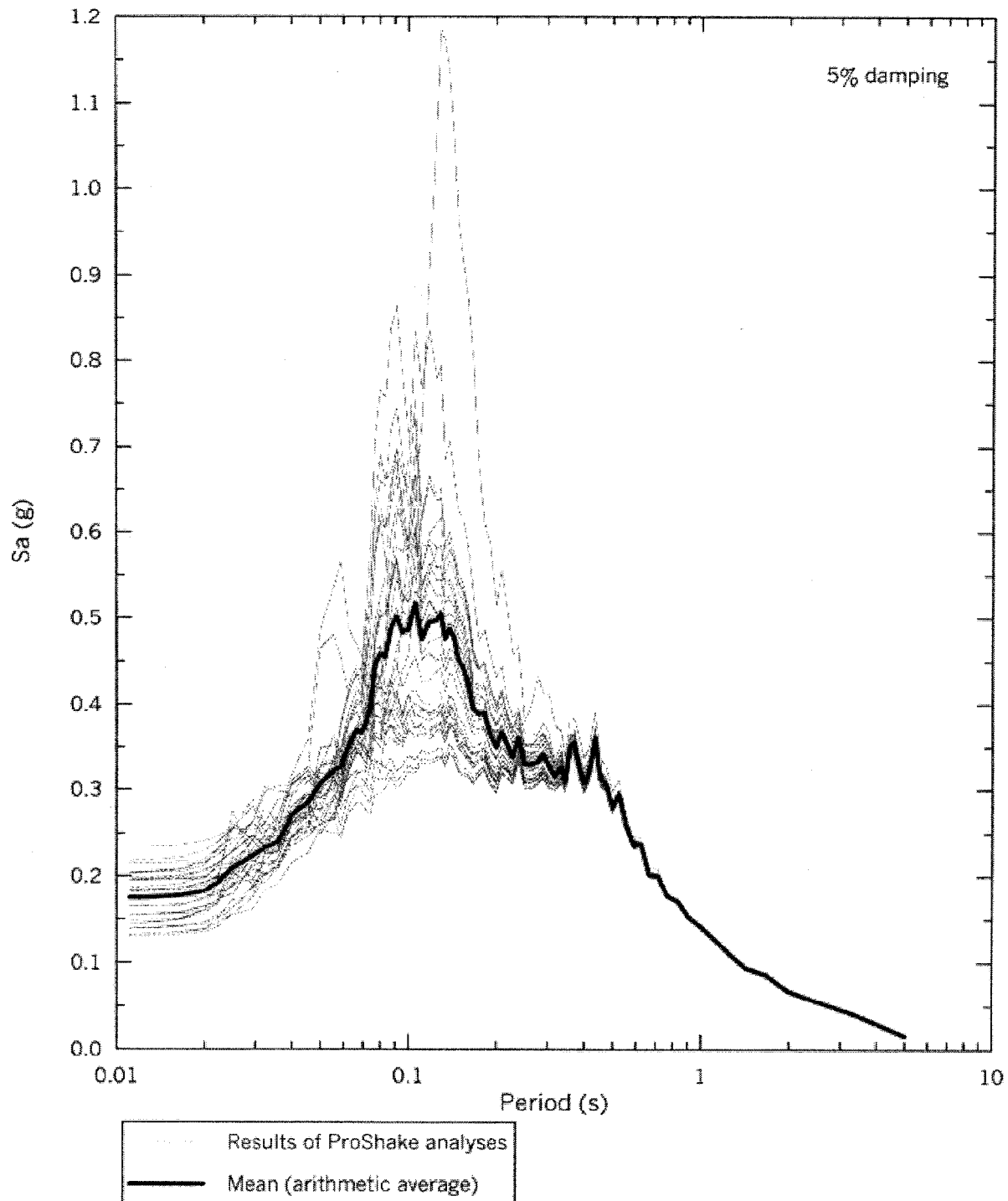


Figure 2.6-46
Strain-Iterated Shear Modulus versus Depth

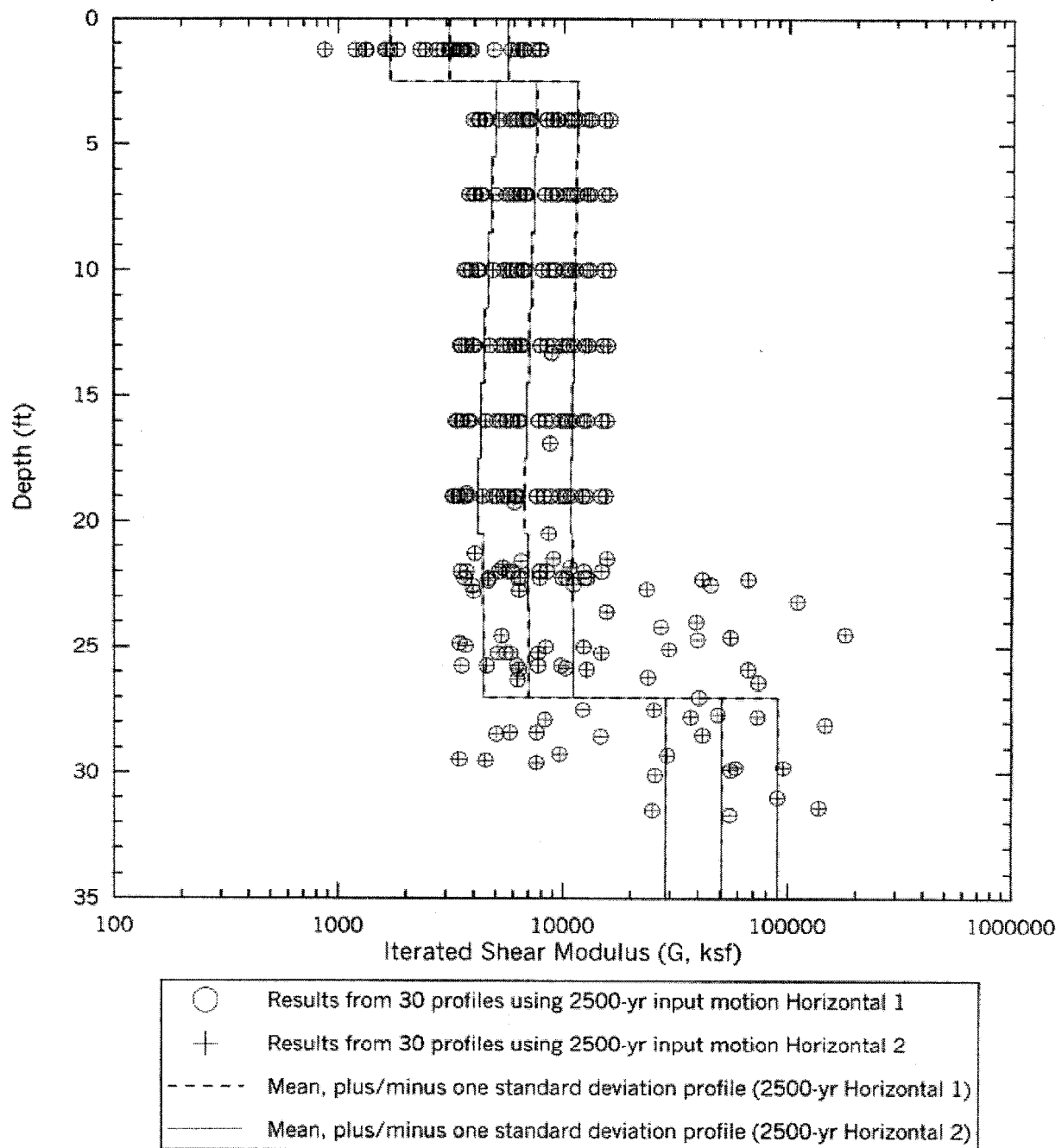


Figure 2.6-47
Strain-Iterated Damping Ratio versus Depth

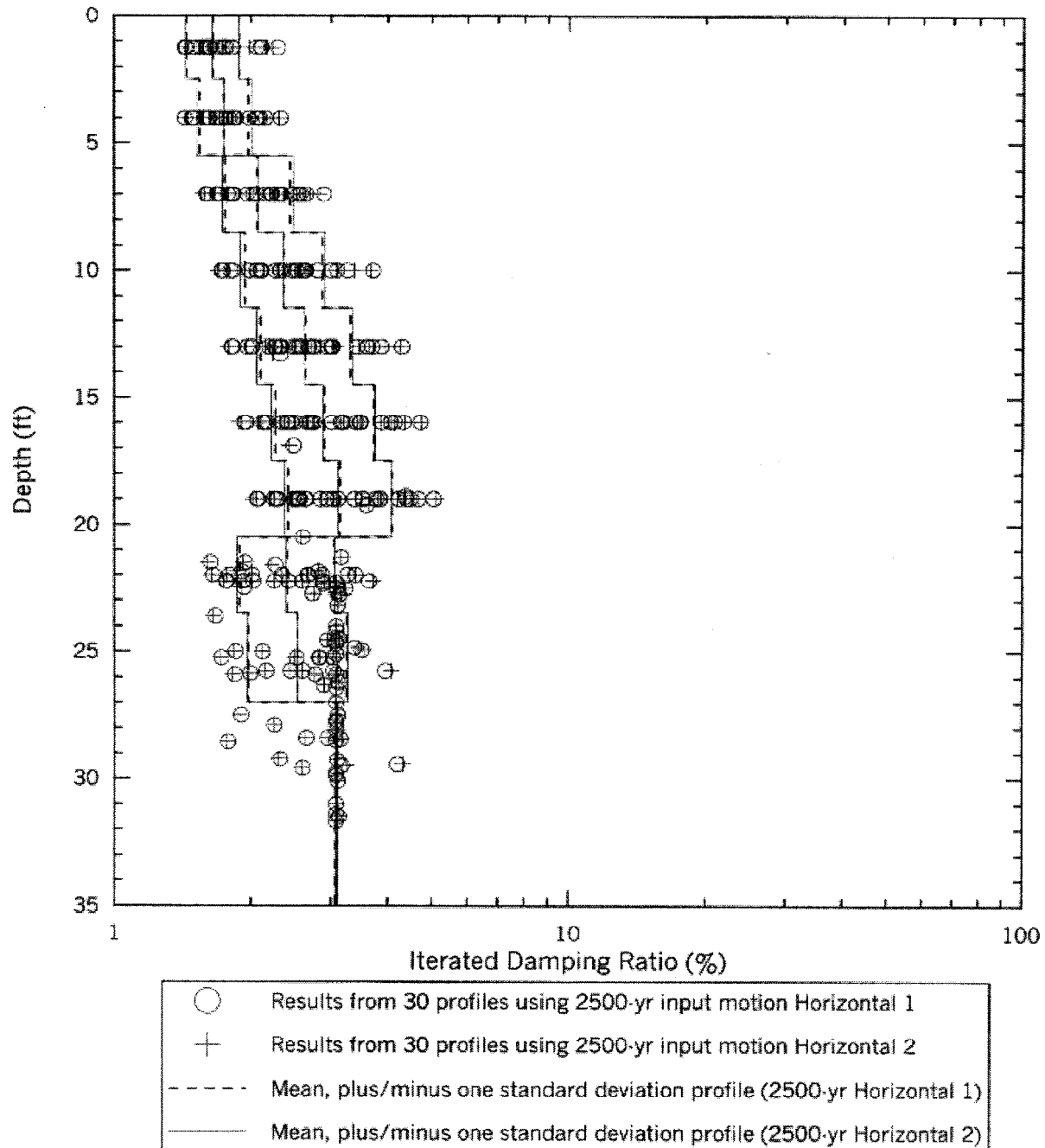


Figure 2.6-48
Soil Property Degradation Models

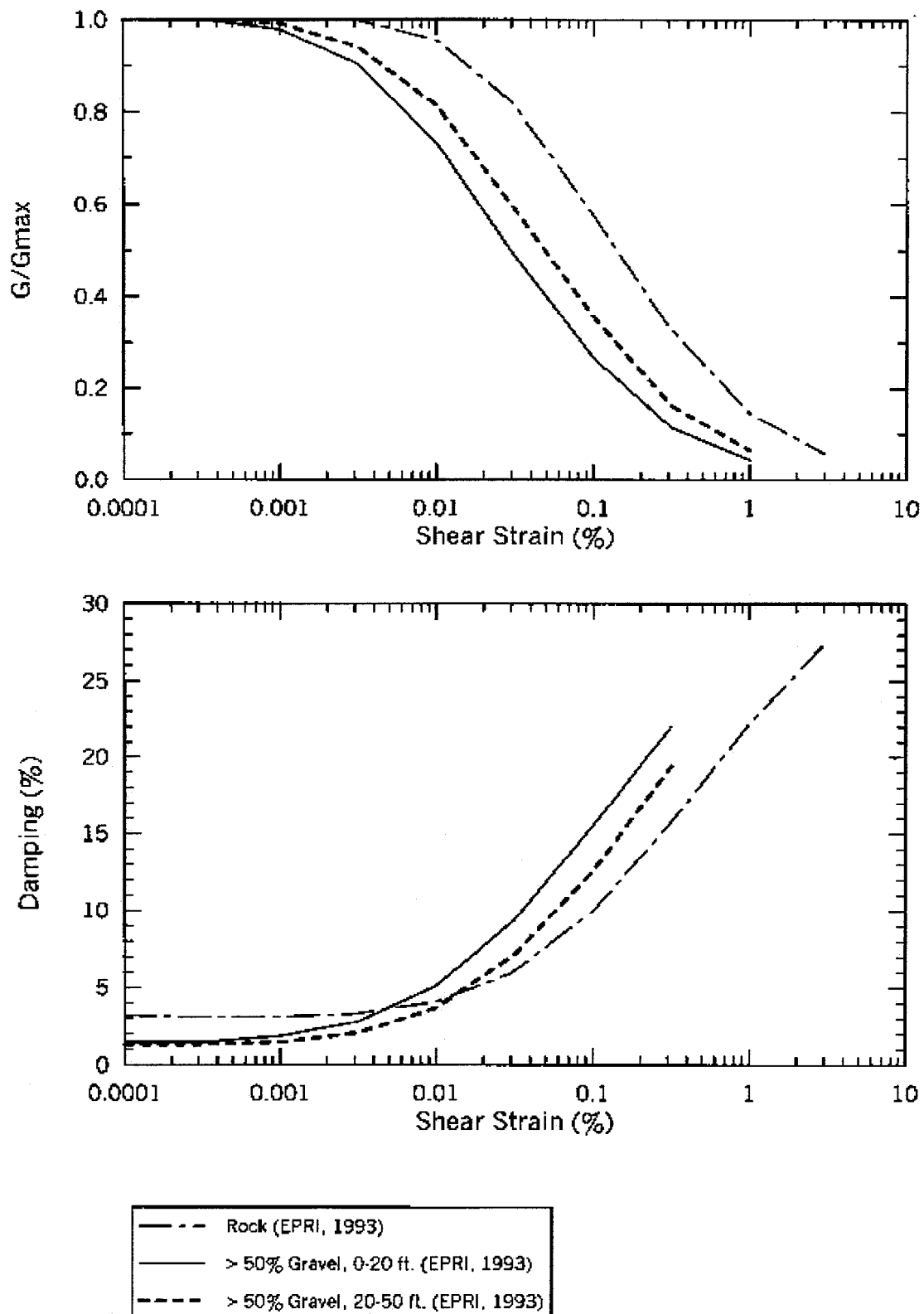


Figure 2.6-49
Horizontal Response Spectra of Strain-Iterated Profiles
(Horizontal 1)

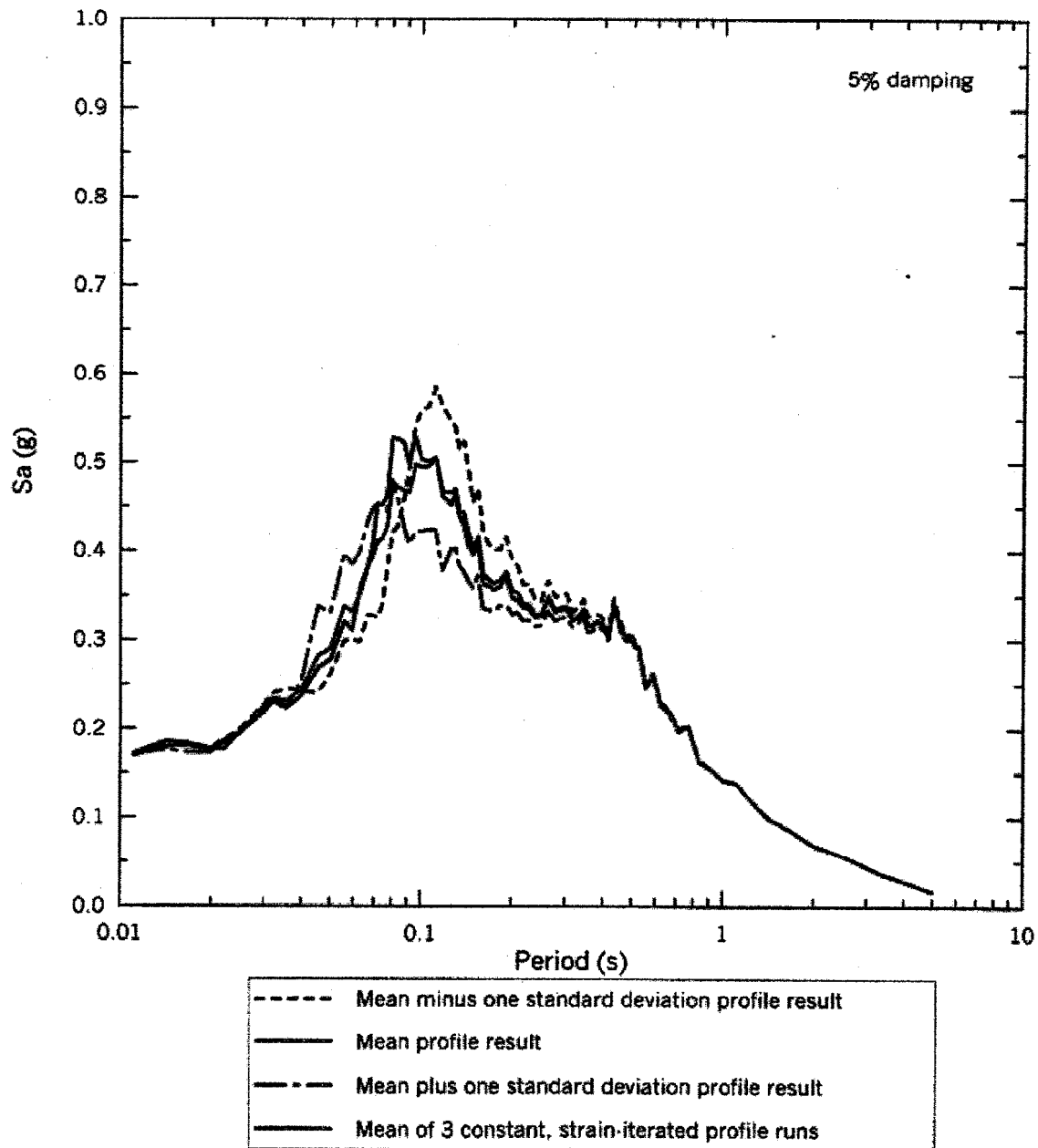


Figure 2.6-50
Horizontal Response Spectra of Strain-Iterated Profiles
(Horizontal 2)

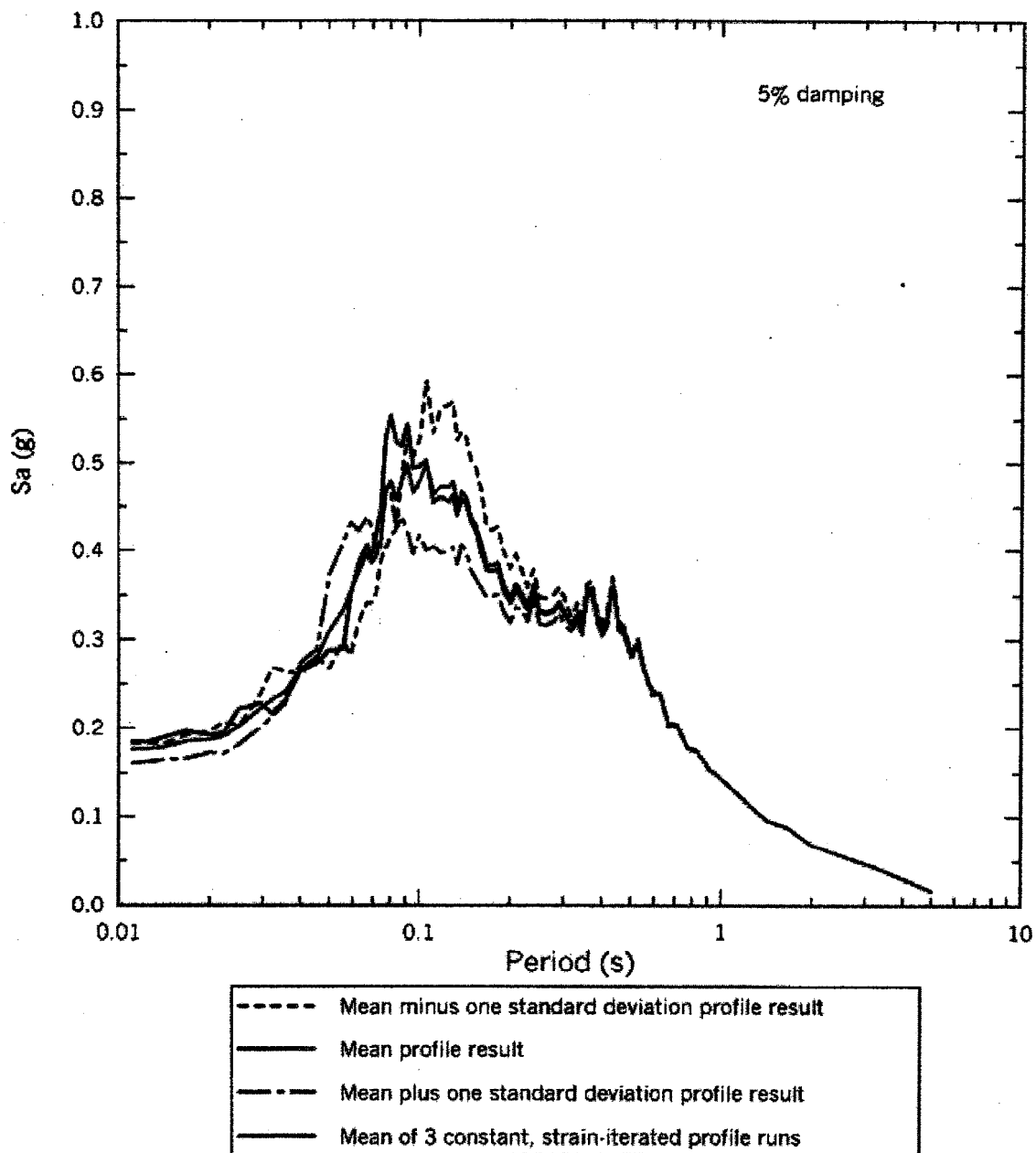


Figure 2.6-51
Comparison of Mean Response Spectra
(2500-Year Input Horizontal 1)

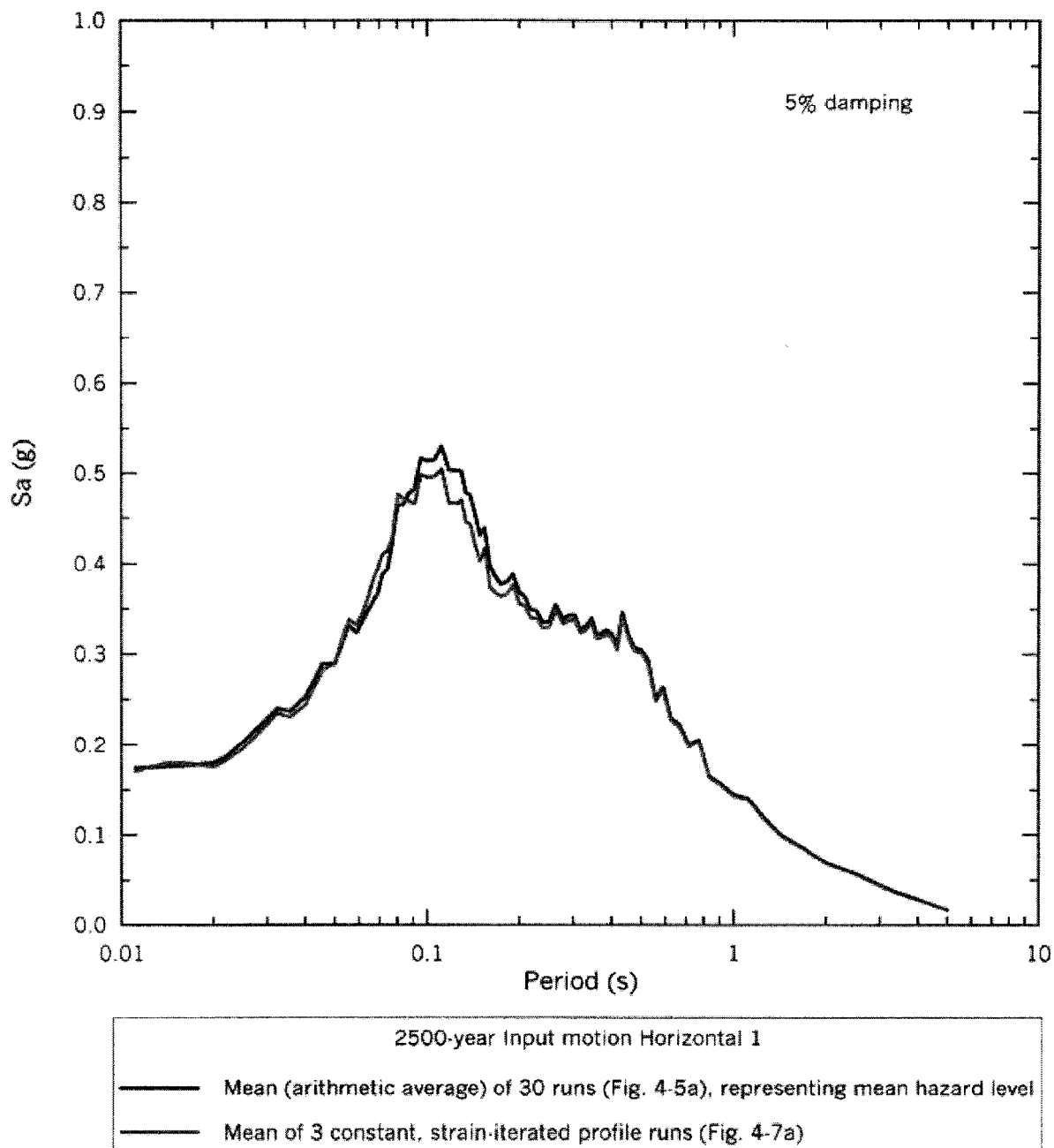


Figure 2.6-52
Comparison of Mean Response Spectra
(2500-Year Input Horizontal 2)

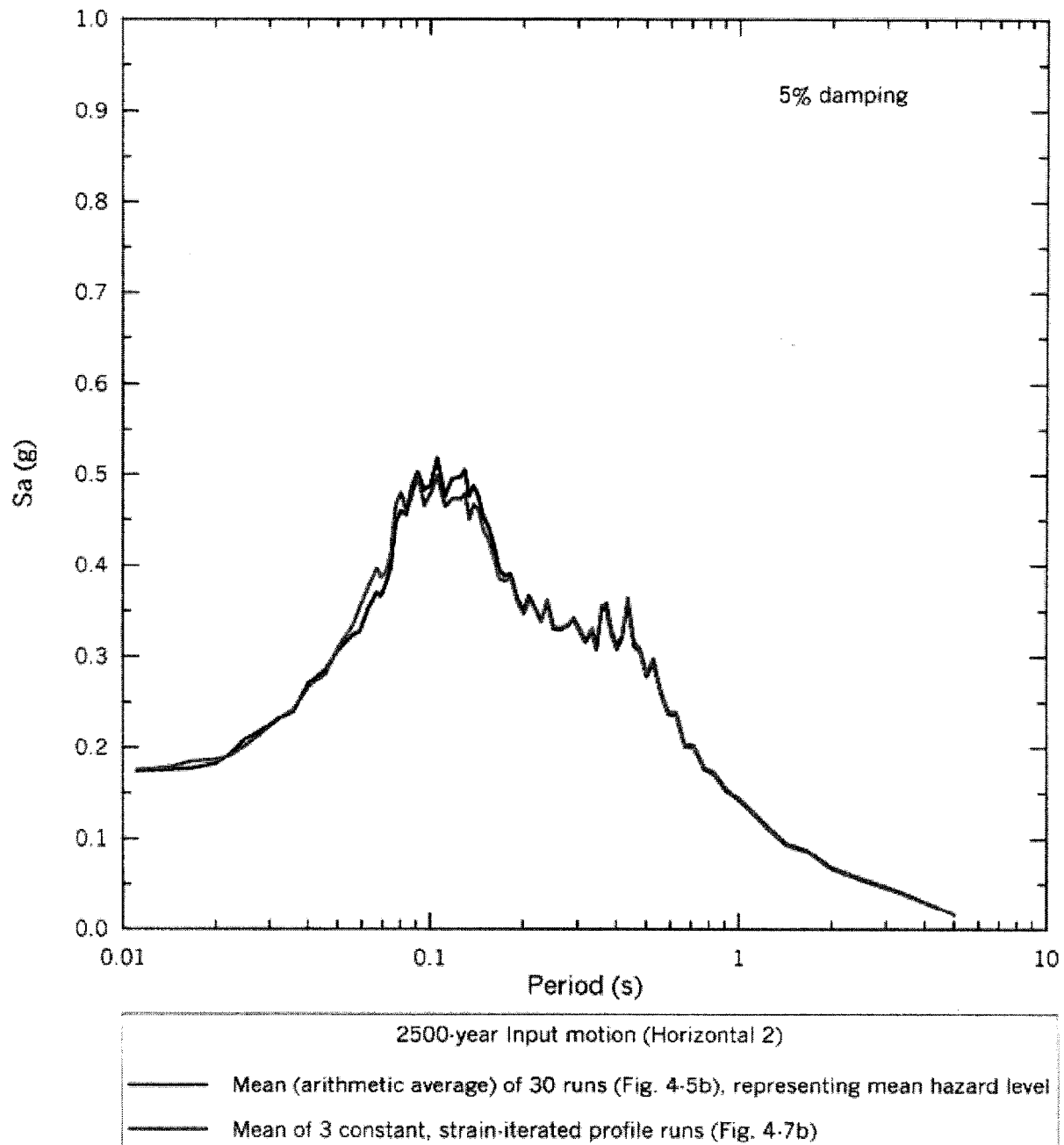


Figure 2.6-53
Ground Acceleration Time-Histories
(mean minus one standard deviation)

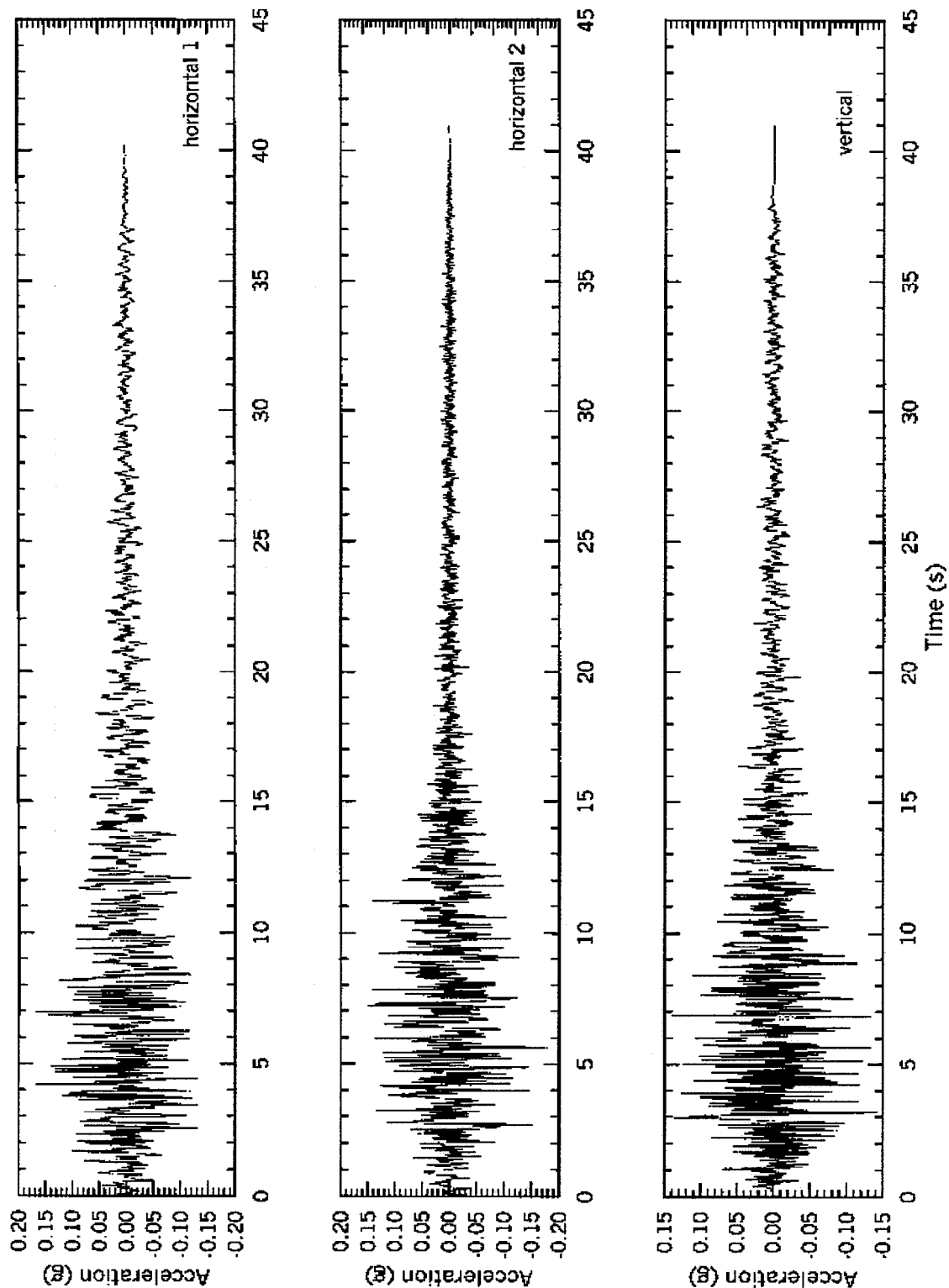


Figure 2.6-54
Ground Acceleration Time-Histories
(Mean Profile)

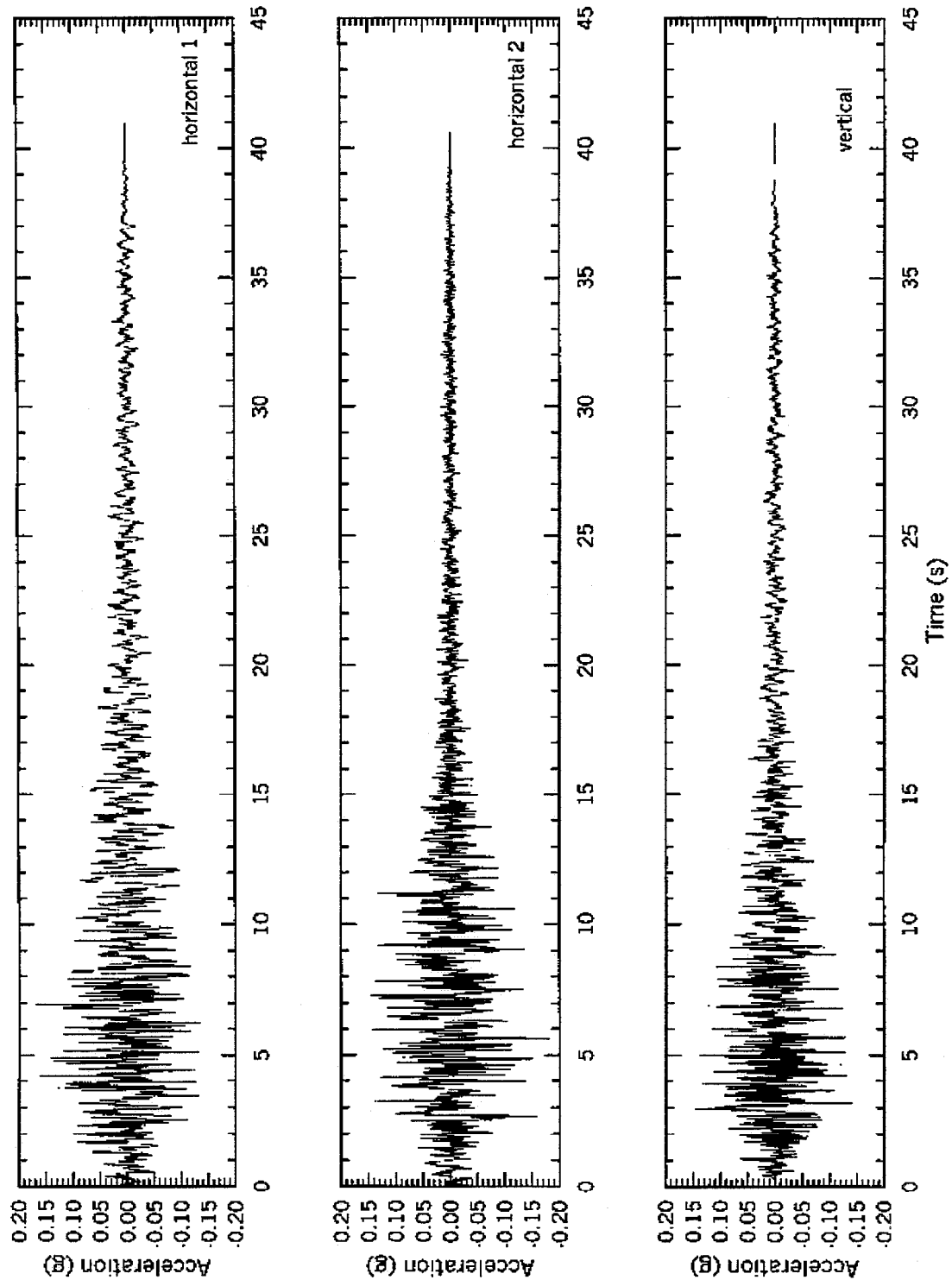


Figure 2.6-55
Ground Acceleration Time-Histories
(mean plus one standard deviation)

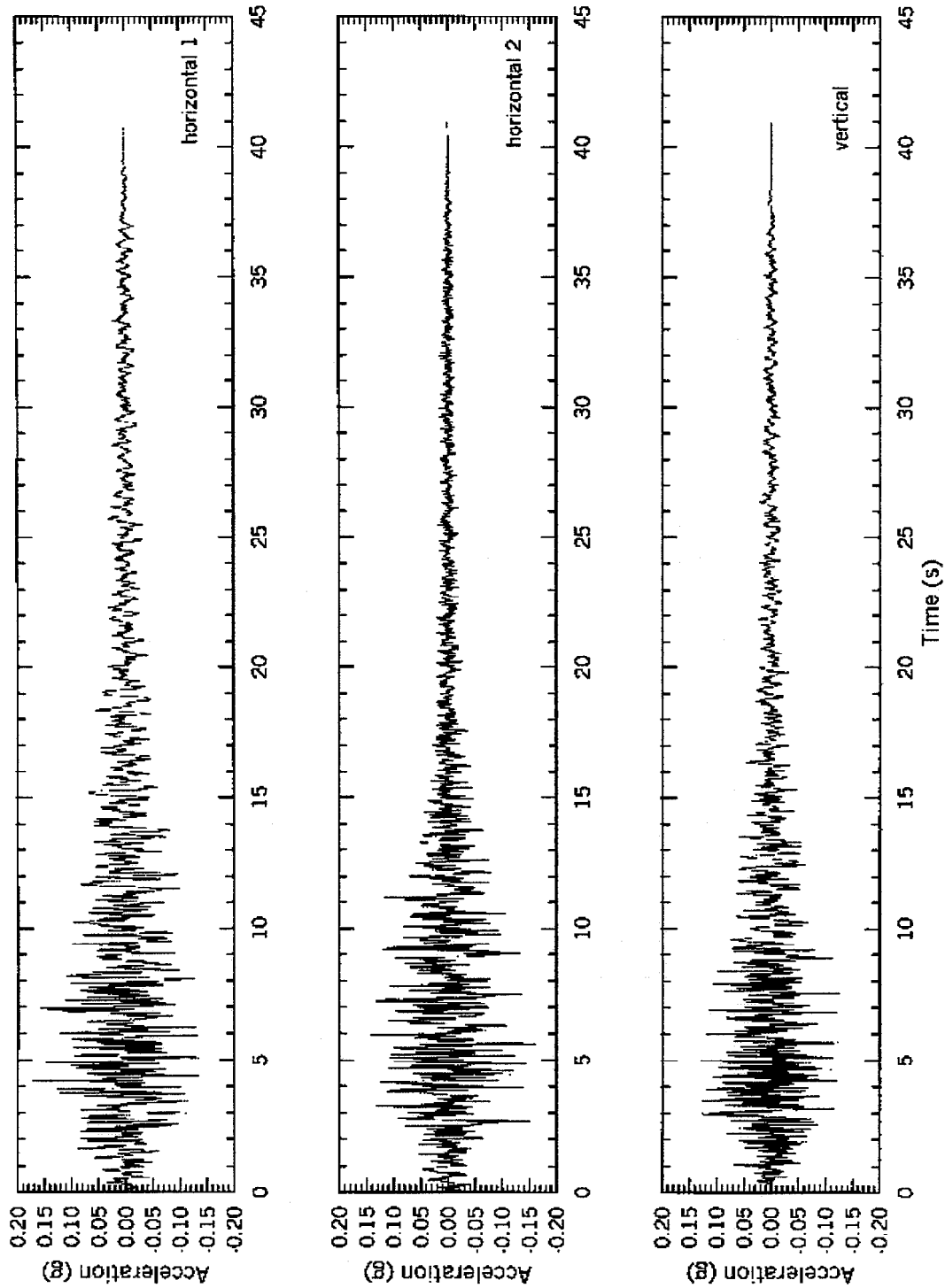
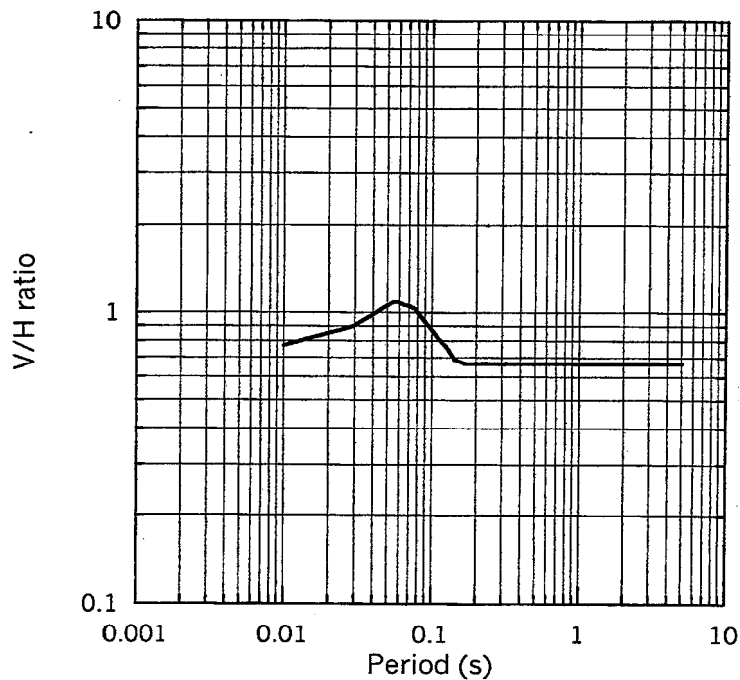


Figure 2.6-56
Vertical to Horizontal Spectra Ratio



Period (s)	V/H ratio	Period (s)	V/H ratio
0.010	0.770	0.080	1.000
0.020	0.770	0.083	0.975
0.022	0.807	0.087	0.949
0.025	0.850	0.091	0.923
0.030	0.897	0.095	0.897
0.032	0.925	0.100	0.870
0.033	0.936	0.105	0.842
0.036	0.954	0.111	0.813
0.040	0.985	0.118	0.789
0.045	1.030	0.125	0.765
0.050	1.060	0.129	0.746
0.056	1.090	0.133	0.728
0.057	1.090	0.138	0.709
0.059	1.090	0.143	0.690
0.063	1.070	0.148	0.685
0.067	1.060	0.154	0.679
0.069	1.060	0.160	0.673
0.071	1.050	0.167	0.667
0.074	1.040	1.000	0.667
0.077	1.030	10.000	0.667

Figure 2.6-57
Vertical Ground Response Spectrum (mean minus one standard deviation)

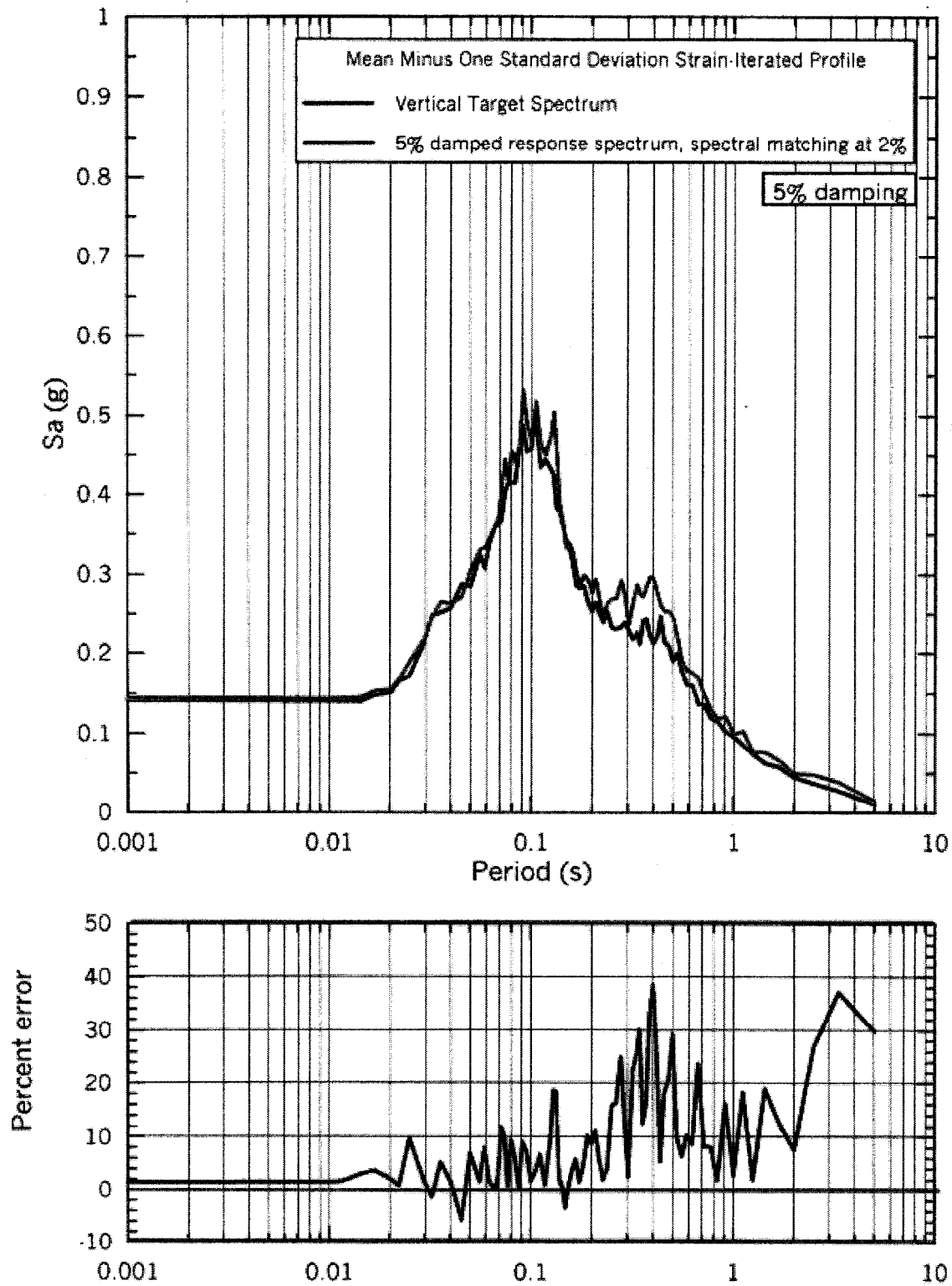


Figure 2.6-58
Vertical Ground Response Spectrum (mean)

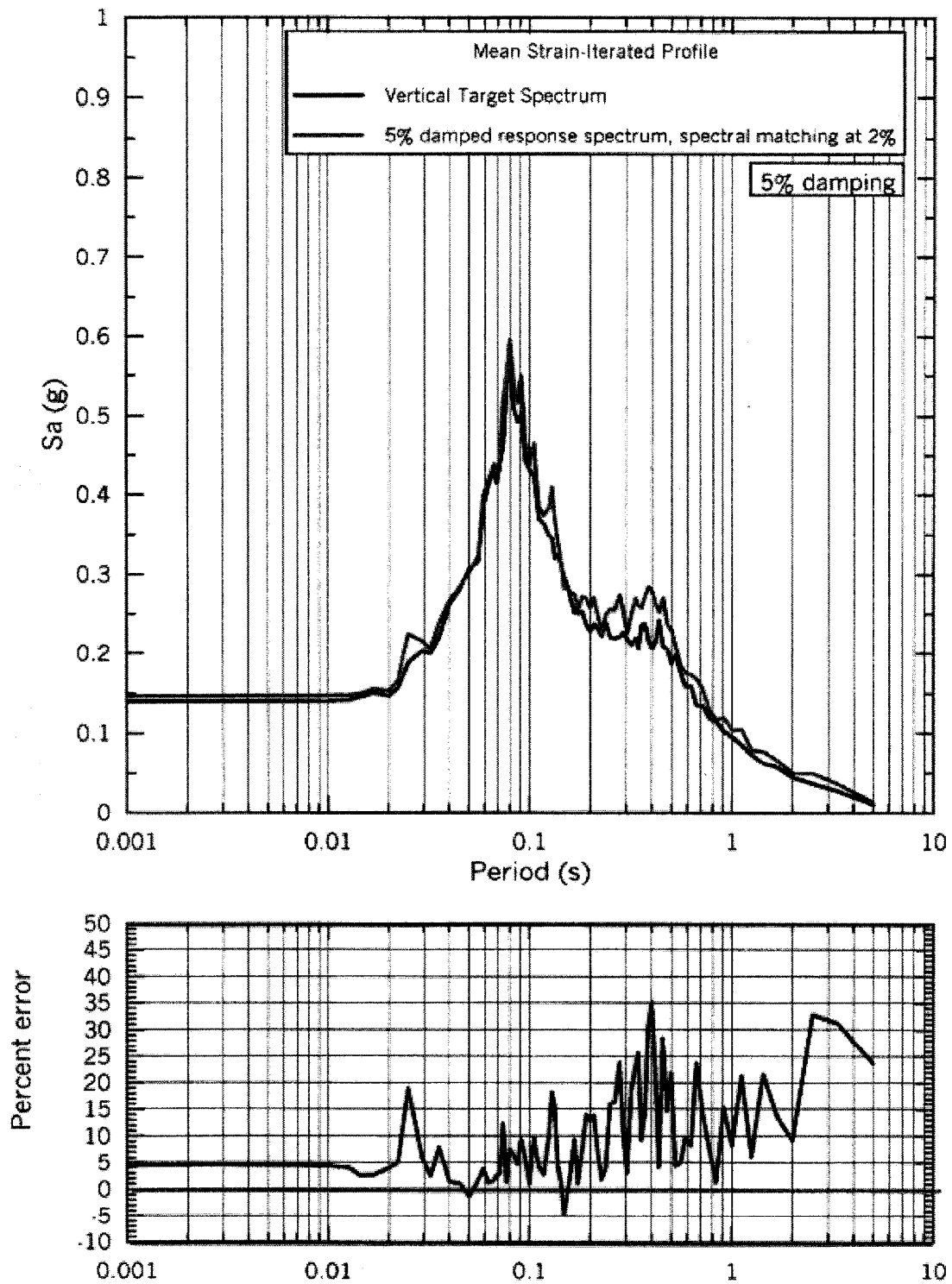


Figure 2.6-59
Vertical Ground Response Spectrum (mean plus one standard deviation)

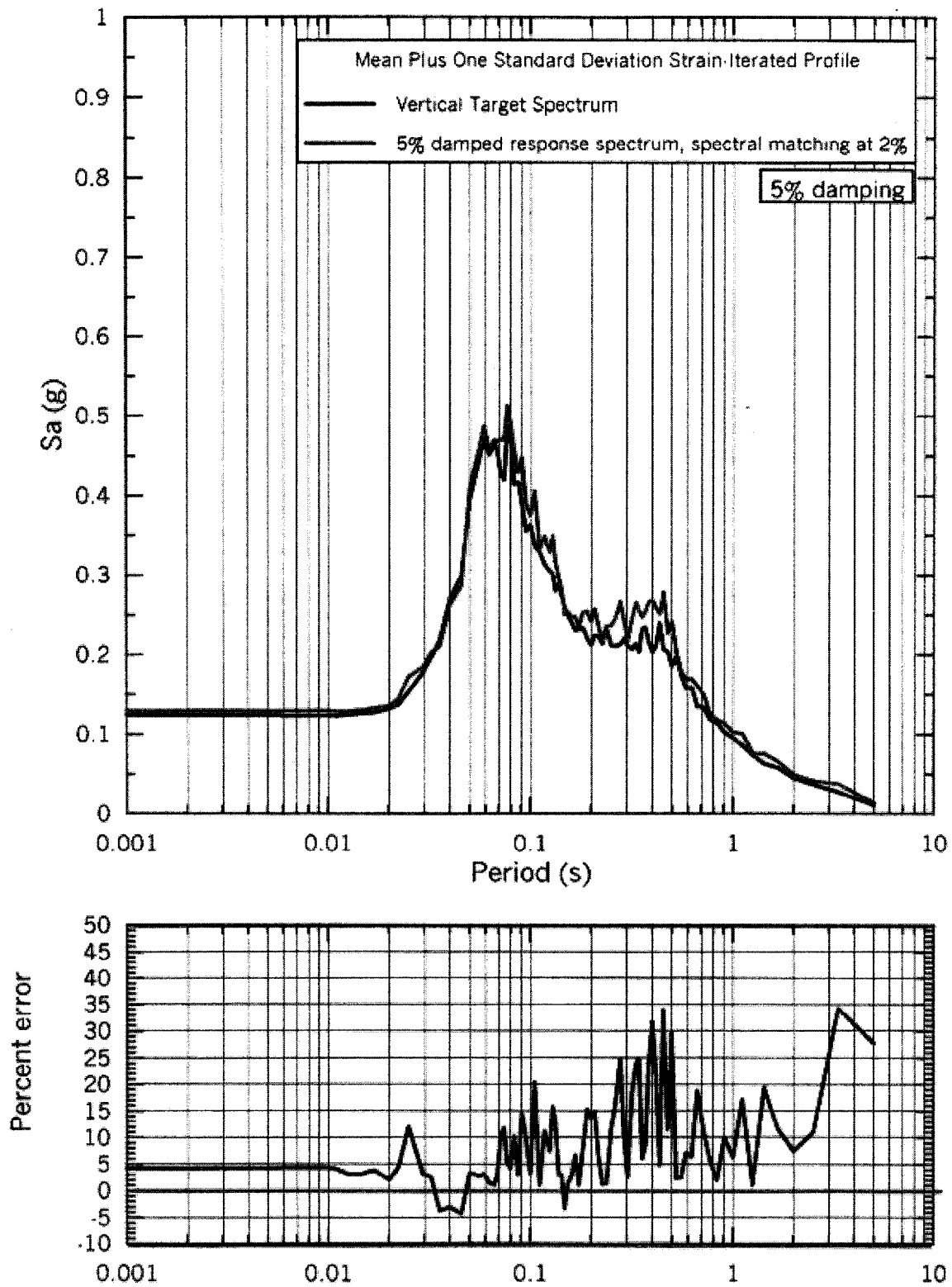


Figure 2.6-60
INEEL Volcanic Rift Zones, Axial Volcanic Zones, and Fissures

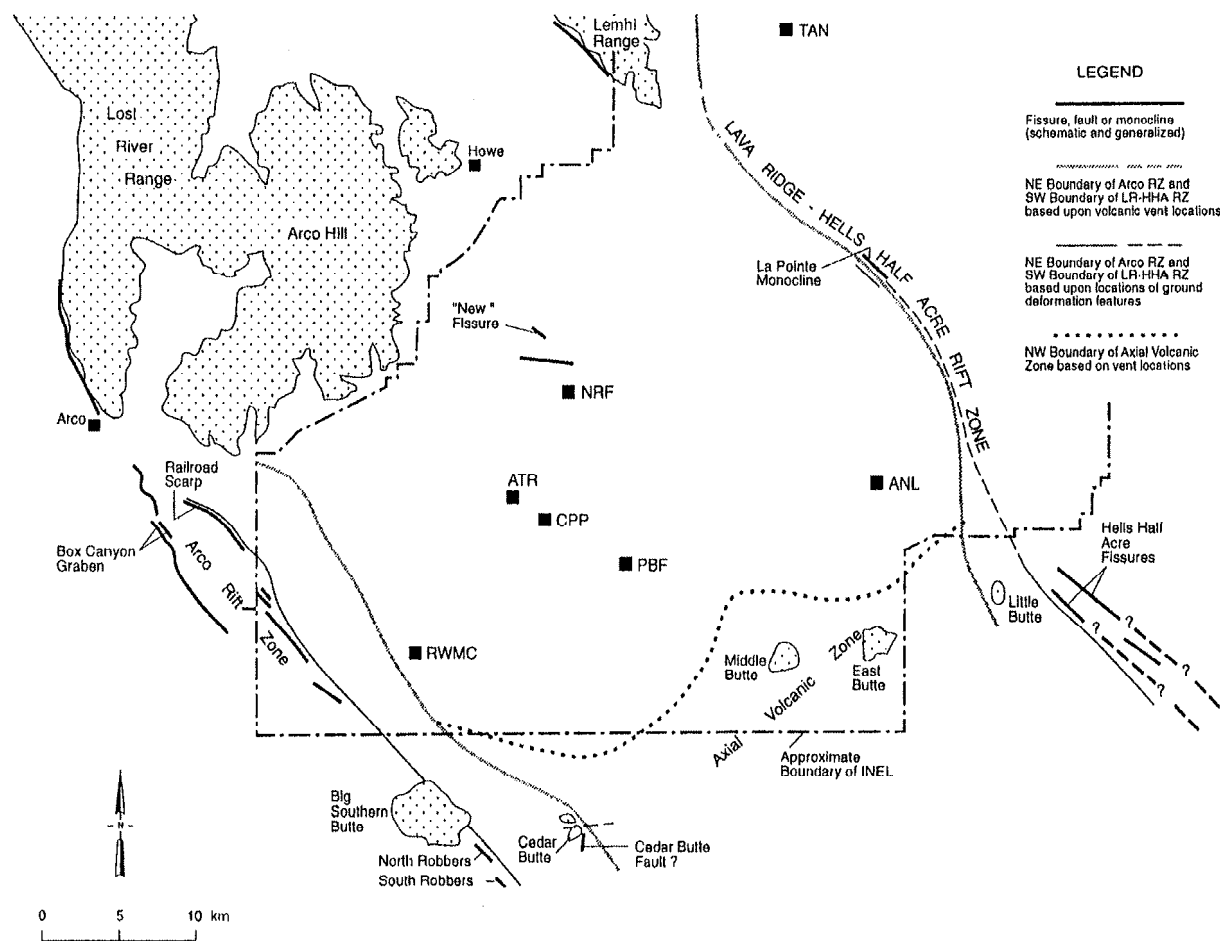


Figure is adapted from the TMI-2 ISFSI SAR (Ref. 2-1). The ICPP is an earlier name for the INTEC, which is adjacent to the ISF Facility site.

Figure 2.6-61
Stress Field and Displacement & Volcanic Rift Zone Structures

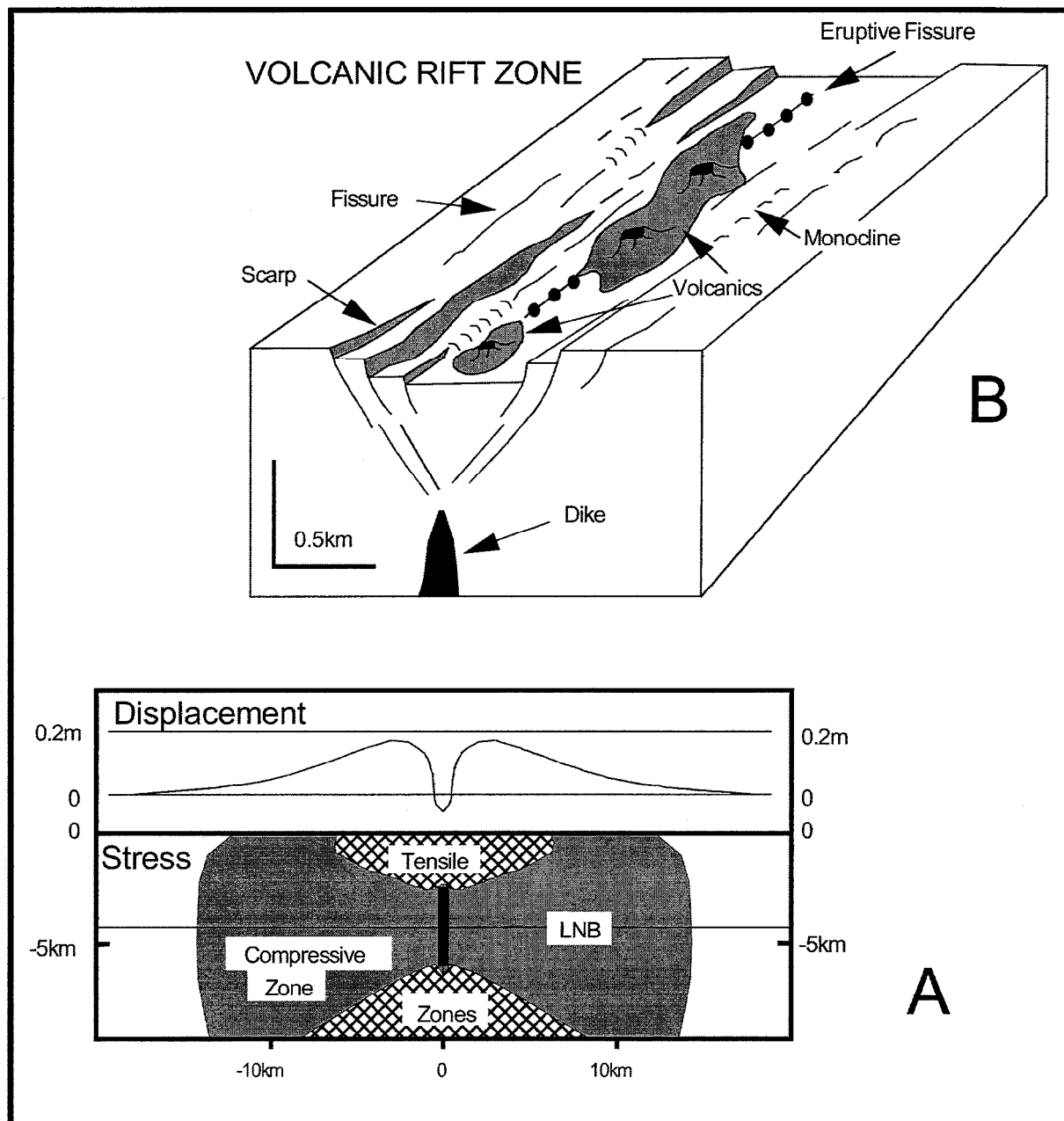


Figure 2.6-62
Map of Volcanic Vents and Volcanic Zones with Estimated Recurrence Intervals

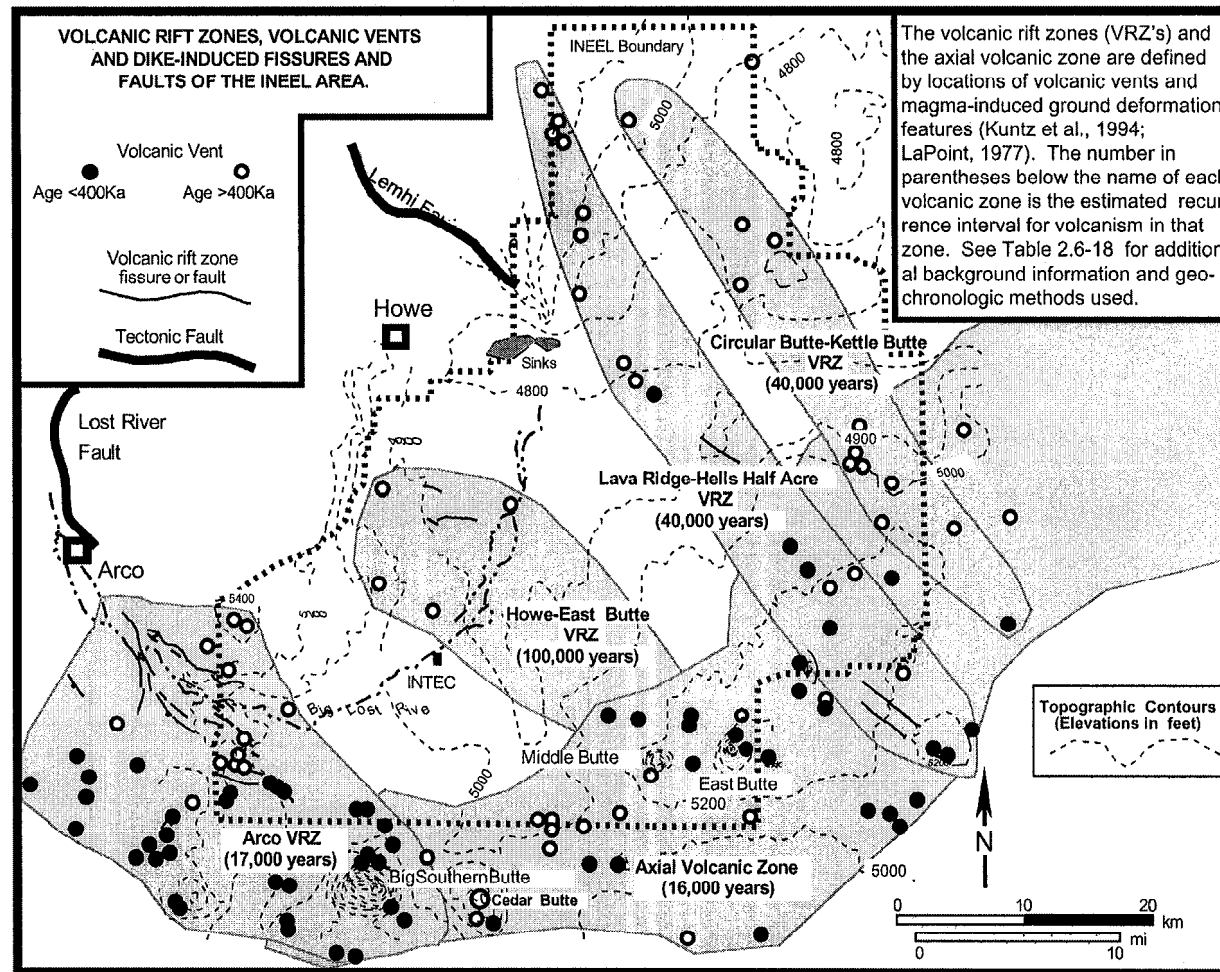


Figure is adapted from the TMI-2 ISFSI SAR (Ref. 2-1). The ISF Facility site is adjacent to the INTEC depicted in the figure.